Microglial dynamics in physiological conditions : a vigilance state and neuronal activity-driven mechanism

Ines Hristovska

▶ **To cite this version:**

Ines Hristovska. Microglial dynamics in physiological conditions : a vigilance state and neuronal activity-driven mechanism. Neuroscience. Université de Lyon, 2019. English. NNT : 2019LYSE1306 . tel-03462627

HAL Id: tel-03462627
https://theses.hal.science/tel-03462627v1

Submitted on 2 Dec 2021

HAL is a multi-disciplinary open access archive for the deposit and dissemination of scientific research documents, whether they are published or not. The documents may come from teaching and research institutions in France or abroad, or from public or private research centers.

L'archive ouverte pluridisciplinaire **HAL**, est destinée au dépôt et à la diffusion de documents scientifiques de niveau recherche, publiés ou non, émanant des établissements d'enseignement et de recherche français ou étrangers, des laboratoires publics ou privés.

N°d'ordre NNT : 2019LYSE1306

THESE de DOCTORAT DE L'UNIVERSITE DE LYON
opérée au sein de
l'Université Claude Bernard Lyon 1

Ecole Doctorale N° 476
Neurosciences et Cognition (NSCo)

Spécialité de doctorat : Neurosciences
Discipline : Neurobiologie cellulaire

Soutenue publiquement le 4/12/2019, par :
Ines Hristovska

Dynamique microgliale en conditions physiologiques : un mécanisme contrôlé par les états de vigilance et l'activité neuronale

---

Devant le jury composé de :

Bessereau, Jean-Louis, PU Université Lyon 1	Président du Jury
Fabre, Véronique, CR INSERM	Rapporteure
Nadjar, Agnès, MCU Université de Bordeaux	Rapporteure
Didier, Anne, PU Université Lyon 1	Examinatrice
Gressens, Pierre, DR INSERM	Examinateur
Pascual, Olivier, CR INSERM	Directeur de thèse
Comte, Jean-Christophe, IR CNRS	Co-directeur de thèse (Invité)

UNIVERSITE Claude BERNARD – LYON 1

Président de l'Université	M. Frédéric FLEURY
Président du Conseil Académique	M. Hamda BEN HADID
Vice-Président du Conseil d'Administration	M. Didier REVEL
Vice-Président du Conseil des Etudes et de la Vie Universitaire	M. Philippe CHEVALLIER
Vice-Président de la Commission de Recherche	M. Fabrice VALLEE
Directeur Général des Services	M. Damien VERHAEGHE

COMPOSANTES SANTE

Faculté de Médecine Lyon-Est – Claude Bernard	Doyen : M. Gilles RODE
Faculté de Médecine et Maïeutique Lyon Sud Charles. Mérieux	Doyenne : Mme Carole BURILLON
UFR d'Odontologie	Doyenne : Mme Dominique SEUX
Institut des Sciences Pharmaceutiques et Biologiques	Directrice : Mme Christine VINCIGUERRA
Institut des Sciences et Techniques de la Réadaptation	Directeur : M. Xavier PERROT
Département de Formation et Centre de Recherche en Biologie Humaine	Directrice : Mme Anne-Marie SCHOTT

COMPOSANTES & DEPARTEMENTS DE SCIENCES & TECHNOLOGIE

UFR Biosciences	Directrice : Mme Kathrin GIESELER
Département Génie Electrique et des Procédés (GEP)	Directrice : Mme Rosaria FERRIGNO
Département Informatique	Directeur : M. Behzad SHARIAT
Département Mécanique	Directeur M. Marc BUFFAT
UFR - Faculté des Sciences	Administrateur provisoire : M. Bruno ANDRIOLETTI
UFR (STAPS)	Directeur : M. Yannick VANPOULLE
Observatoire de Lyon	Directrice : Mme Isabelle DANIEL
Ecole Polytechnique Universitaire Lyon 1	Directeur : Emmanuel PERRIN
Ecole Supérieure de Chimie, Physique, Electronique (CPE Lyon)	Directeur : Bernard BIGOT
Institut Universitaire de Technologie de Lyon 1	Directeur : M. Christophe VITON
Institut de Science Financière et d'Assurances	Directeur : M. Nicolas LEBOISNE
ESPE	Administrateur Provisoire : M. Pierre CHAREYRON

ACKNOWLEDGMENTS

It is quite overwhelming to reflect on several years of one's (still youthful student 😉) life that have been filled with many exciting and uplifting, sometimes difficult scientific moments, which come with a great deal of emotional turmoil and many, many wonderful exchanges. You may not think of science this way, but it is as dramatic (if not more!) as my beloved Spanish telenovelas. Just ask Kassandre and Mélisse before and during our surgeries… Nevertheless, the first thing that comes to mind is the gratitude to be able to do so many interesting things and be surrounded by amazing people. Everybody brings a little bit of themselves, their knowledge, their passion and their (often undervalued) support which makes everything easier and more meaningful. It is often difficult to remember this at a day-to-day basis, but it is surely something that I would like to give more thought to.

I would like to begin by thanking the members of my jury that accepted to evaluate my work and honor me with their presence: Prof. Jean-Louis Bessereau, Dr. Véronique Fabre, Dr. Agnès Nadjar, Prof. Anne Didier and Prof. Pierre Gressens.

I would especially like to thank Olivier Pascual for his support, teaching me and giving me the amazing opportunity to be able to work with "sci-fi" techniques and tools that I have never dreamed of. Your theoretical and technical knowledge and openness towards so many fields (except for Mylène and Eurovision 😉…) is fascinating and I hope that one day I will be able to contemplate scientific concepts as you do. Jean-Christophe, your input and work on the data has been priceless, you are our "microglia team magician" and I would like to thank you for everything, because we could not have done this without you. I would also like to thank Prof. Jerome Honnorat for welcoming me in his lab and allowing me to do this work.

To my friends at the lab: first, the ones I met when I arrived and that have since gone to conquer other horizons: Chloé, the sunshine of the "bureau du bonheur", such happiness to get to know you! Aude, I admire you so much in so many ways and I know you will do amazing things! I miss our heart-opening conversations over coffee and "running/phone-breaking" sessions at Laennec! Fuyuko, my Japanese sunshine, thank you for so many wonderful (and funny!!!) moments. Marie-Eve and Céline, you are one of the most kind and heart-to-heart people I know, thank you for all that you have taught me and keep using your super-powers! Fabrice, we need to continue our bars and concert quests and discover many more! Lucie-Orianne, Do, Elodie, Chloé, Déborah, Margaux, Laurent, Pauline, Mathilde, Bastien, thank you for all the moments we shared, and I wish you so much success!

And the newbies!! Alanah and our tales in the old and new bureau… I will just say "U slay!", I believe in your alternative career as impersonator, and you are one of the funniest and smartest people I know! Mélisse, I am so happy that I got to know you, you will crack microglia-neuron communication and I

can’t wait for you to tell me about it! Those Saturday and Sunday mornings in the 2photon “fridge” were the best I had! Delphine, we were kind of an improbable match, but you became a very good friend and I love our crazy moments and never-ending conversations on anything and everything! And of course, l’amour pour la France…😊 Violaine, I am so happy that we became friends and it was always a pleasure to work, talk, have coffee with you, our long sessions at the 2photon and the “study” sessions at the bureau! Kassandre, I hope Saint-Etienne wins against Lyon next time 😊. In between, I am sure that you will discover many amazing things on microglia!

Naura and Chantal, you are the backbone of the lab, and always in good spirits, it has been a pleasure to work with you! Thank you, Chantal, my savior, for everything! 😊

Thank you Virginie, Claire, Nelly, Vero, Roger for all the moments we shared together, all the conversations, scientific and about life, politics, love...

To my wonderful friends in Lyon and Macedonia who have helped me enormously during this adventure: Bertrand, you were my rock through all of this, and I do not have the words to express how grateful I am for having you in my life. Nade, Paulina, Sarah, Yoann, David, Lucas, Marie, thank you for all your support, never-ending conversations, parties and craziness!

To my family that has been here for me always, emotionally and physically. Your love and support have meant the world to me and this work is for you.

When it's over, I want to say: all my life
I was a bride married to amazement.
I was the bridegroom, taking the world into my arms.

Tell me, what else should I have done?
Doesn’t everything die at last, and too soon?
Tell me, what is it you plan to do
with your one wild and precious life?

Mary Oliver

ABBREVIATIONS

5-HT(R):	5-hydroxytryptamine receptors
AAV:	Adeno-associated virus
Ach:	Acetylcholine
AMPA(R):	α-amino-3-hydroxy-5-methyl-4-isoxazolepropionic acid (receptors)
Arc:	Activity-regulated cytoskeleton associated protein
Arg-1:	Arginase 1
ATP:	Adenosine triphosphate
BDNF:	Brain-derived neurotrophic factor
BF:	Basal forebrain
C1q:	Complement component 1q
C3:	Complement component 3
CaMKII:	Ca^{2+}/calmodulin-dependent protein kinase II
CatS:	Cathepsin S
CCL2:	C-C motif chemokine ligand 2
CD11b (ITGAM):	Integrin subunit alpha M
CD39/ NTPDase1:	Ectonucleoside triphosphate diphosphohydrolase 1
CD47:	Cluster of differentiation 47, integrin associated protein (IAP)
CDK5:	Cyclin dependent kinase 5
CR3:	Complement receptor 3
CREB:	Cyclic-AMP response element-binding protein
CSF1:	Colony stimulating factor 1
CXCL10:	C-X3-C motif chemokine ligand 10
CX3CL1/CX3CR1:	C-X3-C motif chemokine ligand/receptor 1
DAP12/KARAP:	DNAX activating protein of 12kDa/Killer cell activating receptor-associated protein
DG:	Dentate gyrus
EEG:	Electroencephalogram
EMG:	Electromyogram
ERK:	Extracellular signal-regulated kinase
GABA:	Gamma-aminobutyric acid
GCaMP6	GFP-Calmodulin fusion protein
GluR1/2:	Glutamate receptor 1/2
GluN2A/B:	Glutamate binding NMDA receptor subtype 2A/2B
Gpr43/FFRA2:	Free fatty acid receptor 2
GDNF:	Glial cell-derived neurotrophic factor
EPSC:	Excitatory postsynaptic current
HA:	Histamine
Hexb:	Hexosaminidase subunit beta
HFS:	High-frequency stimulation
Homer-1a:	Homer scaffold protein 1
Hoxb8:	Homeobox B8
HSC:	Hematopoietic stem cells
Fcrls:	Fc receptor-like S scavenger receptor
FGF:	Fibroblast growth factor
FIZZ1:	Resistin-like beta
Iba1:	Ionized calcium-binding adapter molecule 1
IGF:	Insulin-like growth factor
IFNy:	Interferon gamma
IL:	Interleukin
iNOS:	Inducible nitric oxide synthase
IPSC :	Inhibitory postsynaptic potential
LC:	Locus coeruleus

LF:	Low-frequency
LFP:	Local field potential
LGN:	Lateral geniculate nucleus
LH:	Lateral hypothalamus
LDT:	Laterodorsal tegmental nucleus
LTD:	Long-term depression
LTP:	Long-term potentiation
LPS:	Lipopolysaccharide
MCH (neurons):	Melanin-concentrating hormone
Mertk:	MER proto-oncogene tyrosine-protein kinase
mGlu1/5:	Metabotropic glutamate receptor
MHC-I:	Major histocompatibility complex I
MnPN:	Median preoptic nucleus
mPFC:	Medial prefrontal cortex
NA:	Norepinephrine
NGF:	Nerve growth factor
NMDA(R):	N-Methyl D-Aspartate (receptor)
NREM:	Non-rapid eye movement
NT:	Neurotransmitter
ODP:	Ocular dominance plasticity
Olfml3:	Olfactomedin like 3
OPC:	Oligodendrocyte progenitor cell
P2X/P2Y:	Purinergic ionotropic (P2X) and metabotropic (P2Y) receptors
PAMP:	Pathogen-associated molecular pattern molecules
PB:	Parabrachial nucleus
PCD:	Programmed cell death
PKA:	Protein kinase A
POA:	Preoptic area
PPT:	Pedunculopontine tegmental nucleus
Pros1:	Protein S
PRP:	Plasticity-related proteins
PSD:	Postsynaptic density
PV-Ins:	Parvalbumin interneurons
RGC:	Retinal ganglion cells
REM:	Rapid eye movement
ROS:	Reactive oxygen species
Sall1:	Spalt-like transcription factor 1
SCN:	Suprachiasmatic nucleus
SHY:	Synaptic homeostasis hypothesis
SiglecH:	Sialic acid binding Ig-like lectin H
SNAP25:	Synaptosomal-associated protein 25
SNARE:	Soluble N-ethylmaleimide-sensitive factor attachment protein receptors
SNIPPs:	Sleep-need-index-phosphoproteins
SOM-Ins:	Somatostatin interneurons
STC:	Synaptic tagging and capture hypothesis
THIK-1:	Two-pore domain halothane-inhibited K^+ channel type 1
TM:	Tuberomammillary nuclei
Tgfβ:	Transforming growth factor beta 1
Tmem119:	Transmembrane protein 119
TNFα:	Tumor necrosis factor alpha
TREM2:	Triggering receptor expressed on myeloid cells 2
TrkB:	Tropomyosin/tyrosine receptor kinase B
TRN:	Thalamic reticular nucleus
TTX:	Tetradotoxin
Syn:	Synapsin

SV40:	Simian vacuolating virus 40
SVZ:	Subventricular zone
SWS:	Slow-wave sleep
vGLUT:	Vesicular glutamate transporter
VLPO:	Ventrolateral preoptic nucleus
WPRE:	WHV (Woodchuck hepatitis virus) post-transcriptional regulatory element
Ym-1:	Chitinase-like 3

RESUME

Les microglies, cellules immunitaires résidentes du système nerveux central (SNC), étaient traditionnellement décrites comme ayant un rôle uniquement lors de blessures ou de maladies du SNC. De manière frappante, dans le cerveau sain, les microglies effectuent une surveillance active du parenchyme en étendant et en rétractant leurs prolongements ramifiés. Ce mouvement est connu sous le nom de motilité microgliale et peut être dirigé vers les synapses. La régulation de ces mouvements et le but des contacts microglie-épines dendritiques restent inconnus. Nous avons examiné l'influence de l'activité neuronale sur la motilité et la morphologie microgliale ainsi que sur les interactions microglies-épines pendant l'éveil et le sommeil. Nous avons observé que les propriétés morpho-dynamiques des microglies sont modulées par les états de vigilance. Les prolongements microgliaux sont attirés par les synapses actives, particulièrement lors de l'éveil, alors que le sommeil régule négativement la proximité des prolongements microgliaux ainsi que les contacts dépendants de l'activité qui lient les prolongements microgliaux aux épines. Le contact des épines avec les prolongements microgliaux entraîne une augmentation de l'activité des épines, principalement observée pendant le sommeil lent. Pour conclure, ces résultats montrent un contrôle complexe de la morpho-dynamique microgliale par l'activité et les états de vigilance. Appréhender les mécanismes régulant la dynamique microgliale et les interactions microglie-épines dendritiques pendant les états de vigilance permettra de mieux comprendre comment les cellules microgliales sont impliquées dans la régulation de l'homéostasie synaptique, l'apprentissage et de la mémoire, des fonctions associées au sommeil. La compréhension des interactions microglies-neurones dans des conditions physiologiques est cruciale pour élucider le fonctionnement synaptique et ses altérations lorsque la microglie est impliquée dans ses fonctions immunes, une caractéristique commune à la plupart des pathologies cérébrales.

Mots-clés : microglie, motilité, interaction microglie-épine, synapse, éveil, sommeil, imagerie calcique, *in vivo*

ABSTRACT

Microglia, the resident immune cells of the central nervous system (CNS), were traditionally believed to be set into action only by injury or diseases. Strikingly, in the healthy brain, microglia actively carry out parenchyma patrolling by extending and retracting their ramified processes. These movements are referred to as microglial motility and may be to some extent directed toward synapses. However, motility regulation and the purpose of microglia-spine contacts remain elusive. We thus examined the influence of neuronal activity on microglial motility, morphology and microglia-spine interactions during sleep and wakefulness. We found that microglial motility and morphology are modulated by vigilance states. Microglial processes were found to be attracted by active synapses particularly during wake, whereas sleep downregulates microglial proximity and activity-dependent contact with spines. Microglial contact resulted in increased spine activity which was mainly observed during sleep. Understanding the mechanisms regulating microglial dynamics and microglia-spine interactions across the vigilance states will provide further insights into how microglial cells may be involved in sleep-associated functions such as synaptic homeostasis, learning and memory. Grasping these cellular interactions in physiological conditions is crucial to understanding synaptic functioning and alterations when microglia are engaged in their immune functions, a hallmark of most brain pathologies.

Key words: microglia, motility, microglia-spine interactions, synapse, wake, sleep, calcium imaging, *in vivo*

Table of contents

INTRODUCTION

I. Overview of microglial cells

1. Glial cells – coming out from the shadows

From a passive role as elements that form an "adhesive substance connecting neurons", glial cells have been recently recognized as key players in many aspects of brain physiology and disease (Rasband, 2016). This new status is due to growing body of evidence, especially in the past 20 years or so, reporting critical involvement of glial cells in many physiological mechanisms (Figure 1). These roles include shaping the central nervous system (CNS) architecture, promoting neuronal survival, offering metabolic support to neurons, regulating ionic extracellular environment, as well as sensing and modulating neuronal activity via gliotransmitters or contact-dependent mechanisms (Akiyoshi et al., 2018; Araque et al., 2014; Eyo et al., 2014; Jha and Morrison, 2018; Mosser et al., 2017; Olsen et al., 2015; Volterra and Meldolesi, 2005). These processes are highly dependent on bidirectional neuron-glial and glial-glial communication (Dzyubenko et al., 2016; Shaham, 2005). Disruption of these mechanisms leading to and/or caused by glial cell dysfunction are common in a broad spectrum of pathologies, including neurodevelopmental, neurodegenerative and neuropsychiatric disorders (Arranz and De Strooper, 2019; Bachiller et al., 2018; Booth et al., 2017; Li et al., 2018; Szepesi et al., 2018).

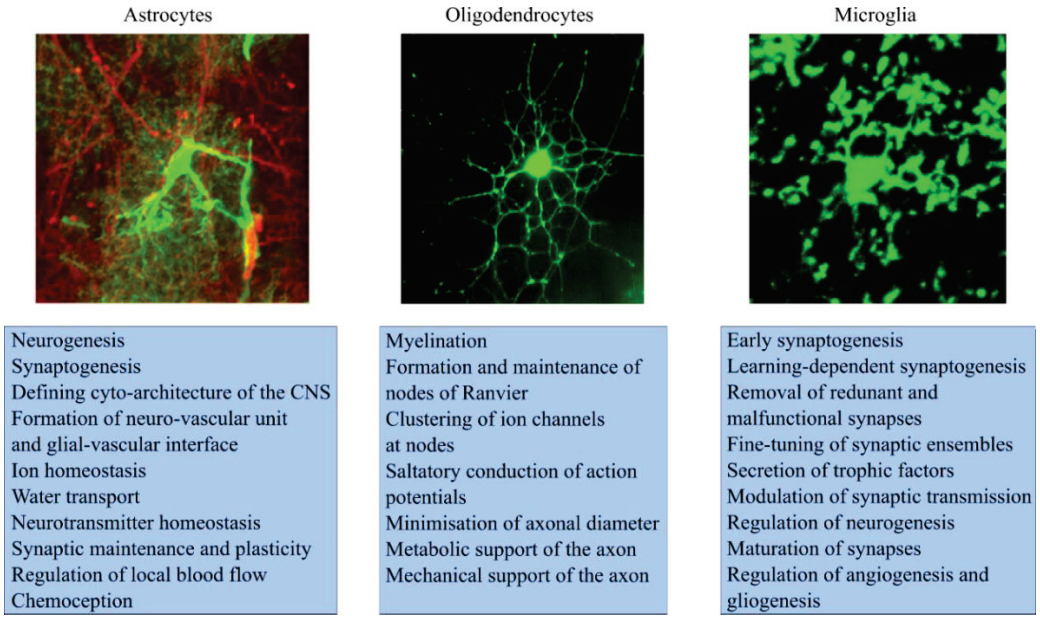

Figure 1: Major types of glial cells (astrocytes, oligodendrocytes and microglial cells) in the central nervous system (CNS) and their main functions. Adapted from (Butt and Verkhratsky, 2018; Giaume et al., 2007; Osterhout et al., 1999)

2. General description of microglial cells in physiology and pathology

2.1 First description of microglial cells

The earliest description of microglia was reported by Nissl, who described "rod cells" in patients with general paresis (Nissl, 1899). Rod microglia are a unique type of activated microglia, with a strikingly different morphology from amoeboid microglia (Holloway et al., 2019). Using tannin and ammoniacal silver nitrate staining method, Achúcarro, an alumnus of Ramon y Cajal, described "granuloadipose cells" that appeared to phagocytose degradation material (Achúcarro, 1913, Figure 2). Ramon y Cajal later developed a staining method (gold chloride sublimate) allowing for an excellent depiction of astrocytes but failed to distinguish other glial cells types. Instead, he observed "corpuscles without process" assembling apolar, adendritic dwarf cells, that he named "the third element" (Ramon y Cajal 1913a). The mystery of the third element was later resolved by Pio del Rio-Hortega, another Cajal alumnus (Rio-Hortega, 1919a). Using modified ammoniacal silver carbonate staining method, del Rio-Hortega managed to distinguish two other cell types: microglia and oligodendroglia, endowed with distinct cytoplasmic expansions. He characterized microglial cells as having small, dark nucleus with little protoplasm and long ramified processes with lateral spines, suggesting that "their shape is mutable and conditional; that their protoplasm is capable of plasticity" (Rio-Hortega, 1919b). Hence, he documented their proliferation, migratory and phagocytic activity upon injury from stab wounds (Rio-Hortega, 1919b). He also described their distribution throughout the brain, revealing a higher density in the gray matter (Rio-Hortega, 1919c). Due to delayed occurrence of microglia in the brain and close apposition with vascular elements, del Rio-Hortega proposed that microglial cells are of mesodermic origin. Regarded as the "father of microglia biology", Del Rio-Hortega provided fascinating insights on microglial origin, morphology, distribution and function that have been mostly confirmed 100 years later.

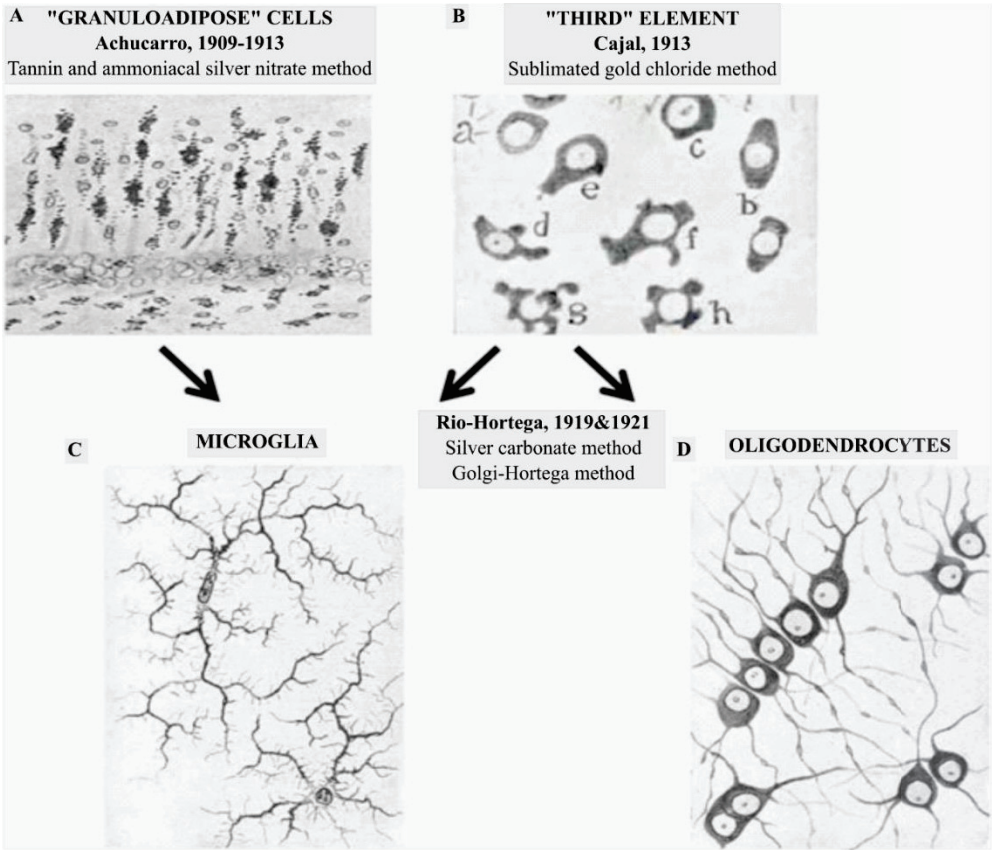

Figure 2: Describing the composition of the third element. (A) Using the tannin and ammoniacal silver nitrate method, Achúcarro visualized "granuloadipose" cells that seemed to phagocytose degradation material. (B) Later, Cajal used sublimated gold chloride method leading to an excellent visualization of astrocytes but poor staining of other glial cells. These cells resembling "corpuscles without processes" were named "the third element". (C, D) Del Rio-Hortega managed to distinguish between microglia (C) and oligodendrocytes (D) using modified silver carbonate method (Tremblay et al., 2015).

2.2 Origin and maintenance of microglial cells

Microglial cells are the resident immune cells of the central nervous system (CNS). They account for ~10% of cells in the brain, after oligodendrocytes (40-60%) and astrocytes (20-40%), with considerable differences between brain regions, developmental stage and species (von Bartheld et al., 2016). Most tissue resident macrophages, with the exception of microglia and partially epidermal Langerhans cells, are derived from classic hematopoietic stem cells (HSC) (Sheng et al., 2015a). Microglial cells were found to derive from yolk-sac precursors (Ginhoux and Guilliams, 2016; Ginhoux et al., 2010; Hoeffel and Ginhoux, 2015), however the precise nature of these precursors remains a matter of debate. Ginhoux *et al*. found that adult microglia come from primitive macrophages during embryogenesis (Ginhoux et al., 2010), whereas two other studies recognized erythromyeloid progenitors as sole precursors of

embryonic and perinatal microglia (Gomez Perdiguero et al., 2015; Kierdorf et al., 2013). The issue in studying microglial ontogeny lies in the difficulty of labeling *in utero* and discriminating subsets of hematopoietic precursors that emerge in a very narrow time interval during development. Using a zebrafish model where each possible precursor is spatially and temporally distinct during embryonic development, Ferrero *et al.* showed that erythromyeloid progenitors did not contribute to microglial development (Ferrero et al., 2018). It was primitive macrophages that generated a first transient wave, followed by embryonic HSC that gave rise to definitive adult microglia (Ferrero et al., 2018). Since this study was conducted in zebrafish, these findings are yet to be confirmed in rodents.

Even though precise microglial ontogeny is to be elucidated, it is well-established that most microglial colonization of the neuroepithelium begins from E9.5 concurrently with the generation of first neurons and prior to astrogliogenesis and oligodendrogenesis (Ginhoux et al., 2010; Malatesta et al., 2000; Qian et al., 2000; Swinnen et al., 2013). Microglia enter via the leptomeninges and lateral ventricles and then spread throughout the cortical wall. Thus, microglial recruitment, positioning and proliferation at the early stages are crucially dependent on bi-directional cross talk between microglia and neural progenitor cells (Arnò et al., 2014). In addition, a microglial subpopulation with a delayed appearance in the brain was recently identified (Chen et al., 2010a). This minoritarian Hoxb8+ population was suggested to enter the brain at embryonic day 12.5 (E12.5) from a hematopoietic source within the embryo (De et al., 2018).

During the early embryonic period and the first two postnatal weeks microglia proliferate rapidly (Nikodemova et al., 2015). Microglial cell numbers start to decline in the third postnatal week and are reduced by 50% in adulthood. In terms of morphology, during the first stages of development, microglial cells have ameboid-like morphologies, with a large soma and no processes (Arnoux et al., 2013). The morphological change from “amoeboid” to “ramified” starts around P10, with the loss of transcription factor Runx, and the ramification process is complete by P28 (Nayak et al., 2014; Zusso et al., 2012).

Under physiological conditions, microglial maintenance is not dependent on the peripheral hematopoietic system (Ajami et al., 2007, 2011). The consensus is that microglia are maintained by self-renewal in steady state, and the initial proliferation rate was found to be very low (0.05%) (Lawson et al., 1992). Questioning this study and the established paradigm that microglial population is long-lived and almost never renewed, a recent study proposed approximately 10 times higher proliferation rate for microglia in mice (Askew et al., 2017).

This study showed that microglial turnover depended on temporal and spatial coupling of microglial proliferation and death, and that proliferation in steady conditions did not depend on local nestin-positive progenitors as it has been shown after transgenic microglial depletion (Bruttger et al., 2015). Furthermore, microglia proliferation rate differed between brain regions and corresponded to the overall proliferation rate in their local environment (Arnoux et al., 2013; Swinnen et al., 2013).

2.3 Microglial cells are a many-splendored thing

Over the course of their development, microglia exhibit discrete transcriptional phases due to changes in their chromatin landscape (Matcovitch-Natan et al., 2016). These phases include early microglia (E10.5 to E14), pre-microglia (E14 to P9) and adult microglia (4 weeks and onward). Strikingly, microglial transcriptional signature reflects their function and parallels brain homeostasis requirements. For instance, early microglia specific genes were associated with defense response and multiple hematopoietic fates. At the pre-microglia stage, clusters enriched for genes related to migration, proliferation and cytokine secretion were common. Interestingly, the transcriptional signatures at early and pre-microglia stages were highly correlated, even though their respective environment was different.

Furthermore, the number of molecularly distinct subpopulations peaked at young ages (E14.5 and P5) and was later reduced (Hammond et al., 2019). Some genes were strongly upregulated in specific states, suggesting a definable transcriptional program for each state. For instance, a $Spp1^{+}$ microglial state, highly concentrated at the axon tracts of pre-myelinated brain, was found only at P4-P5, and was enriched with genes associated with immune cell activation, lysosomal activity and phagocytosis.

Adult microglia express canonical microglial genes associated with tissue maintenance and signaling (Matcovitch-Natan et al., 2016). Under homeostatic conditions, microglia have a specific transcriptome that contains genes that are expressed exclusively by microglia or at higher levels than other CNS or myeloid cell types. In fact, after recruitment and under the influence of the CNS environment, microglial gene expression profile diverges from other tissue-resident macrophages. With regards to CNS macrophages, including perivascular, meningeal and choroid plexus macrophages (Prinz and Priller, 2014, Figure 3), microglial transcriptional profile was found to be closely related in particular to perivascular macrophages (Goldmann et al., 2016; Prinz et al., 2017).

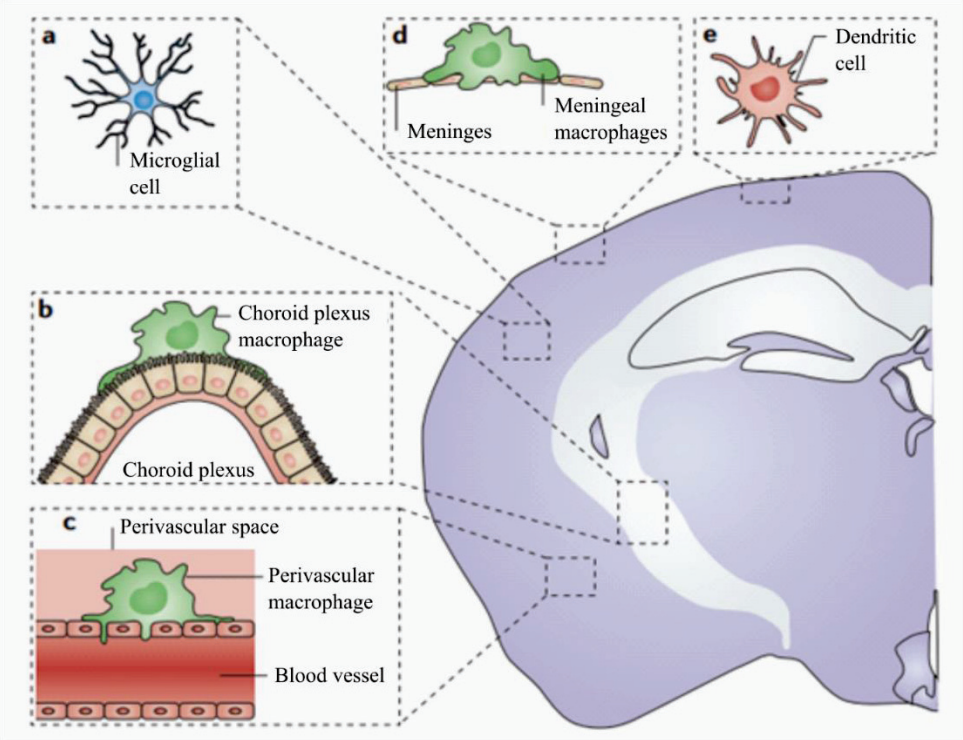

Figure 3: Myeloid cell types in the CNS. The CNS accommodates several populations of myeloid cells: microglial cells in the brain parenchyma (a); and macrophages at outer borders of the brain, including the choroid plexus (b), perivascular space (c) and the meninges (d). Finally, blood-derived dendritic cells (e) are found to a lesser extent at similar locations as macrophages (Prinz and Priller, 2014).

This transcriptome is referred to as homeostatic microglial signature genes and includes Sall1, Hexb, Fcrls, Gpr43, CX3CR1, Olfml3, Tmem119, Trem2, P2RY12, Mertk, Pros1 and SiglecH (Bennett et al., 2016; Buttgereit et al., 2016; Goldmann et al., 2016). These genes allow the maintenance of microglial identity and their homeostatic phenotype. Even though canonical microglial genes (P2RY12, CX3CR1, Trem2, C1qa, Fcrls) were highly expressed in most microglial cells, systematic expression was found only for C1qa, Fcrls and Trem2 (Hammond et al., 2019). Homeostatic microglial transcriptome is crucially regulated by Tgfβ, since its removal is accompanied with a reduction of microglial numbers and microglial homeostatic gene expression (Butovsky et al., 2014).

Genome-wide analysis shows that microglial cells exhibit age- and region-specific transcriptional profiles (Grabert et al., 2016). Even in a single anatomical structure such as the basal ganglia, microglia in different nuclei exhibited different transcriptomes, membrane properties and lysosome content (De Biase et al., 2017). Interestingly, these differences re-emerged in repopulated microglia after microglial ablation, suggesting that local specific cues shape microglial diversity incessantly.

Interestingly, adult microglia also presented sexually dimorphic transcriptomic signatures (Thion et al., 2018). Microglia were in a more immune-activated state in females, with a higher expression level of inflammatory response genes, including TNF, CXCL10, CCl2. Microglial baseline morphology in males was found to be more complex and significantly reduced upon LPS stimulation (Hanamsagar et al., 2017). On the contrary, LPS stimulation did not affect microglia in females. Furthermore, environmental challenges such as the absence of maternal microglia had sexually dimorphic impact on microglial transcriptome that also depended on the developmental stage (Thion et al., 2018).

2.4 Microglial functions in pathology

The traditional roles of microglial cells as immune-competent cells in the CNS have been extensively studied (Bachiller et al., 2018; Wolf et al., 2017). In addition to being the primary cells in the innate immune response, they also activate pathways leading to the initiation of adaptive immune responses, such as antigen presentation to T lymphocytes (Town et al., 2005).

2.4.1 M1/M2 polarization paradigm and its demise

Microglial cells may sense brain microenvironment disturbance via a plethora of pattern recognition receptors (PRRs), including Toll-like receptors (Kielian, 2006; Kigerl et al., 2014). Cell dysfunction, damage and foreign pathogens are detected by danger and pathogen-associated molecular patterns recognition (DAMPs and PAMPs, respectively). Under these conditions, microglial cells become "activated", with morphological changes and modifications of gene expression adapted to challenge the immune outbreak. Many neurological conditions, including acute injury, neurodevelopmental, neurodegenerative and neuropsychiatric diseases, are accompanied by microglial activation (Nayak et al., 2014; Peng et al., 2016; Ransohoff and Perry, 2009). The traditional view has been that microglia acquire customized phenotype upon activation, with polarization towards proinflammatory neurotoxic M1-state or anti-inflammatory neuroprotective M2-state depending on the circumstances (Franco and Fernández-Suárez, 2015; Kabba et al., 2018; Tang and Le, 2016, Figure 4). For instance, following stroke and trauma, microglia polarize towards M1-like state, characterized by increased production of proinflammatory cytokines (TNFα, IL1, IL6), reactive oxygen species (ROS) and inducible nitric oxide synthase (iNOS), as well as expression of high amounts of MHC class I or II. On the other hand, following mild ischemia, microglia polarize to M2-like

state and upregulate arginase-1, anti-inflammatory molecules (IL-10 and TGFβ), secrete growth factors (IGF-I, FGF, CSF1) as well as neurotrophic factors (NGF, BDNF, GDNF). This dichotomous model of microglial activation is overly simplified because a broad spectrum of microglia activation states were found to exist *in vivo* (Dubbelaar et al., 2018; Ransohoff, 2016; Vogel et al., 2013). These activation states have been shown to be highly complex in terms of immune cell phenotypes, encompassing changes in morphology, gene and protein expression (Hammond et al., 2019; Keren-Shaul et al., 2017; Mathys et al., 2017). For instance, it has been suggested that microglia may have neuroprotective functions in ischemia, while evidence for neurotoxic activity also exists (Tian et al., 2016; Wu et al., 2012).

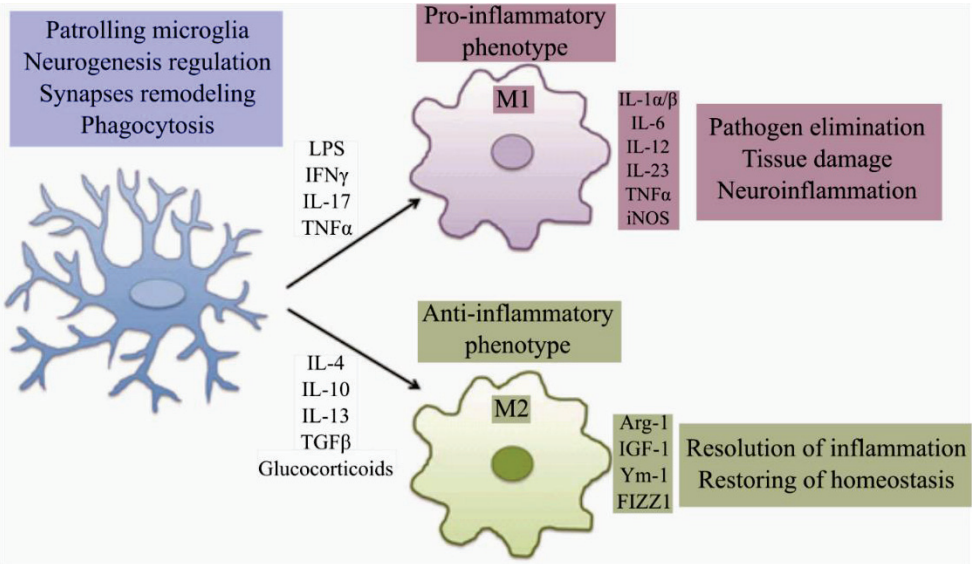

Figure 4: M1/M2 polarization of microglial cells. Classical (M1) and alternative (M2) activation lead to different functional states of microglial cells. Classical activation is induced by LPS and pro-inflammatory cytokines, leading to M1 polarization favoring neuroinflammation and oxidant state. In presence of Th2 type cytokines, microglia polarize to alternative M2 phenotype characterized by arginase, anti-inflammatory cytokine and neurotrophic factor production. This phenotype is associated with reparative and neuroprotective functions (Salvi et al., 2017).

2.4.2 Unexpected roles for microglial cells in pathology

Even though microglia have been mostly related to initiation of immune response after CNS injury and disease, microglial dysfunction may also be the cause for disease initiation. The recent discovery that many risk genes for Alzheimer's disease (AD) are exclusively expressed by microglia suggests that microglia might also be a driving mechanism in disease onset and progression (Bonham et al., 2019).

Microglial cells were thought to be restricted to the CNS even in the case of pathology or injury. However, a recent study in the zebrafish showed that microglial cells may squeeze through the spinal boundary in the case of brachial plexus injury model (BPNS) (Green et al., 2019). They may cross into the peripheral nervous system (PNS) and emerge as the main debris-cleaning cells at the point of injury. From the PNS, they return in the spinal cord in an altered state and may carry the debris back into the CNS, with possible long-term implications in CNS physiology.

In addition to their well-described roles as resident immune cells in the brain, microglial cells were found to serve many functions in physiological conditions.

3. Microglial functions in physiological conditions

3.1 Microglial functions during embryonic and post-natal development

Many roles have emerged for microglial cells during the embryonic and postnatal period. As mentioned previously, microglia start invading the brain very early during embryogenesis and are present when neuronal circuits start to assemble (Swinnen et al., 2013). During the embryonic period, microglial functions include: regulation of the axon tract formation, interneuron migration, phagocytosis of neural progenitors, as well as regulation of gliogenesis and angiogenesis (Thion and Garel, 2017, Figure 5). Indeed, embryonic depletion of microglia led to abnormal outgrowth of dopaminergic axons in the forebrain and laminar positioning of subsets of neocortical interneurons, as well as defasciculation of dorsal callosal axons (Pont-Lezica et al., 2014; Squarzoni et al., 2014).

During the postnatal period, microglial cells promoted proliferation of neuronal precursors and neuronal survival. At early stages, microglial cells were required for layer V neuronal survival through insulin-like growth factor 1 (IGF-1) and CX3CL1 signaling (Ueno et al., 2013); while IL-1β, IL6, TNFα and IFNγ were needed for cortical SVZ neuron survival (Shigemoto-Mogami et al., 2014).

Microglia also participated in programmed cell death (PCD), by phagocytosing dead or dying neurons and debris. *In vitro* studies found that microglial cells triggered PCD by at least two mechanisms: TNFα release inducing death of motor neurons (Sedel et al., 2004) and superoxide ion production leading to PCD of Purkinje neurons (Marín-Teva et al., 2004). In favor of this

role, microglia deficiency for DAP12 and CD11b resulted in decreased apoptosis in the hippocampus (Wakselman et al., 2008).

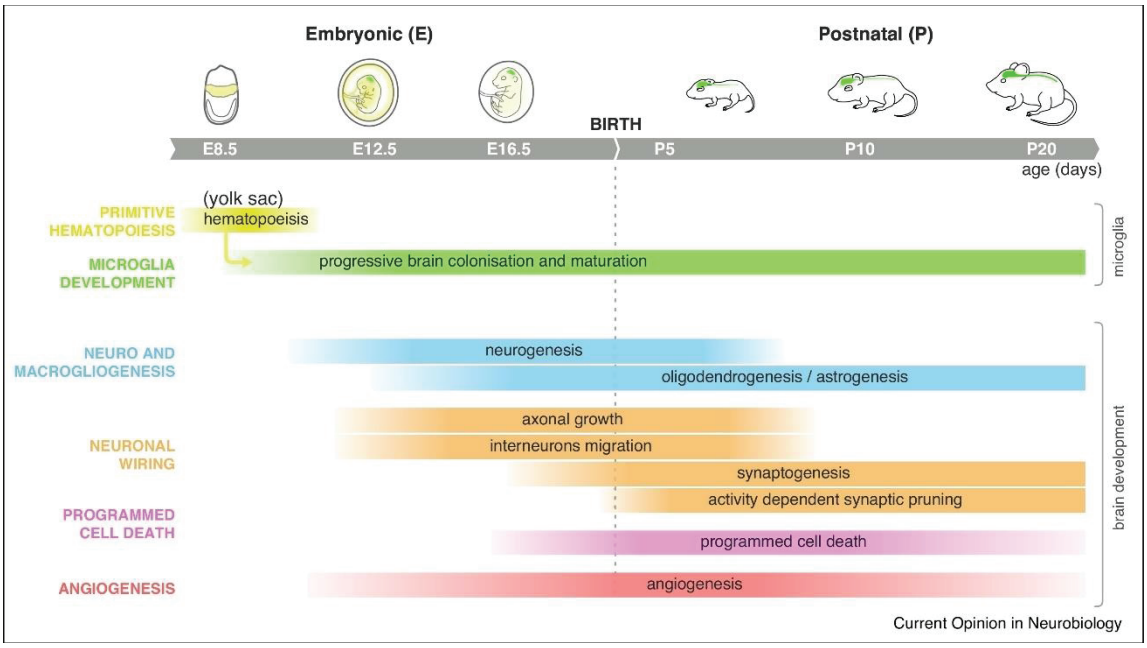

Figure 5: Timeline of microglial and brain development during embryonic and early postnatal period. Illustration of microglial generation and brain colonization (top panel) concurrent with major developmental events (bottom panel) with established and potential involvement of microglial cells (Thion and Garel, 2017).

In addition to participating in large-scale neuronal turnover, microglia contribute considerably to the proper establishment of neuronal circuits by mechanisms involving spine remodeling and functional maturation of synapses.

3.1.1 Synapse formation

Early postnatal period is characterized by a massive burst of synapse formation. Microglia were found to be involved in synapse formation in the developing somatosensory cortex during this period (Miyamoto et al., 2016, Figure 6B). From P8 to P10, microglia-dendrite contacts were often followed by filopodia formation which was initiated by Ca^{2+}-induced actin accumulation. Interestingly, this effect seemed restricted to this specific time frame since the rate of microglia-induced filopodia formation was not increased at P12-P14 and P26-P30. Importantly, filopodia formation was critically dependent on microglial activated phenotype since minocycline administration reduced filopodia formation rate.

Microglial role in synapse formation was also found in organotypic hippocampal slices (Weinhard et al., 2018). Microglial contact elicited transient filopodia formation, which was proposed to involve several mechanisms, including application of tension for pulling, loosening up of the extracellular matrix (ECM) or release of chemotactic factors. Intriguingly, the majority of filopodia originated from mature spine heads, suggesting a role in reorganization of postsynaptic sites.

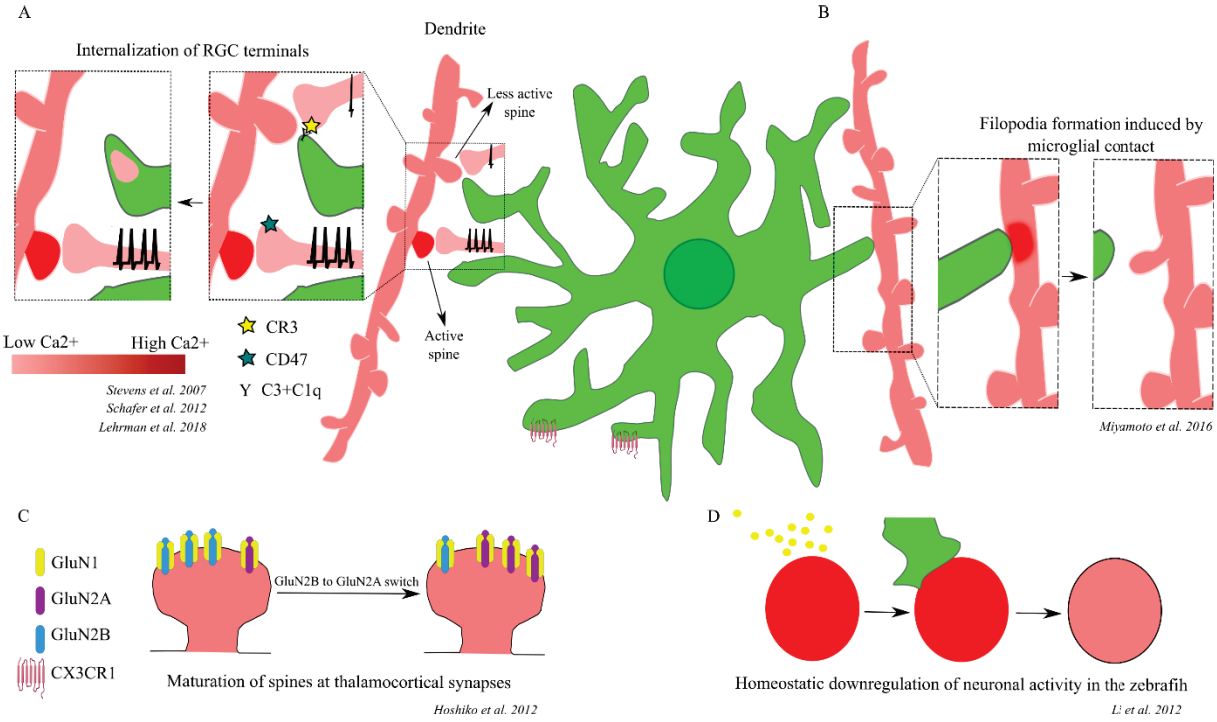

Figure 6: Synthesizing literature on neuron-related microglial functions during development. (A) "Weak" synapses are selectively pruned by microglia in a complement-dependent manner, while others are protected with the presence of "don't eat me" signals. (B) Microglial contact of aspiny dendrites induces Ca^{2+}-dependent actin accumulation and filopodia formation. (C) Microglial fractalkine signaling is necessary for NMDA receptor maturation at thalamocortical synapses. (D) Microglial contact with highly active neurons resulted in downregulation of neuronal activity in larval zebrafish.

3.1.2 Synapse elimination

The period of intense spinogenesis is accompanied by synaptic refinement, termed pruning, during which specific synapses are eliminated to obtain proper brain connectivity. Pruning was initially considered to occur by shedding excess material or to be solely dependent on neuronal mechanisms (Schuldiner and Yaron, 2015), but recent studies suggest that microglia are potent regulators of this mechanism.

3.1.2.1 The complement system and MHC-I molecules

First evidence of microglial involvement in synaptic pruning implicated the classical complement cascade in the mouse retinogeniculate system (Figure 6A). This system undergoes extensive activity-dependent pruning that is crucial for eye-specific segregation (Guido, 2008). Using *in vivo* engulfment essay, the authors showed an internalization of retinal ganglion cell (RGC) axonal terminals within microglial cytoplasm and lysosomal compartments during the period of highest synaptic remodeling (P5-P8) (Stevens et al., 2007). In the developing LGN (lateral geniculate nucleus), synapse elimination was dependent on the expression of complement cascade components C1q and C3 at immature synapses (Stevens et al., 2007). C1q and C3-tagged synapses were recognized and eliminated by microglia via the complement receptor (CR3). Several mechanisms regulating microglia and complement-mediated pruning have been described even though molecular actors for synaptic tagging are still unknown. Engulfment of RGC inputs was found to be performed in an activity-dependent manner, where weaker inputs were selectively pruned (Schafer et al., 2012). C1q expression and localization to synapses was dependent on astrocyte-derived transforming growth factor (TGF)-β and inhibition of TGF-β signaling in postnatal retina led to significant impairment in eye-specific segregation (Bialas and Stevens, 2013). Contrary to "eat-me" signals, synapses may also express "don't eat me" signals that protect them from microglia-mediated pruning. In the dorsal lateral geniculate nucleus, CD47 was localized to more active inputs and its deficiency increased functional pruning and reduced synapse density (Lehrman et al., 2018). Thus, the extent and timing of microglia-dependent pruning during development might be dependent on the joint action of neuronal activity and context-dependent molecular cues.

Another candidate from the immune system that might be involved in synaptic remodeling includes major histocompatibility complex (MHC) class I molecules. MHC-1 colocalizes with PSD-95, a major scaffolding protein in the excitatory postsynaptic density (Goddard et al., 2007) and is involved in segregation of retinal fibers in dLGN (Huh et al., 2000). Alterations in MHC-I expression levels at neuronal synapses were associated with alterations in synaptic elimination and eye-specific segregation (Lee et al., 2014). In the immune system, MHC-I is involved in tagging cells for phagocytosis, therefore, it is possible that the pruning is performed by the resident immune cells of the CNS.

3.1.2.2 Fractalkine signaling

Fractalkine signaling (CX3CR1/CX3CL1) is a specific microglia-neuron communication pathway with a debated role in synaptic pruning. Fractalkine (CX3CL1) is a chemokine almost exclusively expressed by neurons (Ransohoff, 2009; Tarozzo et al., 2003) and may exist in a membrane-bound and soluble form. Importantly, the fractalkine receptor (CX3CR1) is expressed only by microglia in the healthy brain (Cardona et al., 2006; Combadiere et al., 1998). CX3CR1-deficient mice presented a transient increase in dendritic spine density in pyramidal neurons and electrophysiological characteristics of immature circuitry (Paolicelli et al., 2011). However, CX3CR1 KO mice also showed reduced microglial density in the maturing hippocampus between P8 and P28. This was proposed to be the reason for the reduced synaptic pruning, even though a direct contribution of CX3CR1 should not be excluded. Paolicelli *et al*. also showed microglial engulfment of both pre- and postsynaptic material in the developing hippocampus. PSD95, marker of excitatory postsynaptic density, as well as presynaptic SNAP25, were observed both inside clathrin- and nonclatrin-coated vesicles within microglial processes (Paolicelli et al., 2011).

3.1.2.3 Hoxb8 signaling

Pruning may also be mediated, at least partly and probably indirectly, by Hoxb8 signaling. Genetic ablation of Hoxb8 was associated with increased spine density in the frontal cortex and several sub-regions of the striatum, suggestive of pruning deficits (Nagarajan et al., 2018). However, this was not due to synaptic pruning behavior of Hoxb8+ cells, since it was found to be similar to non-Hoxb8+ microglia (De et al., 2018).

3.1.2.4 Phagocytosis or trogocytosis?

The microglial mechanism of synaptic material elimination was presumed to be phagocytosis, defined as cellular uptake of particles over 0.5µm of size (Gordon, 2016). A very recent study using correlated light and EM microscopy coupled with *ex vivo* imaging did not find evidence for phagocytosis of whole synapses (Weinhard et al., 2018). Instead, in the developing hippocampus, microglial processes were engulfing smaller fragments of presynaptic components, with an average diameter of 250nm. This mechanism is known as trogocytosis. Trogocytosis was limited to presynaptic boutons and axons, and was CR3-independent. This mechanism was recently suggested to be mediated by phosphatidylserine (PS), another “eat-me

signal", and might be the underlying mechanism for microglial trogocytosis (Perry and Ravichandran, 2017).

3.1.2.5 Impact of microglial spatial arrangement on spine turnover

Interestingly, the spatial arrangement of microglia was found to be critical for spine stability in the somatosensory cortex in juvenile mice and to be a factor for neuronal circuit remodeling (Iida et al., 2019). The frequency of microglia-spine contacts as well as dendritic spine turnover was higher in the microglial proximal zone (7-20µm from microglia cell body). Microglial spatial arrangement defined alternating domains on dendritic segments with variable distances from microglia, indicating that spine turnover may not be uniformly regulated even in the same dendrites.

3.1.3 Synapse maturation

During development, deficiencies in several neuron-microglia communication pathways also result in synaptic maturation deficits.

3.1.3.1 KARAP/DAP12

KARAP/DAP12 is a transmembrane signaling protein, whose expression is restricted to hippocampal microglia during development (Roumier et al., 2004). Loss-of-function mutation of DAP12 led to enhanced long-term potentiation (LTP) and significant reduction in the synaptic accumulation of GluR1, GluR2 and the postsynaptic targeting of BNDF receptor TrkB (Roumier et al., 2004). These synapses were characterized with a higher ratio of AMPA/NMDA receptor EPSCs (Roumier et al., 2008), suggestive of an immature phenotype due to microglial deficiency.

3.1.3.2 Fractalkine signaling

Maturation deficits were also found in mice deficient for CX3CR1 signaling in the thalamocortical synapses and hippocampus. Between the first and second postnatal weeks, synaptic NMDAR content is known to switch from GluN2B to GluN2A at thalamocortical synapses. CX3CR1 deficiency resulted in altered NMDAR composition, characterized with a higher proportion of GluN2B-containing NMDARs and consequently slower kinetics of

NMDAR-mediated synaptic current (Hoshiko et al., 2012, Figure 6C). These deficits were not found at later times (P27-P32).

As neuronal circuits mature, the ratio between spontaneous and miniature excitatory postsynaptic currents increases (sEPSC and mESPC, respectively) (Hsia et al., 1998). At P15 and P40, the sEPSC/mESPC ratio was reduced in CX3CR1 KO hippocampal slices. The density of multi-synaptic boutons was significantly reduced at P40, as well as the coherence between the hippocampus and prefrontal cortex in adult mice, suggesting a deficit in maturation of synaptic connectivity (Paolicelli et al., 2011; Zhan et al., 2014).

CX3CR1 deficiency also affected glutamatergic presynaptic properties, resulting in synaptic release deficits and higher number of silent synapses in the developing hippocampus (Basilico et al., 2019). These deficits led to immature AMPA/NMDA ratio and defective hippocampal functional connectivity that persisted at later developmental stages.

3.1.3.3 Inhibitory synapses

Apart from excitatory synapses, a possible functional relationship between microglia and inhibitory synapses has been suggested. In fact, the frequency of miniature inhibitory post-synaptic currents (mIPSC) in the hippocampus at P15 was reduced in CX3CR1 KO mice (Zhan et al., 2014).

3.1.4 Baseline and experience-dependent plasticity

In addition to targeting specific microglial pathways, another approach to study microglial function consists in depleting microglial cells. Microglial depletion at P19 and P30 caused a significant reduction in baseline and motor learning-induced spine formation and elimination, associated with learning deficits (Parkhurst et al., 2013). This was associated with significant changes in protein levels at glutamatergic synapses. Altered protein levels concerned those mostly involved in synaptic plasticity and function, such as post-synaptic GluN2B and presynaptic vesicular glutamate transporter 1 (VGLUT1). Whole-cell patch clamp recordings revealed a significant reduction in the frequency of NMDA and AMPA mEPSC in microglia-depleted mice. In addition, the decay time of NMDA was reduced, consistent with a GluN2B containing receptor decrease. These alterations were replicated with specific removal of BNDF in microglia, suggesting a crucial role of microglial BDNF during development.

Another pathway for activity-dependent remodeling of neuronal networks by microglial cells seems to be P2Y12R (Sipe et al., 2016). Alteration of P2Y12R signaling led to disruption of the shift of ocular dominance from the closed eye to the open eye following monocular deprivation. Thus, it is posited that microglial P2Y12R expression is crucial for proper development of the visual cortex and ocular dominance. Contrary to P2Y12R, CX3CR1 signaling was not required for plasticity in the developing visual system, since CX3CR1 KO mice did not present any deficits in lateral geniculate nucleus refinement or ocular dominance plasticity (Lowery et al., 2017).

3.1.5 Modulation of neuronal activity

During development, microglia may also play a role in the homeostatic downregulation of neuronal activity. In a recently developed model of supramaximal stimulation, increased neuronal activity elicited axon swelling and large, sustained depolarization of soma membrane potential (Kato et al., 2016a). Microglial processes migrated towards and wrapped the affected axons, and in some case removed axonal debris which induced rapid soma membrane repolarization back to resting potentials. Thus, neuronal hyperactivity was accompanied with an acute and highly localized neuroprotective action by microglial cells. In larval zebrafish, microglia-neuron contact downregulated both spontaneous and visually-evoked activity of contacted highly active neurons (Li et al., 2012, Figure 6D).

In conclusion, during development, a period of rich synaptic remodeling, microglia are critically involved in neural circuit sculpting and maintenance of neuronal homeostasis and proper synaptic function. This raised intriguing questions about whether these functions are specific to microglia during development or they may also be major contributors to normal physiology in adulthood.

3.2 Microglial physiology in the adult brain

In the healthy adult brain, microglial cells have a small soma (~10µm) and highly ramified primary, secondary and tertiary processes. Primary branches protrude directly from the soma, whereas secondary and tertiary processes emerge from primary and secondary processes, respectively. At the tip of large processes, microglial cells have thin, hair-like processes called filopodia that were described very recently (Bernier et al., 2019). The distribution of microglial cells appears to be uniform across brain regions. Intriguingly, it could not be explained by

random distribution (Iida et al., 2019), suggestive of a potential regulatory mechanism for microglial-specific distribution pattern that needs to be assessed. Nevertheless, each microglial cell occupies a non-overlapping territory with distances of 50-60µm between cell bodies.

Microglial cell bodies were assumed to be stable and immobile in physiological conditions, contrary to the dynamic nature of their processes discussed in the next section. However, a recent study reported 5.8% of translocating microglia daily, suggestive of microglia migratory capacities in the healthy brain (Eyo et al., 2018a). These capacities differed between brain areas: microglia in the cerebellum exhibited higher migration rate compared to the visual cortex (Stowell et al., 2018). Regional differences were even observed within the same region, with a higher percentage of rearrangement in the limb/trunk region compared to the barrel cortex in the somatosensory cortex (Eyo et al., 2018a).

In vivo imaging of microglia dramatically changed our view of these "resting" immune cells. Several tools were pivotal for their unprecedented observation in physiological conditions: 1) technological advances in two-photon microscopy, 2) the development of CX3CR1-GFP/Iba1-GFP transgenic mouse line for specific labeling of microglia in the healthy brain (Hirasawa et al., 2005; Jung et al., 2000), and 3) the use of minimally invasive thin-skull cortical window preparation allowing imaging up to ~250µm below the cortical surface (Jung et al., 2000; Shih et al., 2012). Benefiting from these advances, two pioneering studies revealed that microglial processes show continuous extensions and retractions in the healthy brain (Davalos et al., 2005; Nimmerjahn et al., 2005, Figure 7A). This remarkable dynamics is termed microglial motility and relies on actin polymerization and depolymerization (Hines et al., 2009). Primary processes were found to be less dynamic compared to higher-order processes that displayed an average velocity of 1.47µm/min, and may even reach >4µm/min (Davalos et al., 2005; Nimmerjahn et al., 2005). Thus, microglial cells were posited to monitor the surrounding brain parenchyma in a few hours (Davalos et al., 2005; Nimmerjahn et al., 2005).

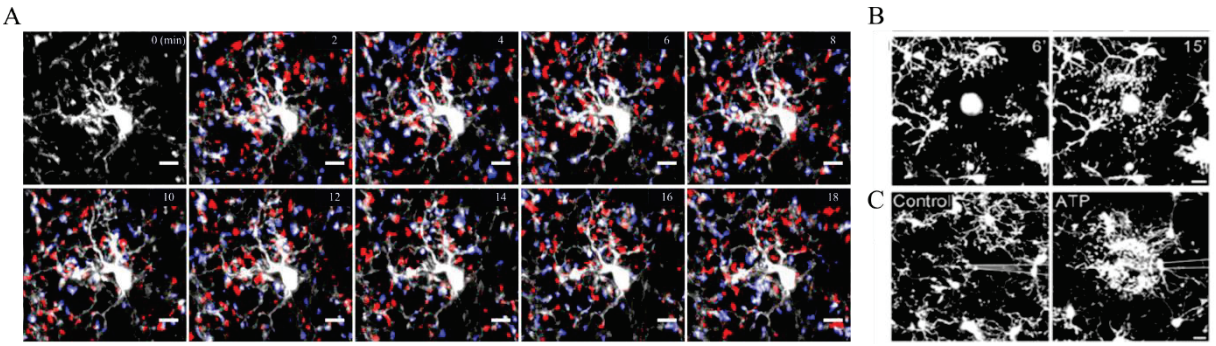

Figure 7: Cortical two-photon imaging of microglial cells. (A) Resting microglia are highly ramified and motile in the mouse cerebral cortex. Microglia are labeled by enhanced green fluorescent protein (eGFP) expressed under the control of microglial promoter CX3CR1. Microglial motility is shown by means of representative color-coded time-lapse images of a single microglial cell showing rapid process extensions (in blue) and retractions (in red) with a 2-minute interval over the time course of 18 minutes (Hristovska and Pascual, 2016) (B) Time-lapse microglial imaging after localized laser injury (center). Neighboring microglial processes extend towards the ablation site within minutes. (C) Microglial processes are attracted towards microelectrode containing ATP, but not towards artificial cerebrospinal fluid (ACSF) containing microelectrode, suggesting chemoattractant effect of ATP. Scale bar=10µm. (Davalos et al., 2005)

Microglial dynamics was first proposed as a mechanism for continuous surveillance of the brain microenvironment. That way, microglial cells would be able to detect cell damage and preserve brain homeostasis. Indeed, focal lesions induced by two-photon laser (Avignone et al., 2015; Davalos et al., 2005; Haynes et al., 2006) in the mouse cortex resulted in a rapid extension (reported velocity ~4.5µm/min of microglial processes (Avignone et al., 2015) towards the lesion site (Figure 7B)). These processes presented bulbous termini and the injured site was quickly isolated from the rest of the parenchyma (Davalos et al., 2005).

Besides the anticipated response in case of injury, the remarkable motility of microglial processes in the uninjured brain has drawn a lot of interest concerning its regulation and biological significance.

3.2.1 Regulation of microglial morphodynamics

3.2.1.1 THIK-1 channels

Microglial surveillance and ramification were recently found to depend on microglial resting potential. In rat brain slices, microglia exhibit a membrane potential of -40mV, which is depolarized compared to neurons and other glial cells (Madry et al., 2018a). This resting potential is maintained in part by the tonic activity of two-pore domain halothane-inhibited K+ channel type 1 (THIK-1). Indeed, genetic deletion or pharmacological blockade of THIK-1, or raising $[K+]_e$, lead to microglial depolarization and subsequent reduction in microglial ramification and surveillance (Madry et al., 2018a). In the same vein, highly ramified cells are characterized with hyperpolarized resting potential compared to less ramified cells, and possibly express more THIK-1 receptors (De Biase et al., 2017).

3.2.1.2 ATP and metabolites

Until recently, it was well-accepted that extracellular nucleotide levels drove a tonically active signaling mechanism regulating microglial ramification and motility, using ATP as key regulator. ATP is released in an activity-dependent manner by neurons and astrocytes, via hemichannels, secretory vesicles and transporters (Burnstock, 2008). Upon release, it may act on specific ionotropic (P2X) and metabotropic (P2Y) purinergic receptors expressed on neurons and glia (Puchałowicz et al., 2014). In the extracellular space, ATP may also be quickly metabolized to other purine molecules by ectonucleotidases, creating a gradient of ATP metabolites (Dunwiddie et al., 1997).

Several studies have shown that ATP and its metabolites may regulate baseline microglial morphology and dynamics. Application of ATP increased basal microglial motility and complexity in retinal explants (Fontainhas et al., 2011), whereas antagonizing P2Y receptors using Reactive blue 2 (RB2) significantly reduced microglial motility (Dou et al., 2012; Wu et al., 2007). Manipulation of extracellular nucleotide levels by applying exogenous apyrase or knocking out endogenous ecto-ATPase NTPDase1/CD39 reduced baseline motility and ramifications (Braun et al., 2000; Davalos et al., 2005; Eyo and Dailey, 2012; Kurpius et al., 2007; Matyash et al., 2017). However, a recent study showed that commercial apyrase was contaminated by K^+ which caused microglial depolarization and subsequent reduction of ramification and motility (Madry et al., 2018b). The same study found that blocking ecto-ATPases did not affect microglial ramification and surveillance, nor did it evoke P2Y12R-evoked electrical response (Madry et al., 2018b). They argued that NTPDase1/CD39 KO mice may exhibit microglial deramification due to functions beyond its enzymatic activity or NTPDase1-mediated effects from other cells (Lanser et al., 2017; Wu et al., 2006). Considering these findings, the effect of ATP on baseline motility and morphology is highly plausible but may be less dependent on ATP degradation than previously thought.

3.2.1.3 Purinergic receptors

P2Y12R is an ATP/ADP receptor, specifically expressed by microglial cells in the brain (Sasaki et al., 2003). In acute hippocampal slices or *in vivo*, microglial motility was not altered in P2Y12R-deficient mice (Eyo et al., 2014; Sipe et al., 2016). On the other hand, microglial cells exhibited a reduced baseline morphology in the visual cortex (Sipe et al., 2016). This was not the case in hippocampal slices, where blocking P2Y12R did not affect membrane potential,

ramification or surveillance (Madry et al., 2018a). Thus, it is possible that P2Y12R regulation is region-specific or that the type of preparation may affect this mechanism.

P2Y13R is the second most expressed NT receptor in microglial cells at the mRNA level (Zhang et al., 2014b). Even though its expression could not be detected at the protein level (Kyrargyri et al., 2019), P2Y13R invalidation led to reduction of microglial process length (Kyrargyri et al., 2019; Stefani et al., 2018), and consequently, reduction of microglial surveillance (Kyrargyri et al., 2019). The reduction of microglial morphology could not be ascribed to changes in microglial membrane potential, but possibly to different functional state of microglial cells since Il-1β protein levels were significantly increased. All things considered, baseline motility seems to be independent from P2Y12R and P2Y13R signaling, but both purinergic receptors seem to regulate baseline microglial morphology.

3.2.1.4 Fractalkine signaling

Fractalkine signaling manipulation has yielded inconsistent results in terms of its involvement in baseline microglial morphology and motility. In adult mice, cell and arborization area were increased in the CA1 in CX3CR1-deficienct mice (Milior et al., 2016), whereas a subsequent study found that microglial morphology was not affected by CX3CR1 deficiency (Hellwig et al., 2016). Furthermore, fractalkine signaling did not seem to be involved in microglial morphology and motility regulation in the visual cortex in adolescent and young adult mice (Lowery et al., 2017).

3.2.2 Microglial interaction with synapses

3.2.2.1 Baseline and activity-modulated microglia-spine interaction

Physical interactions between microglial processes and synapses in physiological conditions were first reported in 2009 by Wake *et al.* in the adult mouse visual cortex (Wake et al., 2009). Two-photon *in vivo* imaging of fluorescent-labeled microglia and neurons showed that microglial processes contacted axon terminals and dendritic spines transiently (~5 minutes) but frequently, at a rate of about one microglial contact per hour. To investigate the impact of synaptic activity on microglial contacts, basal neuronal activity was reduced by binocular eye enucleation, injection of TTX and reduction of neuronal temperature. Reducing neuronal activity resulted in significant reduction of the contact frequency between microglial processes

and synapses, which shortened to a rate of 0.5 per hour. However, following transient ischemia, contacts were prolonged (~1h) and were occasionally followed with disappearance of the presynaptic bouton. Several fascinating findings emerged from this study and have been since confirmed: 1) microglial processes may respond to the functional status of synapses, 2) the frequency of microglia-spine contacts may be related to basal neuronal activity, and 3) microglial processes may participate in activity-dependent synaptic remodeling.

A subsequent study showed that at the ultrastructural level, 94% of microglial processes in the juvenile mouse visual cortex directly contacted synapse-associated elements at any given time point (Tremblay et al., 2010). Even though most contacts appeared to be without any morphological evidence of specialization, 3D reconstructions revealed finger-like protrusions from distal microglial processes that enveloped dendritic spines contacted by an axon terminal. Furthermore, clathrin-coated pits were occasionally observed at interfaces between microglia and synapse-associated elements, suggesting molecular communication between them.

During normal visual experience, microglial processes were preferentially in contact with small dendritic spines (Tremblay et al., 2010). This specificity was not found in the somatosensory cortex, suggesting that spine-microglia interactions are not uniform between brain areas (Iida et al., 2019). The contact duration in the visual cortex was highly variable (5-50 minutes) (Tremblay et al., 2010). Interestingly, spines expanded transiently during interactions with microglial processes; however, over the course of two days, they disappeared more often than non-contacted spines. These findings further confirmed that microglial sampling does not seem to occur randomly. Indeed, microglial processes seemed to target a subset of synapses that were rather transient and displayed structural synaptic changes. Microglial processes were surrounded by pockets of extracellular space and a minority of processes showed phagocytic specializations and cellular inclusions containing material that was possibly synapse-associated elements.

Sensory modulation such as light deprivation resulted in preferential localization of microglial processes at the vicinity of larger dendritic spines that persistently shrank (Tremblay et al., 2010). In this case, extracellular spaces were extended with increased occurrence of cellular inclusions. These effects were reversed following re-exposure to light, except for microglial phagocytosis. In conclusion, as suggested by Wake *et al.*, microglial interaction with synapses and regulation of structural changes may be performed in an experience-dependent manner.

A subsequent electron microscopy immunogold study reported that only 3.5% of synapses were contacted by microglial processes in the rat frontal cortex (Sogn et al., 2013). The authors suggested that this percentage might be a slight underestimation of the true frequency because the majority of microglial processes are labelled with the Iba1 antibody, but not all of them. In line with Tremblay *et al*., they observed electron-lucent pockets around microglial cell bodies and processes, possibly representing extracellular space with matrix proteins, as well as vesicle like-structures inside microglial cells.

In acute hippocampal slices, only 1.5% of dendritic spines were found to be in contact with a microglial process (~1.5 min) at any given time, reaching on average 12% after 80 minutes time-lapse imaging (Pfeiffer et al., 2016). High frequency LTP-inducing stimulation resulted in decreased number of microglia-spine contacts which lasted longer, showing activity-dependent microglial-spine contact and suggestive of possible microglial involvement in spine remodeling. Microglial morphological dynamics and interaction with spines were NMDAR-dependent, as suggested by previously described studies in the hippocampus and cortex.

Microglial contact with dendritic spines was also found to be directly related to spine activity (Akiyoshi et al., 2018). In the motor cortex of non-anesthetized mice, contacted spines had significantly higher basal rates of Ca^{2+} transients compared to non-contacted spines. Interestingly, the frequency of Ca^{2+} transients in parent dendrites was not different between contacted and non-contacted spines, suggesting that a very localized change of neuronal activity may influence microglial processes.

3.2.2.2 Fractalkine signaling

CX3CR1 pathway contribution to baseline microglial behavior was recently assessed (Lowery et al., 2017). In CX3CR1 KO mice, baseline microglia-spine contact dynamics and spine turnover were unaffected. However, the number of contacts with axon terminals was reduced and was accompanied with increase in the perimeter of contact with perisynaptic astrocytic processes. Furthermore, a significant increase in the number of cellular inclusions within microglial processes was observed in CX3CR1 deficient mice. Thus, CX3CR1 signaling had a limited effect on microglia-synapse interactions and synaptic dynamics.

3.2.3 Modulation of microglial motility and morphology by neuronal activity

The discovery that microglial processes transiently contacted synapses raised the intriguing possibility that neuronal activity may guide microglial motility (Tremblay et al., 2010; Wake et al., 2009). To assess this hypothesis, neuronal activity was modulated by genetic, pharmacological and sensory means, and microglial motility was assessed in these conditions. Initial findings have rather negative. Reducing neuronal activity by surface TTX (tetradotoxin, Na^+ channel blocker) application did not impact baseline microglial motility (Nimmerjahn et al., 2005), nor did high frequency stimulation (HFS) in acute hippocampal slices (Wu and Zhuo, 2008). Reducing basal neuronal activity in the visual cortex by TTX injection or body temperature reduction did not decrease microglial motility (Wake et al., 2009), and only binocular eye nucleation resulted in retraction of microglial processes. However, several studies described hereafter have suggested an impact of neurotransmission modulation on microglial morphodynamics.

3.2.3.1 Glutamate and GABA

Modulation of glutamatergic and GABAergic neurotransmission resulted in altered microglial dynamics and morphology in retinal explants. Application of GABA receptor blocker bicuculline on cortical surface significantly increased microglial volume sampling and dynamism (Fontainhas et al., 2011; Nimmerjahn et al., 2005). Along the same line, GABA bath application induced significant but smaller decrease in microglial morphology and process velocity (Fontainhas et al., 2011). In the same model, ionotropic glutamatergic transmission positively regulated microglial morphology and motility through AMPA and kainate receptors, and to a smaller extent through NMDA receptors (Fontainhas et al., 2011, Figure 8A). However, glutamate application, which serves as agonist in both ionotropic and metabotropic glutamate receptors, did not affect microglial morphology nor motility in retinal explants (Fontainhas et al., 2011).

The effect of glutamate application on microglial cells in hippocampal and cortical slices was a different matter. Although baseline motility and morphology were not assessed, bath application of glutamate resulted in significant microglial process extension towards neuronal elements in acute hippocampal slices, and to a lesser degree in cortical slices (Eyo et al., 2014, Figure 8B). These findings were also corroborated *in vivo*. Glutamate and NMDA-induced microglial process extension was dependent on ATP release secondary to NMDAR activation,

and relied on microglial P2Y12 receptors that accumulated at the bulbous tips during outgrowth (Dissing-Olesen et al., 2014; Eyo et al., 2014). Even activation of dendritic NMDAR events on single neurons was sufficient to trigger process outgrowth, proposing a direct link between microglial process motility and neuronal activity (Dissing-Olesen et al., 2014). These interactions were found to be regulated by neuronal NMDAR GluN2A subunit, possibly conferring different regional sensitivities to microglial process extension depending on GluN2A localization (Eyo et al., 2018b). Thus, tissue-specific regulation of microglia-neuron communication is highly conceivable on several levels and may be linked to local architecture and activity of neuronal circuits.

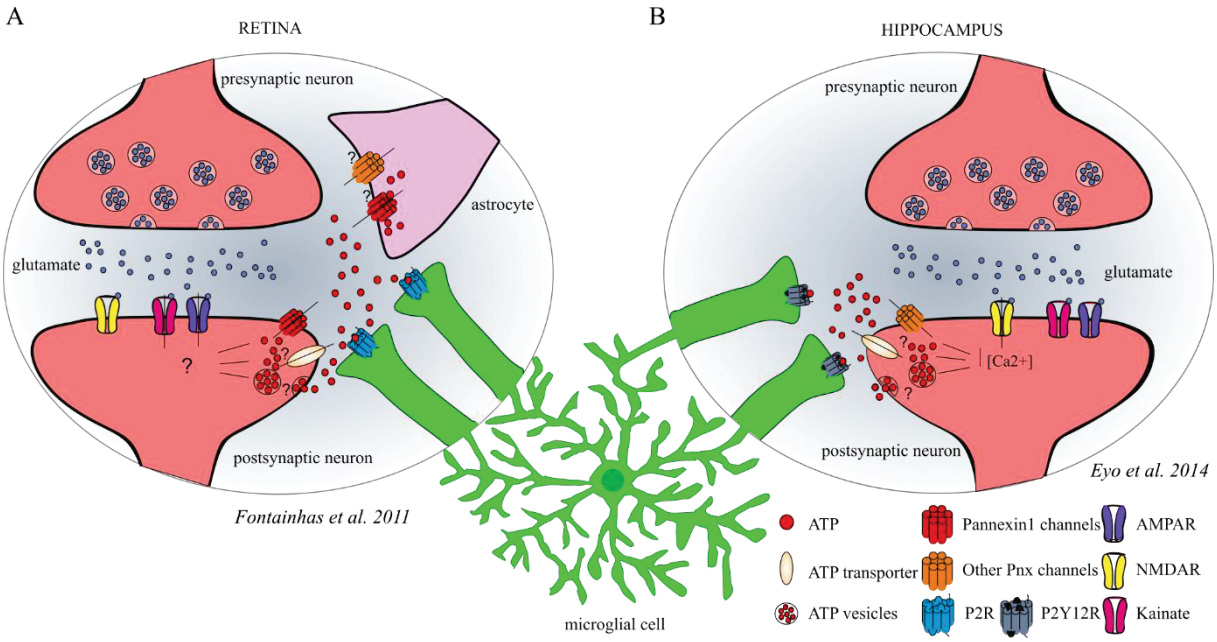

Figure 8: Schematic representation of glutamatergic neurotransmission-induced microglial process outgrowth in the retina and hippocampus. (A) In the retina, AMPAR/kainate activation leads to ATP release through pannexin-1 and possibly other mechanisms from neurons and astrocytes, ultimately leading to microglial response through P2 receptors. (B) In the hippocampus, glutamate-induced microglial process outgrowth is dependent on NMDA receptor. NMDAR activation leads to significant Ca^{2+} influx that is required for ATP release through currently unknown mechanisms but independent of pannexin-1 and astrocyte hemichannels. ATP diffuses in the extracellular space and activates microglial purinergic receptor P2Y12, eliciting microglial process extension. Adapted from (Hristovska and Pascual, 2016)

In the zebrafish optic tectum, local and global elevation of neuronal activity did not change the overall microglial cell area, process tip number and deformation speed, but affected the number of bulbous endings, suggestive of microglia-neuron interactions (Li et al., 2012). Neuronal activity had an instructive role in the oriented movement of microglial processes with underlying mechanisms resembling those described in mammals. Glutamate uncaging caused

ATP-induced outgrowth of microglial processes towards the source of glutamate. This attraction was mediated by the accumulation of P2Y12R at the tip of microglial processes, as well as Rho GTPase Rac, a key regulator of cytoskeleton reorganization. This led to bulbous endings formation, possibly underlying microglia-neuron interactions. Thus, even though the impact of global neuronal activity on microglial dynamics is not straightforward, it is rather well-established that neuronal activity has an instructive role in microglia process extension and microglia-neuron contact via ATP and P2Y12R-dependent mechanisms.

3.2.3.2 *Neuromodulators and neurotransmitters*

An important matter is whether neurotransmission may signal directly to microglial cells, but this does not seem to be the prevailing mechanism. Even though microglia express a variety of NT receptors in cultured microglia, they lack electrical responses to local application of glutamatergic and GABAergic agonists (Eyo et al., 2014; Färber and Kettenmann, 2005; Fields and Burnstock, 2006; Fontainhas et al., 2011; Wu and Zhuo, 2008). On the contrary, it is well-established that extracellular nucleotides elicit strong microglial inward and outward membrane currents through ionotropic P2X and G protein-coupled P2Y receptors respectively (Arnoux et al., 2013; Avignone et al., 2008; Boucsein et al., 2003; Fontainhas et al., 2011; Ulmann et al., 2013; Wu et al., 2007).

Thus, it has been proposed that neurotransmission signals to microglial cells by modulating extracellular levels of nucleotides, such as ATP and metabolites. Even though we described extensively the regulation of microglial dynamics by ATP, the exact molecular mechanisms and cell types involved in ATP release remain to be determined (Dissing-Olesen et al., 2014; Eyo et al., 2014; Fontainhas et al., 2011; Li et al., 2012). Apart from ATP, adenosine is another potential candidate for regulating microglial motility. Microglial cells express high levels of adenosine A1 and A3 receptors and A3R was found to be necessary for microglial process extension *in vitro* (Hammarberg et al., 2003; Ohsawa et al., 2012).

Very few studies have assessed the effect of NTs other than glutamate and GABA on microglial morphodynamics. Bath application of norepinephrine in acute brain slices caused retraction of microglial processes and reduction of baseline surveillance (Gyoneva and Traynelis, 2013). This effect was mediated by β2 adrenergic receptor that is highly expressed in microglia (Gyoneva and Traynelis, 2013; O'Donnell et al., 2012; Zhang et al., 2014). Interestingly,

norepinephrine abolished microglial process extension caused by ATP (Gyoneva and Traynelis, 2013), raising an interesting possibility of norepinephrine regulation of purinergic signaling in microglia.

Contrary to norepinephrine, serotonin application led to chemotactic attraction of microglial processes, possibly through 5-HT2B receptors (Kolodziejczak et al., 2015; Krabbe et al., 2012). These effects may be region-dependent since acetylcholine, serotonin and norepinephrine did not have any effect on microglial motility in the spinal cord dorsal horn (Chen et al., 2010b).

Apart from neurotransmission, extracellular ion concentrations may also regulate microglial dynamics. In addition to K^+ regulation of baseline motility, reduction in extracellular Ca^{2+} induced microglial process convergence towards dendrites in mouse brain slices and *in vivo* (Eyo et al., 2015). Interestingly, this phenomenon was independent of neuronal action potential firing and was mediated by purinergic signaling through microglial P2Y12R.

To summarize, several mechanisms regulating microglial baseline microglial motility have been described, involving THIK-1 channels and ATP. Interestingly, the mechanism(s) by which ATP may regulate baseline motility may not be the same as those involved in microglial process extension towards sites of increased neuronal activity. Even though studies have yielded inconsistent results, changes in neuronal activity seem to affect microglial morphology and dynamics, as well as microglial interactions with neuronal elements, and this seems to be preparation-, age- and region-dependent. Glutamate and GABA, major excitatory and inhibitory NT, seem to signal indirectly to microglial cells via changes in extracellular nucleotide concentrations, whereas others such as NA and serotonin seem to present functional receptors at microglial surface. Future studies elucidating the impact of neuronal activity and microglia-neuron interactions should investigate these points in the most physiological models possible, without the use of anesthetics, and taking advantage of novel available tools for specific microglial cell manipulation.

3.2.4 Microglial functions in the adult brain

Compared to studies during development, much less research has been done to elucidate microglial function in the adult brain. The reason might be that this period is accompanied with relatively minor changes compared to large-scale turnover in the developing brain. Nevertheless, microglial cells have emerged as important regulators of synaptic and structural plasticity even in the adult brain.

3.2.4.1 Roles in innate responses, learning and memory

Genetic microglial depletion in adult mice caused a significant reduction in motor learning-dependent spine formation, accompanied with a lack of performance improvement after learning (Parkhurst et al., 2013). Deficits in other behavioral tasks were also observed: reduced fear response in auditory-cued fear conditioning and lack of preference for a new object in novel object recognition test. BDNF removal in microglial cells specifically recapitulated both the alterations in learning-induced spine remodeling and the behavioral deficits in all tests, except for novel object recognition (Figure 9B and 9C). This finding indicates that depending on the learning paradigm, different cellular and molecular microglial mechanisms might be involved. Microglial BDNF is thought to act on neuronal tyrosine kinase receptor (TrkB), since microglia-conditioned media was found to phosphorylate TrkB *in vitro* in cultures of purified neurons (Parkhurst et al., 2013). Moreover, TrkB signaling may modulate synaptic transmission and plasticity, including the induction of dendritic spine formation (Rex et al., 2007).

A subsequent study used another method for microglial depletion: administration of selective inhibitor of colony-stimulating factor 1 receptor (CSF1R) leading to decreased microglial survival (Elmore et al., 2014). Surprisingly, microglia-depleted adult mice did not present any behavioral and cognitive abnormalities nor changes in synaptic properties. The discrepancy in these results raises the intriguing possibility that the method of microglial elimination (genetic or pharmacological) might impact results and needs to be assessed.

Apart from BDNF, CX3CR1 pathway may be critically involved in microglial functions in adulthood. Alterations in several forms of learning and memory were reported in adult mice with CX3CR1 deficiency: 1) motor learning in the rotarod test, 2) associative learning in a fear conditioning paradigm, and 3) hippocampal-dependent learning in the water maze (Rogers et al., 2011, Figure 9C). These effects might be mediated by IL-1β release since intrahippocampal infusion of antagonist IL-1Ra significantly reversed cognitive deficits.

Other microglial signature receptors may also mediate physiological microglial functions in adulthood. In addition to microglial P2Y12R role in experience-depending plasticity in the developing visual cortex, this receptor was found to be important for innate fear behaviors in adult and developing mice (Peng et al., 2019). Microglia with conditional deletion of P2Y12R in adulthood showed enhanced innate fear responses (Figure 9C), surprisingly without affecting conditional or learned fear responses. These mice presented abnormal ventral hippocampus

CA1 neuronal excitability as action potential firing threshold was lower and sEPSC amplitude was significantly increased.

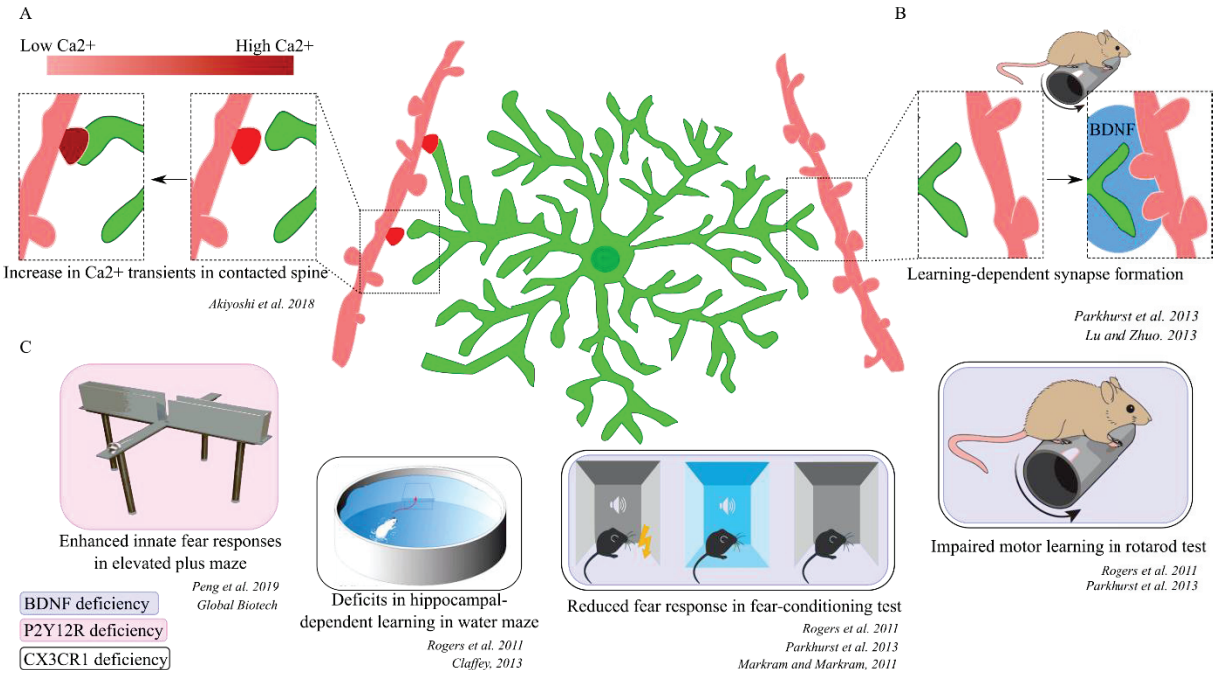

Figure 9: Synthesizing literature on microglial functions in the adult brain. (A) Microglial processes preferentially contact active spines and microglia-spine contact results in increased frequency of spine Ca^{2+} transients. (B) Microglial cells are involved in learning-dependent synapse formation through BDNF release. (C) Deficiencies in microglial signaling pathways significantly impact innate responses, as well as learning and memory.

3.2.4.2 Modulation of neuronal activity and "tag" setting

Microglia-spine contact had functional consequences at the level of synapses and neuronal circuits in adult mice (Akiyoshi et al., 2018). Microglial contact resulted in enhanced activity in the contacted spine and a corresponding increase in back-propagating action potential along the parent dendrite (Figure 9A). At the circuit level, microglial ablation resulted in reduced synchronous firing of L2/3 neurons, especially for those close to each other, which may result from reduced microglia-synapse contact modulation of neuronal activity. Moreover, reduced firing synchrony of spatially close L2/3 neurons was also decreased in case of microglial activation by LPS. Thus, the increase in synaptic activity caused by microglial contact may enhance neuronal population synchronization only in physiological conditions.

A very recent study put forward a role for microglia in synaptic tag setting during the early phase of activity-dependent plasticity in hippocampal slices (Raghuraman et al., 2019). Synaptic tag setting and its subsequent interactions with plasticity related proteins (PRP)

regulate late LTP induction and maintenance (Redondo and Morris, 2011). Hippocampal slices were treated with clodronate, which resulted in activation of microglial cells. Chlodronate treatment did not affect early LTP, but its administration before or 60 minutes after LTP induction prevented LTP maintenance. On the contrary, later activation of microglia (2h post-LTP) did not affect long lasting maintenance.

3.2.4.3 Regulation of neurogenesis

Microglia are also involved in the regulation of proliferation and differentiation of neuronal precursors in the adult neurogenic zones via TNFα, IGF-1, IL-1 and CX3CL1 (Sato, 2015). CX3CR1 deficiency resulted in a dramatic reduction of adult hippocampal neurogenesis due to upregulation of proinflammatory signaling (Bachstetter et al., 2011; Rogers et al., 2011). Microglia may also phagocytose apoptotic cells from the neurogenic niche, by recognizing phosphatidylserine expressed by apoptotic cells (Diaz-Aparicio and Sierra, 2019; Païdassi et al., 2008).

In conclusion, microglial deficiencies impact significantly learning and memory in adult mice, potentially in part by reduction of spine formation and failure to induce local network synchronization. Microglial functions during adulthood do not seem exclusive to learning, because they are also crucial for maintenance of synaptic properties and innate behavior.

II. Neurobiology of the vigilance states

The alternation of sleep and wake is a fundamental biological phenomenon conserved across the animal kingdom that has never ceased to fascinate mankind (Siegel, 2008). Ever since the first observation of distinct brain electrical wave patterns in awake and sleeping humans by Hans Berger in 1929, much research has been done to understand the expression, regulation and function of the vigilance states. Even though many of these aspects have been elucidated, some remain poorly understood. Pioneering research has been exploring new and exciting ventures leading to the discovery of local sleep-wake states, homeostatic regulation of sleep, and central to this thesis, glial involvement in sleep-wake regulation and function. In the following chapters, I will first provide evidence on the current understanding of sleep and wake neurobiology, to conclude with the recent discoveries implicating glial cells in its regulation and functions.

1. General description of the vigilance states, with focus on neuronal activity

Apart from different behavioral manifestations, a major characteristic of the vigilance states is the presence of different cortical brain activity, reflected in particular waveforms in electroencephalogram (EEG) recordings (Scammell et al., 2017, Figure 10). For vigilance states and sub-states identification, EEG recordings are often accompanied with muscle and ocular activity assessment using EMG (electromyogram) and EOG (electrooculogram) recordings, respectively. The wake state is characterized by prominent theta (high-frequency, low-amplitude) EEG activity, a variable amount of EMG activity and presence of ocular movements. Sleep can be divided in two main states: non-rapid eye movement (NREM), also called slow-wave sleep (SWS), and rapid-eve movement (REM), also known paradoxical sleep (PS). NREM sleep is distinguished by slow delta (low frequency, high amplitude) oscillations, low muscular activity and absence of ocular movements, whereas REM sleep shows predominant theta rhythm comparable to wake, absence of muscle tone and occurrence of rapid eye movements.

1.1 Description of the wake state

The characteristic waveforms during wake mirror mostly desynchronized activity associated with continuous irregular firing (5-9Hz). Wake can be further decomposed into sub-states that

differ in terms of cortical activity and synchronization, such as active (AW) and quiet (QW) wake. During active wake, including active exploratory behavior, theta activity is increased, whereas quiet wake contains large amplitude slow oscillations (Bennett et al., 2013; Crochet and Petersen, 2006; Polack et al., 2013; Poulet and Petersen, 2008)

1.2 Description of NREM sleep

NREM sleep is characterized by two major oscillatory events, slow wave activity (0.5-4Hz) and spindles (9-16Hz) (Dijk, 1995). Slow wave activity is considered a major hallmark of NREM sleep. During slow wave activity, local populations of cortical neurons display synchronous membrane potential oscillations, alternating between a depolarized state caused by active neuronal firing and synaptic activity (*up state*), and hyperpolarized state associated with absence of synaptic activity and spiking state (*down-state*) (Amzica and Steriade, 1998; Neske, 2015; Steriade et al., 1993, 2001). It is proposed that the up- and down-states result from a sustained balance between a positive feedback loop (recurrent excitation) with negative feedback control within neuronal networks (Haider et al., 2006; Sanchez-Vives and McCormick, 2000).

Up states seem to be initiated by a subset of layer 5 (L5) pyramidal neurons that fire low-frequency (0.2-2Hz) brief bursts of action potentials (Lőrincz et al., 2015). Slow-frequency rhythmic activity was also observed in reduced preparations such as cortical slices and is generated in the cortical network even without driving thalamic inputs (Steriade et al., 1993). Nevertheless, the removal of thalamic inputs *in vivo* reduced the occurrence of up-states in the slow oscillation, which was stabilized within two weeks (Lemieux et al., 2014).

Sleep spindles, another characteristic pattern of NREM sleep, are rhythmic discharges of neurons throughout the thalamocortical system in the frequency range of 9-16Hz with durations ranging from 0.5 to 3s (De Gennaro and Ferrara, 2003; Dijk, 1995; Vyazovskiy et al., 2004). Spindles generation is thought to occur from the rhythmic burst activity of thalamic reticular nucleus (TRN) during the up state of slow oscillations and is self-maintained by reciprocal interaction between cortical, thalamocortical and TRN neurons (von Krosigk et al., 1993; Steriade et al., 1993).

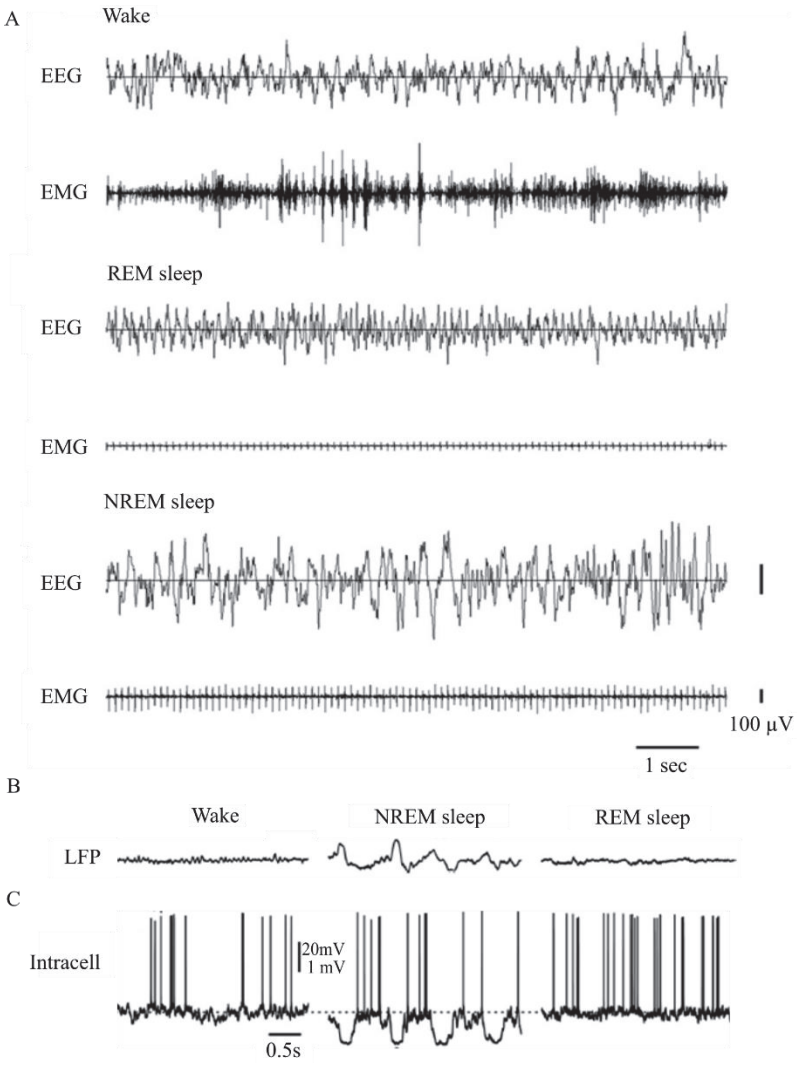

Figure 10: Electrophysiological recordings during the vigilance states. (A) Representative EEG/EMG, (B) local field potential (LFP) and (C) intracellular recordings during wake, NREM and REM sleep showing muscle tonus and different patterns of neuronal activity at the global and local level during the vigilance states. (Luo et al., 2013, unpublished data from Chauvette and Timofeev)

1.3 Description of REM sleep

REM sleep is a unique sleep state, since it is accompanied by the behavioral components of sleep while the forebrain EEG patterns resemble those during wake (Mizuseki and Miyawaki, 2017). Indeed, REM is characterized with a prominent theta rhythm and low-voltage desynchronized activity originating from the hippocampal formation (Buzsáki, 2002). Upon entering REM sleep, acetylcholine release increases to the level of waking while other wake-promoting NT levels are decreased (Hasselmo, 1999). From slow-oscillation fluctuations and burst firing during NREM sleep, thalamocortical neurons switch to tonic neuronal firing during

REM sleep with high arousal threshold (Hirsch et al., 1983; Mizuseki and Miyawaki, 2017). Compared to wake, theta oscillations are slower during REM sleep, except during phasic REM sleep, and the amplitude of CA1 gamma oscillations are significantly lower (Montgomery et al., 2008). Interestingly, theta and gamma synchrony between DG and CA3 are significantly higher during NREM than waking, which is not the case for gamma frequency coherence between CA3 and CA1. Thus, even though REM sleep activity may resemble waking activity, fundamental differences exist in terms of neuromodulation, activity pattern characteristics and network synchrony.

1.4 Electrophysiological and in vivo Ca^{2+} imaging assessment of activity during the vigilance states

The different patterns of neuronal activity underlying wake and sleep are well-established. However, whether overall neuronal activity is different between the vigilance states remains a matter of debate. To answer this question, electrophysiological and calcium imaging studies have assessed neuronal activity of both excitatory and inhibitory cortical populations.

In electrophysiological studies, excitatory and inhibitory neurons are distinguished indirectly by the difference in their discharge patterns: pyramidal cells are mostly regular-spiking, whereas interneurons are fast-spiking. During wake, pyramidal cells discharged in a single spiking mode which shifted to burst firing mode during NREM sleep (Steriade et al., 2001). Surprisingly, the average firing rate increased slightly, even though not significantly, during NREM and REM sleep compared to wake. Fast-spiking neurons exhibited tonic firing pattern during wake which turned to phasic during sleep, accompanied with a decrease in average spiking rate during NREM sleep compared to wake and REM sleep.

In view of the above-described findings, discordant evidence has been provided with two recent *in vivo* Ca^{2+} imaging studies combined with cell-specific labeling of neuronal circuits (Figure 11). Using two-photon imaging of GCaMP6f in superficial and deep layers in adult mice, Niethard *et al.*, reported that activity in pyramidal neurons was highest during wake, lower during SWS and lowest during REM sleep (Niethard et al., 2016). Two major classes of GABAergic neurons, parvalbumin (PV-INs) and somatostatin (SOM-INs) presented different profiles: SOM-INs displayed an activity pattern comparable to those of pyramidal cells, whereas PV-INs showed highest activity during wake and intermediate activity levels during

REM sleep. Seibt *et al.* corroborated some of these findings, in particular the reduction of cortical population activity in L5 during SWS and REM sleep (Seibt et al., 2017). Interestingly, contrary to Ca^{2+} transients in the soma, L5 dendritic shafts exhibited highest Ca^{2+} transients during spindle-rich oscillations, and lowest during wake. In L2/3 neurons, both population activity and dendrites showed an important decrease during quiet wake and all sleep stages compared to active wake, whereas dendrites showed an increase in activity both during individual NREM and REM sleep episodes.

The discrepancies between these studies may arise from several reasons. In electrophysiological studies, the recorded cells are classified indirectly based on their spike shape and more active neurons are likely to be selected for extracellular recordings, which may lead to an overestimation of the firing rates (Harris et al., 2016). On the other hand, calcium imaging is unlikely to faithfully reflect single spikes, especially with regards to high-frequency spike bursts (>100Hz), as found in pyramidal neurons during slow oscillations (Chen et al., 2013). Future use of genetically encoded voltage indicators (GEVI), capable of detecting subthreshold voltage changes of neuronal populations with subcellular resolution, might be able to clarify these discrepancies.

A recent study has assessed more precisely the interaction between neuronal populations during different NREM oscillatory events. Indeed, Niethard *et al.*, studied Ca^{2+} activity in excitatory and inhibitory populations when slow oscillations occurred independently or simultaneously with sleep spindles (Niethard et al., 2018). Interestingly, when spindles nested in the up state of the slow oscillation, these events were accompanied with three-fold higher pyramidal cell Ca^{2+} activity, which occurred in the presence of strong perisomatic inhibition through PV-INS, but not via SOM-Ins. In contrast, during solitary slow oscillations up state, pyramidal cells and SOM-Ins displayed significant increases in activity, without difference in PV-Ins activity. Thus, there seems to be an added complexity in the balance between the activity of excitatory and inhibitory neurons within circuits depending on whether slow oscillations and spindles events are solitary or concurrent.

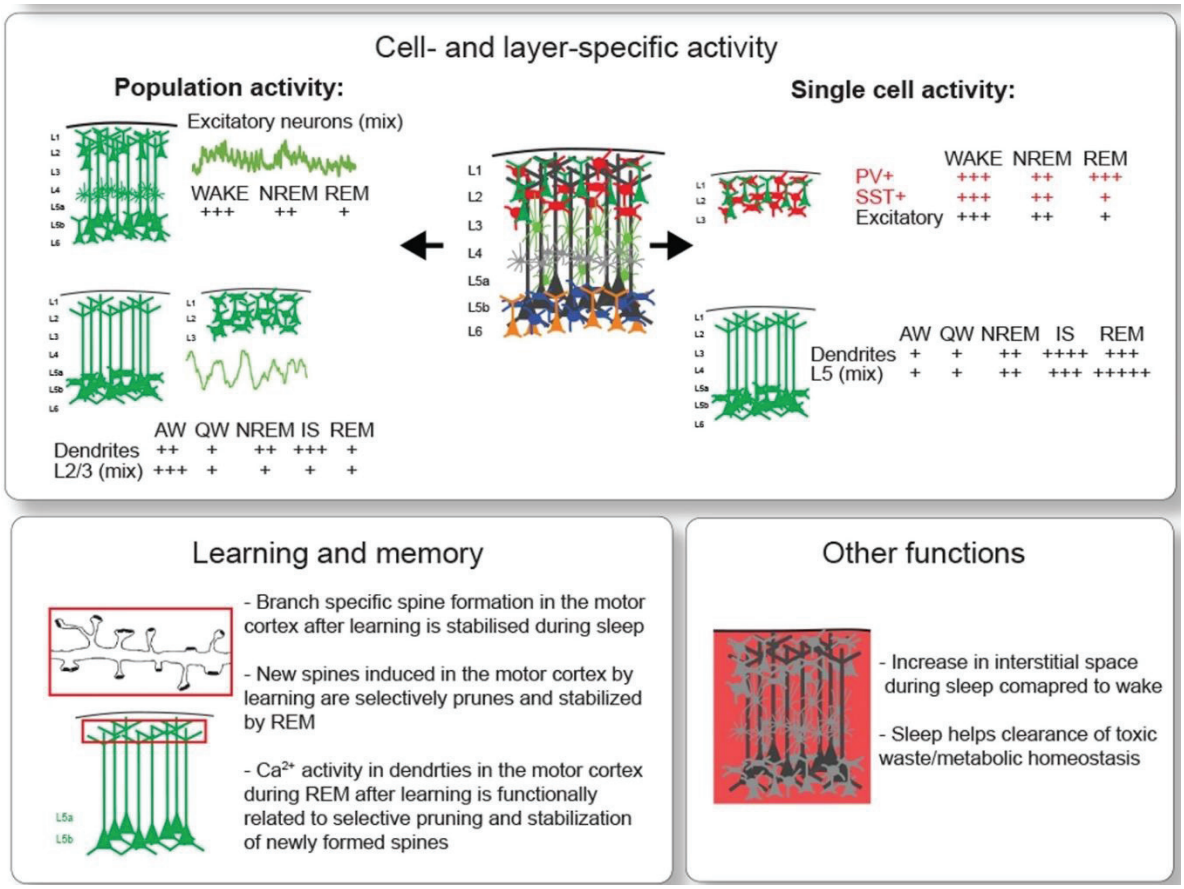

Figure 11: Main findings for vigilance state-dependent neuronal activity and functions using *in vivo* imaging. (A) Characterization of cell-, layer- and neuronal compartment-specific activity during different vigilance states and substates. (B) Specific sleep-related processes associated with cognitive and housekeeping functions. (Sigl-Glöckner and Seibt, 2019)

In conclusion, wake and sleep are characterized with important difference in patterns of neuronal activity, but the underlying activity in different compartments of excitatory and inhibitory neuronal populations still needs to be elucidated. These populations present an elaborate interplay associated with different oscillatory events that might underlie, at least partly, some of the functions of sleep and needs to be studied further.

2. *Regulation of the sleep-wake cycle*

2.1 Global regulation of the sleep-wake cycle

Sleep-wake states are regulated by arousal- and sleep-promoting networks based on the principle of reciprocal inhibition (Figure 12).

2.1.1 Wake-promoting networks and neurotransmitters

The cortical state during wake is dependent on the activation of specific nuclei that belong to the ascending reticular activating system (serotoninergic neurons localized in the dorsal raphe nucleus, noradrenergic neurons in the locus coeruleus, cholinergic neurons in the pontine brainstem, glutamatergic neurons in the medial parabrachial nucleus and dopaminergic neurons in the ventral tegmental area) and the forebrain (cholinergic neurons in the basal forebrain, histaminergic neurons in the tuberomammillary nucleus and GABAergic and orexin neurons in the lateral hypothalamus) (Saper and Fuller, 2017).

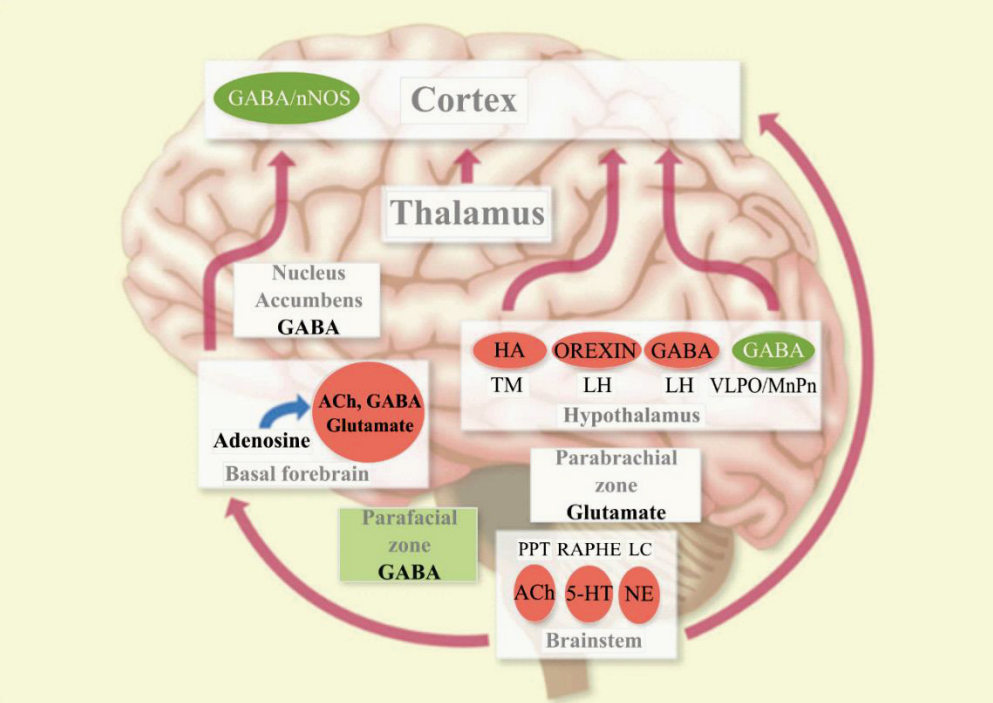

Figure 12: Overview of neuronal networks responsible for sleep and wake regulation. Wake- (in red) and sleep-promoting (in green) nuclei send their projections to the cortex to regulate vigilance states. (Wigren and Porkka-Heiskanen, 2018)

These small group of cells send their axonal projections to the thalamus and/or cortex and release specific neurotransmitters upon activation (Fuller et al., 2011). Thus, levels of wake-promoting NT, such as acetylcholine and serotonin, were found to increase significantly during wake in cortical and subcortical areas (Marrosu et al., 1995; Portas et al., 2000). Norepinephrine levels were also increased in both regions that were assessed: the medial prefrontal (mPFC) and

motor (M1) cortex, with higher relative levels in mPFC (Bellesi et al., 2016). Interestingly, NA levels presented different nadir and build-up dynamics in these two regions, suggesting region-dependent fluctuations of neurotransmitters. Moreover, some neuromodulators, such as norepinephrine, are endowed with rather uniform projections in cortical regions (Berridge and Waterhouse, 2003), whereas others, such as dopamine, preferentially target prefrontal areas (Arnsten, 1997).

A well-described function of wake-promoting neuromodulators includes their capacity of changing membrane properties, spiking activity and intracellular signaling pathways in neurons and glia (O'Donnell et al., 2012). In addition, a wake-promoting neuromodulators cocktail remarkably influenced the ionic composition during the vigilance states whose variations were initially considered a consequence of different patterns of neuronal activity (Ding et al., 2016; Seigneur et al., 2006). In turn, it was extracellular ions that impacted neuronal activity patterns and ion homeostasis regulation was sufficient to alter behavioral states both locally and globally (Ding et al., 2016). Transitions from wake to sleep were accompanied with rapid and sustained decrease in $[K^+]_e$ and a progressive increase in $[Ca^{2+}]_e$ and $[Mg^{2+}]_e$. Wake was found to induce opposite changes in both parameters, that showed faster transitions from sleep towards wake. Interestingly, blocking neuronal activity by TTX did not alter basal $[K^+]_e$ nor did it suppress the neuro-modulator-cocktail induced $[K^+]_e$ increase, suggesting that synaptic transmission did not influence changes of $[K^+]_e$.

2.1.2 Sleep-promoting networks and neurotransmitters

At the onset of sleep, sleep-active neurons depolarize strongly, releasing inhibitory neurotransmitters onto wake-promoting regions, leading to reduced release of wake-promoting neurotransmitters (Saper and Fuller, 2017; Saper et al., 2005). Sleep-active neurons constitute a subset of GABAergic and galaninergic neurons in the preoptic area (POA) of anterior hypothalamus, including ventrolateral preoptic nucleus (VLPO) and median preoptic nucleus (MnPn) (Sherin et al., 1996; Suntsova et al., 2007). Since lesions in the POA resulted in partial sleep loss, additional sleep-active areas have been recently described in other brain areas including the basal forebrain, lateral hypothalamus, cortex and the medulla of the brain stem (Anaclet et al., 2014; Gerashchenko et al., 2008; Luppi et al., 2017). Sleep-promoting neurons are themselves inhibited by the wake-promoting ascending arousal system: wake-promoting neurotransmitters noradrenaline, acetylcholine and serotonin, but not histamine, inhibited

sleep-active VLPO neurons (Gallopin et al., 2000). Thus, these interactions between wake- and sleep-promoting regions make this system act as a "flip-flop switch", characterized by a fast switch between these states (Saper et al., 2001, 2010).

Similar to previously described regional variations of NA, GABA also presented sleep-stage-specific changes between different regions (Vanini et al., 2012). For instance, in the cortex, GABA levels were significantly decreased both during wake and REM sleep compared to NREM sleep. On the other hand, GABA levels were significantly reduced only during REM sleep in the substantia insomnata (SI) of the basal forebrain. Furthermore, several studies indicate that GABA may promote sleep or wake depending on a brain region-by-region basis. For instance, in the pontine reticular formation, GABA may promote wake and inhibit REM sleep (Camacho-Arroyo et al., 1991; Flint et al., 2010; Sanford et al., 2003; Watson et al., 2008; Xi et al., 1999). On the contrary, GABA may promote REM sleep generation in the locus coeruleus and in the dorsal raphe nucleus (Nitz and Siegel, 1997a, 1997b). On the other hand, in the posterior hypothalamus and thalamus, GABA was found to promote NREM sleep and slow wave activity, respectively (Kékesi et al., 1997; Nitz and Siegel, 1996).

Wake-promoting influence was believed to be mostly due to monoaminergic and cholinergic neurons. However, specific lesions of these cell groups, as well as large lesions affecting the thalamus, had little effect on the amount of wake and sleep in rodents (Blanco-Centurion et al., 2007; Fuller et al., 2011; Gerashchenko et al., 2001, 2004; Gompf et al., 2010; Petrovic et al., 2013). Sleep-wake duration was profoundly affected by glutamatergic inputs both from parabrachial nucleus (PB) and pedunculopontine tegmental nucleus (PPT) to the basal forebrain (BF), as well as GABAergic populations in BF and the lateral hypothalamus (LH) (Fuller et al., 2011; Saper and Fuller, 2017). These findings shift the traditional view and propose monoaminergic, cholinergic and peptidergic systems as being modulatory systems. Future studies will need to assess the interaction between these components in the regulation of sleep and wakefulness.

2.2 Local regulation of the sleep-wake cycle

2.2.1 Evidence of local regulation

Sleep has traditionally been viewed as a global state relying on the previously described top-down regulatory mechanisms. Recent evidence suggests that sleep may originate locally in neuronal circuits, and that synchronization of several circuits would result in global sleep (Krueger and Obäl, 1993; Roy et al., 2008; Van Dongen et al., 2011). Pioneering study by Pigarev *et al.* found that sleep developed asynchronously in cortical areas in behaving monkeys and was specific to local networks (Pigarev et al., 1997). Sleep-like functional states were localized in regions at least as small as cortical columns, functional units of tightly connected neurons in the cortex (Rector et al., 2005, 2009). Moreover, the cortical column sleep-like state was found to be homeostatically regulated: the likelihood of being in sleep-like state depended on the duration of the previous wake state. In addition, when cortical columns associated with a particular task were in a sleep-like state, the task performance was affected. For instance, after learning a task that consisted in licking a sweet solution when a specific whisker was stimulated, if the cortical column receiving input from that whisker was in a sleep-like state, more mistakes were committed by the animal.

This phenomenon was also found at the level of cortical neurons since brief episodes of neuronal silence ("off periods") were observed after prolonged wake and were accompanied with emergence of slower waves locally (Vyazovskiy et al., 2011). The incidence of "off periods" increased with wake duration and tended to appear asynchronously across cortical areas even though rats displayed active waking behavior and typical waking EEG activity. Yet again, off periods occurring in the motor cortex during sugar pellet reaching task led to an impaired performance.

2.2.2 Potential mechanisms involved in local regulation

The mechanistic origin of local wake and sleep is probably fundamentally different from previously described global state switching that is controlled by specific neural circuits. Since local sleep is associated with prior activity, it might be initiated by activity-dependent release of molecules, such as ATP, into the extracellular space. ATP may bind to P2 receptors, and ATP-dependent P2X7R activation was found to affect cytokine (IL1 and TNFα) and

neurotrophin release from glia or neurons (Bianco et al., 2005; Hide et al., 2000; Krueger, 2008). Indeed, endogenous TNFα expression was enhanced in the corresponding barrel column by increased whisker stimulation *in vivo* (Churchill et al., 2008). Cytokines and neurotrophins influence neuromodulator (adenosine) and NT (glutamate and GABA) receptor trafficking (Imeri and Opp, 2009; Krueger, 2008; Reyes-Vázquez et al., 2012), which may result in altered network responsiveness, leading to oscillations within small networks. In support of this theory, cortical TNFα application induced sleep-like state within cortical columns (Churchill et al., 2008; Jewett et al., 2015). Local application of IL1 to the cortex also induces local cortical delta waves (Yasuda et al., 2005), but it also increased neuronal activation in hypothalamic sleep regulatory circuit (Yasuda et al., 2007). Considering these findings, the effect of somnogens on global states through a top-down influence of local sleep or a bottom-up effect on subcortical networks needs to be assessed more precisely.

2.3 Homeostatic and circadian regulation of sleep

Borbely proposed a two-process model on sleep regulation, comprised of two anatomically independent mechanisms that jointly regulate sleep duration and propensity: a homeostatic, sleep-dependent process (process S) and circadian, sleep-independent process (process C) (Borbély, 1982).

2.3.1 Process C

Process C reflects the circadian rhythm, that is coordinated by a master clock located in the suprachiasmatic nucleus (SCN) in the anterior hypothalamus (Leak and Moore, 2001; Vansteensel et al., 2008). The circadian clock controls rhythms of many physiological functions, including sleep. A major role of SCN in vigilance state regulation was proposed because SCN lesioning resulted in abolishment of diurnal and nocturnal distribution of sleep-wake rhythms (Edgar et al., 1993; Mistlberger et al., 1983; Tobler et al., 1983; Trachsel et al., 1992). In addition, shorter endogenous sleep-wake periods observed in mutant mice were reproduced in wild-type host mice with SCN transplantation (Ralph et al., 1990).

Rhythmic SCN firing rate relies on the activity of photoreceptive retinal ganglion cells (RGC) that detect light signals and project to the SCN via the retinohypothalamic tract (RHT). In turn, SCN projects mostly to intrahypothalamic zones, including the previously described sleep- and

wake-active nuclei, as well as the pineal gland that drives the synthesis and secretion of melatonin, a sleep inducing hormone (Gooley et al., 2001; Hattar et al., 2002; Lucas et al., 2001; Mistlberger, 2005; Provencio et al., 2000; Rusak and Zucker, 1979; Saper et al., 2005).

2.3.2 Process S

Sleep is also regulated by a homeostatic mechanism that represents the sleep-wake-dependent pressure to sleep (Deboer, 2015). Sleep homeostasis is based on the principle that when sleep is lost, it is compensated with modulation of sleep duration and intensity during the following sleep period. A reliable marker of homeostatic sleep need is slow-wave activity (SWA). Indeed, the first hours of sleep are characterized by maximal SWA, reflecting the highest "sleep need". SWA power progressively decreases over the course of sleep, exhibiting the homeostatic decrease in sleep need (Borbély et al., 2016). Along the same line, prolonged wakefulness or sleep restriction gave rise to an overall increase of SWA during subsequent sleep.

At the cellular level, homeostatic sleep need is proposed to be driven by progressive accumulation of endogenous somnogenic molecules during wake (Brown et al., 2012; Joiner, 2018). The best-known agent of sleep need is adenosine (Huang et al., 2011). Adenosine is created during the day as a metabolic by-product of the energy-storage molecule ATP. Adenosine levels assessed by microdialysis in several brain regions showed a 15-20% decline during episodes of sleep compared to wake (Porkka-Heiskanen et al., 2000). Furthermore, adenosine accumulated significantly in the cholinergic region of the basal forebrain in sleep deprivation, suggesting that sleep-promoting effects due to prolonged wake may be mediated by adenosinergic inhibition of basal forebrain arousal system. Adenosine may promote sleep using several mechanisms in different brain areas, via inhibitory A1R (on several sleep-promoting nuclei) or excitatory $A2_AR$ (on several striatum nuclei, nucleus accumbens and VLPO) signaling (Huang et al., 2011). Intriguingly, adenosine may also promote wakefulness by A1R activation in the lateral preoptic area of the hypothalamus (Methippara et al., 2005).

As mentioned previously, adenosine is supplied by ATP which represents the actual "energy currency of the brain". During spontaneous wake, ATP levels were maintained at a steady state and increased significantly in the initial hours of sleep in predominantly wake-active regions (Dworak et al., 2010). In these regions, ATP surge was positively correlated to the intensity of slow-wave delta activity, suggesting that ATP levels are directly related to SWA in NREM

sleep. These findings open new questions about the possible physiological role of ATP and its metabolites in sleep regulation in the cortex or connecting hypothalamic and cortical signaling.

3. Sleep function

Evolutionary speaking, a strong selective pressure not to sleep exists, since the animal is at increased risk of predation and has less opportunities to find mates and resources (Lima and Rattenborg, 2007; Lima et al., 2005). Despite that, sleep appears to be a universally conserved phenomenon across evolution and is therefore posited to serve at least one fundamental biological function. Theories about the function of sleep revolve around its involvement in serving higher-order cognitive functions and housekeeping/restorative processes (Frank and Heller, 2019). The first implies a role for sleep in synaptic plasticity, learning and memory, whereas the latter involves many contributions, including metabolic regulation (Knutson et al., 2007; Van Cauter et al., 2008), restoring and replenishing energy stores (Oswald, 1980), and removal of metabolic waste (Xie et al., 2013). In this chapter, we will discuss evidence of the role of sleep in learning and memory, which is central to my research. The housekeeping/restorative functions will be addressed briefly in the final chapter, with regards to glial cells involvement in these mechanisms. Nevertheless, these functions are certainly crucial for promoting normal cognitive functioning.

3.1 The role of sleep in memory

Sleep is known to support plasticity and memory consolidation (Datta and Maclean, 2007; Diekelmann and Born, 2010; Stickgold and Walker, 2013; Tononi and Cirelli, 2014). The standard model for memory formation involves two specific processes: 1) temporary encoding of new memories, that are still labile and vulnerable to interference, and 2) repeated memory activation, transfer and integration of stable memory representations into long-term memory networks (Rasch and Born, 2013). With regards to the vigilance states, wake is a period of intense information processing and encoding, whereas sleep, characterized by minimal sensory input, is considered as optimal for memory stabilization and reorganization into a permanent form of long-term storage.

Both encoding and memory consolidation are thought to involve changes in single synapses, and up to entire circuits. Experience-dependent activity during wake leads to short-lived

synaptic changes associated with induction of synaptic plasticity. These mainly rely on post-translational modifications of proteins and rapid morphological alterations of dendritic spines (Bailey et al., 2015; Hernandez and Abel, 2008; Lang et al., 2004). NMDAR are crucially involved in the induction of synaptic plasticity. Their activation leads to increase in postsynaptic intracellular Ca^{2+} concentration, which may result in activation of different kinases and phosphatases, that have been shown to play important roles in long-term plasticity (LTP) and long-term depression (LTD) (Ho et al., 2011; Malenka et al., 1989). Potent enzymatic activity is followed by changes in the activity and distribution of AMPAR, ionotropic receptors that mediate fast excitatory transmission, thus influencing synaptic strength. Phosphorylation-dependent changes also affect actin cytoskeleton dynamics resulting in structural modification of spines.

Experience may also activate induction of gene expression in neuronal ensembles. Experience-dependent transcription is the first step towards consolidation of plastic changes in neurons (Flavell and Greenberg, 2008). Thus, it is well-established that wake leads to induction of early forms of plasticity. However, the precise role of sleep on plasticity and learning is not clear and two theories have been suggested: the synaptic homeostasis hypothesis (SHY) and the active system consolidation hypothesis.

3.1.1 Synaptic homeostasis hypothesis (SHY)

The SHY theory proposes that sleep promotes global synaptic weakening (downscaling) that counteracts overall increase of synaptic strength that occurs during wake due to sensory processing and coding (Tononi and Cirelli, 2014). This mechanism would serve to preserve an overall balance of synaptic strength and avoid synaptic saturation. A recent expansion of SHY asserts that subsets of spines may not be affected by synaptic downscaling, which would allow them to maintain their increased signal-to-noise ratio. Nevertheless, it suggests that under physiological conditions, sleep is not involved in synaptic strengthening and synaptogenesis.

Global downscaling during sleep has been supported by evidence at the molecular, structural and electrophysiological level. At the molecular level, the levels of AMPAR, a marker of synaptic potentiation, were decreased during sleep both in the cortex and hippocampus. These results are suggestive of a net decrease of synaptic strength during sleep (Lanté et al., 2011; Vyazovskiy et al., 2009). A recent study showed that synapse weakening due to AMPAR

removal and dephosphorylation was driven by immediate early gene Homer1a and metabotropic glutamate receptors mGlu1/5 (Diering et al., 2017). This study proposed that during wake, Homer1a was excluded from the synapses due to high levels of norepinephrine. At the onset of sleep, Homer1a was targeted to synapses due to low norepinephrine and increase in adenosine levels and bound mGluR1/5, whose activation induced synaptic weakening. A major regulatory mechanism underlying synaptic and sleep homeostasis might involve the recently discovered phosphorylation/dephosphorylation cycle of a particular set of sleep-need-index-phosphoproteins (SNIPPs) (Wang et al., 2018). Wakefulness progressively increased phosphorylation (mostly on synaptic proteins associated with pre-synaptic short-term plasticity, post-synaptic density structure and glutamate receptors) and phosphorylation states paralleled changes of sleep need.

At the structural level, 3D measurements of synaptic size from both motor and somatosensory cortex were obtained during the sleep-wake cycle using serial block-face scanning electron microscopy (SBEM) (de Vivo et al., 2017). The axon-spine interface decreased by almost 20% after sleep, indicative of scaling, but engaged only small-to-medium synapses. In support of this theory, overall spine density showed a net decrease during sleep in the adolescent mouse brain, but was not observed in adult mice (Maret et al., 2011).

At the electrophysiological level, sleep was associated with a significant decrease of the slope of cortical evoked responses, an electrophysiological marker of synaptic efficacy (Vyazovskiy et al., 2009). Furthermore, the frequency and amplitude of miniature EPSC (mEPSC) from frontal cortex slices in mice and rats were decreased after sleep and increased after waking. Importantly, these studies were done during development and might not be replicated in adult animals, as suggested previously. Furthermore, neocortical and hippocampal firing rates generally increased during wake, followed by a subsequent decrease during sleep (Grosmark et al., 2012; Miyawaki and Diba, 2016; Mizuseki and Buzsáki, 2013; Vyazovskiy et al., 2009).

3.1.1.1 NREM mechanisms involved in synaptic downscaling

Synaptic downscaling and renormalization in networks are believed to be mostly due to slow-wave activity (SWA) (Tononi and Cirelli, 2014). SWA was found to be higher or lower in cortical areas that were respectively more or less active, potentially reflecting the different need for downscaling (Huber et al., 2004, 2006). Experimentally generated firing rates resembling

SWA led to LTD induction of glutamatergic synapses *in vitro* (Bliss and Lomo, 1973; Czarnecki et al., 2007). However, low frequency stimulation was insufficient for LTD induction *in vivo* in the hippocampus and cortex and seemed to critically depend on the level of spontaneous activity of neural circuits (Abraham et al., 1996; Errington et al., 1995; Hager and Dringenberg, 2010; Jiang et al., 2003). On the other hand, burst-mode firing, observed in NREM thalamocortical activation patterns, was able to elicit LTD with and without pairing with post-synaptic EPSPs (Birtoli and Ulrich, 2004; Czarnecki et al., 2007; Lanté et al., 2011). In acute slices of entorhinal cortex, spontaneous pattern of NREM up state spiking was found to induce synaptic weakening of connections between L3 pyramidal neurons (Bartram et al., 2017). On the other hand, pairing synaptic inputs with postsynaptic spiking during up states maintained synaptic strength that was protected against subsequent up state-induced synaptic weakening. Thus, slow-wave activity may be biased towards synaptic weakening, but a subset of synaptic connections may be preserved, in particular those within active neuronal circuits.

3.1.1.2 Evidence challenging SHY

Several findings seem to challenge SHY, providing evidence of synaptic strengthening during sleep. Presynaptic stimulation mimicking slow-wave activity was found to increase EPSP amplitude in cortical neurons, suggesting that NREM firing patterns may induce long-term potentiation (Chauvette et al., 2012). Following visual experience, sleep was found to promote cortical response potentiation in adult mice (Aton et al., 2014) and somatosensory-evoked potentials were also enhanced after a slow-wave sleep episode (Chauvette et al., 2012). SWS also promoted formation of new spines following motor learning on a subset of branches of individual layer V pyramidal neurons (Yang et al., 2014a). Interestingly, most of these studies hint to synaptic strengthening during sleep when sleep was specifically preceded by novel task or experience.

Others propose a Wide Dynamic Range hypothesis (WIDER SHY) in agreement with new findings suggesting that sleep does not simply reduce overall firing rates in neuronal populations. Instead, NREM sleep was found to reduce the activity of high firing rate neurons and tended to increase firing of slow firing neurons, resulting in homogenization of firing rate distribution during sleep (Miyawaki et al., 2019; Watson et al., 2016). This relationship proves to be even more complex because another study suggested that firing rate homeostasis was found to be inhibited during sleep (Hengen et al., 2016). In this case, V1 neurons maintained

their average firing rate around an individual set-point, but when perturbed, firing homeostasis was induced only during wake.

In line of these results, it is possible that the effects of sleep on synaptic plasticity and networks are not as uniform as SHY proposes, but depend on the species, developmental stage and the circuit examined, with a special importance of waking experience preceding sleep.

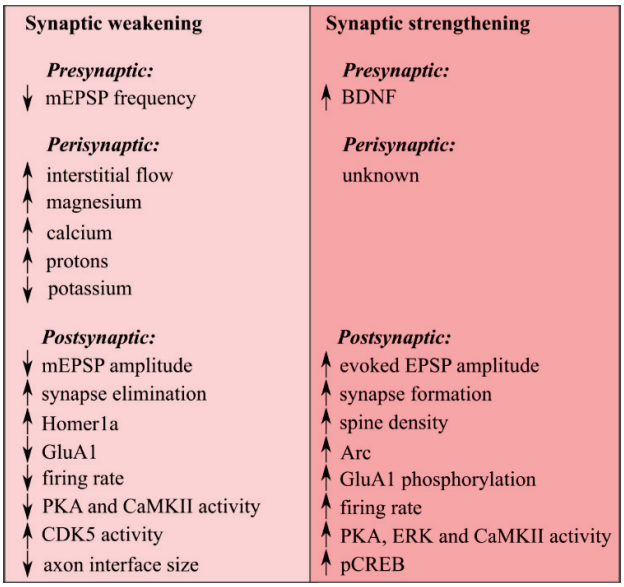

Figure 13: Pre-, peri- and postsynaptic changes associated with sleep-dependent synaptic weakening and strengthening at the molecular, structural and electrophysiological level. (Puentes-Mestril and Aton, 2017)

3.1.2 Active system consolidation hypothesis

Based on the previously described two-stage model, this hypothesis proposes that sleep, in particular NREM sleep, is highly involved in the "active system consolidation" of memory (Born and Wilhelm, 2012). This theory implies that repeated reactivation of specific memory traces that need to be consolidated occurs during sleep and that memories undergo qualitative changes when they are transferred to long-term memory store.

Reactivation was observed for the first time in hippocampal "place cells". These are a subset of cells that fire when an animal is at different locations in an environment during active behavior (Rowland et al., 2016). Recently, the ordered reactivation of neurons was observed optically using two-photon in vivo Ca^{2+} imaging of hippocampal cells in running and inactive mice

(Malvache et al., 2016). During wake, replay sequences were related to functional binding of different anatomically preconfigured cell ensembles.

Recordings from a large ensemble of hippocampal “place cells” showed that the cells that fire together during active exploration had an increased predisposition to fire together during subsequent NREM sleep. Thus, during NREM sleep, these memories are reactivated (“hippocampal replay”) as part of the consolidation process at compressed timescales (approximately 20-fold), and gradually transferred to the long-term stores in the neocortex (Lee and Wilson, 2002; Wilson and McNaughton, 1994, Figure 14). The replay sequences were reactivated during hippocampal sharp-wave ripple oscillations (100-200Hz) that were recently found to induce LTP during replay and thus promote synaptic plasticity (Diekelmann and Born, 2010; Sadowski et al., 2016). Hippocampal-dependent memory consolidation and redistribution towards neocortical networks was found to require slow oscillations, thalamo-cortical spindles and hippocampal sharp wave-ripples and relied on the hierarchical settlement of these rhythms (Buzsáki et al., 1992; Diekelmann and Born, 2010; Steriade et al., 1993). More specifically, phase-locking was achieved when sleep spindles coincided with the early part of the up state of the slow wave and sharp-wave ripples nested into the excitable troughs of the spindle oscillation (Latchoumane et al., 2017). As described previously, spindle nesting in the up states of the slow oscillation was recently found to be accompanied with particular activity of cortical excitatory and inhibitory cell populations, suggestive of conditions that might optimize synaptic plasticity within cortical circuits (Niethard et al., 2018).

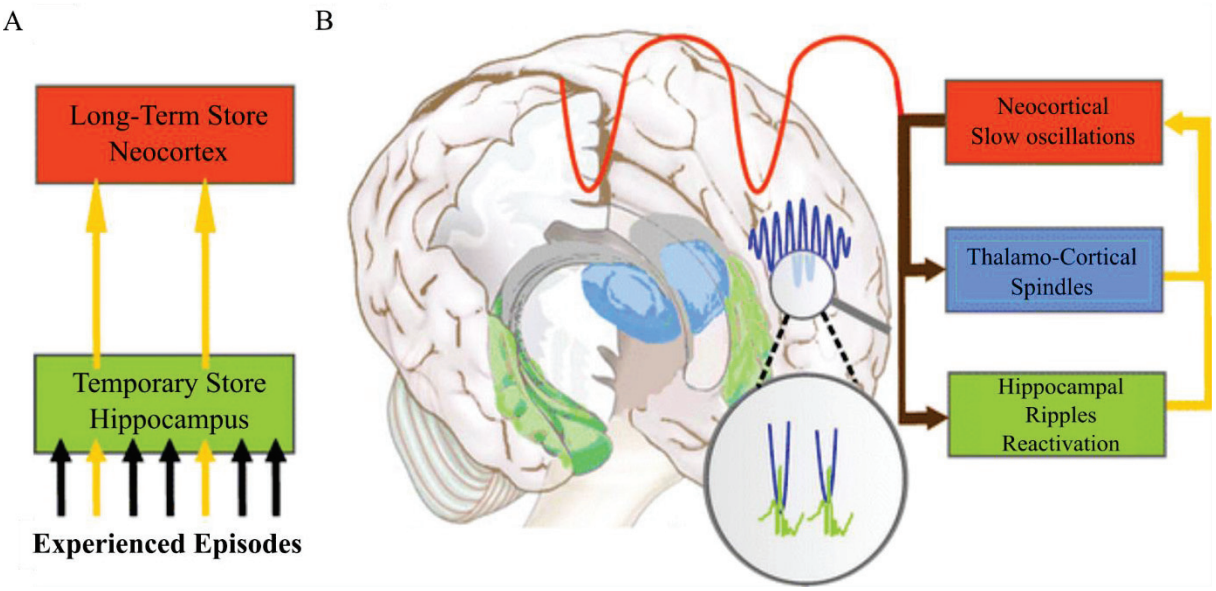

Figure 14: Active system consolidation during sleep. (A) Temporary memory representations are reactivated during NREM sleep, leading to distribution to long-term cortical stores. (B) Hippocampal-dependent memory consolidation and redistribution require precise settlement of neocortical slow oscillations, thalamo-cortical spindles and hippocampal sharp wave-ripples (Born and Wilhelm, 2012).

It is important that reactivation during NREM sleep occurs in the same neurons activated during wake. One of the theories providing an attractive framework for an underlying mechanism is the synaptic tagging and capture hypothesis (STC). This theory proposes that at the time of memory encoding, "synaptic tags" are set on synapses, creating the potential for long-term remodeling (Lesburgueres et al., 2011). Importantly, these tags may mark synapses depending on their prior waking experience and may result in subsequent strengthening or weakening during sleep. Thus, plasticity related proteins (PRPs), such as Arc, Homer1a and BDNF, were found to be transcribed in an experience-dependent manner and targeted to dendrites during wake. Later reactivation of primed neurons and synapses during oscillatory NREM activity promoted PRP capture by tagged synapses. Furthermore, localized spindle activity may target different subsets of dendrites, leading to PRP capture for specific fate depending on the levels of intracellular Ca^{2+}. The ultimate stabilization of synaptic strength, dependent on PRP translation, is proposed to occur during REM sleep (Almeida-Filho et al., 2018).

4. *Role of glial cells in sleep regulation and function*

Past research on sleep has mostly been conducted in a "neurocentric" manner, without considering an active involvement of glial cells. This is probably due to the fact that initial description of the wake-sleep cycle was done using EEG that reflects electrical activity of cortical neurons, whereas glial cells are electrically non-excitable cells. Over the recent years, a growing body of evidence has suggested that glial cells may be directly involved in sleep regulation and may mediate sleep functions.

4.1 Role of astrocytes

Astrocytes are known to play important roles in maintaining brain homeostasis and regulating synaptic transmission. More precisely, they are involved in regulation of brain energy metabolism, blood flow, local concentrations of ions and neurotransmitters, as well as synapse function, formation and elimination (Butt and Verkhratsky, 2018).

4.1.1 Involvement in sleep regulation and homeostasis

We already addressed the importance of adenosine accumulation for sleep homeostasis. Even though all cell types are capable of releasing adenosine, a more direct evidence of astrocytic involvement in sleep homeostasis was reported using conditional astrocytic suppression of SNARE-dependent gliotransmission. This resulted in impaired exocytosis and loss of tonic adenosine-mediated presynaptic inhibition of excitatory synaptic transmission (Pascual et al., 2005). In this model, the compensatory NREM SWA mechanisms were affected due to a reduced supply of adenosine acting on A1R (Halassa et al., 2009).

Astrocytes were also proposed to modulate sleep homeostasis by regulating slow oscillations. Suppressing the previously described astrocytic SNARE gliotransmission led to reduction of the slow oscillation power in whole cell recordings of pyramidal neurons (Fellin et al., 2009). Another mechanism by which astrocytes may assist slow local oscillations includes short-range spatial buffering of extracellular K+, because during slow sleep oscillations (<1Hz), astrocyte membrane polarization oscillated in close synchrony with NREM SWA (Amzica, 2002; Amzica and Neckelmann, 1999).

New tools allowing optogenetic activation of astrocytes *in vivo* has provided further evidence for the role of astrocytes in sleep-wake regulation. Optogenetic stimulation of astrocytes in posterior hypothalamus mostly affecting orexin and MCH neurons resulted in increased NREM and REM sleep time, without changes in the delta power (Pelluru et al., 2016). This manipulation allows for increase in intracellular Ca2+ (Losi et al., 2017), resulting in increased gliotransmission and possible release of ATP, D-serine, glutamate and cytokines mediating the observed effect.

In addition, astrocytic gene expression and ultrastructure were critically regulated by the sleep-wake cycle (Bellesi et al., 2015). 1.4% of all astrocytic transcripts in the forebrain were dependent on the vigilance states. Upregulated genes during wake included those associated to metabolism, extracellular matrix and cytoskeleton, including genes involved in the elongation of peripheral astrocytic processes (PAP). At the ultrastructural level, astrocytic processes were found to be closer to the synaptic cleft during wake, with reduced astrocytic coverage during sleep. This configuration might promote neurotransmitter clearance or supply of glial-derived

signals for synaptic plasticity during wake. During sleep, it may support glutamate spillover and participate in the promotion of neuronal synchronization.

4.1.2 Involvement in glymphatic pathway

Astrocytes may play an important role in "brain cleaning" via the glymphatic pathway which is highly active during sleep. The glymphatic pathway facilitates the clearance of solutes, including Aβ, from the interstitial fluid (Iliff et al., 2012). This clearance pathway is critically dependent on aquaporin-4 (AQP-4) water channels that are mostly localized on astrocytic endfeet in the brain (Camassa et al., 2015; Papadopoulos and Verkman, 2013). During slow-wave sleep, both the interstitial space and the glymphatic influx were highly increased, compared to wakefulness (Xie et al., 2013), suggesting higher waste clearance during sleep.

4.1.3 Astrocyte-neuron metabolic interactions in sleep/wake cycle

Even though brain activity during wake is associated with higher metabolic rates, brain expenditure remains relatively high during NREM sleep (~85% of the rate during wake) (Stender et al., 2016). Astrocytes are known to supply energy metabolites to neurons via gap junction-mediated networks (Giaume et al., 2010). The major constituent of gap junctions in astrocytes is connexin 43 (Nagy and Rash, 2000). Mice with conditional deletion of astrocyte gap-junction protein connexin 43 manifested excessive sleepiness and fragmented wake during the nocturnal active phase. This effect was mediated by a reduced excitability of orexin neurons in the lateral hypothalamic area (Clasadonte et al., 2017), due to reduced diffusion of glucose and lactate. Thus, astrocyte-neuron metabolic interactions contribute to the regulation of the sleep-wake cycle.

4.2 Role of oligodendrocytes

In contrast to well-described functions for astrocytes, much less is known about the roles of oligodendrocytes and microglia in the regulation of sleep. Oligodendrocytes may secrete prostaglandin D2, which was found to be a robust sleep-promoting substance when applied exogenously (Urade and Hayaishi, 2011). Genome-wide profiling of oligodendrocytes during the vigilance state also showed that, similar to astrocytes, oligodendrocyte gene expression was affected by sleep (Bellesi et al., 2013). Genes related to promotion of OPC proliferation as well

as phospholipid synthesis and myelination were transcribed preferentially during sleep, whereas genes involved in apoptosis, cellular stress response and OPC differentiation were expressed at higher levels during wake.

4.3 Role of microglial cells

4.3.1 Regulation of sleep homeostasis

Microglia, as well as astrocytes, are capable of secreting many somnogenic substances *in vitro*, including IL-1, TNFα and neurotrophines. As mentioned earlier, these molecules may influence sleep pressure and enhance NREM duration when injected intraventricularly or following cortical application (Yasuda et al., 2007). In addition, mice lacking TNFα or IL-1 present a sleep phenotype characterized with reduction of NREM sleep duration and intensity. A more direct effect of microglia was suggested when sleep-deprived mice were administered with minocycline (Wisor et al., 2011). Minocycline administration leads to microglial reactivity attenuation and caused a reduction in total sleep time and abolished compensatory EEG SWA in sleep-deprived mice. The molecular mechanism did not seem to involve IL-1β, IL6 and TNFα, since their mRNA levels were not altered. On the other hand, TNFα was suggested to exert its somnogenic effects by promoting microglial attraction to synapses (Karrer 2015). Indeed, TNFα induced neuronal production of chemokines (CCL2, CCL7 and CXCL10) and colony stimulating factor 1 (CSF-1) *in vitro*, promoting elongation of microglial processes. Furthermore, chronic sleep restriction, but not acute, resulted in microglia activation and promoted its phagocytic activity without overt signs of neuroinflammation (Bellesi et al., 2017).

4.3.2 Involvement in sleep-dependent plasticity

Microglia might also be involved in sleep-dependent plasticity, with mechanisms closely linked with the microglial circadian clock. Microglial morphology and microglia-spine interactions exhibited diurnal variations (Hayashi, 2013). These were critically dependent on P2Y12R expression that was driven by the intrinsic microglial clock. Microglia extended their processes and increased contacts with dendritic spines during the dark phase, when P2Y12R expression was highest. Furthermore, microglial P2Y12R expression was found to be critical for ocular dominance plasticity (ODP), a process highly dependent on sleep (Frank et al., 2001; Sipe et al., 2016). Cortical microglia also presented circadian expression of cathepsin S (CatS)

(Hayashi et al., 2013). CatS is a microglia-specific lysosomal cysteine protease that is able to modify the perisynaptic environment. CatS was secreted during the dark phase and led to downscaling of synaptic strength during the subsequent light phase.

With these evidence, we may affirm that glial cells are very well positioned to control the regulation of sleep-wake cycles and mediate sleep functions. Indeed, many functions that are mediated by glial cells are found to be modulated during the sleep-wake cycle. Thus, better characterization of the functions of glial cells in general, as well as specifically related to the sleep-wake cycle will undoubtedly provide much insight into the sleep-wake mechanisms that are not properly understood.

5. *Sleep vs other brain states: general anesthesia and coma*

Even though anesthesia is a pharmacologically induced state, it shares many physiological hallmarks with the naturally occurring sleep state. These include reversible loss of consciousness, slow synchronous cortical waves, immobility and reduction of body temperature (Franks, 2008). Anesthesia may be induced by administration of two types of anesthetic agents: intravenous, including propofol, thiopental and ketamine; and halogenated agents, such as isoflurane and halothane. The exact mechanism of action of general anesthetics remains largely unknown, but evidence show that ion channels are the most probable molecular targets, in particular GABA receptors, two-pore-domain K^+ (2PK) channels and NMDA receptors (Franks, 2008). In general, anesthetics do not affect single but multiple ion channels in agent-specific permutations resulting in increased neural inhibition and/or decreased synaptic excitation (Garcia et al., 2010).

To achieve unconsciousness, it is possible that anesthetics may hijack networks involved in the regulation of the sleep-wake cycle. Currently, it is unclear whether anesthetics primarily affect cortical or subcortical regions with subsequent repercussions (Brown et al., 2011; Hutt et al., 2018), but evidence point to distinct regulation for different anesthetics. For instance, sleep-promoting GABAergic neurons in the preoptic area were activated with $GABA_A$ agonist propofol and pentobarbital administration, as well as several halogenated anesthetics, but not with ketamine (Lu et al., 2008; Moore et al., 2012; Nelson et al., 2003). Another example of agent-specific pharmacological mechanisms is that lesioning of cholinergic neurons in the

nucleus basalis amplified the anesthetic potency of propofol and pentobarbital, but not halothane (Leung et al., 2011).

Even though the regulation of these mechanisms needs to be elucidated, the specific combination of targeted channels and circuits is likely reflected in the distinct EEG oscillatory patterns for each anesthetic drug. Neuronal oscillations generated by anesthetics such as ketamine/xylazine and urethane resemble particularly those during sleep. Indeed, ketamine/xylazine reproduces the predominant EEG signature of NREM sleep: slow cortical activity with states of hyperpolarization and depolarization (Chauvette et al., 2011). Nevertheless, more precise LFP and intracellular recordings reveal several differences: ketamine/xylazine administration exhibited increased amplitude of slow oscillations and duration of silent states compared to sleep, as well as increased gamma activity power (Chauvette et al., 2011). Other anesthetics may produce activity that is quite different from sleep. For instance, propofol, thiopental and isoflurane administration leads to high amplitude burst suppression activity separated by brief episodes of isoelectric activity (Lukatch et al., 2005).

Taking into consideration these findings, the distinct activity patterns generated by different anesthetic agents resembling more or less those during sleep, may serve as substrates for studying the impact of sleep-like and other states.

Other brain states exist and may be studied, such as coma, characterized with minimal brain activity and globally depressed metabolism (Brown et al., 2010). In terms of activity, low-amplitude delta activity and bursts of theta and alpha activity and possibly burst suppression are mostly observed in humans.

6. *Somatosensory cortex organization and sleep-wake activity*

Due to its somatotopic organization, the (primary) somatosensory cortex, provides an excellent model to study active sensory processing and experience-dependent plasticity. Sensory information from peripheral receptors are first transduced to the dorsal root and trigeminal ganglion cells. The information is then conveyed to neurons in the spinal cord and hindbrain, that project in turn to specific somatosensory thalamic relays. The major thalamic somatosensory nucleus is the ventral posterior group, which projects to somatosensory areas in

the cerebral cortex where sensory information processing is taking place. Interestingly, the barrel (whisker-related) cortex occupies more than two thirds of the total S1 area in the mouse (Franklin and Paxinos 2008). Apart from the area representing the whiskers and other parts of the face, the somatosensory cortex also includes the forelimb, trunk and hindlimb area. These areas are separated between them by territories with few granule cells in L4. In turn, the somatosensory cortex has widespread projections to cortical and subcortical areas.

During active wakefulness, global cortical activation was observed in the somatosensory cortex (Fernandez et al., 2017). Quiet wakefulness was accompanied with prominence of low-frequency (LF) activity. This differed from other regions, such as mPFC, that showed only a slight increase in frequency during active wakefulness compared to quiet wakefulness. During NREM sleep, LF oscillations increased in all cortical regions, with the highest mean amplitude observed in the somatosensory cortex (Figure 15). In addition, NREM sleep was enriched in fast spindles compared to prefrontal cortex (Fernandez et al., 2018). Interestingly, somatosensory areas showed increased coherence in the LF band during NREM sleep with regions such as the motor cortex that communicate via direct corticocortical connections.

In addition to the important changes of activity during sleep and wake, many studies have shown sleep-dependent changes at the molecular, structural and electrophysiological level in the somatosensory cortex.

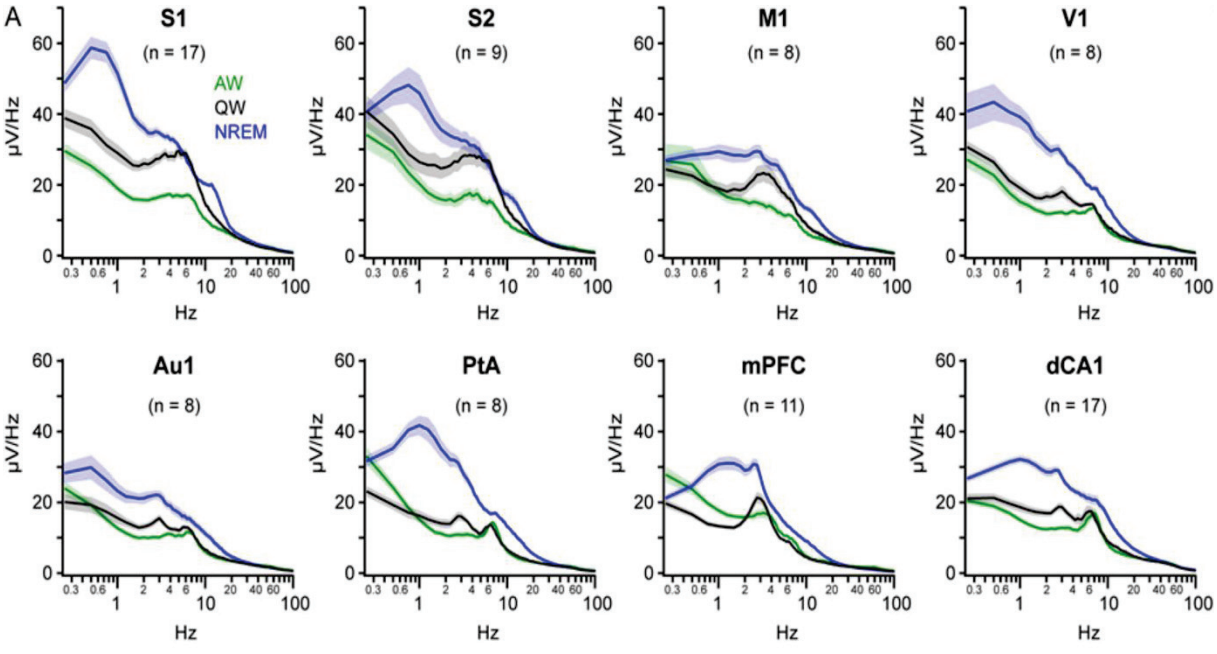

Figure 15: LFP spectral analysis during active wakefulness (AW), quiet wakefulness (QW), and NREM sleep in different cortical regions. The somatosensory cortex shows highest mean amplitude of low-frequency (LF) activity during NREM sleep and notable separations in the power spectra during wake and sleep. (Fernandez et al., 2017)

To summarize, the wake and sleep-related activity changes and the topographic organization of the somatosensory cortex, in particular the barrel cortex, constitute a great model for sleep-wake study, which might be further supplemented with modulation of sensory experience and plasticity mechanisms.

METHODOLOGICAL CONSIDERATIONS

1. *Use of CX3CR1$^{eGFP/+}$ and CX3CR1$^{CreERT2/+}$ mice*

To visualize microglial cells in the brain, we used the CX3CR1$^{eGFP/+}$ mouse model, where enhanced green fluorescent protein (eGFP) is expressed under the control of endogenous CX3CR1 locus (Jung et al., 2000). In fact, this model is the tool *par excellence* for visualizing microglial cells in the healthy brain. For study of microglial dynamics at the spine level, we generated CX3CR1$^{CreERT2/+}$Rosa26-STOP-tdTomato$^{-/-}$ mouse model where Cre recombinase is expressed under the control of the CX3CR1 promotor (Parkhurst et al., 2013). The resulting genotype in both cases bears one functional copy of the CX3CR1 gene. Consequently, mice may be partially deficient for CX3CR1, which mediates neuron-microglia communication. Several studies found no effect of CX3CR1 heterozygosity on many microglial parameters in physiological conditions, while others have observed a mild impact both in physiological and pathological conditions. In CX3CR1$^{eGFP/+}$ mice, several parameters relevant to our study were similar to Iba1$^{eGFP/+}$ mice, another model for microglia visualization without CX3CR1 heterozygosity (Hirasawa et al., 2005; Paolicelli et al., 2014). These parameters included microglial morphology and motility (Nimmerjahn et al., 2005; Wake et al., 2009), dendritic spine turnover (Parkhurst et al., 2013) and interaction with synapses (Tremblay et al., 2010; Wake et al., 2009). However, to exclude any effect of CX3CR1 heterozygosity, all these parameters should be compared between CX3CR1$^{eGFP/+}$ and wild type mice. In other studies, CX3CR1 deficiency showed a gene dose-dependent effect, with intermediate phenotype for CX3CR1$^{eGFP/+}$ mice in memory tests or LTP induction, even though the latter was not significantly different from wild type mice (Lee et al., 2010; Maggi, 2011; Rogers et al., 2011). In our case we assess sleep and wake within the same phenotype (CX3CR1$^{eGFP/+}$), and the results we observed are thus due to the change of the vigilance states rather than the decrease of CX3CR1 protein expression.

2. *Surgical procedure: thin-skull cortical window preparation and electrode implantation*

The two most common approaches for *in vivo* imaging include thinned-skull and cranial window preparations. In the case of thinned-skull preparation, the skull is carefully thinned to approximately 20µm leaving an intact periosteal layer as structural support for the thinned area.

For cranial window preparation, a part of the skull is completely removed. Even though cranial window preparation provides more imaging depth, the thinned-skull is a more immunologically inert preparation, thus better suited for studying microglial cells in physiological conditions. Indeed, possibly due to extensive activation of microglial cells in the cranial window preparation, rates of spine turnover were higher using this preparation compared to the thinned-skull preparation (24.7% to 4.9%) (Xu et al., 2007). In our case, we used a variation of the thinned-skull preparation, called thinned-skull cortical window preparation, where a coverslip is placed on top of the thinned skull allowing long-term imaging of the intact mouse brain.

For electrophysiological recordings, we implanted two EEG electrodes over the frontal and parietal cortex. Fronto-parietal electrodes are often used for sleep-wake studies since SWA signal is stronger in frontal derivations, allowing for a good detection of sleep-wake states (Huber et al., 2000; Vyazovskiy et al., 2002). EEG screws were placed contralaterally to the thinned-skull preparation due to the large place occupied by the thinned-skull preparation and, most importantly, to avoid injury. Since EEG allows for global monitoring of the vigilance states, we cannot rule out appearance of local wake/sleep states in our imaging region. However, local assessment at the imaging site would be highly invasive since electrode placement would cause an important microglial activation. In any case, the somatosensory region remains a good choice for studying sleep and wake cycles because high mean amplitudes of low-frequency activity are observed in this area, as well as substantial separations in the power spectra during wake and NREM sleep.

3. Genetically encoded calcium indicator GCaMP6m injection

To visualize fluctuations of neuronal activity, mice were injected with a genetically encoded calcium indicator AAV1.Syn.GCaMP6m.WPRE.SV40 in the somatosensory cortex (Chen et al., 2013). To avoid inflammation and injury at the imaging site, the injection was performed with an angle of 60º at a speed of 0.1µl/min, using a glass pipette with a small 20µm diameter tip. Two-photon imaging was done at a distance from the injection site where microglial cells were highly ramified and resembled microglial cells in physiological conditions. Taking into consideration the fact that we perform imaging fairly soon after injection, the expression of GCaMP6 indicators should not perturb the function of cortical circuits during this period (Chen et al., 2013).

4. Head-restriction

Two-photon imaging *in vivo* in unanesthetized mice requires contention and we chose head-restriction of the animal. Mouse immobilization may cause difficulties for the mouse to sleep and may increase stress levels. To improve animal well-being, prior to the imaging sessions, mice were progressively habituated to head-restriction (from 10 minutes to 4 hours) and were given a reward at the beginning and end of each session. Mice did not exhibit stress signs during imaging session and exhibited both NREM and REM episodes, which we believe reflects minimal stress. We observed relatively long NREM sleep periods that were occasionally followed by REM sleep, resembling natural sleep-wake cycles. However, due to head-restriction, both NREM and REM sleep duration was reduced, and sleep was more fragmented compared to freely moving mice (Franken et al., 1999). An individual episode of NREM sleep lasted on average 52 seconds and was often adjacent to other sleep episodes. These individual juxtaposed sleep episodes constituted one longer sleep episode (on average 5.8 minutes) that was interrupted by micro-wake episodes. Since individual episodes were too short for quantification of microglial parameters, we selected longer sleep episodes that contained more than >75% sleep. We found this to be a good compromise since the longer episodes still contained ~90% of sleep on average. Future experiments may use more recent knowledge to optimize head-fixation in order to mimic natural sleep position or incorporate gentle techniques, such as rocking, that may increase sleep duration (Kompotis et al., 2019; Yüzgeç et al., 2018).

THESIS OBJECTIVES

The regulation and functional role of the continuous movement of microglia is one of the great mysteries of neuroscience currently. Recent evidence has suggested that neuronal activity may regulate microglial motility and interaction with spines. Several brain states such as sleep, wake and anesthesia exhibit different patterns of neuronal activity. Sleep and wake are also associated with molecular mechanisms of synaptic plasticity important for synaptic homeostasis, learning and memory. Taking into consideration the growing body of evidence of microglial guidance by neuronal activity and its potent involvement in synaptic plasticity, this thesis had two objectives: 1) assess the impact of the brain states on global microglial motility and morphology, and 2) study how microglial dynamics at the spine level and microglia-spine interactions are impacted by the vigilance states and local neuronal activity, as well as the functional consequences of microglia-spine contact.

1. *Aim 1*

In physiological conditions, microglial cells have a highly ramified morphology and motile processes that extend and retract continuously. This movement is characterized with high energy expenditure and may serve functions other than immune surveillance of the surrounding parenchyma. Studies assessing the impact of neuronal activity on global motility and morphology in several brain areas and preparations have proposed a regulation of microglial dynamics by neuronal activity. However, these studies remain inconclusive and were done either using *ex vivo* models or anesthetized animals and/or sensory deprivation. To study the regulation of microglial morphology and motility by neuronal activity in physiological conditions, we used wake and sleep as two physiological states that are characterized with different patterns of neuronal activity (Article 2). We also assessed the impact of two different anesthetics: ketamine/xylazine, that reproduces the main features of sleep; and pentobarbital, characterized with a more divergent EEG pattern (Article 1). For this reason, I set up the simultaneous placement of thinned-skull cortical window preparation over the somatosensory cortex and EEG/EMG electrodes to assess neuronal activity and muscle tonus. We were thus able to combine two-photon imaging in vigil CX3CR1$^{eGFP/+}$ with electrophysiological recordings which allowed us to visualize microglial morphology and motility during the brain states.

2. *Aim 2*

To a greater extent than global microglial motility, previous studies found microglial dynamics at the spine level to be activity-dependent. For the most part, microglial processes appear to sense neuronal activity and to be attracted towards active spines. However, in physiological conditions, this attraction may be influenced by the vigilance states. Sleep and wake are fundamentally distinct states characterized with changes in neuronal activity, neuromodulation, ion and purine concentrations and are involved in different mechanisms of synaptic plasticity. Combining the previously described technique with stereotaxic injection of genetically encoded calcium indicators in the somatosensory cortex, we were able to simultaneously visualize both microglial dynamics and the fluctuations of Ca^{2+} activity at the spine level and the underlying vigilance state (Article 2). Using this mode we examined: 1) the regulation of microglial dynamics at the spine level and microglia-spine interactions by local neuronal activity and the vigilance states, 2) whether the proposed positive attraction between microglial processes and spines is vigilance state-dependent, and 3) the functional consequences of microglia-spine contact during the vigilance states.

RESULTS

1. ***Article 1: Anesthetics alter microglial morphology and motility***

2. ***Article 2: Sleep decreases neuronal activity control of microglial dynamics***

ARTICLE 1

In preparation

Anesthetics alter microglial morphology and motility

Hristovska I[1]*, Verdonk F[2,3,4]*, Comte JC[5], Desestret V[1], Honnorat J[1], Chrétien F[2,6,7]#, Pascual O[1]#

[1]INSERM U1217, CNRS UMR5310, Institut NeuroMyoGène, Lyon, France; Université Claude Bernard Lyon 1, Lyon, France

[2]Institut Pasteur, Experimental Neuropathology Unit, Infection and Epidemiology Department, Paris, France

[3]Department of Anaesthesiology and Intensive Care, Saint Antoine Hospital, Assistance Publique-Hôpitaux de Paris, Paris, France

[4] Sorbonne University, Paris, France

[5]INSERM U1028, CNRS UMR5292, Centre de Recherche en Neuroscience de Lyon, Lyon, France Université Claude Bernard Lyon 1, Lyon, France

[6]Paris Descartes University, Sorbonne Paris Cité, Paris, France

[7]Laboratoire hospitalo-universitaire de Neuropathologie, Centre Hospitalier Sainte Anne, Paris, France

* The authors contributed equally to this manuscript

Abstract

Background: Microglia, the resident immune cells of the brain, are highly ramified and motile and their morphology is strongly linked to their function. Microglia constantly monitor the brain parenchyma and are crucial for maintaining brain homeostasis and fine-tuning of neuronal networks. Besides affecting neurons, anesthetics may have wide-ranging effects mediated by non-neuronal cells and in particular microglia. We thus examined the effect of two commonly used anesthetic agents, ketamine/xylazine and barbiturates, on microglial motility and morphology.

Methods: A combination of two-photon *in vivo* imaging and electroencephalography (EEG) recordings in unanesthetized and anesthetized mice as well as automated analysis of *ex vivo* sections were used to assess morphology and dynamics of microglia.

Results: We found that administration of ketamine/xylazine and pentobarbital anesthesia resulted in quite distinct EEG profiles. Both anesthetics reduced microglial motility, but only ketamine/xylazine administration led to reduction of microglial complexity *in vivo*. The change of cellular dynamics *in vivo* was associated with a reduction of several features of microglial cells *ex vivo,* such as the complexity index, the ramification length and the number of nodes for ketamine/xylazine, whereas barbiturates altered the size of the cytoplasm. Furthermore, ketamine/xylazine and pentobarbital effects on microglial morphological parameters were region dependent.

Conclusions: Anesthetics have considerable effects on neuronal activity and microglial cells. This may have unintended consequences on microglial functions so barbiturates might be a preferred anesthetic agent for the study of microglial morphology. These findings will undoubtedly raise compelling questions about the functional relevance of anesthetics on microglial cells in neuronal physiology and anesthesia-induced neurotoxicity.

Keywords: microglia, motility, morphology, anesthesia, ketamine/xylazine, pentobarbital, immunohistochemistry, two-photon imaging

Introduction

Anesthetics are widely administered in animal research studies. They are commonly used to generate a reversible brain state allowing surgery and *in vivo* imaging of animals with less motion artefacts and stress during contention. Excess of anesthetics can also be used for euthanasia allowing further anatomical studies, such as immunohistochemistry. However, anesthetic agents are major pharmacological modulators of neuronal activity. As such, they may have unwanted effects on animal physiology and possibly bias the outcome of experiments.

For instance, general anesthesia primarily acts on the two main inhibitory and excitatory neurotransmitters of the CNS (1) by targeting Gamma-AminoButyric Acid A ($GABA_A$) receptors and N-methyl-D-aspartate (NMDA) receptors, respectively. Furthermore, recent studies revealed detrimental effects of general anesthetics on morpho-functional changes in the CNS as well as impaired neurocognitive performance (2). Research on the subject was mostly focused on elucidating the impact of anesthetic toxicity on neurons, and little consideration has been given to mechanisms mediated through action on glial cells.

Microglial cells, a part of the glial cell population, are the resident immune cells of the brain and are thus crucial in maintaining brain homeostasis (3). A growing body of evidence indicates that they contribute to the fine-tuning of neuronal circuits, to synaptic and structural plasticity, and that they could be involved in learning and memory (4,5). A hallmark of microglial cells in physiological conditions is the incessant motility of their processes that has been linked to changes of neuronal activity and synaptic functions (6). The effect of anesthesia on their function and more elaborated responses are however poorly documented.

Few studies have examined the effects of anesthetic exposure on microglial cells, and most often as side studies, revealing contradictory findings. Very recently, isoflurane was found to increase the length of microglial processes in acute and chronic preparations *in vivo*, and potentiate motility in acute preparations only (7). The effect of ketamine/xylazine was less potent as it increased microglial

ramification in acute preparation only and had no effect on microglial motility. On another hand, isoflurane was previously reported to inhibit microglial surveillance and ramifications by blocking THIK-1, one of the main K+ channels expressed by microglia *in situ* (8). The same study found that another widely used anesthetic, urethane, had no effect on both microglial ramifications and motility. Other studies have assessed the activation of microglial cells with anesthesia administration. Ketamine caused the activation of microglial cells in the retrosplenial cortex, but not in the cingulate cortex of rats (9). Kannan *et al.* found that in the presence of $GABA_AR$ agonist, pentobarbital, the morphology of microglia in cell culture changed from a ramified to a rounded shape (10). However, neuroleptic anesthetics targeting dopamine and opioid receptors did not cause any activation of microglial cells in the hippocampus of young adult mice (11). Morphological changes of microglia have been associated with different roles in physiological and pathological conditions. For instance, reduction of microglial ramification, accompanied by cell body enlargement, and shortening and thickening of processes, is characteristic of brain inflammation or injury (12,13). In this case, microglial cells secrete pro-inflammatory cytokines, increase their phagocytic activity and decrease neuronal synchrony (14,15). On the other hand, microglia may also hyper-ramify in response to stress (16) and accelerated aging (17), and this phenotype and the potential consequences have been much less described. Considering the importance of microglial cells in brain homeostasis and the routine use of anesthetics, more detailed evidence on the effects of anesthetics on microglial morphology and motility is needed.

In our study, we combined immunohistochemistry and two-photon *in vivo* imaging to study the effects of two anesthetics commonly used in laboratory studies, pentobarbital/ thiopental-based anesthetics ($GABA_AR$ agonist) and ketamine-xylazine cocktail (NMDAR antagonist), on the morphology and motility of microglial cells as well as on neuronal activity assessed by electroencephalography (EEG) and electromyography (EMG). Our findings suggest that these anesthetics differ in their effect on neuronal activity and cause changes in microglial motility and morphology that vary depending on the anesthetics and on the brain region studied.

Materials and methods

Animals

For *in vivo* and *ex vivo* experiments, six to ten week-old male heterozygous CX3CR1$^{eGFP(+/-)}$ mice were used, expressing enhanced green fluorescent protein (eGFP) under the control of CX3CR1 promoter. Mice were housed in individual cages with bedding and running wheels, under normal light/dark conditions and provided with food and water *ad libitum*. All experimental procedures were carried out in accordance with the French institutional guidelines and ethical committee.

In vivo experiments

Surgery and habituation

Mice were handled during one week prior to surgery. For surgery, mice were deeply anesthetized with isoflurane (3-4%, Isovet, Piramal Healthcare, UK Ltd.) and mounted in a stereotaxic apparatus (D. Kopf Instruments). To relieve post-operatory pain and inflammation, Carprofen (5mg/kg s.c.) was administered at the beginning of the surgery and the following two days. For transcranial imaging, a custom-made head plate implant was positioned on the left hemisphere and the skull was carefully thinned over the somatosensory cortex using a high-speed dental drill. For electrophysiological recordings, two EEG screws were inserted in the frontal and parietal cortex of the right hemisphere and two EMG electrodes were inserted in the neck muscles. A custom-made restraint system was used during head-restraining habituation sessions. Our habituation protocol involved daily training sessions over 7-10 days lasting progressively longer (from 10 minutes to 4 hours). A reward of several drops of sweetened concentrated milk was administered at the beginning and end of each session. Mice were imaged at the end of the habituation sessions.

Treatment conditions

Two-photon imaging was performed in the somatosensory cortex in the same mice (n=6) in unanesthetized (control condition) and anesthetized condition. Thus, the same microglial cells were imaged in unanaesthetized condition and subsequently during anesthesia. In the «anesthesia» condition,

mice were injected intraperitoneally with either a mixture of ketamine (100mg/kg) and xylazine (10mg/kg) or pentobarbital (60mg/kg) dissolved in 0.9% saline.

Two-photon *in vivo* imaging microscopy

A two-photon microscope (Olympus) with a mode-locked Ti:Sapphire laser (Mai-Tai, Spectra-Physics) tuned to 900nm (excitation wavelength for eGFP) was used. eGFP-labeled microglia were imaged under a 20x water-immersion objective (0.95 N.A. Olympus). Fluorescence was detected using a 560nm dichroic mirror coupled to a 525/50nm emission filter and a photomultiplier tube in whole-field detection mode. Laser power during imaging was maintained below 20mW. Microglial cells in the somatosensory cortex were imaged at least 15 minutes after general anesthesia. The imaging parameters corresponded to 200x200µm field of view and resolution of 521x521 pixels approximately. Microglia were imaged at a depth of 50-150 µm from the cortical surface and a typical recording lasted approximately 15-20 minutes (30-40 stacks). 25-30 consecutive Z-stack images were acquired every 30 seconds, 1µm/optical section.

EEG/EMG recordings

During the entire imaging session, the vigilance states were monitored using real-time EEG/EMG differential recordings amplifier (Model 3000, A-M systems). Signals were sampled at 1kHz. EEG was filtered in the frequency band [0.5Hz-300Hz], while EMG was filtered in the [10-500Hz] frequency band. EEG data were analyzed using a custom MATLAB© software. Power spectra and probability distributions of EEG magnitude were estimated for the total duration of anesthesia. Time-frequency representation was performed with a 4s duration sliding FFT (fast Fourier transform) window and 0.5s step size.

Imaging analysis

Image processing and analysis were performed using custom-written MatLab© software. From the original image, we manually delimited regions of interest containing the totality of only one microglial cell. In order to correct the drift in the x, y and z planes, each volume was registered to a reference volume (the first volume) using shift estimation from the cross-correlation peak by FFT. After

realignment, standard deviation intensity projections of z stacks were created and used to generate 2D time-lapse movies. For analyses of microglial complexity, we transformed the images into binary and calculated the Hausdorff fractal dimension, thus providing quantitative measure of the complexity of microglial cells. For each series of images, cell complexity was determined by averaging the complexity values obtained for each image. To analyze microglial motility, subtractions between consecutive Z-stack projections were performed. The number of summed pixels in subtracted images determined the global motility coefficient (arbitrary unit). This coefficient was normalized to the volume of the stack.

Ex vivo experiments

Treatment conditions

Three experimental groups were considered. In the anesthesia group, n=6 mice were injected intraperitoneally with either with a mixture of ketamine (100mg/kg) and xylazine (10mg/kg) or thiopental (60mg/kg) dissolved in 0.9% saline and were euthanized by cervical dislocation 5 minutes after anesthesia, followed by collection of the brain. In the control group, n=5 mice were injected with isotonic saline solution (NaCl 0.9%) and were euthanized by cervical dislocation 5 minutes after injection followed by brain collection. Cervical dislocation was authorized by the Ethics Committee of the Institute Pasteur and the French Ministry of National Education and Research in order to avoid any molecular interaction with any type of anesthesia or with carbon dioxide before brain analysis.

Tissue preparation

After euthanasia by cervical dislocation, the brains were immediately removed and sectioned along the inter-hemispherical fissure on a sagittal plane. The left hemisphere, dedicated to the morphological analysis, was fixed for 24 hours in a 4% paraformaldehyde solution (QPath®, VWR Chemicals, Fontenay Sous Bois, France) and then stored in a 0.1% paraformaldehyde solution until carrying out floating sections of 80µm along a sagittal plane using a vibratome (VT 1000 S, Leica®, Germany). The most medial section was then used for the morphological analysis.

Microglial morphology imaging and analysis

Microglial morphologic criteria were determined with an automated confocal tissue imaging system coupled to morphological modelling in CX3CR1$^{GFP/+}$ transgenic mice. This analysis was performed on sagittal cerebral floating sections of the left hemisphere placed on glass slides with FluoroMount (FluoroMount-G Mounting Medium, FluoProbes).

The image acquisition was carried out according to a previously validated protocol (18) using a confocal spinning disk microscope (Cell Voyager - CV1000, Yokogawa®, Japan) equipped with a UPLSAPO objective 40x/NA 0.9. Automatic analysis was applied using analysis script developed with the image analysis software Acapella™ (version 2.7 - Perkin Elmer Technologies, Waltham, USA). The following morphological criteria have been defined for each microglial cell on more than 3,000 microglial cells by group: the area of the cell body and the cytoplasmic area, defined as the area of the cytoplasm included in the primary branches, expressed in µm^2; a second set of calculated criteria extrapolated from the previous ones yielded the complexity index (CI) and the covered environment area (CEA). We defined the CI by the ratio between the number of segments of each ramification of each cell multiplied by the sum of the nodes on one hand and the number of primary branches on the other hand. Thus, we obtained an average complexity relative to the number of primary branches for each microglial cell.

$$CI = \frac{nb\ of\ segments\ \times\ (nb\ of\ nodes 1 + nb\ of\ nodes\ 2)}{nb\ of\ roots}$$

The CEA represents the 2D total surface covered by its ramifications and defined as the area of the polygon formed by linking the extremities of its processes, expressed in µm^2.

Statistical analysis

All statistical analyses were performed using the Prism V statistical analysis software (GraphPad, La Jolla, Ca). Microglial complexity and motility index were compared between groups using the non-parametric paired Wilcoxon test. Significance of $p<0.05$ was used for all analyses.

Results

Ketamine/xylazine and pentobarbital administration generate distinct and specific patterns of neuronal activity *in vivo*

Anesthetic effects on global neuronal activity were monitored using EEG/EMG recordings. EEG signal patterns were different between vigilance states and varied depending on the anesthetic agent (Figure 1A, 1C, 1E). The unanaesthetized condition is characterized with a large spectral range (Width to Mid-Height: WHM) equal to 10Hz, as well as a high dispersion of the amplitudes' distribution (Figure 1A, 1B, 1G, 1H). Ketamine/xylazine anesthesia was characterized with slow and large amplitude waves (Figure 1C, 1D) close to pure bi-chromatic signal (0.5Hz and 2Hz, Figure 1I) continuously present during the anesthesia period (Figure 1J). The 0.5 Hz component is stable during anesthesia while the 2Hz component tends to vanish at the end of the recoded period (Figure 1J). Pentobarbital anesthesia caused states of low electric activity with sporadic bursts of high amplitude (Figure 1E), consistent with the high peak at 0 (around baseline) and the long wings observed on the amplitudes' distribution (Figure 1F). The EEG signal exhibited a more spread spectrum in comparison to ketamine/xylazine (Figure 1I, 1J). The time-frequency representation of pentobarbital anesthesia (Figure 1K, 1L) showed a gradual increase of the spectral range before continuously decreasing until the end of the recording.

Both anesthetics reduce microglial motility, but only ketamine/xylazine affects microglial morphology *in vivo*

We examined microglial morphology, particularly the degree of ramification, assessed by an overall complexity index, and the motility of microglial processes *in vivo* in the somatosensory cortex of $CX3CR1^{GFP/+}$ mice. These cellular parameters where compared in unanaesthetized and anesthetized conditions. We found that microglial complexity was significantly reduced *in vivo* when mice were injected with ketamine/xylazine (1.55±0.016 vs 1.52±0.013, p=0.031; Figure 2A, 2B). However, microglial complexity remained unaltered with thiopental administration (1.56±0.01 vs 1.56±0.008, p=0.56; Figure 2D, 2E). To address the impact of anesthesia on microglial motility, we recorded 3D

time-lapse videos of the same microglial cells when the mouse was not anesthetized and subsequently during ketamine/xylazine or pentobarbital anesthesia. Both ketamine/xylazine and pentobarbital administration resulted in a significantly reduced overall process motility when compared to control (859.6±45.61 vs 707.1±26.28 motility index/μm^3 for ketamine/xylazine and 841.22±29.76 vs 757.12±22.46 motility index/μm^3 for pentobarbital; p=0.031; Figure 2C and 2F).

Ketamine/xylazine and thiopental affect different parameters of microglial morphology *ex vivo*, with inter-regional variability

To further describe the morphological changes of microglia and evaluate their heterogeneity in different brain areas, we studied microglial morphology in brain sections from $CX3CR1^{GFP/+}$ mice administered with ketamine/xylazine, thiopental anesthesia or saline prior to euthanasia (Figure 3 A, B, C). In the whole brain, ketamine/xylazine anesthesia caused a significant reduction of microglial cell complexity in comparison to the control group (3.5±0.1 vs 3.2±0.1; $p<0.05$; Figure 3E). Consequently, the total length of ramifications and the number of nodes were significantly reduced in comparison to the control group (318±19 vs 358±29 µm; $p<0.05$ and 8.3±0.6 vs 7.1±0.5; $p<0.05$; Figure 3H and 3I). In contrast, treatment with thiopental affected exclusively the cytoplasm area, resulting in a significant reduction in comparison to the control group (53.8±2.2 vs 59.7±3.3 μm^2; $p<0.05$; Figure 3D), which was not the case upon ketamine/xylazine administration. Other morphological features such as the cell environment covered by the ramifications (Figure 3F) and the number of segments (Figure 3G) remained unchanged in both conditions.

To investigate possible inter-regional variability, we quantified these morphological parameters in microglial cells separately in the frontal cortex (Figure 4) and the hippocampus (Figure 5). In both regions, the complexity of microglial cells (3.2±0.1 vs 3.4±0.1 for the frontal cortex and 3.3±0.2 vs 3.6±0.2 for the hippocampus; $p<0.05$, Figure 4E and 5B) were significantly reduced with ketamine/xylazine anesthesia. However, we observed a significant decrease of the total length of the ramifications in the frontal cortex only (306±16 vs 349±26 µm; $p<0.05$; Figure 5E). Furthermore, the

previously reported reduction of the cytoplasm area caused by thiopental anesthesia was only observed in the hippocampus but not in the frontal cortex (58.5±4.4 vs 68.3±8.2 μm^2; $p<0.05$; Figure 4D and 5A).

Discussion

Our current findings demonstrate that administration of two commonly used *iv* anesthetic in clinic, ketamine/xylazine and barbiturates resulted in the loss of microglial surveillance rate *in vivo* and morphological alterations that depended on the type of anesthetics administered and the brain region examined. Ketamine/xylazine administration resulted in extensive and widespread reduction of microglial process complexity, whereas barbiturates affected the cytoplasm area in a limited manner. Ketamine/xylazine and barbiturates are commonly used as general anesthetics for surgery, imaging, or euthanasia preceding immunohistochemistry studies. For anesthesia, ketamine, a NMDAR antagonist is often used with an α_2 adrenergic agonist, in our case xylazine, which provides sedation and analgesia (19,20). Importantly, ketamine activates less $GABA_AR$ in comparison with other anesthetics, which allowed us to distinguish the effects of ketamine/xylazine and barbiturates that are $GABA_A$ agonists (21). For the *ex vivo* and *in vivo* experiments, we used two types of barbiturates characterized by different durations of action caused chemical structure differences. Thiopental is an ultra-short acting anesthetic that was used for *ex vivo* experiments whereas pentobarbital was preferred for *in vivo* study because it was reported to have 4 to 8 times longer action than thiopental (22).

Interestingly, different anesthetics generate distinct and specific neuronal activity that might explain the discrepancies that we found on microglial morphology and dynamics. Our EEG recordings indicate that ketamine/xylazine anesthesia is characterized by slow, large amplitude waves with high delta power and it has been shown that different anesthetics affecting delta power in opposite manner impact differently sensory processing in V1 (23). The different effect of anesthetics on cortical activity might thus be related to the divergent impact on microglial cells (7). We found that pentobarbital anesthesia was associated with a different EEG pattern: states of isoelectric activity with bursts of high amplitude activity. Moreover, pentobarbital was found to reduce the firing rate of high and non-high frequency

bursting (HFB and non-HFB respectively) neurons *in vivo* in rats (24). Looking more closely, the pentobarbital power spectrum resembles the power spectrum during anaesthetized condition when compared to ketamine/xylazine. This might explain why pentobarbital had no effect on microglial morphology, suggesting that the frequency pattern of EEG could impact global microglial morphology. These findings need further investigation, to determine whether and how different EEG patterns, in terms of frequency and amplitude, may impact microglial morphology and motility.

Microglial cells continuously survey their surroundings by extending and retracting their motile processes (25,26). They make direct contacts with synapses that seems to be dependent, at least partly, on neuronal activity (14,27–29). Our study found that both anesthetics induced a reduction of microglial motility in the somatosensory cortex. Our results are in line with previous studies showing that blocking NMDAR-mediated glutamatergic transmission induced a significant decrease in microglial motility in retinal explants (−12.5% decrease) while GABA application decreased microglial motility as well (−7.9% decrease) (30). However the reduction that we observed with ketamine/xylazine do not match a recent study that report no or opposite effect of ketamine/xylazine anesthesia on microglial motility (7,31). Even though both studies were performed *in vivo*, several discrepancies should be highlighted: 1) we used a thin-skull cranial preparation, which is more immunologically inert compared to cranial window preparation used by the two studies; 2) in our case, the same microglia is imaged in presence and absence of anesthetics, whereas Sun *et al.* imaged different microglia between the conditions with 2-h rest between the two conditions.

Although we report clear effects of anesthetics, it is rather difficult to determine whether their action is direct on microglial cells. Indeed, various evidence report the presence of glutamate and GABA receptors on microglial surface (32,33). However microglia lack electrical responses to local application of GABA and glutamate in retinal slices (30), as well as to puffs of glutamate or NMDA in hippocampal slices (27) casting doubt on a direct action on microglia. The observed effect could also be due to side effects of anesthetics for example pentobarbital also target alpha-amino-3-hydroxy-5-methyl-4-isoxazolepropionic acid receptors (AMPAR) (34,35) or voltage-dependent Na^+ channels, while

ketamine affects also the cholinergic muscarinic receptors (antagonistic effect) (36,37) and α(alpha) and β(beta) adrenergic receptors (agonistic effect) (38). Ketamine and pentobarbital could also target ion channels expressed by microglial cells and alter membrane properties (39,40). A recent study found a direct impact of gaseous anesthetics on microglial motility by action on tandem pore domain halothane inhibited K(+) channel (THIK)-1, a two-pore domain K^+ channel present on microglial cells (8). Likewise, possible changes in extracellular ion concentration due to altered neurotransmission by anesthesia might affect microglial resting potential and consequently microglial motility.

Anesthetics could also modulate microglia through indirect action. For example, extracellular nucleotides, in particular adenosine triphosphate (ATP), elicit membrane currents in microglial cells via ionotropic (P2X) and metabotropic (P2Y) purinergic receptors and affect microglial motility (27,30,41–44). Importantly, ATP is co-released with the main transmitters from neurons (45) and from astrocytes (46) at synapses in response to neuronal activity. ATP released could lead to a chemotactism of microglial processes toward highly active spines (14) possibly by a NMDAR-dependent ATP release (27). Thus, a reduction of ATP release caused by reduction of neuronal activity may decrease microglial motility. Finally, both *iv* and inhaled anesthetics have been shown to disrupt astrocyte calcium signaling in the cortex (47) and consequently the calcium-dependent release of ATP that could regulate microglial motility.

Morphological changes of microglial cells are often associated with microglial activation. Indeed, immunohistochemistry studies rely on quantification of microglial morphology to characterize inflammation. We found both *in vivo and ex vivo* that ketamine/xylazine and barbiturates affected microglial morphology in different ways. Ketamine/xylazine anesthesia caused a significant reduction of microglial complexity overall, particularly by decreasing the number of segments and branching points. It has previously been found that blocking NMDAR by D-AP5 resulted in significant decreases in all morphological parameters studied, such as the total dendritic length, the total branch point and the dendritic tree area in retinal explants (30). Because β-adrenergic receptor agonist, isoproterenol, has

been shown to induced a considerable decrease in the ramifications of resting microglia in acute slices (48), another effect of ketamine could be through its agonist action on β-adrenergic agonist receptors. We found no effect of pentobarbital on microglial complexity in the somatosensory cortex *in vivo*. More precise *ex vivo* quantifications found that barbiturates affected only the cytoplasm area of microglial cells, which is defined as the cell body area associated with the cytoplasmic area of the primary ramifications. In that regard, the study of Fontainhas *et al.* shows that GABA application in retinal explants affected microglial complexity (30). The discrepancy between these results could be explained by the heterogeneity of microglial cells between retina and CNS. Another explanation could be the use of barbiturates that target specifically $GABA_A$ while the administration of GABA might also target $GABA_C$ and $GABA_B$ receptors.

We then assessed whether the aforementioned morphological changes by anesthesia administration are similar among different brain regions. We studied microglial cells in the hippocampus and the frontal cortex, two areas where microglial cells contribute to neuropsychiatric disorders such as dementia or depression (49,50). Ketamine/xylazine caused a significant reduction in both the complexity and the total ramification length in both regions. This reduction was accompanied by a reduction in the number of segments and nodes rank 1 and 2 in the frontal cortex, but not in the hippocampus. The effects of thiopental also differed depending on the brain region. Thiopental caused a reduction in the cytoplasm area of the hippocampus, but not the frontal cortex. The discrepancy between the effects of anesthetics on microglial cells in these different regions may come from several reasons. First, the composition and function of glutamatergic and GABAergic networks may vary between the hippocampus and cortex. Second, the neuronal NMDA and $GABA_A$ receptor subtype composition may differ between areas. Third, microglial phenotypic heterogeneity: microglial expression profiles, receptor and channel distribution, as well as the resting potential of microglial cells may vary between different regions (51–54), thus contribute to different responses of microglial cells.

Conclusion

Overall, our study shows that both anesthetics reduced microglial surveillance. Ketamine/xylazine had a more considerable effect on microglial morphology, whereas the effect of barbiturates was limited to the cytoplasm area. Even though both anesthetics alter microglial motility, barbiturates seem more appropriate anesthetic agents for the study of microglial morphology.

Our findings have major implications for research studies. Many *ex vivo* studies are based on the characterization of microglial morphology to evaluate the activation status and inflammatory profile of microglial cells and may thus be biased by the type of anesthetic used. Furthermore, the disclosed alterations of microglial motility and morphology may have unintended consequences on microglial responses *in vivo* and thus bias experimental results. Future studies need to assess the potential alterations of additional parameters associated with microglial morphology and motility under anesthesia. These include microglial interaction with spines and neuronal networks, the phagocytic capacity of microglial cells, as well as the cytokine secretion. Furthermore, it is important to determine whether anesthetics maintain their effects on microglial cells' morphology and motility *in vivo* past anesthesia and the potential long-term effects. If this is the case, multiple imaging sessions with repeated animal exposure to anesthesia may have serious consequences on the experimental results. Finally, since the developing brain and the aging brain are more vulnerable to anesthesia-induced neurotoxicity, we need to study the short-term and long-term effects of anesthetic agents on microglial cells in these populations.

Competing interests

The authors declare that none of them have competing interests.

Author Contribution

IH and FV performed research; IH, JCC, FV performed analysis; IH, FV, JCC, OP wrote the manuscript; VD, JH, FC, FV, OP designed research and proofread the manuscript.

Acknowledgements

IH was funded by the French ministry for research. We thank the CRNL and CIQLE imaging facilities for access to the two-photon microscope and ALECS facilities for mice housing. This work was also supported by the Fondation des Gueules Cassées and the SFAR (Société Française d'Anesthésie-Réanimation), ANR MICROMEM and INSERM. The authors thank Dr Anne Danckaert for her help.

List of abbreviations

AMPA: Alpha-amino-3-hydroxy-5-Methyl-4-isoxazolePropionic Acid

ATP: Adenosine TriPhosphate

CEA: Covered Environment Area

CI: Complexity Index

CNS: Central Nervous System

EEG: ElectroEncephaloGraphy

EMG: ElectroMyoGraphy

GABA: Gamma-AminoButyric Acid A

GFP: Green Fluorescent Protein

NMDA: N-methyl-D-aspartate

Figures

Figure 1. Ketamine/xylazine and pentobarbital anesthesia are associated with different patterns of neuronal activity. (A-F) Examples of EEG traces (A, C, E) and their corresponding amplitude distributions (B, D, F) in different conditions: control (A, B), during ketamine/xylazine (C, D) and pentobarbital (E, F) anesthesia. (G-L) Characteristic power spectrum (G, I, K) and normalized color-coded logarithmic amplitude of time-frequency graphs (H, J, L) in control condition (G, H), and during ketamine-xylazine (I, J) and pentobarbital (K, L) anesthesia.

Figure 2. Ketamine/xylazine and pentobarbital anesthesia reduce microglial motility *in vivo,* while microglial complexity is reduced by ketamine/xylazine only. (A, D) Representative images showing microglial complexity between control (in green) and ketamine/xylazine anesthesia (A) or pentobarbital (in red) anesthesia (D). (B, C) Quantification of microglial complexity (B) and motility (C) for control and ketamine/xylazine anesthesia (n=6 $CX3CR1^{GFP/+}$ mice, 3 microglia analyzed per mouse, Wilcoxon test). (E, F) Quantification of microglial complexity (E) and motility (F) for control and pentobarbital anesthesia (n=6 $CX3CR1^{GFP/+}$ mice, 3 microglia analyzed per mouse, Wilcoxon test). Bars represent mean±SEM. *indicates $p<0.05$.

Figure 3. Whole brain variability by morphological criteria in the different conditions. Two regions have been explored: hippocampus (H) and frontal cortex (FC) in three different conditions: control, ketamine/xylazine (ket/xyl) and thiopental. (A-C) Morphological criteria characterizing a representative microglial cell in each condition. The scale bars equal 5µm. (D-I) Microglial morphology was characterized using the following parameters: microglial cytoplasm (D), the complexity index (E), the cell environment area in μm^2 (F), the number of segments by cell (G), the total ramification length in µm (H) and the number of nodes (rank #1 & #2) by cell (I). Data shown are mean±SD in the control, ketamine/xylazine and thiopental conditions (n=5, n=6 and n = 6, respectively). In $CX3CR1^{GFP/+}$ mice, 576 to 988 microglial cells were analyzed by region and by animal. ANOVA Kruskal-Wallis test was used to compare the different regions. *$p<0.05$.

Figure 4. Frontal cortex variability by morphological criteria in the different conditions. (A-C) Microglial modelization characterizing a representative panel of microglial cells in each condition in the frontal cortex. The scale bars equal 10µm. (D-I) Microglial morphology was characterized using the following parameters: microglial cytoplasm (D), the complexity index (E), the cell environment area in μm^2 (F), the number of segments by cell (G), the total ramification length in µm (H) and the number of nodes (rank #1 & #2) by cell (I). Data shown are mean±SD in the control, ketamine/xylazine and thiopental conditions (n=5, n=6 and n=6, respectively). In $CX3CR1^{GFP/+}$ mice, 305 to 582 microglial cells were analyzed by region and by animal. ANOVA Kruskal-Wallis test was used to compare the different regions. *p<0.05.

Figure 5. Hippocampus variability by morphological criteria in the different conditions. Microglial morphology was characterized using the following parameters: microglial cytoplasm (A), the complexity index (B), the cell environment area in μm^2 (C), the number of segments by cell (D), the total ramification length in µm (E) and the number of nodes (rank #1 & #2) by cell (F). Data shown are mean±SD in the control, ketamine/xylazine and thiopental conditions (n = 5, n=6 and n = 6, respectively). In $CX3CR1^{GFP/+}$ mice, 272 to 448 microglial cells were analyzed by region and by animal. ANOVA Kruskal-Wallis test was used to compare the different regions. *p<0.05.

Bibliography:

1. Son Y. Molecular mechanisms of general anesthesia. Korean J Anesthesiol. 2010 Jul;59(1):3–8.

2. Vutskits L, Xie Z. Lasting impact of general anaesthesia on the brain: mechanisms and relevance. Nat Rev Neurosci. 2016 18;17(11):705–17.

3. Gomez-Nicola D, Perry VH. Microglial dynamics and role in the healthy and diseased brain: a paradigm of functional plasticity. Neurosci Rev J Bringing Neurobiol Neurol Psychiatry. 2015 Apr;21(2):169–84.

4. Parkhurst CN, Yang G, Ninan I, Savas JN, Yates JR, Lafaille JJ, et al. Microglia promote learning-dependent synapse formation through brain-derived neurotrophic factor. Cell. 2013 Dec 19;155(7):1596–609.

5. Xavier AL, Menezes JRL, Goldman SA, Nedergaard M. Fine-tuning the central nervous system: microglial modelling of cells and synapses. Philos Trans R Soc B Biol Sci [Internet]. 2014 Oct 19 [cited 2017 Aug 20];369(1654). Available from: http://www.ncbi.nlm.nih.gov/pmc/articles/PMC4173279/

6. Hristovska I, Pascual O. Deciphering Resting Microglial Morphology and Process Motility from a Synaptic Prospect. Front Integr Neurosci. 2015;9:73.

7. Sun W, Suzuki K, Toptunov D, Stoyanov S, Yuzaki M, Khiroug L, et al. In vivo Two-Photon Imaging of Anesthesia-Specific Alterations in Microglial Surveillance and Photodamage-Directed Motility in Mouse Cortex. Front Neurosci. 2019;13:421.

8. Madry C, Kyrargyri V, Arancibia-Cárcamo IL, Jolivet R, Kohsaka S, Bryan RM, et al. Microglial Ramification, Surveillance, and Interleukin-1β Release Are Regulated by the Two-Pore Domain K+ Channel THIK-1. Neuron. 2018 Jan 17;97(2):299-312.e6.

9. Nakki R, Nickolenko J, Chang J, Sagar SM, Sharp FR. Haloperidol prevents ketamine- and phencyclidine-induced HSP70 protein expression but not microglial activation. Exp Neurol. 1996 Feb;137(2):234–41.

10. Kannan G, Kambhampati SP, Kudchadkar SR. Effect of anesthetics on microglial activation and nanoparticle uptake: Implications for drug delivery in traumatic brain injury. J Control Release Off J Control Release Soc. 2017 Mar 21;

11. Zhao Y, Huang L, Xu H, Wu G, Zhu M, Tian J, et al. Neuroinflammation Induced by Surgery Does Not Impair the Reference Memory of Young Adult Mice. Mediators Inflamm. 2016;2016:3271579.

12. Davis EJ, Foster TD, Thomas WE. Cellular forms and functions of brain microglia. Brain Res Bull. 1994;34(1):73–8.

13. Verdonk F, Petit A-C, Abdel-Ahad P, Vinckier F, Jouvion G, de Maricourt P, et al. Microglial production of quinolinic acid as a target and a biomarker of the antidepressant effect of ketamine. Brain Behav Immun. 2019 Jun 28;

14. Akiyoshi R, Wake H, Kato D, Horiuchi H, Ono R, Ikegami A, et al. Microglia Enhance Synapse Activity to Promote Local Network Synchronization. eNeuro. 2018 Oct;5(5).

15. Nakajima K, Kohsaka S. Microglia: activation and their significance in the central nervous system. J Biochem (Tokyo). 2001 Aug;130(2):169–75.

16. Hellwig S, Brioschi S, Dieni S, Frings L, Masuch A, Blank T, et al. Altered microglia morphology and higher resilience to stress-induced depression-like behavior in CX3CR1-deficient mice. Brain Behav Immun. 2016;55:126–37.

17. Raj DDA, Jaarsma D, Holtman IR, Olah M, Ferreira FM, Schaafsma W, et al. Priming of microglia in a DNA-repair deficient model of accelerated aging. Neurobiol Aging. 2014 Sep;35(9):2147–60.

18. Verdonk F, Roux P, Flamant P, Fiette L, Bozza FA, Simard S, et al. Phenotypic clustering: a novel method for microglial morphology analysis. J Neuroinflammation. 2016 Dec 17;13(1):153.

19. Green CJ, Knight J, Precious S, Simpkin S. Ketamine alone and combined with diazepam or xylazine in laboratory animals: a 10 year experience. Lab Anim. 1981 Apr;15(2):163–70.

20. Naccarato EF, Hunter WS. Anaesthetic effects of various ratios of ketamine and xylazine in rhesus monkeys (*Macaca mulatta*). Lab Anim. 1979 Oct;13(4):317–9.

21. Garcia PS, Kolesky SE, Jenkins A. General anesthetic actions on GABA(A) receptors. Curr Neuropharmacol. 2010 Mar;8(1):2–9.

22. Goldstein A, Aronow L. The durations of action of thiopental and pentobarbital. J Pharmacol Exp Ther. 1960 Jan;128:1–6.

23. Michelson NJ, Kozai TDY. Isoflurane and ketamine differentially influence spontaneous and evoked laminar electrophysiology in mouse V1. J Neurophysiol. 2018 01;120(5):2232–45.

24. Kato R, Yamanaka M, Yokota E, Koshikawa N, Kobayashi M. Spike Timing Rigidity Is Maintained in Bursting Neurons under Pentobarbital-Induced Anesthetic Conditions. Front Neural Circuits. 2016;10:86.

25. Davalos D, Grutzendler J, Yang G, Kim JV, Zuo Y, Jung S, et al. ATP mediates rapid microglial response to local brain injury in vivo. Nat Neurosci. 2005 Jun;8(6):752–8.

26. Nimmerjahn A, Kirchhoff F, Helmchen F. Resting microglial cells are highly dynamic surveillants of brain parenchyma in vivo. Science. 2005 May 27;308(5726):1314–8.

27. Eyo UB, Peng J, Swiatkowski P, Mukherjee A, Bispo A, Wu L-J. Neuronal hyperactivity recruits microglial processes via neuronal NMDA receptors and microglial P2Y12 receptors after status epilepticus. J Neurosci Off J Soc Neurosci. 2014 Aug 6;34(32):10528–40.

28. Tremblay M-È, Lowery RL, Majewska AK. Microglial interactions with synapses are modulated by visual experience. PLoS Biol. 2010 Nov 2;8(11):e1000527.

29. Wake H, Moorhouse AJ, Jinno S, Kohsaka S, Nabekura J. Resting microglia directly monitor the functional state of synapses in vivo and determine the fate of ischemic terminals. J Neurosci Off J Soc Neurosci. 2009 Apr 1;29(13):3974–80.

30. Fontainhas AM, Wang M, Liang KJ, Chen S, Mettu P, Damani M, et al. Microglial morphology and dynamic behavior is regulated by ionotropic glutamatergic and GABAergic neurotransmission. PloS One. 2011 Jan 25;6(1):e15973.

31. Liu YU, Ying Y, Li Y, Eyo UB, Chen T, Zheng J, et al. Neuronal network activity controls microglial process surveillance in awake mice via norepinephrine signaling. Nat Neurosci. 2019 Nov;22(11):1771–81.

32. Kaindl AM, Degos V, Peineau S, Gouadon E, Chhor V, Loron G, et al. Activation of microglial N-methyl-D-aspartate receptors triggers inflammation and neuronal cell death in the developing and mature brain. Ann Neurol. 2012 Oct;72(4):536–49.

33. Kuhn SA, van Landeghem FKH, Zacharias R, Färber K, Rappert A, Pavlovic S, et al. Microglia express GABA(B) receptors to modulate interleukin release. Mol Cell Neurosci. 2004 Feb;25(2):312–22.

34. Ticku MK, Kulkarni SK, Mehta AK. Modulatory role of GABA receptor subtypes and glutamate receptors in the anticonvulsant effect of barbiturates. Epilepsy Res Suppl. 1992;8:57–62.

35. Zhu H, Cottrell JE, Kass IS. The effect of thiopental and propofol on NMDA- and AMPA-mediated glutamate excitotoxicity. Anesthesiology. 1997 Oct;87(4):944–51.

36. Lydic R, Baghdoyan HA. Ketamine and MK-801 decrease acetylcholine release in the pontine reticular formation, slow breathing, and disrupt sleep. Sleep. 2002 Sep 15;25(6):617–22.

37. Yamakura T, Chavez-Noriega LE, Harris RA. Subunit-dependent inhibition of human neuronal nicotinic acetylcholine receptors and other ligand-gated ion channels by dissociative anesthetics ketamine and dizocilpine. Anesthesiology. 2000 Apr;92(4):1144–53.

38. Kubota T, Hirota K, Yoshida H, Takahashi S, Anzawa N, Ohkawa H, et al. Effects of sedatives on noradrenaline release from the medial prefrontal cortex in rats. Psychopharmacology (Berl). 1999 Oct;146(3):335–8.

39. Hantal G, Fábián B, Sega M, Jójárt B, Jedlovszky P. Effect of general anesthetics on the properties of lipid membranes of various compositions. Biochim Biophys Acta Biomembr. 2019 01;1861(3):594–609.

40. Zhou C, Liu J, Chen X-D. General anesthesia mediated by effects on ion channels. World J Crit Care Med. 2012 Jun 4;1(3):80–93.

41. Boucsein C, Zacharias R, Färber K, Pavlovic S, Hanisch U-K, Kettenmann H. Purinergic receptors on microglial cells: functional expression in acute brain slices and modulation of microglial activation in vitro. Eur J Neurosci. 2003 Jun;17(11):2267–76.

42. Dissing-Olesen L, LeDue JM, Rungta RL, Hefendehl JK, Choi HB, MacVicar BA. Activation of neuronal NMDA receptors triggers transient ATP-mediated microglial process outgrowth. J Neurosci Off J Soc Neurosci. 2014 Aug 6;34(32):10511–27.

43. Ulmann L, Levavasseur F, Avignone E, Peyroutou R, Hirbec H, Audinat E, et al. Involvement of P2X4 receptors in hippocampal microglial activation after status epilepticus. Glia. 2013 Aug;61(8):1306–19.

44. Wu L-J, Vadakkan KI, Zhuo M. ATP-induced chemotaxis of microglial processes requires P2Y receptor-activated initiation of outward potassium currents. Glia. 2007 Jun;55(8):810–21.

45. Pankratov Y, Lalo U, Verkhratsky A, North RA. Vesicular release of ATP at central synapses. Pflugers Arch. 2006 Aug;452(5):589–97.

46. Hamilton NB, Attwell D. Do astrocytes really exocytose neurotransmitters? Nat Rev Neurosci. 2010 Apr;11(4):227–38.

47. Thrane AS, Thrane VR, Zeppenfeld D, Lou N, Xu Q, Nagelhus EA, et al. General anesthesia selectively disrupts astrocyte calcium signaling in the awake mouse cortex. Proc Natl Acad Sci U S A. 2012 Nov 13;109(46):18974–9.

48. Gyoneva S, Traynelis SF. Norepinephrine modulates the motility of resting and activated microglia via different adrenergic receptors. J Biol Chem. 2013 May 24;288(21):15291–302.

49. Heneka MT, Carson MJ, El Khoury J, Landreth GE, Brosseron F, Feinstein DL, et al. Neuroinflammation in Alzheimer's disease. Lancet Neurol. 2015 Apr;14(4):388–405.

50. Setiawan E, Attwells S, Wilson AA, Mizrahi R, Rusjan PM, Miler L, et al. Association of translocator protein total distribution volume with duration of untreated major depressive disorder: a cross-sectional study. Lancet Psychiatry. 2018;5(4):339–47.

51. De Biase LM, Schuebel KE, Fusfeld ZH, Jair K, Hawes IA, Cimbro R, et al. Local Cues Establish and Maintain Region-Specific Phenotypes of Basal Ganglia Microglia. Neuron. 2017 Jul 19;95(2):341-356.e6.

52. Grabert K, Michoel T, Karavolos MH, Clohisey S, Baillie JK, Stevens MP, et al. Microglial brain region-dependent diversity and selective regional sensitivities to aging. Nat Neurosci. 2016 Mar;19(3):504–16.

53. Guneykaya D, Ivanov A, Hernandez DP, Haage V, Wojtas B, Meyer N, et al. Transcriptional and Translational Differences of Microglia from Male and Female Brains. Cell Rep. 2018 Sep 4;24(10):2773-2783.e6.

54. Hanisch U-K. Functional diversity of microglia - how heterogeneous are they to begin with? Front Cell Neurosci. 2013;7:65.

FIGURE 1

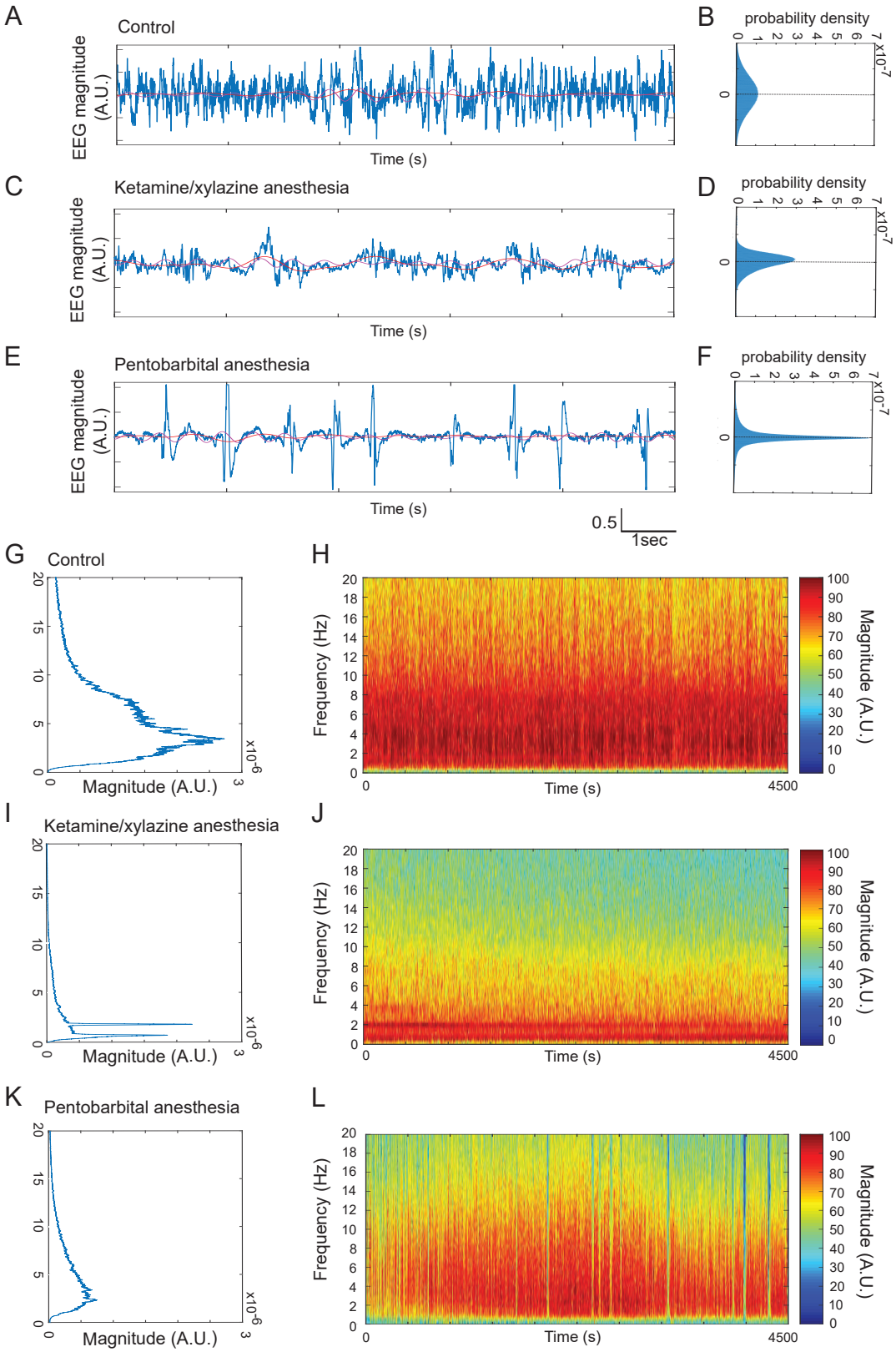
A
Control
EEG magnitude (A.U.)
Time (s)
B
probability density
x10^-7
C
Ketamine/xylazine anesthesia
EEG magnitude (A.U.)
Time (s)
D
probability density
x10^-7
E
Pentobarbital anesthesia
EEG magnitude (A.U.)
Time (s)
0.5
1sec
F
probability density
x10^-7
G
Control
Magnitude (A.U.)
x10^-6
H
Frequency (Hz)
Time (s)
4500
Magnitude (A.U.)
I
Ketamine/xylazine anesthesia
Magnitude (A.U.)
x10^-6
J
Frequency (Hz)
Time (s)
4500
Magnitude (A.U.)
K
Pentobarbital anesthesia
Magnitude (A.U.)
x10^-6
L
Frequency (Hz)
Time (s)
4500
Magnitude (A.U.)

FIGURE 2

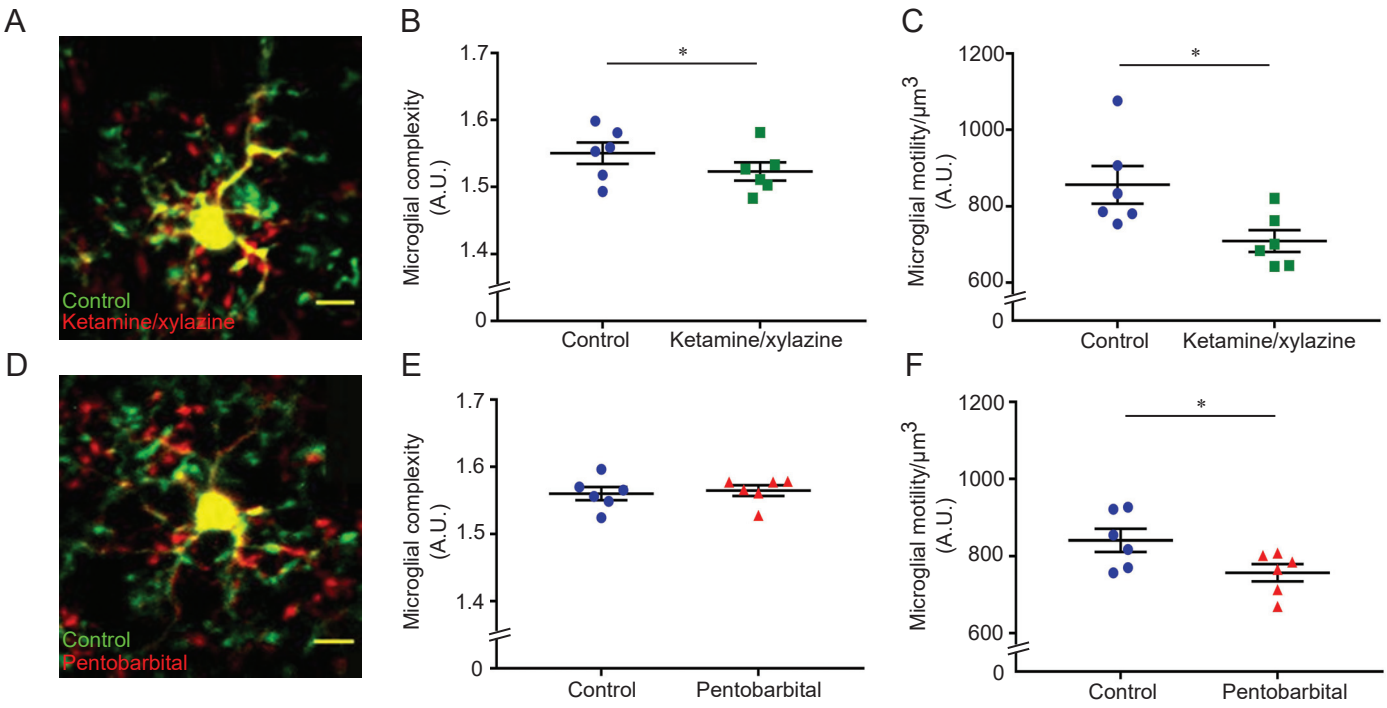
A
Control
Ketamine/xylazine
B
Microglial complexity (A.U.)
1.7
1.6
1.5
1.4
0
*
Control
Ketamine/xylazine
C
Microglial motility/µm3 (A.U.)
1200
1000
800
600
0
*
Control
Ketamine/xylazine
D
Control
Pentobarbital
E
Microglial complexity (A.U.)
1.7
1.6
1.5
1.4
0
Control
Pentobarbital
F
Microglial motility/µm3 (A.U.)
1200
1000
800
600
0
*
Control
Pentobarbital

FIGURE 3

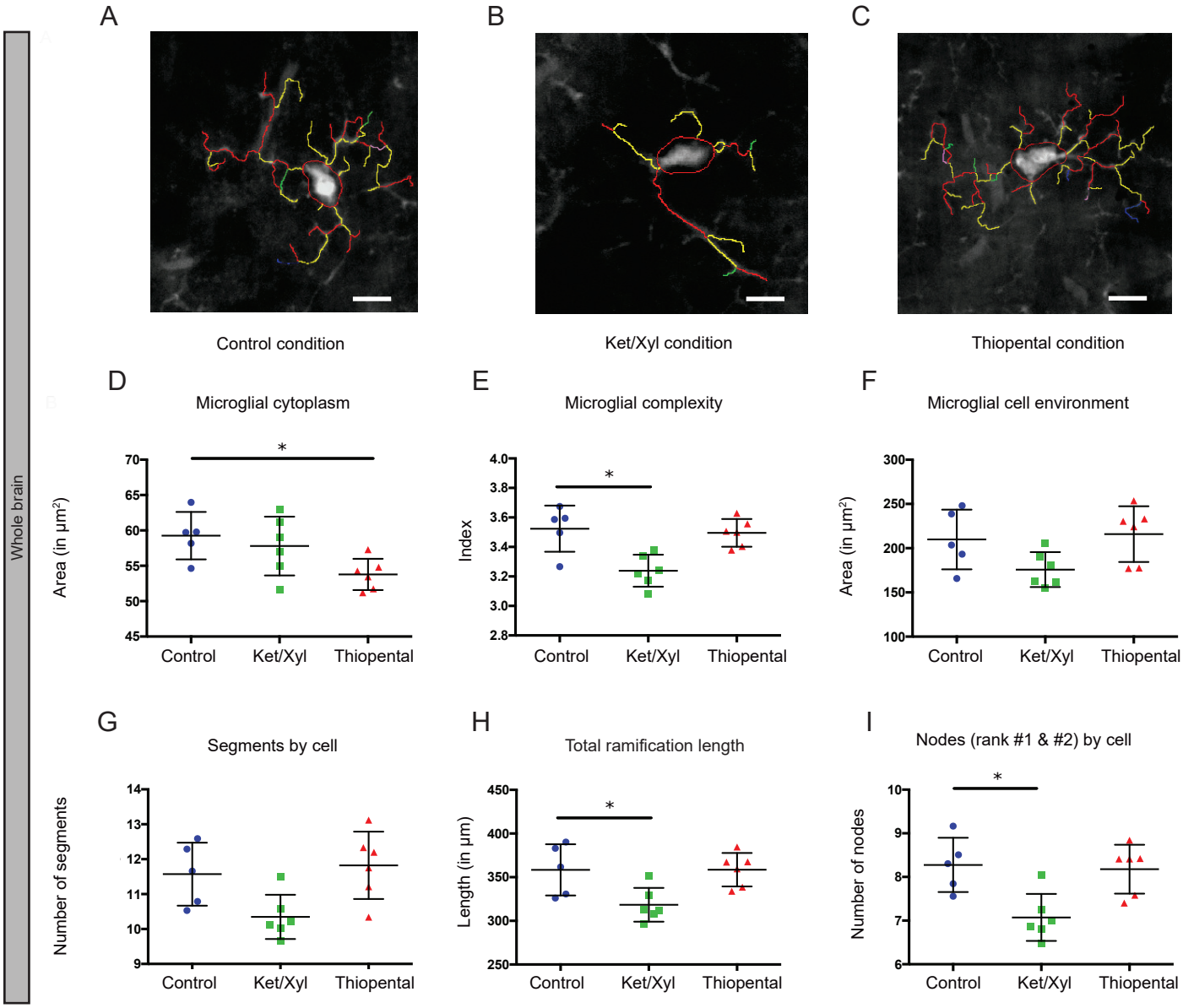
Whole brain
A
B
C
Control condition
Ket/Xyl condition
Thiopental condition
D
Microglial cytoplasm
Area (in µm²)
E
Microglial complexity
Index
F
Microglial cell environment
Area (in µm²)
G
Segments by cell
Number of segments
H
Total ramification length
Length (in µm)
I
Nodes (rank #1 & #2) by cell
Number of nodes
Control
Ket/Xyl
Thiopental

FIGURE 4

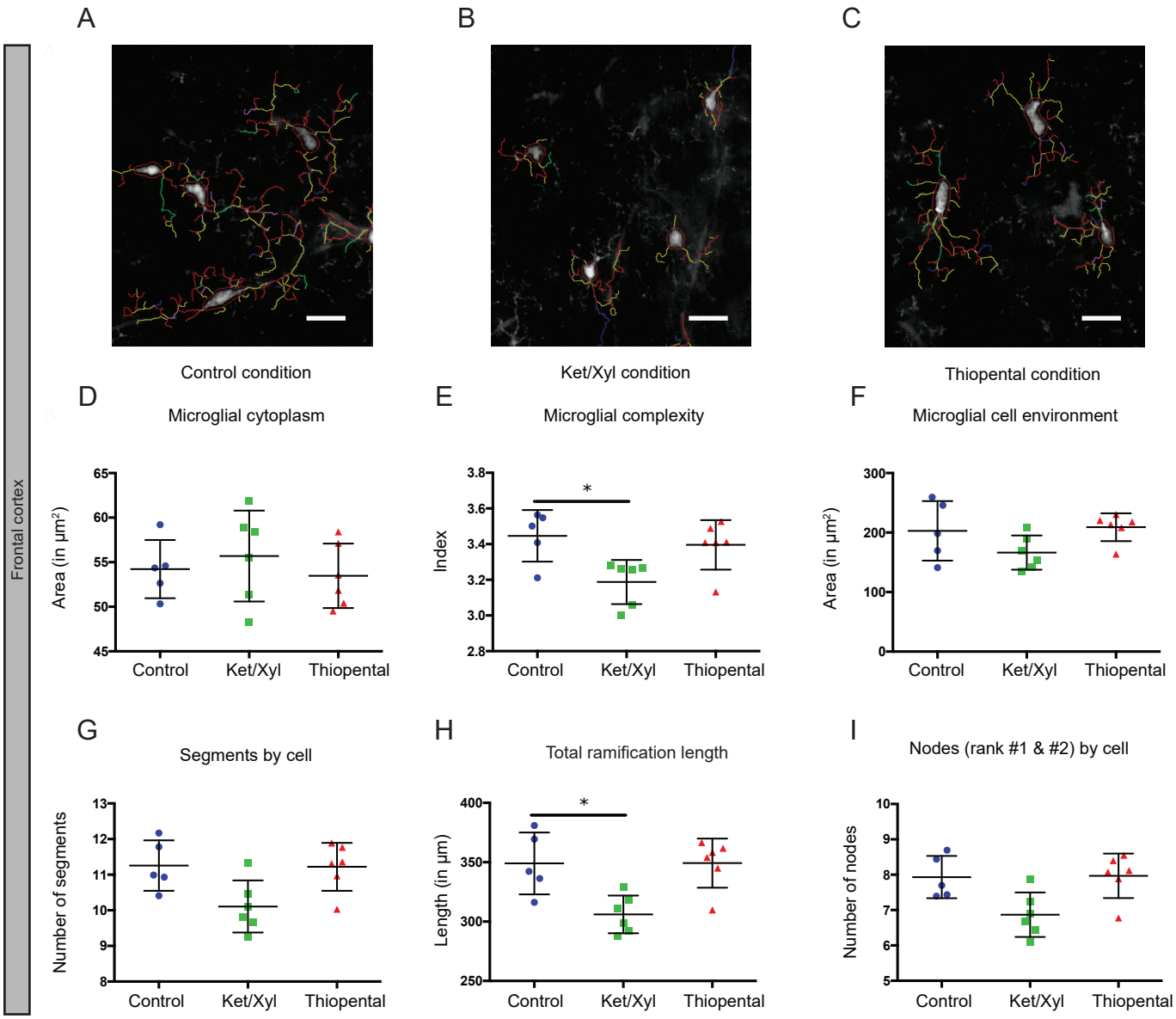
A
B
C
Frontal cortex
Control condition
Ket/Xyl condition
Thiopental condition
D
Microglial cytoplasm
Area (in µm²)
65
60
55
50
45
Control
Ket/Xyl
Thiopental
E
Microglial complexity
Index
3.8
3.6
3.4
3.2
3.0
2.8
*
Control
Ket/Xyl
Thiopental
F
Microglial cell environment
Area (in µm²)
300
200
100
0
Control
Ket/Xyl
Thiopental
G
Segments by cell
Number of segments
13
12
11
10
9
8
Control
Ket/Xyl
Thiopental
H
Total ramification length
Length (in µm)
400
350
300
250
*
Control
Ket/Xyl
Thiopental
I
Nodes (rank #1 & #2) by cell
Number of nodes
10
9
8
7
6
5
Control
Ket/Xyl
Thiopental

FIGURE 5

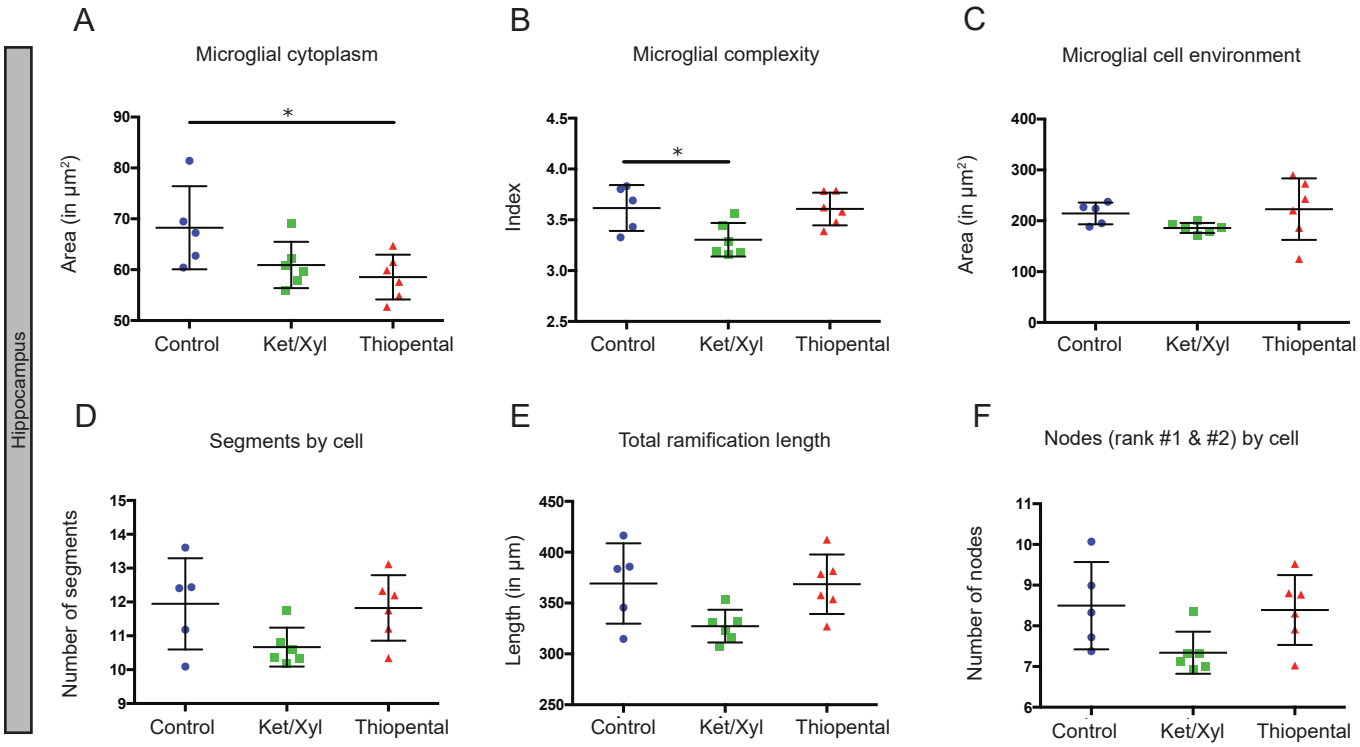
Hippocampus
A
Microglial cytoplasm
Area (in µm²)
90
80
70
60
50
*
Control
Ket/Xyl
Thiopental
B
Microglial complexity
Index
4.5
4.0
3.5
3.0
2.5
*
Control
Ket/Xyl
Thiopental
C
Microglial cell environment
Area (in µm²)
400
300
200
100
0
Control
Ket/Xyl
Thiopental
D
Segments by cell
Number of segments
15
14
13
12
11
10
9
Control
Ket/Xyl
Thiopental
E
Total ramification length
Length (in µm)
450
400
350
300
250
Control
Ket/Xyl
Thiopental
F
Nodes (rank #1 & #2) by cell
Number of nodes
11
10
9
8
7
6
Control
Ket/Xyl
Thiopental

ARTICLE 2

In preparation

Sleep decreases neuronal activity control of microglial dynamics

Hristovska I[1]*, Honnorat J[1], Comte JC[2], Pascual O[1]#

[1]INSERM U1217, CNRS UMR5310, Institut NeuroMyoGène, Lyon, France; Université Claude Bernard Lyon 1, Lyon, France

[2]INSERM U1028, CNRS UMR5292, Centre de Recherche en Neuroscience de Lyon, Lyon, France Université Claude Bernard Lyon 1, Lyon, France

Introduction

Microglial cells are the resident immune cells of the central nervous system (CNS) and their roles in various brain pathologies have been extensively studied (Prinz and Priller, 2014). In the healthy brain, microglia perform many physiological tasks that are essential for neuronal homeostasis and normal synaptic functions. During development, they participate in the refinement of neuronal circuits, including phagocytosis of synapses and trogocytosis of presynaptic structures, and their spatial arrangement is essential for generating domains of spine instability (Iida et al., 2019; Paolicelli et al., 2011; Schafer et al., 2012; Weinhard et al., 2018). They are also important for synapse maturation and filopodia formation in the developing somatosensory cortex (Hoshiko et al., 2012; Miyamoto et al., 2016; Weinhard et al., 2018). In the adult brain, microglia play a central role in learning-induced synapse formation by the secretion of brain-derived neurotrophic factor (BDNF) (Parkhurst et al., 2013). Moreover, microglial contact enhances synaptic activity and promotes neuronal network synchronization (Akiyoshi et al., 2018). These functions are critically dependent on microglial dynamics and functional properties in the healthy brain. Indeed, in non-pathological conditions, microglial cells present a ramified morphology with highly dynamic processes that extend and retract continuously (Davalos et al., 2005; Nimmerjahn et al., 2005). This movements allows them to survey the surrounding parenchyma and make transient contacts with other CNS elements, particularly synapses (Davalos et al., 2005; Nimmerjahn et al., 2005; Tremblay et al., 2010; Wake et al., 2009). The regulation of microglial motility and microglia-spine contact is still not well understood. Even though results are not straightforward, manipulation of neuronal activity revealed that increased neuronal activity is mostly accompanied by enhanced microglial dynamics while it is decreased in low neuronal activity regimen (Fontainhas et al., 2011; Li et al., 2012; Nimmerjahn et al., 2005; Tremblay et al., 2010). Moreover, microglial interactions with synapses seem to be activity dependent. For instance, reduction of neuronal activity in the visual cortex by means of eye nucleation, lowering body temperature or applying tetradotoxin (TTX) decreased microglia-synapse interactions (Wake et al., 2009). LTP induction in hippocampal slices increased the number of microglial processes and the duration of microglia-spine contacts (Pfeiffer et al., 2016). Highly active spines were the preferential target of microglial processes

in the somatosensory cortex, and microglial contact resulted in enhanced activity in the contacted spine (Akiyoshi et al., 2018). Thus, microglial processes seem to be sensing neuronal activity and are attracted towards sites of high neuronal activity, suggestive of microglia-to-neuron physical interactions (Eyo et al., 2014; Li et al., 2012; Wake et al., 2009).

Even though these studies suggest that microglial dynamics and microglia-synapse interactions are activity-dependent, most of them are performed in non-physiological conditions. These include *ex vivo* manipulations and use of anesthetized animals and/or sensory deprivation. Sleep-wake cycles are physiological states characterized by major changes in neuronal activity, including activity patterns and firing rate: wake is characterized by continuous asynchronous firing of cortical neurons, resulting in high-frequency, low-amplitude oscillations, while neurons alternate between synchronous periods of sustained neuronal firing and periods of neuronal silence, producing low-frequency, high-amplitude oscillations during sleep (Steriade, 1994). Beside neuronal activity, these vigilance states present distinct neuromodulation, extracellular space volume, ion and purine concentrations (Ding et al., 2016; Dworak et al., 2010). Although the exact function of sleep is still elusive, its role in synaptic homeostasis and plasticity is consensual as sleep and wake are important for learning and memory consolidation and are associated with molecular mechanisms of synaptic plasticity (Abel et al., 2013; Klinzing et al., 2019).
Taking into consideration the growing body of evidence of microglial guidance by neuronal activity and its potent involvement in synaptic plasticity, we wanted to assess the regulation of microglial dynamics and microglia-spine interactions during the vigilance states.
For this reason, we combined two-photon *in vivo* imaging of microglial cells and neuronal activity with electrophysiological recordings in vigil head-restrained mice. Our results show that global microglial motility and complexity are modulated by wake and sleep. At a single-spine level, microglial proximity and contact with spines were downregulated during NREM sleep in a state-dependent manner. Finally, we found that microglial contact with spines resulted in an increase of spine activity which was mainly observed during NREM sleep.

MATERIAL AND METHODS

Animals

To image microglial motility and complexity, we used six to ten-week-old male heterozygous *CX3CR1*$^{+/eGFP}$ mice, expressing enhanced green fluorescent protein (eGFP) under the control of the fractalkine receptor (CX3CR1) promoter (Jung et al., 2000). For microglial dynamics and spine activity analysis, *CX3CR1*^{CreERT2} mice (Parkhurst et al., 2013a) were crossed with *ROSA26-STOP-tdTomato* mice, to generate *CX3CR1*$^{+/CreERT2}$; *ROSA26-STOP-tdTomato*$^{(-/-)}$ mice. All transgenic mice were derived from the C57BL/6J strain. Mice were housed in individual cages with bedding and running wheels, under 12/12h light/dark cycle and were given access to food and water *ad libitum* at ALECS Facility. All experimental procedures were carried out in accordance with the European institutional guidelines and ethical committee (Apafis #DR2014-14 and Apafis #7839).

Induction of Cre activity with Tamoxifen treatment

Tamoxifen (catalog #T-5648; Sigma-Aldrich) was dissolved in warm sterile olive oil (catalog #8001-25-0, Sigma Aldrich, warmed at 55ºC) at a concentration of 20mg/ml. Six to seven-weeks-old *CX3CR1*$^{+/CreERT2}$*ROSA26-STOP-tdTomato*$^{(-/-)}$ mice were injected subcutaneously in the thigh at 0.4mg/g, twice 48h apart.

Surgery and habituation

For surgery, mice were deeply anesthetized with isoflurane (3-4%, Isovet, Piramal Healthcare, UK Ltd.) and mounted in a stereotaxic frame (D. Kopf Instruments). Isoflurane anesthesia was maintained at concentrations of 1-3% during the surgical procedure. To reduce post-operatory pain and inflammation, we administered Carprofen (5mg/kg s.c.) at the beginning of the surgery, and for two consecutive days following surgery. After the skull was thoroughly cleaned and exposed, two EEG (electroencephalogram) screws were inserted in the frontal and parietal cortex of the right hemisphere and two EMG (electromyogram) electrodes were inserted in the dorsal neck muscles. A custom-designed 0.5-mm diameter cranial implant was firmly glued on the left hemisphere using acrylic-based

dental adhesive resin cement (Super bond; Sun Medical). The skull was carefully thinned over the somatosensory cortex using a high-speed dental drill until reaching 20-30μm bone thickness. Most of the drilling was performed in cold, sterile saline solution which allowed continuous cooling and humidification of the bone to avoid heat-induced tissue injury, desiccation of the bone and inflammation. To visualize Ca^{2+} dynamics in spines of L2/3 pyramidal neurons of the somatosensory cortex, we performed a small craniotomy (300μm) and injected 500-700nl AAV1.Syn.GCaMP6m.WPRE.SV40 (UPenn Vector Core, $\geq 1x10^{13}$ viral genomes/ml) at a speed of 0.1μl/min. We used a glass pipette with a 20μm diameter tip which was maintained in the brain for 10 additional minutes to avoid backflow. We then placed a cover glass on top of a thin layer of cyanoacrylate glue over the thinned skull.

Following surgery, mice were left to recover for one week. Mice were then subjected to daily head-restrained habituation sessions over 7-10 days lasting progressively longer (from 10 minutes to 4 hours). At the beginning and end of each session, mice were rewarded with several drops of sweetened concentrated milk.

Vigilance state recordings

The vigilance states were monitored using real-time EEG/EMG differential recordings amplifier (Model 3000, A-M systems). EEG and EMG signals were sampled at 1kHz and band-pass filtered with 0.5Hz-300Hz and 10-500Hz, respectively. EEG/EMG data were analyzed using a custom-written MATLAB© software considering EEG frequency and power, as well as EMG power in 4-sec epochs. Wake was determined by increased EMG activity and high theta/delta ratio. NREM sleep was defined by low EMG activity and high delta/theta ratio, while REM sleep consisted of high theta activity (6-9Hz) and muscle atonia. Sleep and wake episodes were defined using a manually established threshold. Episodes containing >90% and <25% of wake were recognized as wake and sleep respectively. One episode of a given vigilance state lasted on average 5.86±0.46 minutes.

Two-photon *in vivo* imaging

Two-photon microscope (Olympus) with a mode-locked Ti:Sapphire laser (Mai-Tai, Spectra-Physics) and 20x water-immersion objective (0.95 N.A. Olympus) was used. Fluorescence was detected using a

560nm dichroic mirror coupled to 525/50nm and 650/40nm emission filters for eGFP and tdTomato, respectively. Laser power during imaging was maintained below 20mW.

Microglial motility and complexity during wake and sleep experiments. For imaging of microglial cells only, the laser was tuned to 900nm considering the excitation wavelength for eGFP. Microglial cells were imaged in the somatosensory cortex at a depth of 60-150 µm from the cortical surface. The imaging area was 200x200µm with a resolution of 521x521 pixels and pixel size of 0.38µm. Z-stacks containing 25-35 consecutive images were acquired every 30 seconds, with a step size of 1µm/optical section. A typical recording lasted approximately 30-35 minutes (60-70 Z-stacks).

Microglial dynamics and calcium imaging experiments. Imaging of microglial dynamics and spine calcium activity was performed using a laser tuned to 980nm for simultaneous excitation of both fluorescent proteins, eGFP and tdTomato. Imaging was performed in the L1 of the somatosensory cortex at a depth of 60-120 µm from the cortical surface because of higher spine density. The imaging area was 100x100µm with a resolution of 256x256 pixels and a 0.38µm pixel size. Z-stacks containing 14-16 consecutive images were acquired every 7 seconds, with a step size of 1µm/optical section. A typical recording lasted approximately 35 minutes (300 Z-stacks).

Analysis

Image processing and analysis were performed using ImageJ (National Institute of Mental Health, Bethesda, USA) and custom-written MatLab© code. Prior to realignment, microglial images were uniformly adjusted for contrast and brightness to reduce background noise. The Z-stacks for each microglial cell were then corrected for drift and movements in the x, y and z planes during time-lapse image acquisition. Each volume was registered to a reference volume (the first volume) using shift estimation from the cross-correlation peak by fast Fourier transform (FFT).

Microglial motility and complexity during wake and sleep experiments. We manually delimited and cropped regions of interest containing the totality of one microglial cell from the 200x200µm field of view. After realignment, standard deviation intensity projections from the Z-stacks were added to

generate 2D time-lapse movies. To quantify the complexity of microglial cells during wake and sleep, we converted the projections into binary and calculated the Hausdorff fractal dimension (Fernández-Martínez and Sánchez-Granero, 2014) for each time point. For surface area measurements, we thresholded each microglia, converted the projections into binary and measured microglial area overtime. Microglial complexity coefficient and surface area during wake and sleep were determined by averaging the values obtained for all images during episodes of wake or sleep for each imaging session.

To analyze microglial motility, we performed subtractions between consecutive Z-stack projections. For visualization purposes, the lost and gained pixels between each time point were pseudo colored in red and blue, resulting in images where red and blue points represented lost and newly formed processes, respectively. The number of summed pixels in subtracted images determined the global motility coefficient (arbitrary unit). This coefficient was normalized to the volume of each microglial Z-stack.

Microglial dynamics and spine calcium imaging during wake and sleep experiments. We first identified spines using a maximum intensity projection (MIP) of all the images contained in the time series. We then identified the time point with the higher intracellular Ca^{2+} level for each spine. For that time point, we scrolled through the Z-stack to find the three planes containing the majority of the spine (3µm volume). For each spine, we did a maximum intensity projection (MIP) time-series only from the three planes containing the spine. On the MIP time-series, we delimited a 15x15 µm region of interest (ROI) centered at the spine. For each spine, we generated a new time-series containing only the ROI. To include microglial processes from all planes surrounding the spine, we delimited 7-9 planes encompassing the planes above and below the spine and assessed microglial processes around the spine of interest. We generated standard deviation intensity (STD) projections for microglial cell images. Time-series were cropped at the previously described ROI. The 15x15µm maximum intensity and standard deviation projections were used for further analysis of spine activity and microglial dynamics respectively. For most of the microglia-spine analyses, we used 11-22 spines/mouse from 5 mice. For spine activity during sleep and wake, with and before/after contact, we used 10-18 spines/mouse from 5 mice. Spines that were not in contact with microglial processes during sleep or wake were excluded from analyses (n=16). For microglial proximity with dendritic spines, we used 7-15 spines/mouse from

5 mice, including spines that were never contacted by microglial processes. All spines that were very close to microglial cell bodies or primary processes were excluded from the microglia-spine distance analysis.

To quantify calcium activity in spines, we filtered the signal to remove background noise and measured the fluorescence intensity at the center of the spine and calculated the mean (baseline) and the standard deviation of the fluorescence intensity over time. Significant Ca^{2+} events were defined when the fluorescence intensity exceeded 0.85*std above the baseline. This threshold was determined by visual inspection for several spines allowing us to detect most of the Ca^{2+} transients. Background fluorescence was subtracted for each image.

To measure the distance and contact duration between microglial processes and dendritic spines, we used a custom-made Matlab code that plots the distance between the center of the spine and the moving front of the closest microglial process (Figure S3B). Since the size of the spine is variable, the threshold for microglia-spine contact was defined by visual inspection. Physical contact between microglial processes and dendritic spines was considered when the process was less than 500nm away from the edge of the spine and detectable in more than 3 consecutive focal planes. For contact duration, the totality of the time points below the threshold was added and multiplied by the time for each Z-stack (7 seconds).

For the study of microglial dynamics with regards to activity during sleep or wake, we classified spines in three categories depending on their level of activity during different vigilance states (Figure S3A): 1) for spines active during wake, the ratio of Ca^{2+} events between wake and sleep was > 1.3; this value corresponded approximately to 1*std; 2) for spines mostly active during sleep, the ratio of Ca^{2+} events between sleep and wake was > 1.3 and 3) intermediary spines, active both during wake and sleep, with a ratio of Ca^{2+} events < 1.3.

For illustration purposes, brightness and contrast of the images were adjusted.

Statistics. All statistical analyses were performed using the Prism V statistical analysis software (GraphPad, La Jolla, Ca). For microglial complexity, motility and surface area comparisons during the vigilance states, we used Wilcoxon test and all n-values represent individual animals. For experiments

assessing microglial dynamics and spine activity, n-values represent individual spines obtained from two videos analyzed per animal. For these analyses, we used two-tailed paired t-test where appropriate, Kolmogorov-Smirnoff test for cumulative distributions and Pearson's correlation test for correlation analyses. All values reported are mean±SEM. Significance of $p<0.05$ was used for all analyses.

RESULTS

Vigilance states influence microglial motility and complexity

To examine whether microglial complexity and motility are modified by vigilance states, we performed two-photon imaging of microglial cells in the somatosensory cortex while simultaneously assessing the electroencephalogram (EEG) and the electromyogram (EMG) (Figure 1A, 1B) in unanesthetized head-restrained mice. We imaged microglial cells for 35 minutes, and each session included several episodes of wake (dark blue) and NREM sleep (pale blue), during which microglial parameters for several cells were found to vary (Figure 1C, 1D). The same microglial cell imaged during wake and sleep showed increased motility (extensions in blue and retractions in red) and morphology (in black) during wake compared to sleep (Figure 1C). Quantifications of microglial morphology and motility *in vivo* for 34 microglial cells from 6 mice revealed that microglial surface area (Figure 1E, Wilcoxon test, *$p<0.05$), complexity (Figure 1F, Wilcoxon test, *$p<0.05$) and motility (Figure 1G, Wilcoxon test, *$p<0.05$) were significantly reduced during sleep when compared to wake.

Microglial motility and complexity are regulated by neuronal activity

Sleep and wake are characterized by different patterns of neuronal activity that were clearly observed during our imaging sessions. During wake, low-amplitude high-frequency desynchronized activity with a large spectral range is observed (Figure 2A), whereas sleep contains a larger amount of synchronized high-amplitude low-frequency activity with a lower spectral range (Figure 2B). To examine whether neuronal activity is an important parameter that affects microglial motility and complexity, we performed cross-correlation analysis between these parameters and EEG power. We found that both complexity (Figure 2C) and motility (Figure 2D) were negatively cross correlated with the EEG power.

As cross-correlation analysis indicates that microglia seems to be under the influence of the global network, we wanted to assess whether changes in motility and complexity are synchronized for several microglial cells in a large field of view or if individual microglia behave independently from each other, indicating a rather local regulation of motility and complexity. We thus studied the correlation of

microglial complexity and motility for microglial cells that are close or far apart (Figure 2E). We found that the changes in complexity are well correlated between microglial cells whatever their respective distances (Figure 2F), indicating that complexity might reflect global brain activity. On the other hand, the modifications of motility are not well correlated, and the correlation worsens as microglial cells are further apart (Figure 2G). These data suggest that even though the vigilance states seem to modulate microglial motility and complexity, this is done at different levels of integration. Complexity seems to respond to global neuronal activity, whereas motility could rather depend on the local network, likely at the synaptic level.

Microglial contact with spines is affected by neuronal activity and the vigilance states

To study microglial motility at the synaptic level, we simultaneously visualized microglial cells and fluctuations of intracellular Ca^{2+} concentration as a proxy of neuronal activity during the vigilance states (Figure 3A). To monitor neuronal activity, neurons in the somatosensory cortex were transduced with GCaMP6m in order to monitor neuronal activity in mice expressing the reporter gene tdTomato in microglia. We found contacts between microglial processes and spines with variable duration lasting on average ~4.38±0.42min (Figure S2A). In 35 minutes, active spines were contacted on average 35% of the time by microglial processes, even though this time span was highly variable (Figure S2B).

We next assessed the impact of the vigilance states on local microglia-spine distance and contacts. First, we did not find any significant difference in the proportion of spines contacted by microglial processes during wake and NREM sleep (Figure 3B, Wilcoxon test, *$p<0.05$). This is consistent with the fact that we did not observe a significant difference in spine activity during NREM sleep and wake (Figure S2C). When investigating the distribution of microglial processes around spines during the different vigilance states, we found that microglial processes were closer to spines during wake (Figure 3C, Kolmogorov-Smirnoff, ****$p<0.0001$). Interestingly, this difference was not observed when processes were very close or far from the spine, but for intermediate distances enclosed between 2 and 5µm. Furthermore, microglial processes spent slightly more time in contact with microglial processes during wake when compared to sleep (Figure 3D, paired t-test, two-tailed, *$p<0.05$), indicating that NREM sleep may counterbalance the positive attraction of neuronal activity.

We next wanted to know whether local spine activity affects microglial dynamics. Thus, we studied the correlation between the activity of the spine and the duration of microglia-spine contact. We found that this correlation was positive and that microglial processes seem to stay longer in contact with highly active spines (Figure 3E, Pearson's correlation test, *p<0.05). To test whether this profile may be observed by a random distribution of values for microglia-spine contact and spine activity, we performed the same analysis after randomizing our data. We did not find any correlation for this random data set (Figure 3F, Pearson's correlation test, *p<0.05).

NREM sleep limits the positive attraction of microglial processes towards synaptic activity

Next, we wanted to evaluate the effect of NREM sleep on the positive attraction of microglial processes towards synaptic activity. For this reason, we studied microglia-spine contacts in various regimens of synaptic activity during the vigilance states. To do this, we classified spines in three categories: spines mostly active during wake, spines mostly active during sleep and spines with comparable activity between NREM sleep and wake (Figure S3A). For sake of simplicity, we only report here results from spines that exhibited activity mostly during one of the vigilance states (spines with comparable activity during sleep and wake are presented in supplemental material). As previously, we found that microglial processes were closer to spines active during wake (Kolmogorov-Smirnov test, ****p<0.0001, Figure 4A and S3C). This observation holds true whatever the vigilance state during which the contact was monitored (Kolmogorov-Smirnov test, *p<0.05, Figure S3D and S3E). As suggested previously, microglial processes were closer during wake both for spines active during wake and spines active during sleep, although the difference between wake and NREM sleep was smaller for spine active during NREM sleep (Kolmogorov-Smirnov test, ****p<0.0001, Figure 4B and 4C). Spine activity was well correlated with microglia-spine contact duration for spines active during wake, but not as well for spines active during NREM sleep (Figure 4D and 4E, Pearson's correlation test, **** p<0.0001). In addition, the contact duration was reduced during NREM sleep for spines active during wake (Figure 4F, paired t-test, two-tailed, *p<0.05), indicating that those synapses might have a peculiar faith. This was not detected for spines active during NREM sleep (Figure 4G, paired t-test, two-tailed *p<0.05).

Microglial contact induces spine activity increase during NREM sleep

Since microglial contact was recently found to increase spine activity (Akiyoshi 2018), we wanted to evaluate the impact of the vigilance states in this regard. By quantifying spine Ca^{2+} transients when microglia process where not in contact (before/after contact) or during contact with spines, we confirmed that overall spine activity was significantly increased during contact with microglial processes without considering the vigilance state (Figure 5B, paired t-test, *p<0.05). Intriguingly, during contact, the increase in spine activity was significantly higher during NREM sleep compared to wake (Figure 5C, one-way ANOVA, *p<0.05), indicating that the contact-induced increase in activity may be mainly occurring during NREM.

DISCUSSION

In this work, we investigated the impact of neuronal activity and vigilance states on microglial dynamics at the network and synaptic level. We report here, that global microglial morphology and motility are modulated during the vigilance states and that these variations are at least partly related to changes in neuronal activity. We found that microglial morphology was globally following the changes of neuronal activity associated to the vigilance states, whereas motility was likely regulated at the synaptic level. Interactions between microglial processes and single spines were related to the level of spine activity but were impacted by the vigilance states. Finally, microglial contact increased spine activity, mostly during NREM sleep episodes.

Changes of activity during various vigilance states

We analyzed microglial morphology and motility in head-restrained mice who presented several sleep-wake episodes during a continuous imaging session. Even though sleep episodes were, as anticipated, shorter than those observed in freely moving animals (Franken et al., 1999), changes in neuronal activity characteristic of NREM sleep were well monitored by EEG recordings. Few episodes of REM sleep were detected but too short and rare to be analyzed reliably.

Local neuronal activity during different vigilance states has been an open question for many years. Recent data using imaging combined to electrophysiology indicate that at the somatic level, NREM

sleep is associated with a decrease of neuronal activity compared to wake (Niethard et al., 2016; Seibt et al., 2017). However, when calcium dynamics is monitored at the dendritic level, the decrease in calcium activity is absent (Seibt et al., 2017). In a similar manner, our monitoring of calcium activity in spines indicates that calcium activity does not change between wake and NREM sleep at the spine level (Figure S2C). The decoupling between somatic and dendritic firing has to be interpreted in the light of data indicating that interneurons activity is increased during NREM (Niethard et al., 2016) and that their projections on the somato-axonal compartment might gate dendritic activity. With our approach, we monitored only excitatory synapses as inhibitory neurons exhibit "en passant synapses" lacking spine heads.

EEG activity is coupled with microglial dynamics

Our findings indicate that NREM sleep is associated with a significant reduction of microglial morphological parameters and global motility. Both microglial complexity and surface area were reduced, pointing to a global decrease in microglial ramification during sleep. Cross-correlation analysis confirmed this result since it indicates that during sleep, when the EEG power is high, microglial motility and complexity are low. The opposite relationship holds true during wake. Modifications of microglial morphology and motility were observed for single sleep-wake episodes and were correlated with the corresponding activity patterns, suggesting a close relationship between neuronal activity and microglial dynamics.

An important finding of our study is that changes in morphology were mostly correlated for several microglial cells (<120µm apart) across the sleep-wake cycle, suggesting a global impact of neuronal activity on microglial morphology and its degree of ramification. However, it is difficult to distinguish the impact of neuronal activity versus the vigilance states. On the other hand, motility changes were not well correlated between microglial cells, indicating that motility is intrinsic to each microglia and potentially dependent on local mechanisms. These findings suggest that microglial cells are highly responsive to changes in neuronal activity occurring during the vigilance states and that microglial motility and morphology might rely on different signaling mechanisms.

Possible regulation of microglial dynamics during the vigilance states

The vigilance states are regulated by neuronal populations that send projections over widespread CNS areas (Wigren and Porkka-Heiskanen, 2018). Thus, excitatory and inhibitory neurotransmitters (NTs) fluctuate at the cortical level during the vigilance states. Cortical GABA levels were found to be significantly increased during NREM sleep compared to wake (Vanini et al., 2012). In line with our results, increase in ionotropic GABA transmission in retinal explants resulted in significant reduction of microglial motility and morphology (Fontainhas et al., 2011a). During wake, among other NTs, cortical norepinephrine and serotonin are increased (Bellesi et al., 2016; Portas et al., 2000), but these were found to have divergent effects on microglial cells. Norepinephrine caused microglial process retraction in acute brain slices (Gyoneva and Traynelis, 2013), whereas serotonin was found to have chemotactic effect for microglial processes (Etienne et al., 2019; Krabbe et al., 2012). Thus, even though microglial response to single NTs may be characterized, this should be taken with caution in the complex neuromodulatory environment of the sleep-wake cycles and needs to be further assessed.

Besides NTs, several ions exhibit state-dependent changes of concentration (Ding et al., 2016). For instance, arousal is associated with a rapid rise in $[K^+]_e$, occurring within seconds, along with a slower decrease in $[Ca^{2+}]_e$ and $[Mg^{2+}]_e$. It has been reported that baseline microglial surveillance and morphology are critically regulated by changes in $[K^+]_e$ via two-pore K^+ channel (THIK-1) (Madry et al., 2018). However, $[K^+]_e$ found to induce changes in microglial dynamics (Madry et al., 2018) is far beyond the slight concentration modifications (Ding et al., 2016) observed during the vigilance states, which makes regulation by THIK-1 unlikely. Thus, changes occurring in the extracellular space during the vigilance states are multiple and the exact mechanisms influencing microglial motility and morphology remain to be determined.

Neuronal activity positively attracts microglial processes

In physiological conditions, microglial processes are highly motile, but the properties, the target and the function of this dynamics remain unclear. Several studies *ex vivo* and in anesthetized animals have suggested that neuronal activity could control, at least partly, the dynamism of microglial processes

(Tremblay et al., 2010; Wake et al., 2009). To better understand the local regulation of microglial processes, we first assessed whether spine activity determines the proximity and contact of microglial processes with spines and how vigilance states may impact this process. We found that microglial processes spent more time in contact with spines displaying high calcium transient frequencies. These findings suggest that microglial processes may sense activity and be attracted towards spines depending on their activity. These results are in accordance with a recent study showing that microglia are preferentially in contact with active spines (Akiyoshi et al., 2018). Interestingly, we found that positive attraction toward active spines was affected by NREM sleep as microglial processes where found further away from spines and the correlation between the frequency of Ca^{2+} activity in spines and contact duration was reduced.

Mechanisms affecting changes in attraction towards spines during the vigilance states

The change of microglial processes attraction towards spines between vigilance states warrants further investigation and is beyond the scope of this paper but several explanations might be suggested. Purines, especially ATP and adenosine, are important chemical signaling molecules promoting attraction and retraction of microglial cell processes (Davalos et al., 2005; Dissing-Olesen et al., 2014; Eyo et al., 2014; Ohsawa et al., 2012; Orr et al., 2009) Purine concentrations vary during neuronal activity through local ATP release from active spines and astrocytes. It is thus possible that ATP release and gradient generation, differently regulated during the vigilance states, contribute to the disparity in microglial sensing of activity during sleep. Extracellular concentrations of ATP and adenosine also fluctuate during the vigilance states; adenosine accumulates during wake, while ATP levels increase at the onset of the light phase (Dworak et al., 2010; Porkka-Heiskanen et al., 2000). During this phase, Hayashi found that microglial morphology was reduced and proposed that it was due to the decrease in microglial P2Y12R, that varies due to the circadian rhythm (Hayashi, 2013). Our experiments were performed at the beginning of the light phase when sleep episodes are most frequent. However, the fluctuations of morphological parameters were correlated to the change of vigilance state. Due to the fragmented pattern of the vigilance states in mice, we can exclude the possibility that the circadian variation of P2Y12R expression is responsible for the fast change of morphology that we observed in our 35-minute

recordings. Finally, we do not know if changes observed during wake or sleep are due to different microglial sensibility to NT or to their fluctuation, and future studies need to assess these possibilities.

Microglia-spine contact modulates spine activity

Like previously reported by Akiyoshi *et al.*, we also observed an increase in spine activity during contact with microglial processes. Unexpectedly, this increase took place during sleep. The impact of this change of activity is difficult to assess but raises two intriguing points. First, microglia may modulate neuronal activity. This comes as no surprise since several recent reports indicate that microglia can modulate neuronal activity in given circumstances through the release of neuroactive molecules (Pascual et al., 2012; Zhang et al., 2014a). However, to our knowledge, this is the first report of microglia modulating neuronal activity in a specific vigilance state. Second, microglia could participate to functions associated with NREM sleep. Since sleep function is associated in general with synaptic homeostasis and memory, a tempting speculation would relate these specific contacts with synaptic scaling mechanisms. Two predominant theories of synaptic scaling during sleep are hotly debated. The active system consolidation theory proposes that sleep is involved in molecular and structural strengthening of synapses tagged during wake by active neuronal replay during slow wave sleep (Rasch and Born, 2013). Next to the idea of active system consolidation, the synaptic homeostasis hypothesis (SHY) suggests a global synaptic downscaling during sleep, which counters synaptic potentiation generated during wake (Tononi and Cirelli, 2014). Microglia may find their place in both hypothesis since they may affect synaptic activity by releasing cytokines, and neurotrophic factors, and by direct, contact-dependent mechanisms (Sheng et al., 2015b). A growing body of evidence suggests that microglia could also be involved in structural plasticity during the vigilance states by several mechanisms, including phagocytosing opsonized synapses during sleep (Choudhury et al., 2019). Microglia could also participate in synaptic plasticity through BNDF release since specifically removing BNDF in microglia resulted in reduction of learning-dependent spine formation and that sleep was found to promote branch-specific formation of dendritic spines after learning (Parkhurst et al., 2013; Yang et al., 2014).

Finally, microglia could also drive changes in the sleep-wake cycle. Pro-inflammatory cytokines, including interleukin (IL)-1β and tumor necrosis factor (TNF)α, were found to influence sleep pressure and enhance duration of NREMS and EEG delta wave power during NREM sleep (Krueger et al., 2011). TNFα was further suggested to promote microglial attraction at synapses and participate in the modulation of the sleep-wake cycles (Karrer et al., 2015). The possible role of microglial cells in the regulation of sleep is not mutually exclusive to our findings and needs to be addressed for a full understanding of the contribution of these cells to different and complementary aspects across the sleep-wake cycle.

In conclusion, we demonstrate that microglial motility and morphology are modulated by the vigilance states, both globally and at the level of the spine. Spine activity, and especially the vigilance state in which activity is occurring, impacts microglial proximity and contact with spines, resulting in functional consequences during contact. Based on our findings, we propose that microglial processes may sense neuronal activity particularly during wake and increase spine activity during sleep. These findings provide a foundation for future work understanding the mechanisms regulating microglial dynamics and microglia-spine activity across the vigilance states and excitingly, the potential functions of microglia in synaptic homeostasis. Understanding these mechanisms at the physiological levels is crucial for understanding how sleep disruptions and microglial activation in pathological conditions may impact these processes.

Figures

Figure 1. Microglial complexity and motility are modulated by the vigilance states. **(A, B)** Schematic representation of the experimental setup. **(A)** Head-restrained mice were trained for simultaneous two-photon imaging with electrophysiology (side view). **(B)** Fronto-parietal EEG and neck EMG electrodes were implanted, combined with a thin-skull cortical window preparation and calcium indicator injection (top view). **(C)** Selected frames showing microglial complexity (in black) and motility (extensions in blue and retractions in red) for one cell during wake and sleep. **(D)** Evolution of the complexity and motility for three microglial cells (yellow, red and black lines) during an entire imaging session containing several episodes of wake and sleep. **(E, F, G)** Quantification of **(E)** microglial surface area (51.85±2.38 and 48.605±2.18 for wake and sleep respectively, n=6 mice, 5-7 microglial cells/mouse, Wilcoxon test, *p<0.05), **(F)** microglial complexity (1.571±0.11 and 1.556±0.11 for wake and sleep respectively, n=6 mice, 5-7 microglial cells/mouse, Wilcoxon test, *p<0.05) and **(G)** motility (897.56±25.32 and 835.04±26.91 for wake and sleep respectively, n=6 mice, 5-7 microglial cells/mouse, Wilcoxon test, *p<0.05) during wake and sleep. Scale bar=10µm. Graphs show mean ± SEM. Individual points represent individual animals.

Figure 2. Neuronal activity correlates with microglial complexity and motility. (A, B) Characteristic electroencephalogram (EEG) and electromyogram (EMG) signals (left panel), power spectrum (middle panel) and color-coded time-frequency graph (right panel) during **(A)** wake and **(B)** sleep. **(C, D)** Cross-correlation analysis between **(C)** microglial complexity (r=-0.202, n=6 mice, 5-7 microglial cells/mouse) and **(D)** motility (r=-0.25, n=6 mice, 5-7 microglial cells/mouse) with electroencephalogram (EEG) power. **(E)** Examples of two microglial cells that are close (left panel) or far apart (right panel) with their corresponding correlation coefficients for complexity and motility. **(F, G)** Distribution of the correlation coefficient of the **(F)** complexity (average r=0.63, n=3-7 microglial cells/mouse) and **(G)** motility (average r=0.377, n=5 mice, 3-7 microglial cells/ mouse) between couples of microglial cells as a function of their distance. Scale bar=10µm. Graphs show mean ± SEM.

Figure 3. Microglia-spine contact is influenced by the vigilance states and neuronal activity. (A) Simultaneous imaging of microglial processes (red, arrow) and neuronal GCaMP6 expression (green) in the L1 of the primary somatosensory cortex. The arrowheads indicate contacts between microglial processes and spines. **(B)** Percentage of contacted spines by microglial processes during individual 4.2-minute wake and sleep episodes (0.667±0.027 and 0.608±0.035 for wake and sleep respectively, n=68 spines from 5 mice, Wilcoxon test, *p<0.05). **(C)** Cumulative distribution of the distance between the closest microglial process with spines during wake and sleep episodes (Kolmogorov-Smirnov test, *p<0.05). **(D)** Percentage of time the spine spends in contact with a microglial process during wake and sleep (0.38±0.0285 and 0.342±0.029, n=68 spines from 5 mice, paired t-test, two-tailed, *p<0.05). **(E)** Correlation between Ca^{2+} spike frequency and the duration of microglia-spine contact (r=0.31, n=68 spines from 5 mice, Pearson's correlation test, *p<0.05). **(F)** Correlation between spine activity and duration of microglia-spine contact for random data set (r=-0,09, n=68 spines from 5 mice, Pearson's correlation test, *p<0.05). Graphs show mean ± SEM.

Figure 4. Activity during wake exerts positive attraction towards microglial processes. (A) The cumulative distribution of microglia-spine distance for spines active during wake (blue line) and spines active during sleep (red line) (Kolmogorov-Smirnov test, *p<0.05). **(B, C)** The cumulative distribution of microglia-spine distance for **(B)** spines active during wake and **(C)** spines active during sleep during wake and sleep episodes (Kolmogorov-Smirnov test, *p<0.05). All distances are indicated in μm. **(D, E)** Correlation between microglia-spine contact duration and spine activity during **(D)** wake and **(E)** sleep (r=0.66 and 0.23 for spines active during wake and sleep respectively, n=26 for spines active during wake and n=25 for spines active during sleep, from 5 mice, Pearson's correlation test, *p<0.05). **(F, G)** For episodes of wake and sleep, duration of contact between microglial processes and spines active during **(F)** wake (407.62s±42.36 and 282.15s±39 for wake and sleep respectively, n=26 spines from 5 mice, paired t-test, two-tailed, *p<0.05) and **(G)** spines active during sleep (402.4s±51.5 and 347.8s±54.33 for wake and sleep respectively, n=25 spines from 5 mice, paired t-test, two-tailed, *p<0.05).

Figure 5. Microglial contact with spine increases spine activity during sleep. (A) Selected frames showing spine activity before/after and during contact with microglial processes. **(B)** Frequency of spine Ca^{2+} transients during or before/after contact with microglial processes ($0.88x10^{-2}$±0.00063 and $1.04x10^{-2}$±0.00074, before/after and during contact, respectively, n=68 spines from 5 mice, paired t-test, two-tailed, *p<0.05). **(C)** Frequency of spine Ca^{2+} before/after and during microglial contact during episodes of wake ($9.41x10^{-3}$Hz ± 0.00096 and $8.75x10^{-3}$Hz ±0.0009 during and before/after contact respectively, n=61 spines from 5 mice, one-way ANOVA, *p<0.05) and episodes of sleep ($1.3x10^{-2}$±0.0012 and $9x10^{-3}$±0.00081 during and before/after contact respectively, n=61 spines/mouse from 5 mice, One-way ANOVA, *p<0.05).

Supplementary figures

Figure 1. Characterization of sleep and wake duration and episodes in head-restrained mice. (A, B, C) Quantification of wake and sleep (NREM and REM) from 4-hour recordings in head-restrained mice. **(A)** Percentage of time spent during wake, sleep and REM sleep during a 4-hour session (12 4-hour sessions from 6 mice, 63.43%±1.75%, 35.7%±1.65%, 0.87%±0.16% for wake, sleep and REM sleep respectively). **(B)** Average duration of individual wake, NREM and REM sleep episodes during a 4-hour session (12 4-hour sessions from 6 mice, 59.56s±3, 41.2s±2.3, 14.4±2.3 for wake, NREM sleep and REM sleep respectively). **(C)** Total number of wake, NREM and REM sleep episodes with varying lengths over a 4-hour session (12 4-hour sessions from 6 mice, 163.5±8.24, 131.1±7.4, 6.58±0.99 for wake, NREM and REM sleep respectively). **(D, E)** Quantification of sleep and wake during 35-minute imaging sessions. **(D)** Percentage of time spent awake or in NREM and REM sleep during one imaging session of 35 minutes (16 35-minute sessions from 6 mice, 52.4%±3.38, 46.51%±3.29, 1.04%±0.39 for wake, NREM and REM sleep respectively). **(E)** Average duration of individual wake, NREM and REM sleep episodes for one imaging session of 35 minutes (16 35-minute sessions from 6 mice, 52.48s±5.77, 52.07s±5.5 and 8.88±2.2 for wake, NREM and REM sleep respectively). **(F)** Total number of wake, NREM and REM sleep episodes over 35-minute imaging session (16 35-minute sessions from 6 mice, 23.06s±1.88, 20.19s±1.89 and 1.25±0.37 for wake, NREM and REM sleep respectively). **(G)** Average duration of chosen wake and sleep episodes for morphology and motility quantification (355.68s±39.22 for wake and 350.44s±37.8) **(H)** Average duration of wake and sleep for chosen wake and sleep episodes (for wake episodes: 348.52±39.28 during wake and 7.16s±2.32 during sleep; for sleep episodes: 29.2s±4.21 during wake and 321.25±36.59 during sleep).

Figure 2. Description of microglia-spine contact and spine activity. (A) Average duration of microglia-spine contact (263.82s±25.1, n=48 spines from 5 mice, 7-14 spines/mouse). **(B)** Average percentage of time the spine spends in contact with microglial processes (35.84%±2.76, n=68 spines from 5 mice, 11-22 spines/mouse). **(C)** Average frequency of spine Ca^{2+} transients during wake and during sleep ($0.9x10^{-2}$±0.000695 and $1.04x10^{-2}$±0.00071, during wake and sleep respectively, n=11-22

spines from 5 mice, paired t-test, two-tailed, *p<0.05). **(D)** Correlation between spine activity and number of microglia-spine contacts over 35 minutes (r=0.05, n=6-18 spines/mouse from 5 mice, Pearson's correlation test, *p<0.05)

Figure 3. Definition of spines active during wake and spines active during sleep. (A) An example of a spine active during wake (upper panel) and a spine active during sleep (lower panel). The blue and red arrows indicate calcium events during wake and sleep, respectively. **(B)** Analysis of microglial motility at the level of the spine by measuring the distance between the moving front of the closest microglial process (yellow line) and the spine (encircled). **(C)** Selected frames showing the minimal distances (yellow line) and maximal distances (purple lines) between the closest microglial processes and a spine active during wake (upper panel) and a spine active during sleep (lower panel). Scale bar=5µm. All distances are indicated in micrometers. **(D, E)** The cumulative distribution of microglia-spine distance during **(D)** wake episodes and **(E)** sleep episodes for spines active during wake and spines active during sleep (Kolmogorov-Smirnov test, *p<0.05). All distances are indicated in µm.

Figure 4. Microglia-spine contact duration and activity for intermediary spines. (A) Correlation between microglia-spine contact duration and spine activity for intermediary spines (r=0.017, n=17 from 5 mice, Pearson's correlation test, *p<0.05). **(B)** Duration of contact between microglial processes and intermediary spines during wake and sleep (450.88s±81.09 and 366.47s±62.45 for wake and sleep respectively, n=17 spines from 5 mice, paired t-test, two-tailed, *p<0.05). **(C)** Frequency of spine Ca^{2+} transients before/after and during microglial contact for intermediary spines ($0.936x10^{-2}$±0.0012 and $1.04x10^{-2}$±0.0015, before/after and during contact respectively, n=17 spines from 5 mice, paired t-test, two-tailed, *p<0.05).

Bibliography:

Abel, T., Havekes, R., Saletin, J.M., and Walker, M.P. (2013). Sleep, plasticity and memory from molecules to whole-brain networks. Curr. Biol. CB *23*, R774-788.

Akiyoshi, R., Wake, H., Kato, D., Horiuchi, H., Ono, R., Ikegami, A., Haruwaka, K., Omori, T., Tachibana, Y., Moorhouse, A.J., et al. (2018). Microglia Enhance Synapse Activity to Promote Local Network Synchronization. ENeuro *5*.

Bellesi, M., Tononi, G., Cirelli, C., and Serra, P.A. (2016). Region-Specific Dissociation between Cortical Noradrenaline Levels and the Sleep/Wake Cycle. Sleep *39*, 143–154.

Choudhury, M.E., Miyanishi, K., Takeda, H., Islam, A., Matsuoka, N., Kubo, M., Matsumoto, S., Kunieda, T., Nomoto, M., Yano, H., et al. (2019). Phagocytic elimination of synapses by microglia during sleep. Glia glia.23698.

Davalos, D., Grutzendler, J., Yang, G., Kim, J.V., Zuo, Y., Jung, S., Littman, D.R., Dustin, M.L., and Gan, W.-B. (2005). ATP mediates rapid microglial response to local brain injury in vivo. Nat. Neurosci. *8*, 752–758.

Ding, F., O'Donnell, J., Xu, Q., Kang, N., Goldman, N., and Nedergaard, M. (2016). Changes in the composition of brain interstitial ions control the sleep - wake cycle. Science *352*, 550–555.

Dissing-Olesen, L., LeDue, J.M., Rungta, R.L., Hefendehl, J.K., Choi, H.B., and MacVicar, B.A. (2014). Activation of neuronal NMDA receptors triggers transient ATP-mediated microglial process outgrowth. J. Neurosci. Off. J. Soc. Neurosci. *34*, 10511–10527.

Dworak, M., McCarley, R.W., Kim, T., Kalinchuk, A.V., and Basheer, R. (2010). Sleep and Brain Energy Levels: ATP Changes during Sleep. J. Neurosci. *30*, 9007–9016.

Etienne, F., Mastrolia, V., Maroteaux, L., Girault, J.-A., Gervasi, N., and Roumier, A. (2019). Two-photon Imaging of Microglial Processes' Attraction Toward ATP or Serotonin in Acute Brain Slices. J. Vis. Exp. JoVE.

Eyo, U.B., Peng, J., Swiatkowski, P., Mukherjee, A., Bispo, A., and Wu, L.-J. (2014). Neuronal hyperactivity recruits microglial processes via neuronal NMDA receptors and microglial P2Y12 receptors after status epilepticus. J. Neurosci. Off. J. Soc. Neurosci. *34*, 10528–10540.

Fernández-Martínez, M., and Sánchez-Granero, M.A. (2014). Fractal dimension for fractal structures: A Hausdorff approach revisited. J. Math. Anal. Appl. *409*, 321–330.

Fontainhas, A.M., Wang, M., Liang, K.J., Chen, S., Mettu, P., Damani, M., Fariss, R.N., Li, W., and Wong, W.T. (2011). Microglial morphology and dynamic behavior is regulated by ionotropic glutamatergic and GABAergic neurotransmission. PloS One *6*, e15973.

Franken, P., Malafosse, A., and Tafti, M. (1999). Genetic determinants of sleep regulation in inbred mice. Sleep *22*, 155–169.

Gyoneva, S., and Traynelis, S.F. (2013). Norepinephrine modulates the motility of resting and activated microglia via different adrenergic receptors. J. Biol. Chem. *288*, 15291–15302.

Hayashi, Y. (2013). Diurnal Spatial Rearrangement of Microglial Processes through the Rhythmic Expression of P2Y12 Receptors. J. Neurol. Disord. *01*.

Hoshiko, M., Arnoux, I., Avignone, E., Yamamoto, N., and Audinat, E. (2012). Deficiency of the microglial receptor CX3CR1 impairs postnatal functional development of thalamocortical synapses in the barrel cortex. J. Neurosci. Off. J. Soc. Neurosci. *32*, 15106–15111.

Iida, T., Tanaka, S., and Okabe, S. (2019). Spatial impact of microglial distribution on dynamics of dendritic spines.

Jung, S., Aliberti, J., Graemmel, P., Sunshine, M.J., Kreutzberg, G.W., Sher, A., and Littman, D.R. (2000). Analysis of fractalkine receptor CX(3)CR1 function by targeted deletion and green fluorescent protein reporter gene insertion. Mol. Cell. Biol. *20*, 4106–4114.

Karrer, M., Lopez, M.A., Meier, D., Mikhail, C., Ogunshola, O.O., Müller, A.F., Strauss, L., Tafti, M., and Fontana, A. (2015). Cytokine-induced sleep: Neurons respond to TNF with production of chemokines and increased expression of Homer1a in vitro. Brain. Behav. Immun. *47*, 186–192.

Klinzing, J.G., Niethard, N., and Born, J. (2019). Mechanisms of systems memory consolidation during sleep. Nat. Neurosci.

Krabbe, G., Matyash, V., Pannasch, U., Mamer, L., Boddeke, H.W.G.M., and Kettenmann, H. (2012). Activation of serotonin receptors promotes microglial injury-induced motility but attenuates phagocytic activity. Brain. Behav. Immun. *26*, 419–428.

Krueger, J.M., Clinton, J.M., Winters, B.D., Zielinski, M.R., Taishi, P., Jewett, K.A., and Davis, C.J. (2011). Involvement of cytokines in slow wave sleep. In Progress in Brain Research, (Elsevier), pp. 39–47.

Li, Y., Du, X.-F., Liu, C.-S., Wen, Z.-L., and Du, J.-L. (2012). Reciprocal regulation between resting microglial dynamics and neuronal activity in vivo. Dev. Cell *23*, 1189–1202.

Madry, C., Kyrargyri, V., Arancibia-Cárcamo, I.L., Jolivet, R., Kohsaka, S., Bryan, R.M., and Attwell, D. (2018). Microglial Ramification, Surveillance, and Interleukin-1β Release Are Regulated by the Two-Pore Domain K+ Channel THIK-1. Neuron *97*, 299-312.e6.

Miyamoto, A., Wake, H., Ishikawa, A.W., Eto, K., Shibata, K., Murakoshi, H., Koizumi, S., Moorhouse, A.J., Yoshimura, Y., and Nabekura, J. (2016). Microglia contact induces synapse formation in developing somatosensory cortex. Nat. Commun. *7*, 12540.

Niethard, N., Hasegawa, M., Itokazu, T., Oyanedel, C.N., Born, J., and Sato, T.R. (2016). Sleep-Stage-Specific Regulation of Cortical Excitation and Inhibition. Curr. Biol. CB *26*, 2739–2749.

Nimmerjahn, A., Kirchhoff, F., and Helmchen, F. (2005). Resting microglial cells are highly dynamic surveillants of brain parenchyma in vivo. Science *308*, 1314–1318.

Ohsawa, K., Sanagi, T., Nakamura, Y., Suzuki, E., Inoue, K., and Kohsaka, S. (2012). Adenosine A3 receptor is involved in ADP-induced microglial process extension and migration. J. Neurochem. *121*, 217–227.

Orr, A.G., Orr, A.L., Li, X.-J., Gross, R.E., and Traynelis, S.F. (2009). Adenosine A(2A) receptor mediates microglial process retraction. Nat. Neurosci. *12*, 872–878.

Paolicelli, R.C., Bolasco, G., Pagani, F., Maggi, L., Scianni, M., Panzanelli, P., Giustetto, M., Ferreira, T.A., Guiducci, E., Dumas, L., et al. (2011). Synaptic pruning by microglia is necessary for normal brain development. Science *333*, 1456–1458.

Parkhurst, C.N., Yang, G., Ninan, I., Savas, J.N., Yates, J.R., Lafaille, J.J., Hempstead, B.L., Littman, D.R., and Gan, W.-B. (2013). Microglia promote learning-dependent synapse formation through brain-derived neurotrophic factor. Cell *155*, 1596–1609.

Pascual, O., Ben Achour, S., Rostaing, P., Triller, A., and Bessis, A. (2012). Microglia activation triggers astrocyte-mediated modulation of excitatory neurotransmission. Proc. Natl. Acad. Sci. *109*, E197–E205.

Pfeiffer, T., Avignone, E., and Nägerl, U.V. (2016). Induction of hippocampal long-term potentiation increases the morphological dynamics of microglial processes and prolongs their contacts with dendritic spines. Sci. Rep. *6*.

Porkka-Heiskanen, T., Strecker, R.E., and McCarley, R.W. (2000). Brain site-specificity of extracellular adenosine concentration changes during sleep deprivation and spontaneous sleep: an in vivo microdialysis study. Neuroscience *99*, 507–517.

Portas, C.M., Bjorvatn, B., and Ursin, R. (2000). Serotonin and the sleep/wake cycle: special emphasis on microdialysis studies. Prog. Neurobiol. *60*, 13–35.

Prinz, M., and Priller, J. (2014). Microglia and brain macrophages in the molecular age: from origin to neuropsychiatric disease. Nat. Rev. Neurosci. *15*, 300–312.

Rasch, B., and Born, J. (2013). About sleep's role in memory. Physiol. Rev. *93*, 681–766.

Schafer, D.P., Lehrman, E.K., Kautzman, A.G., Koyama, R., Mardinly, A.R., Yamasaki, R., Ransohoff, R.M., Greenberg, M.E., Barres, B.A., and Stevens, B. (2012). Microglia sculpt postnatal neural circuits in an activity and complement-dependent manner. Neuron *74*, 691–705.

Seibt, J., Richard, C.J., Sigl-Glöckner, J., Takahashi, N., Kaplan, D.I., Doron, G., de Limoges, D., Bocklisch, C., and Larkum, M.E. (2017). Cortical dendritic activity correlates with spindle-rich oscillations during sleep in rodents. Nat. Commun. *8*, 684.

Sheng, L., Leshchyns'ka, I., and Sytnyk, V. (2015). Neural cell adhesion molecule 2 promotes the formation of filopodia and neurite branching by inducing submembrane increases in Ca2+ levels. J. Neurosci. Off. J. Soc. Neurosci. *35*, 1739–1752.

Steriade, M. (1994). Sleep oscillations and their blockage by activating systems. J. Psychiatry Neurosci. JPN *19*, 354–358.

Tononi, G., and Cirelli, C. (2014). Sleep and the price of plasticity: from synaptic and cellular homeostasis to memory consolidation and integration. Neuron *81*, 12–34.

Tremblay, M.-È., Lowery, R.L., and Majewska, A.K. (2010). Microglial interactions with synapses are modulated by visual experience. PLoS Biol. *8*, e1000527.

Vanini, G., Lydic, R., and Baghdoyan, H.A. (2012). GABA-to-ACh Ratio in Basal Forebrain and Cerebral Cortex Varies Significantly During Sleep. Sleep *35*, 1325–1334.

Wake, H., Moorhouse, A.J., Jinno, S., Kohsaka, S., and Nabekura, J. (2009). Resting microglia directly monitor the functional state of synapses in vivo and determine the fate of ischemic terminals. J. Neurosci. Off. J. Soc. Neurosci. *29*, 3974–3980.

Weinhard, L., di Bartolomei, G., Bolasco, G., Machado, P., Schieber, N.L., Neniskyte, U., Exiga, M., Vadisiute, A., Raggioli, A., Schertel, A., et al. (2018). Microglia remodel synapses by presynaptic trogocytosis and spine head filopodia induction. Nat. Commun. *9*, 1228.

Wigren, H.-K., and Porkka-Heiskanen, T. (2018). Novel concepts in sleep regulation. Acta Physiol. *222*, e13017.

Yang, G., Lai, C.S.W., Cichon, J., Ma, L., Li, W., and Gan, W.-B. (2014). Sleep promotes branch-specific formation of dendritic spines after learning. Science *344*, 1173–1178.

Zhang, J., Malik, A., Choi, H.B., Ko, R.W.Y., Dissing-Olesen, L., and MacVicar, B.A. (2014). Microglial CR3 activation triggers long-term synaptic depression in the hippocampus via NADPH oxidase. Neuron *82*, 195–207.

FIGURE 1

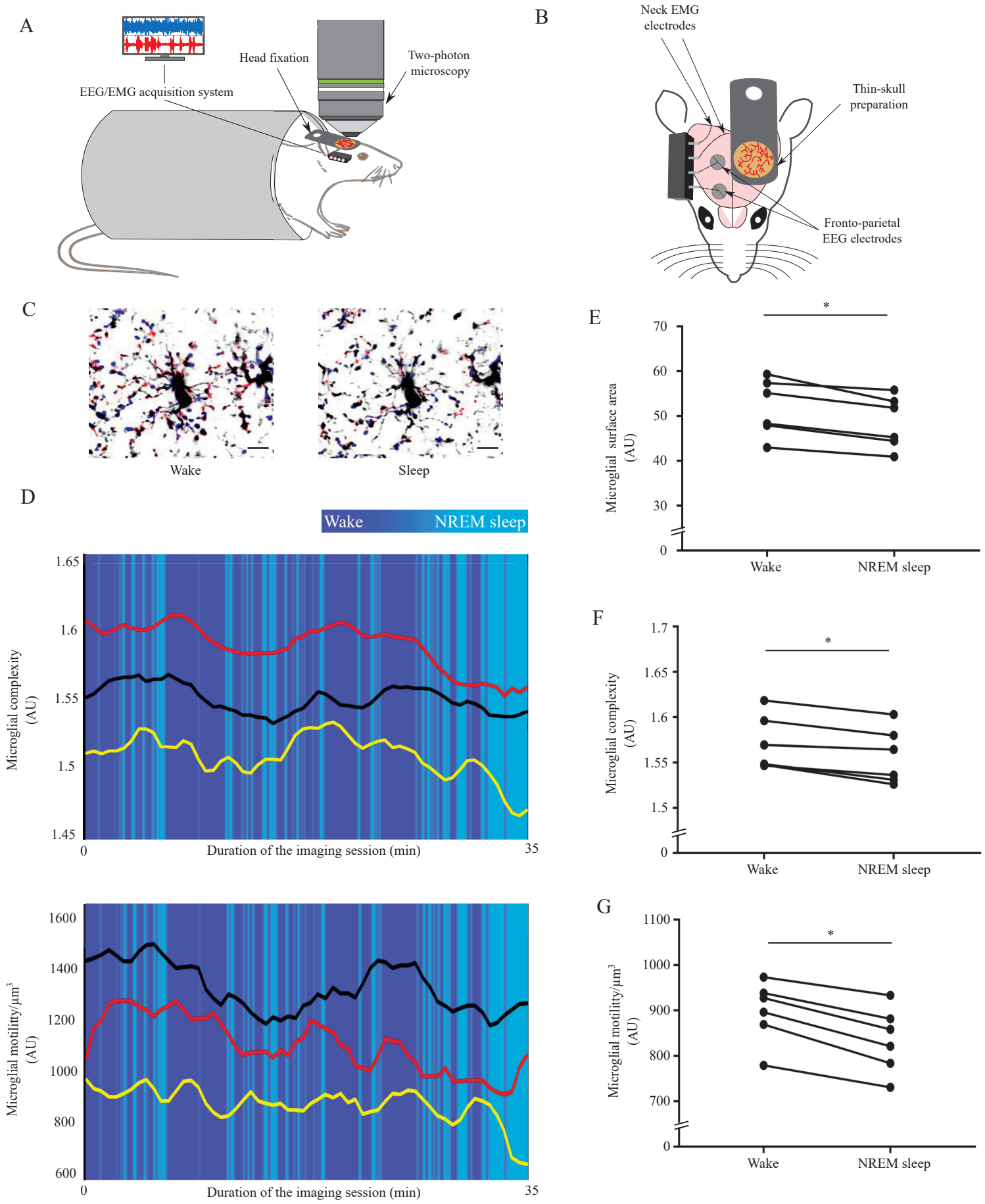
A
EEG/EMG acquisition system
Head fixation
Two-photon microscopy
B
Neck EMG electrodes
Thin-skull preparation
Fronto-parietal EEG electrodes
C
Wake
Sleep
D
Wake
NREM sleep
Microglial complexity (AU)
1.65
1.6
1.55
1.5
1.45
0
Duration of the imaging session (min)
35
Microglial motility/µm³ (AU)
1600
1400
1200
1000
800
600
0
Duration of the imaging session (min)
35
E
Microglial surface area (AU)
70
60
50
40
30
0
Wake
NREM sleep
*
F
Microglial complexity (AU)
1.7
1.65
1.6
1.55
1.5
0
Wake
NREM sleep
*
G
Microglial motility/µm³ (AU)
1100
1000
900
800
700
0
Wake
NREM sleep
*

FIGURE 2

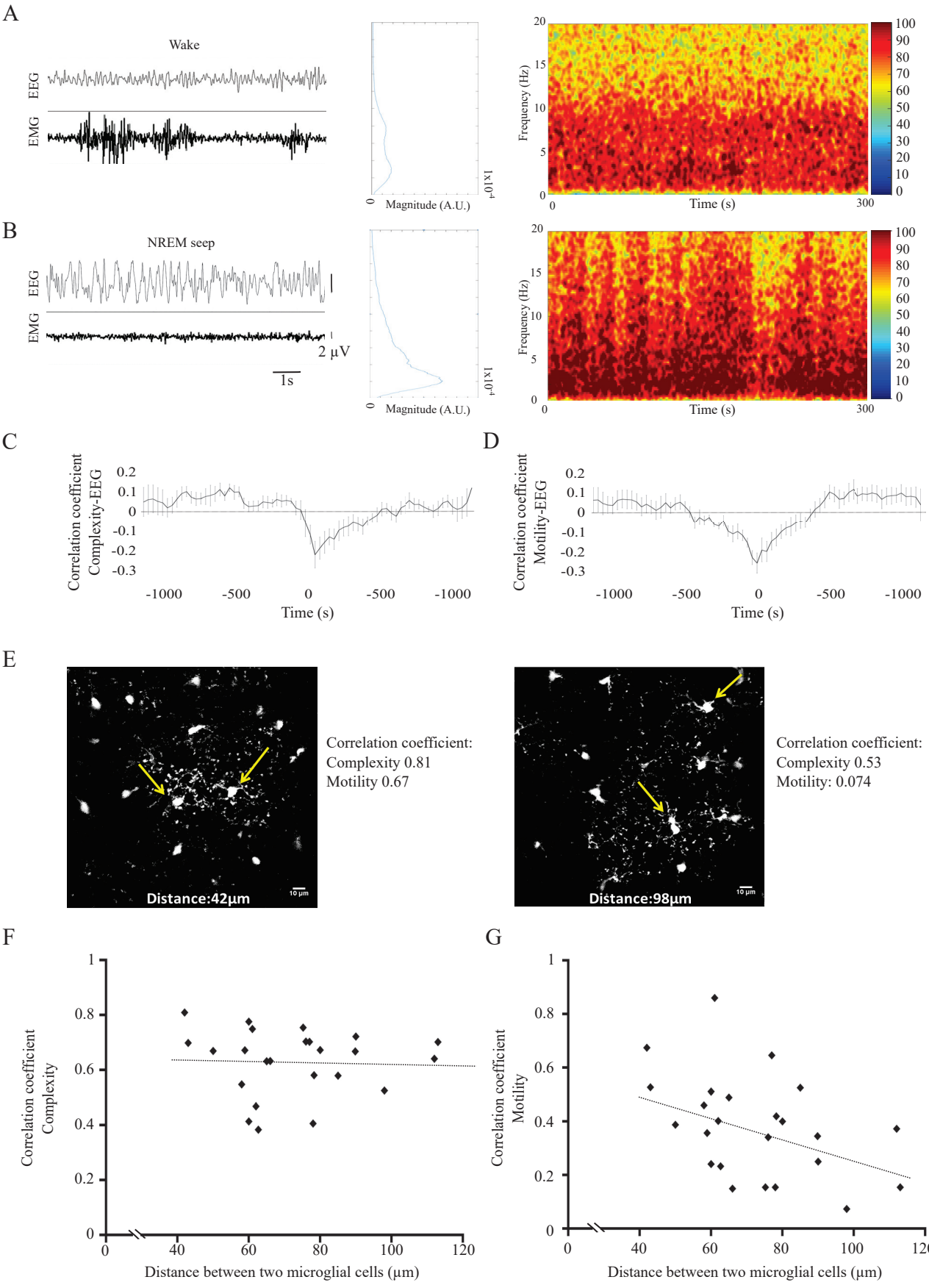
A
Wake
EEG
EMG
Magnitude (A.U.)
Frequency (Hz)
Time (s)
B
NREM seep
2 µV
1s
C
Correlation coefficient
Complexity-EEG
Time (s)
D
Correlation coefficient
Motility-EEG
Time (s)
E
Distance:42µm
Correlation coefficient:
Complexity 0.81
Motility 0.67
Distance:98µm
Correlation coefficient:
Complexity 0.53
Motility: 0.074
F
Correlation coefficient
Complexity
Distance between two microglial cells (µm)
G
Correlation coefficient
Motility
Distance between two microglial cells (µm)

FIGURE 3

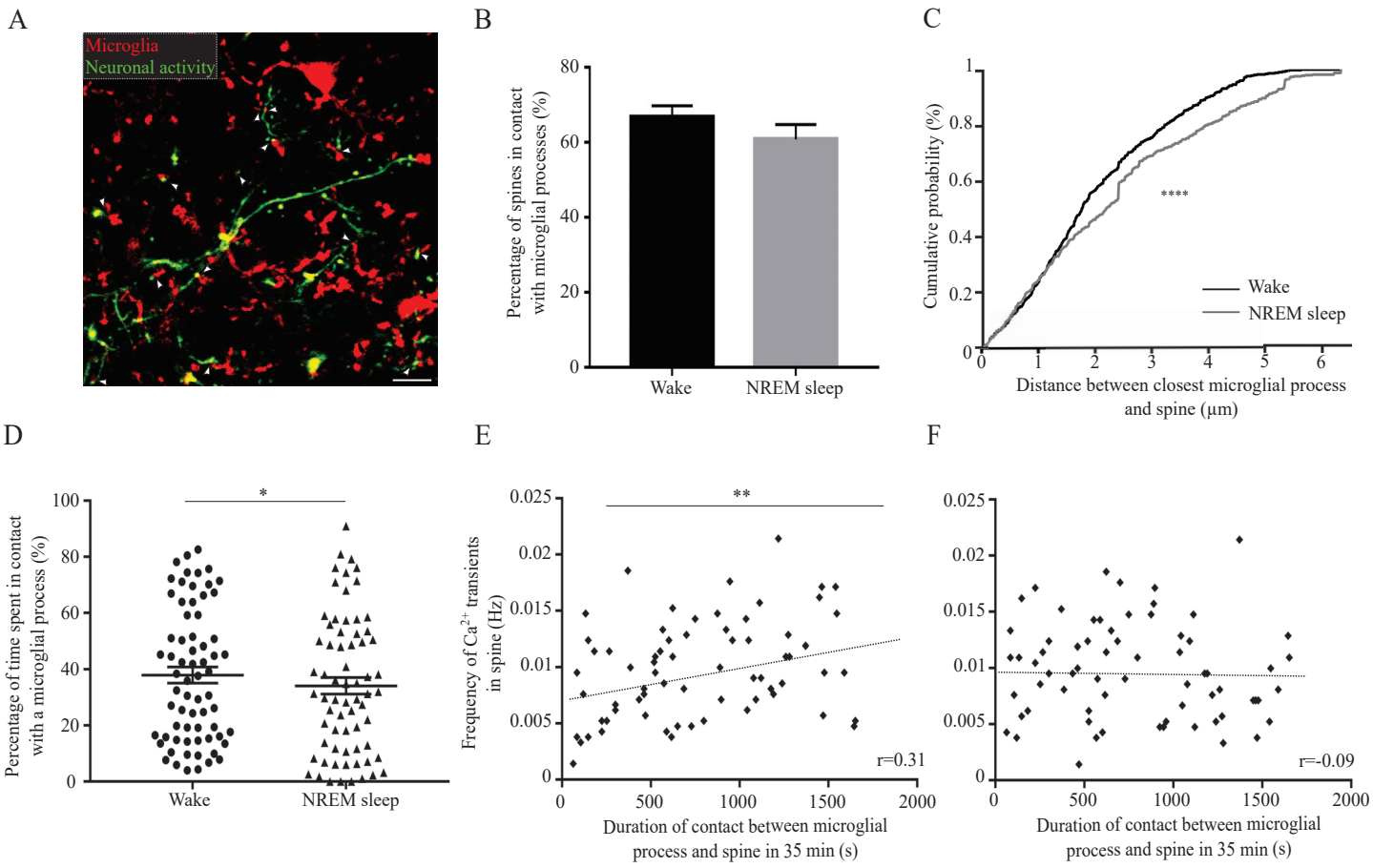
A
Microglia
Neuronal activity
B
Percentage of spines in contact with microglial processes (%)
80
60
40
20
0
Wake
NREM sleep
C
Cumulative probability (%)
1
0.8
0.6
0.4
0.2
0
****
Wake
NREM sleep
0
1
2
3
4
5
6
Distance between closest microglial process and spine (µm)
D
Percentage of time spent in contact with a microglial process (%)
100
80
60
40
20
0
*
Wake
NREM sleep
E
Frequency of Ca2+ transients in spine (Hz)
0.025
0.02
0.015
0.01
0.005
0
**
r=0.31
0
500
1000
1500
2000
Duration of contact between microglial process and spine in 35 min (s)
F
0.025
0.02
0.015
0.01
0.005
0
r=-0.09
0
500
1000
1500
2000
Duration of contact between microglial process and spine in 35 min (s)

FIGURE 4

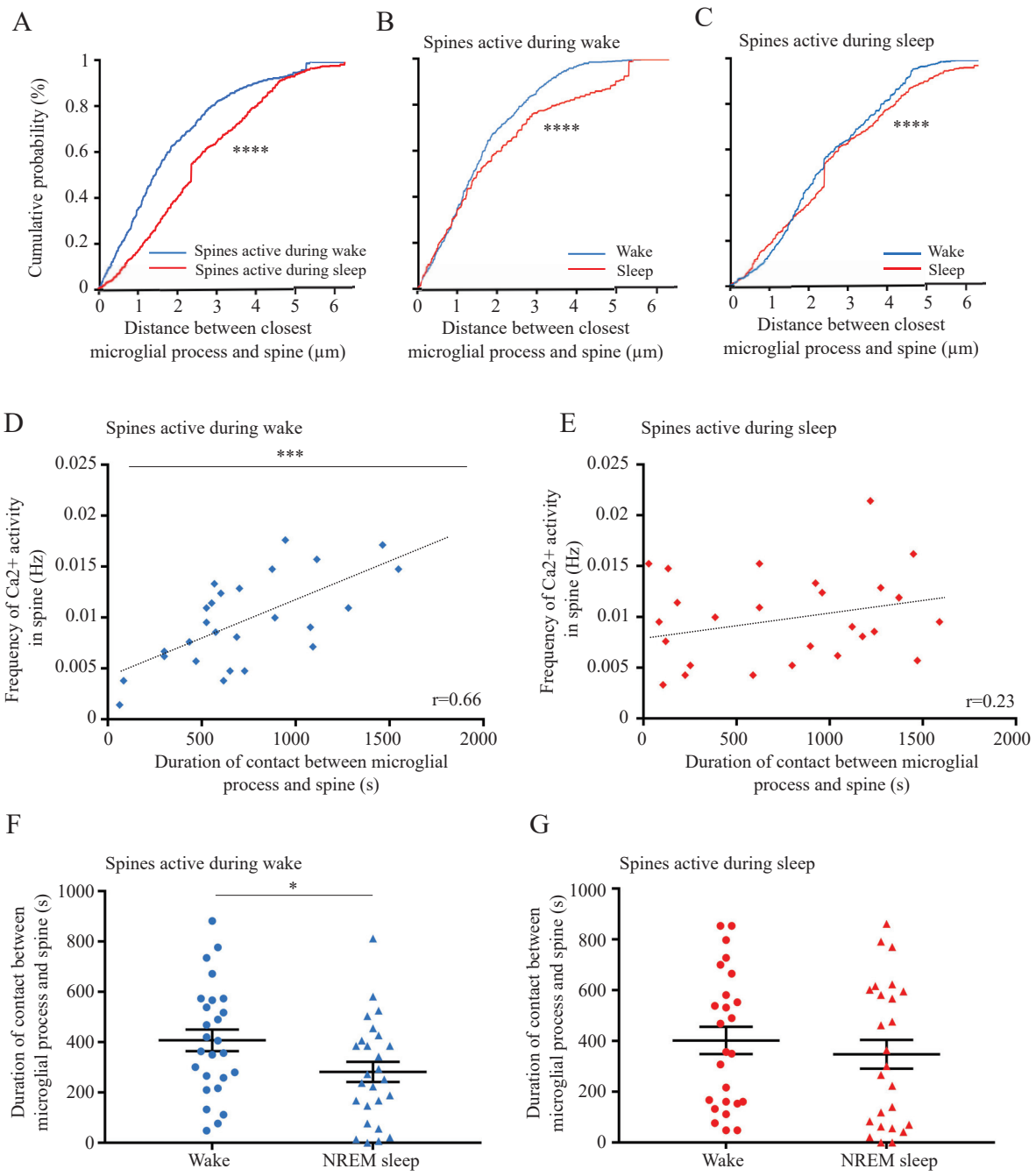
A
B
C
Cumulative probability (%)
Spines active during wake
Spines active during sleep
****
Distance between closest microglial process and spine (µm)
Wake
Sleep
D
E
Frequency of Ca2+ activity in spine (Hz)
***
r=0.66
r=0.23
Duration of contact between microglial process and spine (s)
F
G
Duration of contact between microglial process and spine (s)
*
Wake
NREM sleep

FIGURE 5

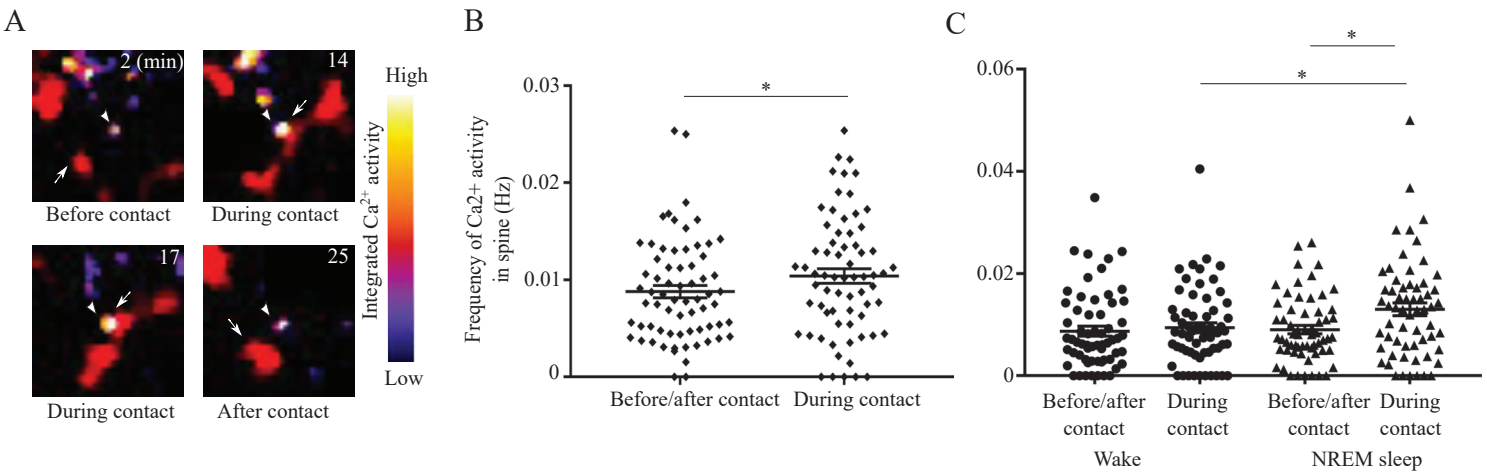
A
2 (min)
14
17
25
Before contact
During contact
During contact
After contact
High
Low
Integrated Ca2+ activity
B
Frequency of Ca2+ activity in spine (Hz)
0.03
0.02
0.01
0
*
Before/after contact
During contact
C
0.06
0.04
0.02
0
*
*
Before/after contact
During contact
Before/after contact
During contact
Wake
NREM sleep

SUPPLEMENTARY FIGURE 1

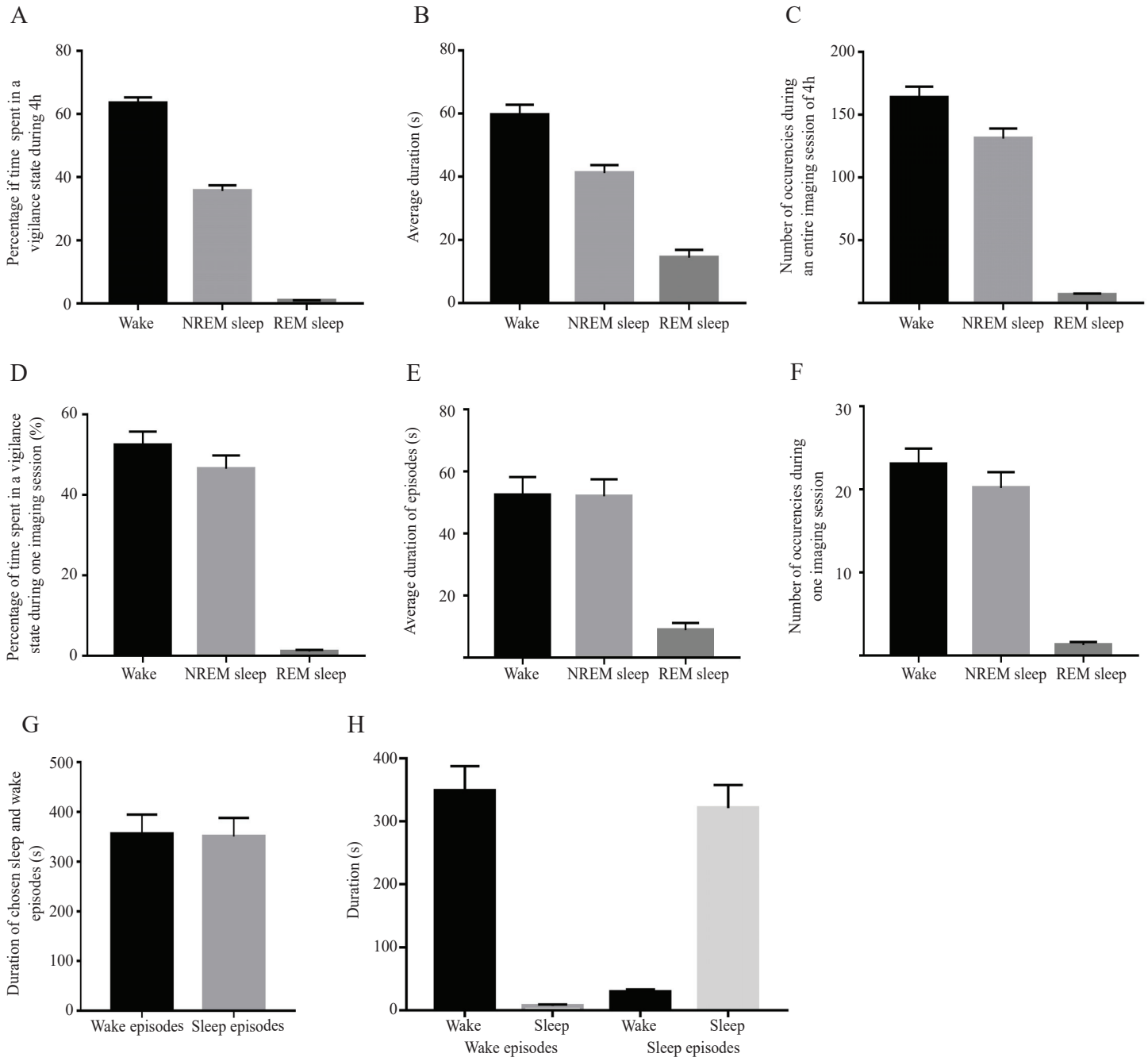

SUPPLEMENTARY FIGURE 2

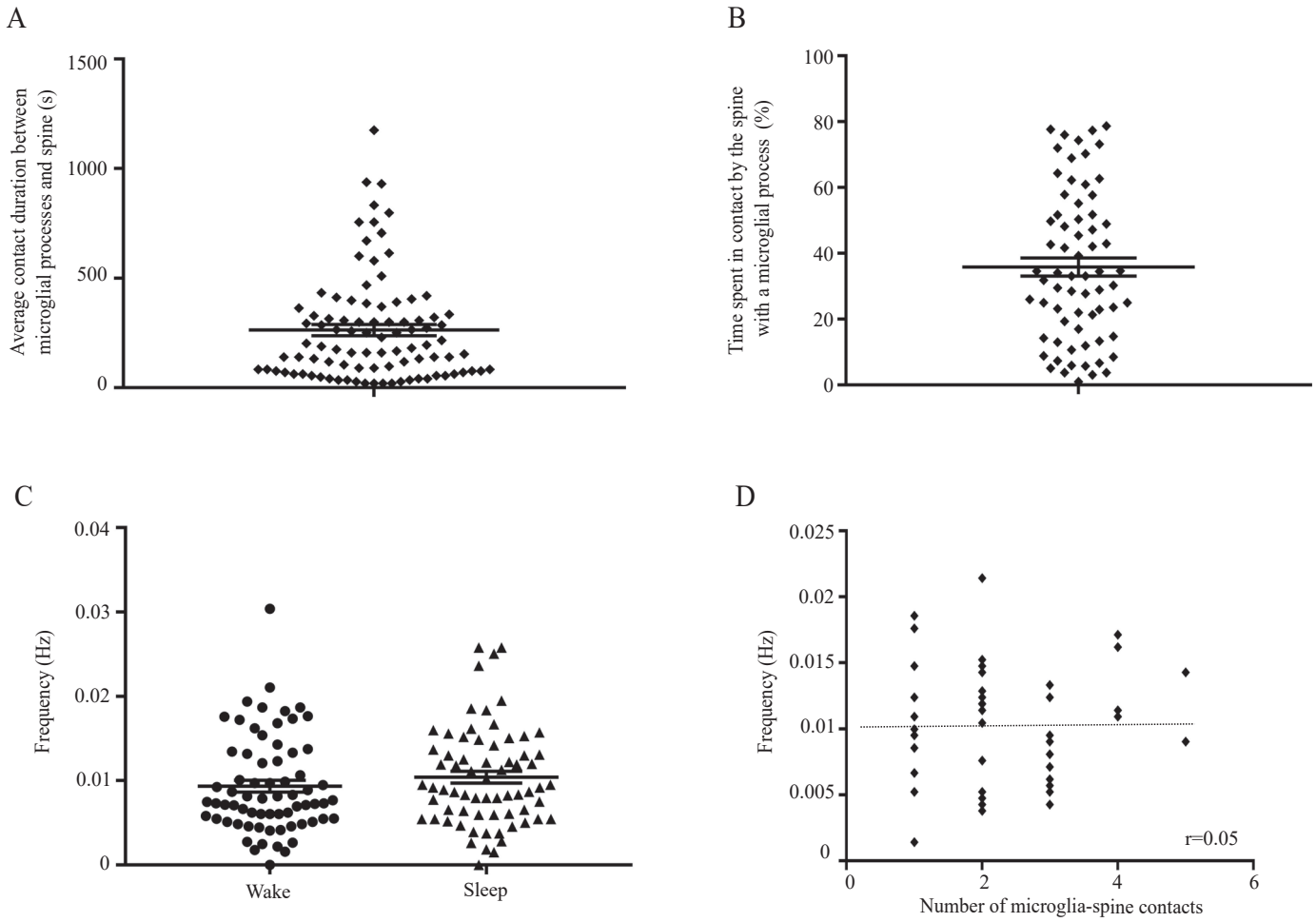

SUPPLEMENTARY FIGURE 3

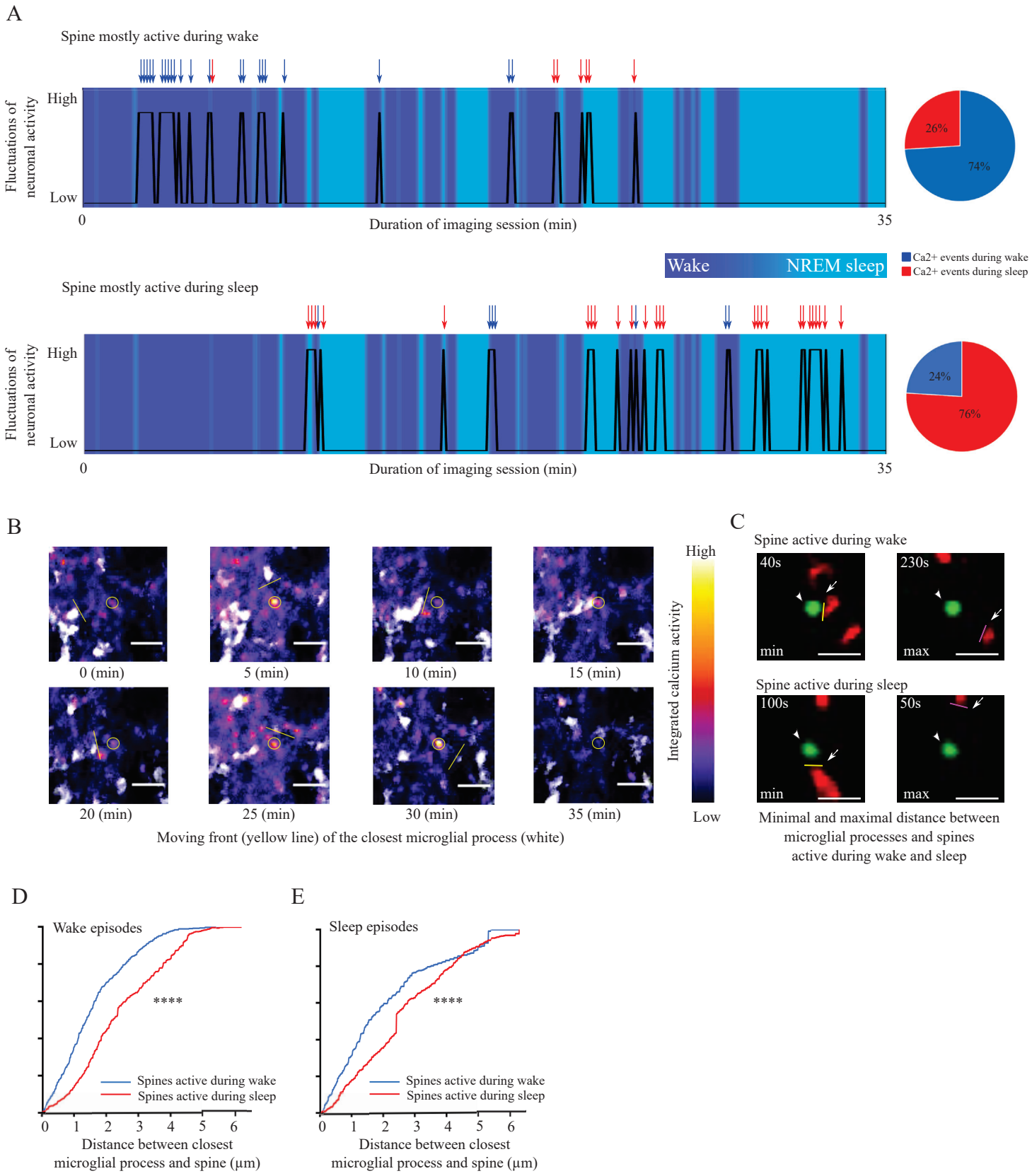

SUPPLEMENTARY FIGURE 4

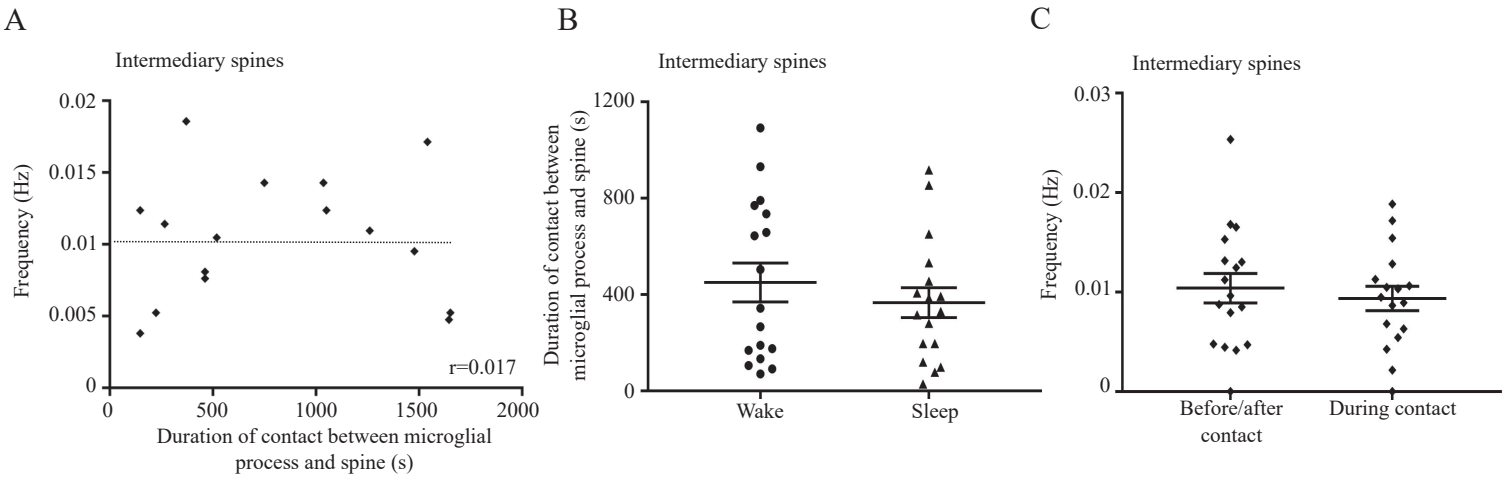

DISCUSSION

Our results suggest that microglial morphodynamic parameters may vary during different brain states and these changes may be directly linked to the level and/or patterns of neuronal activity. At the spine level, the interactions between microglial processes and spines were related to the level of spine activity and were influenced by the vigilance states. Finally, microglia-spine contact resulted in modulation of spine activity, which occurred mainly during NREM sleep episodes.

1. *Limitations of the study*

Using calcium imaging, we were only able to observe excitatory spines that have been active during the imaging period. We were blind towards inactive or inhibitory spines and studied microglial dynamics with this important limitation. Contrary to excitatory spines, very few studies have focused on microglial behavior towards inhibitory spines. These were mostly conducted *in vitro* (Lim et al., 2013) or in pathological conditions (Cantaut-Belarif et al., 2017; Chen et al., 2014). Thus, the occurrence of microglial contact with inhibitory spines in physiological conditions and its functional consequences are currently largely unknown.
Furthermore, we could not assess the possible preference of microglial processes for spines of certain size during the vigilance states due to limited resolution. The size parameter is worth considering because microglia showed preference for contacting smaller spines that subsequently disappeared in the visual cortex during development (Tremblay et al., 2010a). Taking into consideration the absence of structural neuronal marker in our experiments, we were unable to assess the fate and potential structural changes at synapses contacted during wake or sleep, as well as for spines whose activity increased following microglial contact. Future investigations will have to take advantage of these markers in order to obtain a comprehensive assessment of microglial dynamics towards all spines.

For experiments assessing microglial dynamics at the spine level, the frequency of image acquisition was 7 seconds per Z-stack, which is not best suited for neuronal activity assessment. At the time of our experiments, we did not dispose of a resonant scanner with our two-photon imaging system. Thus, in order to maintain a reasonable resolution, and image multiple Z-stacks with a certain number of planes during several sleep-wake cycles, we opted for this acquisition

frequency. Using this acquisition frequency did not result in a significant loss of detection of calcium events, probably due to the use of medium kinetics genetically encoded calcium indicator (GCaMP6m) and the fact that each spine was contained in several planes of the volume.

2. Modulation of microglial morphology and motility in different brain states

In physiological conditions, microglial processes are highly ramified and dynamic, continuously surveying the surrounding parenchyma (Davalos et al., 2005; Nimmerjahn et al., 2005). Despite being the resident immune cells of the brain, recent studies attribute fundamental physiological functions to microglial cells, including contribution to synaptic connectivity and properties, as well as the regulation of neuronal activity and network synchronization (Akiyoshi et al., 2018; Parkhurst et al., 2013; Raghuraman et al., 2019). These newly discovered tasks depend on the integrity of microglial morphology and motility, which are regulated by mechanisms that have just begun to be elucidated.

1.1 Specific patterns of neuronal activity during sleep and anesthesia administration

It has been suggested that neuronal activity could control, at least partly, microglial morphology and dynamics in anesthetized animals and *ex vivo* (Tremblay et al., 2010; Wake et al., 2009), but these findings are almost inexistent in physiological conditions. In two separate studies, we assessed microglial morphology and motility during sleep and anesthesia. These states are characterized by specific patterns of neuronal activity, with the common denominator being increased delta power, suggestive of slow-wave activity dominated states particularly during sleep and ketamine/xylazine anesthesia. Barbiturate anesthesia administration also slowed neuronal activity but led to isoelectric activity with bursts of high amplitude activity.

1.2 Global reduction of microglial motility during sleep and anesthesia

In all conditions, microglial motility in the somatosensory cortex was decreased compared to wake. This finding suggests that global reduction in neuronal activity and/or increased delta power may result in global decrease in microglial motility. The degree to which microglial motility was reduced in all conditions varied: sleep (~7.5%), pentobarbital (~9%) and ketamine-xylazine anesthesia (~17%). The observation that the reduction of microglial motility during

sleep is significant, but not major, might be explained by several reasons: 1) sleep remains an unstable physiological state with regards to anesthesia and microglial processes still need to continuously survey the tissue, 2) even though sleep has been perceived as a "passive" state, its metabolic rate is only slightly reduced compared to wake, and 3) sleep may play vital functions that might involve microglial cells. The reduction of microglial motility was higher in anesthetized conditions, which may result from the increased duration and proportion of silent states and isoelectric activity during anesthesia (Chauvette et al., 2011; Lukatch et al., 2005). The difference we observed between pentobarbital and ketamine-xylazine anesthesia is quite interesting and might be associated with the different pathways that are targeted by these anesthetics that might impact microglial motility to different extents. Isoflurane anesthesia was also found to impact microglial morphology and motility, however, with inconclusive results between studies. Microglial surveillance and ramifications were reduced in slices and *in vivo* (Madry et al., 2018a), whereas isoflurane administration increased microglial ramifications *in vivo* (Sun et al., 2019).

1.3 Different regulation of microglial morphology by anesthetic agents

Microglial complexity was significantly reduced with sleep and ketamine/xylazine anesthesia administration, but not with pentobarbital anesthesia. This may be due to the shared slow oscillations between the first two states, even though these do not present similar cellular and network features. For instance, the duration of silent states or the degree of synchrony of slow waves differs between sleep and ketamine/xylazine anesthesia (Chauvette et al., 2011). Thus, it is possible that microglial morphology is shaped more specifically by the patterns of neuronal activity, and not as much the level of activity, like it seems to be the case for motility.

1.4 Variable decrease of microglial morphodynamic parameters during sleep

The design of our sleep/wake experiments allowed us to observe fluctuations of microglial morphology and motility within individual consecutive wake and sleep episodes. Even though we found a global reduction of microglial motility and morphology in the majority of NREM sleep episodes, the extent of this decrease was variable. This might result from the presence of different proportions of slow-wave and spindle-rich activity in NREM sleep episodes. Furthermore, transitions between states and preceding circumstances might impact these parameters. For instance, some sleep episodes were preceded by wake whilst others by periods

of fragmented sleep. Thus, neuronal activity might not be similar within these sleep episodes and microglial cells might not respond in the same way. It is also possible that the shift from one state to another does not influence microglial parameters at the same pace. For instance, extracellular ion concentrations change far more consistently and rapidly from wake to sleep relative to falling asleep (Ding et al., 2016). In future experiments, faster acquisition frequencies may give accurate measurements and assess these aspects more precisely.

3. *May microglia contribute to change of vigilance states?*

Following the observation of a concurrent fluctuation of microglial parameters and neuronal activity during the vigilance states, an important point is to ascertain whether microglial changes are following or preceding changes in neuronal activity. Cross-correlation analysis suggests that changes in microglial motility may precede changes in EEG power, suggesting that microglial motility may start to increase just before or at the transition between states and possibly contribute to the state change. Since our acquisition frequency is rather slow (1 Z-stack=30s), we are not entirely convinced that this is the case and faster acquisition frequencies may help ascertain the validity of these results. Nevertheless, the possibility that microglia may contribute in switching between states is not completely unexpected since several studies point towards a role for microglial cells in driving changes in the sleep-wake cycle. First, microglia are greatly equipped to sense adenosine and ATP that mediate sleep pressure and local sleep homeostasis (Bjorness and Greene, 2009; Dworak et al., 2010; Madry and Attwell, 2015). Microglial cells are capable of releasing pro-inflammatory cytokines, including IL-1β and TNFα that are found to influence sleep pressure and enhance EEG delta wave power and duration of NREM sleep (Krueger et al., 2011). Furthermore, genetic deletion of cathepsin S, a microglia-specific lysosomal cysteine protease in the brain, resulted in a significant reduction of EEG delta power during the light phase (Hayashi et al., 2013), suggesting that microglia may induce changes in neuronal activity over the sleep-wake cycle. Even if this is the case, global motility variation prior to activity change does not exclude the possible regulation of microglial motility by neuronal activity at the local level once the vigilance state is established.

On the other hand, microglial morphology appeared to follow changes in neuronal activity, suggesting that microglial cells would ramify following the onset of low-amplitude activity as observed during wake and *vice versa*. Taking into consideration our previous observation of the potential major influence of patterns of neuronal activity on microglial morphology, it is

probable that fluctuations of microglial morphology require sustained changes in patterns of neuronal activity and possibly the characteristic neuromodulatory tones observed during the vigilance states.

4. *Microglial morphology and motility are regulated at different integration levels*

Is the temporal evolution of global microglial morphology and motility comparable between microglial cells or is it intrinsic to each microglia? Interestingly, our results hint to a contrasting regulation of these parameters. Microglial cells in a larger field (~120µm) presented similar changes in microglial morphology across the sleep-wake cycle, suggesting a global impact of the vigilance states on microglial ramification. On the contrary, changes in microglial motility did not evolve in the same manner and were quite dissimilar for cells that were far. The modest correlation observed for neighboring microglial cells may arise from the potential presence of localized patterns of synchronous neural activity, as it has been observed during running, grooming or level pulling in neighboring motor cortical L2/3 neurons (Dombeck et al., 2009; Hira et al., 2013). Nevertheless, our observations indicate that microglial motility seems more likely to be regulated at the local level.

In addition to the already-described surveillance by large microglial processes, microglia also possess thin actin-dependent filopodia processes that allow nanoscale surveillance (Bernier et al., 2019). These are found at the tip of microglial processes and their regulation is distinct from large processes. In fact, norepinephrine and nitric oxide, both involved in the regulation of sleep-wake cycles, drive filopodia extension. It is thus possible that even though the complexity and motility of large processes is reduced during sleep, this nanoscale surveillance is affected differently during the vigilance states and may serve different functions.

5. *Distinct regulation of microglial processes by neuronal activity during the vigilance states*

Several studies provide evidence that microglial dynamics is not random, but rather activity-dependent. Microglial processes may be attracted towards sites of increased neuronal activity via mechanisms involving NMDAR-dependent ATP release and microglial P2Y12R (Dissing-Olesen et al., 2014; Eyo et al., 2014). Spines contacted by microglia exhibited higher basal rates

of Ca^{2+} transients *in vivo* (Akiyoshi et al., 2018) and processes extended their contact with spines after LTP induction in hippocampal slices (Pfeiffer et al., 2016). Our results are in agreement with this hypothesis since we observed that microglial processes spent more time in contact with highly active spines.

5.1 Activity during wake attracts microglial processes, but is impeded during sleep

Since activity at the spine level does not seem to differ between sleep and wake, and these are profoundly distinct states, we investigated their influence on microglial sensing of neuronal activity. During wake, microglial processes were overall closer to spines and spent longer time in contact with spines that exhibited higher frequency of Ca^{2+} transients. Sleep was associated with an important weakening of this relationship. Thus, microglial processes seem to sense neuronal activity predominantly during wake and sleep might hinder this attraction. These findings may lead to intriguing theories regarding the purpose for microglial sensing of activity during wake and the mechanisms underlying the weakening of microglial attraction during sleep.

5.2 May microglial processes sense and tag active synapses during wake?

A recent study suggested that microglia may play a critical role in setting synaptic tags during the early phase of activity-dependent plasticity (Raghuraman et al., 2019). Thus, a pleasant speculation could be that by sensing activity during wake, microglial processes are directed towards synapses that need to be "tagged" for further activity-dependent plasticity. Induction of synaptic plasticity and setting of a synaptic tag involved NMDAR activation (Moncada et al., 2015) and activity-dependent microglial process outgrowth is also dependent on NMDAR activation (Dissing-Olesen et al., 2014; Eyo et al., 2014), providing an intriguing link for microglial involvement in the setting of synaptic tags. The candidate molecules employed by microglial cells to facilitate mechanisms for long-term potentiation may involve pro-inflammatory cytokines TNF-α and IL-1β (Raghuraman et al., 2019).

5.3 What mechanisms may contribute to the impediment of microglial process attraction during sleep?

Since microglial processes seem to be attracted towards spines mostly during wake, what are the mechanisms that might change this attraction during sleep? The first reason might be purely physical. The increased distance between microglial processes and spines during sleep might lead to a critical gap between them, rendering microglial processes too far to sense ATP gradient. This is not very likely because even though ATP has a very short half-life, its metabolite and in particular ADP may still act as a long-range signal for process outgrowth even for distant microglia. The mechanisms responsible for long-range chemoattraction by ATP are not known but may include ATP amplification by means of other signaling molecules or enhancing ATP response by mechanisms such as ATP-induced ATP release from astrocytes (Davalos et al., 2005; Pascual et al., 2012). It is possible that the regulation of these mechanisms differs between the vigilance states, contributing to the incapacity of microglial processes in properly sensing ATP and purine gradient. Indeed, astrocytic processes were found to be farther from the synaptic cleft during sleep, possibly leading to disparity in activity sensing, NT recapture and astrocytic gliotransmitter release between the vigilance states. Furthermore, the change in extracellular ion concentration during the sleep-wake cycle may impact ectonucleotidases activity, and consequently ATP gradient generation and process attraction (Wang and Guidotti, 1996). In addition to the signaling molecules, microglial processes also need to be properly equipped to sense them and the expression of these receptors may vary with the circadian rhythm and possibly the vigilance states (Hayashi 2013).

5.4 May microglial processes sense activity from other neuronal compartments?

Apart from synaptic clefts, it is possible that microglial processes may sense activity from other neuronal compartments, such as dendrites and axons. This might occur to a much lesser extent because most microglial processes were in direct apposition to synapse-associated elements (Tremblay et al., 2010). However, an argument opposed to this hypothesis is that the frequency of Ca^{2+} transients in the parent dendrite did not differ between contacted and non-contacted spines (Akiyoshi et al., 2018), suggesting that Ca^{2+} transients in dendrites may not drive microglial process extension. However, to our knowledge, this study did not assess potential contacts at the dendrite level with regards to dendritic activity. Taken into consideration the increased and synchronized activity in dendrites during spindle-rich NREM sleep (Seibt et al., 2017), it would be interesting to address microglial dynamics at the dendritic level during the sleep-wake cycle.

In conclusion, even though the basic mechanism of ATP-dependent attraction of microglial processes has been described, there are many gaps and inconsistencies in our understanding and much research needs to be done to obtain a comprehensive view. Not much is known about how these mechanisms are regulated during the vigilance states and need to be elucidated. Nevertheless, the impediment of microglial process attraction during sleep raises fascinating questions not only about the underlying circumstances of this phenomenon, but also its functional consequences.

6. *Microglial contact increases spine activity*

Microglial contact with neuronal components has previously been found to increase local spine activity or homeostatically downregulate neuronal activity (Akiyoshi et al., 2018; Li et al., 2012). In our study, we observed an increase in spine activity during contact with microglial process. The exact mechanism remains unknown, but microglia possess an arsenal of molecular tools serving this purpose. They may secrete many soluble molecules locally, such as cytokines, neurotrophic factors and neurotransmitters capable of influencing neuronal activity (Szepesi et al., 2018). They may also release extracellular vesicles (EVs) that may increase glutamate release at presynaptic sites of neuronal synapses (Antonucci et al., 2012). Finally, they may also trigger intracellular Ca^{2+} elevation by contact-dependent mechanism mediated by neural cell adhesion molecules (NCAM) (Sheng et al., 2015b).

6.1 Microglial contact-induced increase in spine activity occurs during NREM sleep

Increase in spine activity during microglial contact took place during NREM sleep. Unfortunately, due to our limited acquisition frequency, we were unable to assess with certainty whether this increase occurs during slow-wave activity or spindle-rich episodes. Taking into consideration the different activity rhythms that constitute NREM sleep and their respective functions, assessing the context in which microglia-induced activity increase occurs is primordial for understanding its function.

Nevertheless, our findings suggest that, during sleep, microglial roles may be less oriented towards sensing neuronal activity, but potentially towards exerting specific functions at synapses. One hypothesis is that after having sensed and "tagged" active spines, microglia may participate in their strengthening during sleep by increasing their activity. Activity increase

might lead to enhanced spine growth, since activity-dependent growth of spines has already been established (Kwon and Sabatini, 2011; Maletic-Savatic et al., 1999). Microglia may enhance spine formation by secreting BDNF and IL-10 (Lim et al., 2013; Parkhurst et al., 2013). In the adult brain, microglia were indeed found to be involved in learning-dependent spine formation, but their role in baseline spine formation was not assessed in adults. Our study might suggest that even in the absence of a learning paradigm, microglia could modulate spine activity through contact with spines.

Akiyoshi *et al.* suggested that microglia-dependent increase in spine activity was accompanied with increased frequency of back-propagating action potentials reflected as dendritic Ca^{2+} transients, that may serve in local network synchronization (Akiyoshi et al., 2018). Taking into consideration that spindle-rich NREM sleep is associated with increased and synchronized activity in dendrites, it is possible that microglia may participate in local dendritic spindle-related plasticity, implied by the decoupling of dendritic and somatic firing during sleep. Bearing in mind these findings, future studies need to determine the temporal and spatial requirements for increased network synchronization caused by contact-dependent microglial increase in spine activity.

6.2 Microglia may contribute to global downscaling during sleep

Microglial roles during sleep are without doubt not limited to increasing spine activity. A very recent study suggested that microglia might be engaged in selective elimination of opsonized synapses during each sleep phase (Choudhury et al., 2019). In addition to recognizing specific "tagged" synapses, microglia may be involved in global downscaling of synaptic strength via proteolytic modification of perisynaptic environment. This might be due to microglial cathepsin S secretion which was involved in functional changes in glutamate receptor (Liu et al., 2010; Vyazovskiy et al., 2008) and spine density (Maret et al., 2011; Yang and Gan, 2012), as well as reduction of the mEPSC mean amplitude (Hayashi et al., 2013).

Taking into consideration the role of the sleep-wake cycles in information processing, learning and memory, and the emerging microglial roles in adulthood linked with these processes, future experiments need to combine two-photon imaging and electrophysiology with sensory modulation and behavioral learning paradigms to assess more precisely the interplay between all these parameters.

CONCLUSION

In conclusion, we report that microglial dynamics is modulated by the brain states, and these variations are related to changes in neuronal activity. Two physiological states, sleep and wake affect microglial morphology globally, whereas microglial motility seems to be intrinsically linked to local spine activity. We propose that microglial processes may sense neuronal activity and are attracted towards active synapses particularly during wake; however, this relationship seems to be hindered during sleep. Microglial contact increases spine activity, and this increase takes place mainly during NREM sleep. Our findings contribute to the accumulating evidence of the regulation and function of microglial cells in physiological conditions. The novelty of our study is in determining how the vigilance states may add another level of complexity to the established regulation by neuronal activity and in describing specific microglial functions dependent on the vigilance state. Taking into consideration the critical and separate involvement of the wake/sleep cycles in information processing, learning and memory, and their distinct impact on microglial properties, their concerted action may guide microglia-mediated fine-tuning of neuronal networks in the adult brain. Sleep disruption, and age- and pathology-related changes in microglial parameters may lead to failure of microglia to fulfill these emerging homeostatic functions and restoring microglial function is crucial for maintaining synaptic homeostasis.

BIBLIOGRAPHY

Abel, T., Havekes, R., Saletin, J.M., and Walker, M.P. (2013). Sleep, plasticity and memory from molecules to whole-brain networks. Curr. Biol. CB *23*, R774-788.

Abraham, W.C., Mason-Parker, S.E., and Logan, B. (1996). Low-frequency stimulation does not readily cause long-term depression or depotentiation in the dentate gyrus of awake rats. Brain Res. *722*, 217–221.

Ajami, B., Bennett, J.L., Krieger, C., Tetzlaff, W., and Rossi, F.M.V. (2007). Local self-renewal can sustain CNS microglia maintenance and function throughout adult life. Nat. Neurosci. *10*, 1538–1543.

Ajami, B., Bennett, J.L., Krieger, C., McNagny, K.M., and Rossi, F.M.V. (2011). Infiltrating monocytes trigger EAE progression, but do not contribute to the resident microglia pool. Nat. Neurosci. *14*, 1142–1149.

Akiyoshi, R., Wake, H., Kato, D., Horiuchi, H., Ono, R., Ikegami, A., Haruwaka, K., Omori, T., Tachibana, Y., Moorhouse, A.J., et al. (2018). Microglia Enhance Synapse Activity to Promote Local Network Synchronization. ENeuro *5*.

Almeida-Filho, D.G., Queiroz, C.M., and Ribeiro, S. (2018). Memory corticalization triggered by REM sleep: mechanisms of cellular and systems consolidation. Cell. Mol. Life Sci. CMLS *75*, 3715–3740.

Amzica, F. (2002). Physiology of sleep and wakefulness as it relates to the physiology of epilepsy. J. Clin. Neurophysiol. Off. Publ. Am. Electroencephalogr. Soc. *19*, 488–503.

Amzica, F., and Neckelmann, D. (1999). Membrane capacitance of cortical neurons and glia during sleep oscillations and spike-wave seizures. J. Neurophysiol. *82*, 2731–2746.

Amzica, F., and Steriade, M. (1998). Electrophysiological correlates of sleep delta waves. Electroencephalogr. Clin. Neurophysiol. *107*, 69–83.

Anaclet, C., Ferrari, L., Arrigoni, E., Bass, C.E., Saper, C.B., Lu, J., and Fuller, P.M. (2014). The GABAergic parafacial zone is a medullary slow wave sleep-promoting center. Nat. Neurosci. *17*, 1217–1224.

Antonucci, F., Turola, E., Riganti, L., Caleo, M., Gabrielli, M., Perrotta, C., Novellino, L., Clementi, E., Giussani, P., Viani, P., et al. (2012). Microvesicles released from microglia stimulate synaptic activity via enhanced sphingolipid metabolism: Microglial MVs increase sphingolipid metabolism in neurons. EMBO J. *31*, 1231–1240.

Araque, A., Carmignoto, G., Haydon, P.G., Oliet, S.H.R., Robitaille, R., and Volterra, A. (2014). Gliotransmitters travel in time and space. Neuron *81*, 728–739.

Arnò, B., Grassivaro, F., Rossi, C., Bergamaschi, A., Castiglioni, V., Furlan, R., Greter, M., Favaro, R., Comi, G., Becher, B., et al. (2014). Neural progenitor cells orchestrate microglia migration and positioning into the developing cortex. Nat. Commun. *5*, 5611.

Arnoux, I., Hoshiko, M., Mandavy, L., Avignone, E., Yamamoto, N., and Audinat, E. (2013). Adaptive phenotype of microglial cells during the normal postnatal development of the somatosensory “Barrel” cortex. Glia *61*, 1582–1594.

Arnsten, A.F. (1997). Catecholamine regulation of the prefrontal cortex. J. Psychopharmacol. Oxf. Engl. *11*, 151–162.

Arranz, A.M., and De Strooper, B. (2019). The role of astroglia in Alzheimer's disease: pathophysiology and clinical implications. Lancet Neurol. *18*, 406–414.

Askew, K., Li, K., Olmos-Alonso, A., Garcia-Moreno, F., Liang, Y., Richardson, P., Tipton, T., Chapman, M.A., Riecken, K., Beccari, S., et al. (2017). Coupled Proliferation and Apoptosis Maintain the Rapid Turnover of Microglia in the Adult Brain. Cell Rep. *18*, 391–405.

Aton, S.J., Suresh, A., Broussard, C., and Frank, M.G. (2014). Sleep promotes cortical response potentiation following visual experience. Sleep *37*, 1163–1170.

Avignone, E., Ulmann, L., Levavasseur, F., Rassendren, F., and Audinat, E. (2008). Status epilepticus induces a particular microglial activation state characterized by enhanced purinergic signaling. J. Neurosci. Off. J. Soc. Neurosci. *28*, 9133–9144.

Avignone, E., Lepleux, M., Angibaud, J., and Nägerl, U.V. (2015). Altered morphological dynamics of activated microglia after induction of status epilepticus. J. Neuroinflammation *12*, 202.

Bachiller, S., Jiménez-Ferrer, I., Paulus, A., Yang, Y., Swanberg, M., Deierborg, T., and Boza-Serrano, A. (2018). Microglia in Neurological Diseases: A Road Map to Brain-Disease Dependent-Inflammatory Response. Front. Cell. Neurosci. *12*, 488.

Bachstetter, A.D., Morganti, J.M., Jernberg, J., Schlunk, A., Mitchell, S.H., Brewster, K.W., Hudson, C.E., Cole, M.J., Harrison, J.K., Bickford, P.C., et al. (2011). Fractalkine and CX 3 CR1 regulate hippocampal neurogenesis in adult and aged rats. Neurobiol. Aging *32*, 2030–2044.

Bailey, C.H., Kandel, E.R., and Harris, K.M. (2015). Structural Components of Synaptic Plasticity and Memory Consolidation. Cold Spring Harb. Perspect. Biol. *7*, a021758.

von Bartheld, C.S., Bahney, J., and Herculano-Houzel, S. (2016). The search for true numbers of neurons and glial cells in the human brain: A review of 150 years of cell counting: Quantifying neurons and glia in human brain. J. Comp. Neurol. *524*, 3865–3895.

Bartram, J., Kahn, M.C., Tuohy, S., Paulsen, O., Wilson, T., and Mann, E.O. (2017). Cortical Up states induce the selective weakening of subthreshold synaptic inputs. Nat. Commun. *8*, 665.

Basilico, B., Pagani, F., Grimaldi, A., Cortese, B., Di Angelantonio, S., Weinhard, L., Gross, C., Limatola, C., Maggi, L., and Ragozzino, D. (2019). Microglia shape presynaptic properties at developing glutamatergic synapses. Glia *67*, 53–67.

Bellesi, M., Pfister-Genskow, M., Maret, S., Keles, S., Tononi, G., and Cirelli, C. (2013). Effects of Sleep and Wake on Oligodendrocytes and Their Precursors. J. Neurosci. *33*, 14288–14300.

Bellesi, M., de Vivo, L., Tononi, G., and Cirelli, C. (2015). Effects of sleep and wake on astrocytes: clues from molecular and ultrastructural studies. BMC Biol. *13*, 66.

Bellesi, M., Tononi, G., Cirelli, C., and Serra, P.A. (2016). Region-Specific Dissociation between Cortical Noradrenaline Levels and the Sleep/Wake Cycle. Sleep *39*, 143–154.

Bellesi, M., de Vivo, L., Chini, M., Gilli, F., Tononi, G., and Cirelli, C. (2017). Sleep Loss Promotes Astrocytic Phagocytosis and Microglial Activation in Mouse Cerebral Cortex. J. Neurosci. Off. J. Soc. Neurosci. *37*, 5263–5273.

Bennett, C., Arroyo, S., and Hestrin, S. (2013). Subthreshold mechanisms underlying state-dependent modulation of visual responses. Neuron *80*, 350–357.

Bennett, M.L., Bennett, F.C., Liddelow, S.A., Ajami, B., Zamanian, J.L., Fernhoff, N.B., Mulinyawe, S.B., Bohlen, C.J., Adil, A., Tucker, A., et al. (2016). New tools for studying microglia in the mouse and human CNS. Proc. Natl. Acad. Sci. U. S. A. *113*, E1738-1746.

Bernier, L.-P., Bohlen, C.J., York, E.M., Choi, H.B., Kamyabi, A., Dissing-Olesen, L., Hefendehl, J.K., Collins, H.Y., Stevens, B., Barres, B.A., et al. (2019). Nanoscale Surveillance of the Brain by Microglia via cAMP-Regulated Filopodia. Cell Rep. *27*, 2895-2908.e4.

Berridge, C.W., and Waterhouse, B.D. (2003). The locus coeruleus-noradrenergic system: modulation of behavioral state and state-dependent cognitive processes. Brain Res. Brain Res. Rev. *42*, 33–84.

Bialas, A.R., and Stevens, B. (2013). TGF-β signaling regulates neuronal C1q expression and developmental synaptic refinement. Nat. Neurosci. *16*, 1773–1782.

Bianco, F., Pravettoni, E., Colombo, A., Schenk, U., Möller, T., Matteoli, M., and Verderio, C. (2005). Astrocyte-derived ATP induces vesicle shedding and IL-1 beta release from microglia. J. Immunol. Baltim. Md 1950 *174*, 7268–7277.

Birtoli, B., and Ulrich, D. (2004). Firing mode-dependent synaptic plasticity in rat neocortical pyramidal neurons. J. Neurosci. Off. J. Soc. Neurosci. *24*, 4935–4940.

Bjorness, T., and Greene, R. (2009). Adenosine and Sleep. Curr. Neuropharmacol. *7*, 238–245.

Blanco-Centurion, C., Gerashchenko, D., and Shiromani, P.J. (2007). Effects of saporin-induced lesions of three arousal populations on daily levels of sleep and wake. J. Neurosci. Off. J. Soc. Neurosci. *27*, 14041–14048.

Bliss, T.V., and Lomo, T. (1973). Long-lasting potentiation of synaptic transmission in the dentate area of the anaesthetized rabbit following stimulation of the perforant path. J. Physiol. *232*, 331–356.

Bonham, L.W., Sirkis, D.W., and Yokoyama, J.S. (2019). The Transcriptional Landscape of Microglial Genes in Aging and Neurodegenerative Disease. Front. Immunol. *10*, 1170.

Booth, H.D.E., Hirst, W.D., and Wade-Martins, R. (2017). The Role of Astrocyte Dysfunction in Parkinson's Disease Pathogenesis. Trends Neurosci. *40*, 358–370.

Borbély, A.A. (1982). A two process model of sleep regulation. Hum. Neurobiol. *1*, 195–204.

Borbély, A.A., Daan, S., Wirz-Justice, A., and Deboer, T. (2016). The two-process model of sleep regulation: a reappraisal. J. Sleep Res. *25*, 131–143.

Born, J., and Wilhelm, I. (2012). System consolidation of memory during sleep. Psychol. Res. *76*, 192–203.

Boucsein, C., Zacharias, R., Färber, K., Pavlovic, S., Hanisch, U.-K., and Kettenmann, H. (2003a). Purinergic receptors on microglial cells: functional expression in acute brain slices and modulation of microglial activation in vitro. Eur. J. Neurosci. *17*, 2267–2276.

Braun, N., Sévigny, J., Robson, S.C., Enjyoji, K., Guckelberger, O., Hammer, K., Di Virgilio, F., and Zimmermann, H. (2000). Assignment of ecto-nucleoside triphosphate diphosphohydrolase-1/cd39 expression to microglia and vasculature of the brain. Eur. J. Neurosci. *12*, 4357–4366.

Brown, E.N., Lydic, R., and Schiff, N.D. (2010). General Anesthesia, Sleep, and Coma. N. Engl. J. Med. *363*, 2638–2650.

Brown, E.N., Purdon, P.L., and Van Dort, C.J. (2011). General anesthesia and altered states of arousal: a systems neuroscience analysis. Annu. Rev. Neurosci. *34*, 601–628.

Brown, R.E., Basheer, R., McKenna, J.T., Strecker, R.E., and McCarley, R.W. (2012). Control of sleep and wakefulness. Physiol. Rev. *92*, 1087–1187.

Bruttger, J., Karram, K., Wörtge, S., Regen, T., Marini, F., Hoppmann, N., Klein, M., Blank, T., Yona, S., Wolf, Y., et al. (2015). Genetic Cell Ablation Reveals Clusters of Local Self-Renewing Microglia in the Mammalian Central Nervous System. Immunity *43*, 92–106.

Burnstock, G. (2008). Purinergic signalling and disorders of the central nervous system. Nat. Rev. Drug Discov. *7*, 575–590.

Butovsky, O., Jedrychowski, M.P., Moore, C.S., Cialic, R., Lanser, A.J., Gabriely, G., Koeglsperger, T., Dake, B., Wu, P.M., Doykan, C.E., et al. (2014). Identification of a unique TGF-β-dependent molecular and functional signature in microglia. Nat. Neurosci. *17*, 131–143.

Butt, A., and Verkhratsky, A. (2018). Neuroglia: Realising their true potential. Brain Neurosci. Adv. *2*, 239821281881749.

Buttgereit, A., Lelios, I., Yu, X., Vrohlings, M., Krakoski, N.R., Gautier, E.L., Nishinakamura, R., Becher, B., and Greter, M. (2016). Sall1 is a transcriptional regulator defining microglia identity and function. Nat. Immunol. *17*, 1397–1406.

Buzsáki, G. (2002). Theta oscillations in the hippocampus. Neuron *33*, 325–340.

Buzsáki, G., Horváth, Z., Urioste, R., Hetke, J., and Wise, K. (1992). High-frequency network oscillation in the hippocampus. Science *256*, 1025–1027.

Camacho-Arroyo, I., Alvarado, R., Manjarrez, J., and Tapia, R. (1991). Microinjections of muscimol and bicuculline into the pontine reticular formation modify the sleep-waking cycle in the rat. Neurosci. Lett. *129*, 95–97.

Camassa, L.M.A., Lunde, L.K., Hoddevik, E.H., Stensland, M., Boldt, H.B., De Souza, G.A., Ottersen, O.P., and Amiry-Moghaddam, M. (2015). Mechanisms underlying AQP4 accumulation in astrocyte endfeet. Glia *63*, 2073–2091.

Cantaut-Belarif, Y., Antri, M., Pizzarelli, R., Colasse, S., Vaccari, I., Soares, S., Renner, M., Dallel, R., Triller, A., and Bessis, A. (2017). Microglia control the glycinergic but not the GABAergic synapses via prostaglandin E2 in the spinal cord. J. Cell Biol. *216*, 2979–2989.

Cardona, A.E., Pioro, E.P., Sasse, M.E., Kostenko, V., Cardona, S.M., Dijkstra, I.M., Huang, D., Kidd, G., Dombrowski, S., Dutta, R., et al. (2006). Control of microglial neurotoxicity by the fractalkine receptor. Nat. Neurosci. *9*, 917–924.

Chauvette, S., Crochet, S., Volgushev, M., and Timofeev, I. (2011). Properties of Slow Oscillation during Slow-Wave Sleep and Anesthesia in Cats. J. Neurosci. *31*, 14998–15008.

Chauvette, S., Seigneur, J., and Timofeev, I. (2012). Sleep oscillations in the thalamocortical system induce long-term neuronal plasticity. Neuron *75*, 1105–1113.

Chen, S.-K., Tvrdik, P., Peden, E., Cho, S., Wu, S., Spangrude, G., and Capecchi, M.R. (2010a). Hematopoietic origin of pathological grooming in Hoxb8 mutant mice. Cell *141*, 775–785.

Chen, T., Koga, K., Li, X.-Y., and Zhuo, M. (2010b). Spinal microglial motility is independent of neuronal activity and plasticity in adult mice. Mol. Pain *6*, 19.

Chen, T.-W., Wardill, T.J., Sun, Y., Pulver, S.R., Renninger, S.L., Baohan, A., Schreiter, E.R., Kerr, R.A., Orger, M.B., Jayaraman, V., et al. (2013). Ultrasensitive fluorescent proteins for imaging neuronal activity. Nature *499*, 295–300.

Chen, Z., Jalabi, W., Hu, W., Park, H.-J., Gale, J.T., Kidd, G.J., Bernatowicz, R., Gossman, Z.C., Chen, J.T., Dutta, R., et al. (2014). Microglial displacement of inhibitory synapses provides neuroprotection in the adult brain. Nat. Commun. *5*, 4486.

Choudhury, M.E., Miyanishi, K., Takeda, H., Islam, A., Matsuoka, N., Kubo, M., Matsumoto, S., Kunieda, T., Nomoto, M., Yano, H., et al. (2019). Phagocytic elimination of synapses by microglia during sleep. Glia glia.23698.

Churchill, L., Rector, D.M., Yasuda, K., Fix, C., Rojas, M.J., Yasuda, T., and Krueger, J.M. (2008). Tumor necrosis factor alpha: activity dependent expression and promotion of cortical column sleep in rats. Neuroscience *156*, 71–80.

Clasadonte, J., Scemes, E., Wang, Z., Boison, D., and Haydon, P.G. (2017). Connexin 43-Mediated Astroglial Metabolic Networks Contribute to the Regulation of the Sleep-Wake Cycle. Neuron *95*, 1365-1380.e5.

Combadiere, C., Salzwedel, K., Smith, E.D., Tiffany, H.L., Berger, E.A., and Murphy, P.M. (1998). Identification of CX3CR1. A chemotactic receptor for the human CX3C chemokine fractalkine and a fusion coreceptor for HIV-1. J. Biol. Chem. *273*, 23799–23804.

Crochet, S., and Petersen, C.C.H. (2006). Correlating whisker behavior with membrane potential in barrel cortex of awake mice. Nat. Neurosci. *9*, 608–610.

Czarnecki, A., Birtoli, B., and Ulrich, D. (2007). Cellular mechanisms of burst firing-mediated long-term depression in rat neocortical pyramidal cells. J. Physiol. *578*, 471–479.

Datta, S., and Maclean, R.R. (2007). Neurobiological mechanisms for the regulation of mammalian sleep-wake behavior: reinterpretation of historical evidence and inclusion of contemporary cellular and molecular evidence. Neurosci. Biobehav. Rev. *31*, 775–824.

Davalos, D., Grutzendler, J., Yang, G., Kim, J.V., Zuo, Y., Jung, S., Littman, D.R., Dustin, M.L., and Gan, W.-B. (2005). ATP mediates rapid microglial response to local brain injury in vivo. Nat. Neurosci. *8*, 752–758.

Davis, E.J., Foster, T.D., and Thomas, W.E. (1994). Cellular forms and functions of brain microglia. Brain Res. Bull. *34*, 73–78.

De, S., Van Deren, D., Peden, E., Hockin, M., Boulet, A., Titen, S., and Capecchi, M.R. (2018). Two distinct ontogenies confer heterogeneity to mouse brain microglia. Development *145*, dev152306.

De Biase, L.M., Schuebel, K.E., Fusfeld, Z.H., Jair, K., Hawes, I.A., Cimbro, R., Zhang, H.-Y., Liu, Q.-R., Shen, H., Xi, Z.-X., et al. (2017). Local Cues Establish and Maintain Region-Specific Phenotypes of Basal Ganglia Microglia. Neuron *95*, 341-356.e6.

De Gennaro, L., and Ferrara, M. (2003). Sleep spindles: an overview. Sleep Med. Rev. *7*, 423–440.

Deboer, T. (2015). Behavioral and electrophysiological correlates of sleep and sleep homeostasis. Curr. Top. Behav. Neurosci. *25*, 1–24.

Diaz-Aparicio, I., and Sierra, A. (2019). C1q is related to microglial phagocytosis in the hippocampus in physiological conditions. Matters.

Diekelmann, S., and Born, J. (2010). The memory function of sleep. Nat. Rev. Neurosci. *11*, 114–126.

Diering, G.H., Nirujogi, R.S., Roth, R.H., Worley, P.F., Pandey, A., and Huganir, R.L. (2017). Homer1a drives homeostatic scaling-down of excitatory synapses during sleep. Science *355*, 511–515.

Dijk, D.J. (1995). EEG slow waves and sleep spindles: windows on the sleeping brain. Behav. Brain Res. *69*, 109–116.

Ding, F., O'Donnell, J., Xu, Q., Kang, N., Goldman, N., and Nedergaard, M. (2016). Changes in the composition of brain interstitial ions control the sleep-wake cycle. Science *352*, 550–555.

Dissing-Olesen, L., LeDue, J.M., Rungta, R.L., Hefendehl, J.K., Choi, H.B., and MacVicar, B.A. (2014). Activation of neuronal NMDA receptors triggers transient ATP-mediated microglial process outgrowth. J. Neurosci. Off. J. Soc. Neurosci. *34*, 10511–10527.

Dombeck, D.A., Graziano, M.S., and Tank, D.W. (2009). Functional clustering of neurons in motor cortex determined by cellular resolution imaging in awake behaving mice. J. Neurosci. Off. J. Soc. Neurosci. *29*, 13751–13760.

Dou, Y., Wu, H., Li, H., Qin, S., Wang, Y., Li, J., Lou, H., Chen, Z., Li, X., Luo, Q., et al. (2012). Microglial migration mediated by ATP-induced ATP release from lysosomes. Cell Res. *22*, 1022–1033.

Dubbelaar, M.L., Kracht, L., Eggen, B.J.L., and Boddeke, E.W.G.M. (2018). The Kaleidoscope of Microglial Phenotypes. Front. Immunol. *9*, 1753.

Dunwiddie, T.V., Diao, L., and Proctor, W.R. (1997). Adenine nucleotides undergo rapid, quantitative conversion to adenosine in the extracellular space in rat hippocampus. J. Neurosci. Off. J. Soc. Neurosci. *17*, 7673–7682.

Dworak, M., McCarley, R.W., Kim, T., Kalinchuk, A.V., and Basheer, R. (2010). Sleep and Brain Energy Levels: ATP Changes during Sleep. J. Neurosci. *30*, 9007–9016.

Dzyubenko, E., Gottschling, C., and Faissner, A. (2016). Neuron-Glia Interactions in Neural Plasticity: Contributions of Neural Extracellular Matrix and Perineuronal Nets. Neural Plast. *2016*, 1–14.

Edgar, D.M., Dement, W.C., and Fuller, C.A. (1993). Effect of SCN lesions on sleep in squirrel monkeys: evidence for opponent processes in sleep-wake regulation. J. Neurosci. Off. J. Soc. Neurosci. *13*, 1065–1079.

Elmore, M.R.P., Najafi, A.R., Koike, M.A., Dagher, N.N., Spangenberg, E.E., Rice, R.A., Kitazawa, M., Matusow, B., Nguyen, H., West, B.L., et al. (2014). Colony-stimulating factor 1 receptor signaling is necessary for microglia viability, unmasking a microglia progenitor cell in the adult brain. Neuron *82*, 380–397.

Errington, M.L., Bliss, T.V., Richter-Levin, G., Yenk, K., Doyère, V., and Laroche, S. (1995). Stimulation at 1-5 Hz does not produce long-term depression or depotentiation in the hippocampus of the adult rat in vivo. J. Neurophysiol. *74*, 1793–1799.

Etienne, F., Mastrolia, V., Maroteaux, L., Girault, J.-A., Gervasi, N., and Roumier, A. (2019). Two-photon Imaging of Microglial Processes' Attraction Toward ATP or Serotonin in Acute Brain Slices. J. Vis. Exp. JoVE.

Eyo, U., and Dailey, M.E. (2012). Effects of oxygen-glucose deprivation on microglial mobility and viability in developing mouse hippocampal tissues. Glia *60*, 1747–1760.

Eyo, U.B., Peng, J., Swiatkowski, P., Mukherjee, A., Bispo, A., and Wu, L.-J. (2014). Neuronal hyperactivity recruits microglial processes via neuronal NMDA receptors and microglial P2Y12 receptors after status epilepticus. J. Neurosci. Off. J. Soc. Neurosci. *34*, 10528–10540.

Eyo, U.B., Gu, N., De, S., Dong, H., Richardson, J.R., and Wu, L.-J. (2015). Modulation of microglial process convergence toward neuronal dendrites by extracellular calcium. J. Neurosci. Off. J. Soc. Neurosci. *35*, 2417–2422.

Eyo, U.B., Mo, M., Yi, M.-H., Murugan, M., Liu, J., Yarlagadda, R., Margolis, D.J., Xu, P., and Wu, L.-J. (2018a). P2Y12R-Dependent Translocation Mechanisms Gate the Changing Microglial Landscape. Cell Rep. *23*, 959–966.

Eyo, U.B., Bispo, A., Liu, J., Sabu, S., Wu, R., DiBona, V.L., Zheng, J., Murugan, M., Zhang, H., Tang, Y., et al. (2018b). The GluN2A Subunit Regulates Neuronal NMDA receptor-Induced Microglia-Neuron Physical Interactions. Sci. Rep. *8*, 828.

Färber, K., and Kettenmann, H. (2005). Physiology of microglial cells. Brain Res. Brain Res. Rev. *48*, 133–143.

Fellin, T., Halassa, M.M., Terunuma, M., Succol, F., Takano, H., Frank, M., Moss, S.J., and Haydon, P.G. (2009). Endogenous nonneuronal modulators of synaptic transmission control cortical slow oscillations in vivo. Proc. Natl. Acad. Sci. U. S. A. *106*, 15037–15042.

Fernandez, L.M., Vantomme, G., Osorio-Forero, A., Cardis, R., Béard, E., and Lüthi, A. (2018). Thalamic reticular control of local sleep in mouse sensory cortex. ELife *7*.

Fernandez, L.M.J., Comte, J.-C., Le Merre, P., Lin, J.-S., Salin, P.-A., and Crochet, S. (2017). Highly Dynamic Spatiotemporal Organization of Low-Frequency Activities During Behavioral States in the Mouse Cerebral Cortex. Cereb. Cortex N. Y. N 1991 *27*, 5444–5462.

Fernández-Martínez, M., and Sánchez-Granero, M.A. (2014). Fractal dimension for fractal structures: A Hausdorff approach revisited. J. Math. Anal. Appl. *409*, 321–330.

Ferrero, G., Mahony, C.B., Dupuis, E., Yvernogeau, L., Di Ruggiero, E., Miserocchi, M., Caron, M., Robin, C., Traver, D., Bertrand, J.Y., et al. (2018). Embryonic Microglia Derive from Primitive Macrophages and Are Replaced by cmyb-Dependent Definitive Microglia in Zebrafish. Cell Rep. *24*, 130–141.

Fields, R.D., and Burnstock, G. (2006). Purinergic signalling in neuron-glia interactions. Nat. Rev. Neurosci. *7*, 423–436.

Flavell, S.W., and Greenberg, M.E. (2008). Signaling mechanisms linking neuronal activity to gene expression and plasticity of the nervous system. Annu. Rev. Neurosci. *31*, 563–590.

Flint, R.R., Chang, T., Lydic, R., and Baghdoyan, H.A. (2010). GABAA Receptors in the Pontine Reticular Formation of C57BL/6J Mouse Modulate Neurochemical, Electrographic, and Behavioral Phenotypes of Wakefulness. J. Neurosci. *30*, 12301–12309.

Fontainhas, A.M., Wang, M., Liang, K.J., Chen, S., Mettu, P., Damani, M., Fariss, R.N., Li, W., and Wong, W.T. (2011a). Microglial morphology and dynamic behavior is regulated by ionotropic glutamatergic and GABAergic neurotransmission. PloS One *6*, e15973.

Franco, R., and Fernández-Suárez, D. (2015). Alternatively activated microglia and macrophages in the central nervous system. Prog. Neurobiol. *131*, 65–86.

Frank, M.G., and Heller, H.C. (2019). The Function(s) of Sleep. Handb. Exp. Pharmacol. *253*, 3–34.

Frank, M.G., Issa, N.P., and Stryker, M.P. (2001). Sleep enhances plasticity in the developing visual cortex. Neuron *30*, 275–287.

Franken, P., Malafosse, A., and Tafti, M. (1999). Genetic determinants of sleep regulation in inbred mice. Sleep *22*, 155–169

Franklin KBJ, Paxinos G. The Mouse Brain in Stereotaxic Coordinates. 3. New York: Elsevier; 2008.

Franks, N.P. (2008). General anaesthesia: from molecular targets to neuronal pathways of sleep and arousal. Nat. Rev. Neurosci. *9*, 370–386.

Fuller, P.M., Fuller, P., Sherman, D., Pedersen, N.P., Saper, C.B., and Lu, J. (2011). Reassessment of the structural basis of the ascending arousal system. J. Comp. Neurol. *519*, 933–956.

Gallopin, T., Fort, P., Eggermann, E., Cauli, B., Luppi, P.H., Rossier, J., Audinat, E., Mühlethaler, M., and Serafin, M. (2000). Identification of sleep-promoting neurons in vitro. Nature *404*, 992–995.

Garcia, P.S., Kolesky, S.E., and Jenkins, A. (2010). General anesthetic actions on GABA(A) receptors. Curr. Neuropharmacol. *8*, 2–9.

Gerashchenko, D., Kohls, M.D., Greco, M., Waleh, N.S., Salin-Pascual, R., Kilduff, T.S., Lappi, D.A., and Shiromani, P.J. (2001). Hypocretin-2-saporin lesions of the lateral hypothalamus produce narcoleptic-like sleep behavior in the rat. J. Neurosci. Off. J. Soc. Neurosci. *21*, 7273–7283.

Gerashchenko, D., Chou, T.C., Blanco-Centurion, C.A., Saper, C.B., and Shiromani, P.J. (2004). Effects of lesions of the histaminergic tuberomammillary nucleus on spontaneous sleep in rats. Sleep *27*, 1275–1281.

Gerashchenko, D., Wisor, J.P., Burns, D., Reh, R.K., Shiromani, P.J., Sakurai, T., de la Iglesia, H.O., and Kilduff, T.S. (2008). Identification of a population of sleep-active cerebral cortex neurons. Proc. Natl. Acad. Sci. U. S. A. *105*, 10227–10232.

Giaume, C., Kirchhoff, F., Matute, C., Reichenbach, A., and Verkhratsky, A. (2007). Glia: the fulcrum of brain diseases. Cell Death Differ. *14*, 1324–1335.

Giaume, C., Koulakoff, A., Roux, L., Holcman, D., and Rouach, N. (2010). Astroglial networks: a step further in neuroglial and gliovascular interactions. Nat. Rev. Neurosci. *11*, 87–99.

Ginhoux, F., and Guilliams, M. (2016). Tissue-Resident Macrophage Ontogeny and Homeostasis. Immunity *44*, 439–449.

Ginhoux, F., Greter, M., Leboeuf, M., Nandi, S., See, P., Gokhan, S., Mehler, M.F., Conway, S.J., Ng, L.G., Stanley, E.R., et al. (2010). Fate mapping analysis reveals that adult microglia derive from primitive macrophages. Science *330*, 841–845.

Goddard, C.A., Butts, D.A., and Shatz, C.J. (2007). Regulation of CNS synapses by neuronal MHC class I. Proc. Natl. Acad. Sci. *104*, 6828–6833.

Goldmann, T., Wieghofer, P., Jordão, M.J.C., Prutek, F., Hagemeyer, N., Frenzel, K., Amann, L., Staszewski, O., Kierdorf, K., Krueger, M., et al. (2016). Origin, fate and dynamics of macrophages at central nervous system interfaces. Nat. Immunol. *17*, 797–805.

Goldstein, A., and Aronow, L. (1960). The durations of action of thiopental and pentobarbital. J. Pharmacol. Exp. Ther. *128*, 1–6.

Gomez Perdiguero, E., Klapproth, K., Schulz, C., Busch, K., Azzoni, E., Crozet, L., Garner, H., Trouillet, C., de Bruijn, M.F., Geissmann, F., et al. (2015). Tissue-resident macrophages originate from yolk-sac-derived erythro-myeloid progenitors. Nature *518*, 547–551.

Gomez-Nicola, D., and Perry, V.H. (2015). Microglial dynamics and role in the healthy and diseased brain: a paradigm of functional plasticity. Neurosci. Rev. J. Bringing Neurobiol. Neurol. Psychiatry *21*, 169–184.

Gompf, H.S., Mathai, C., Fuller, P.M., Wood, D.A., Pedersen, N.P., Saper, C.B., and Lu, J. (2010). Locus ceruleus and anterior cingulate cortex sustain wakefulness in a novel environment. J. Neurosci. Off. J. Soc. Neurosci. *30*, 14543–14551.

Gooley, J.J., Lu, J., Chou, T.C., Scammell, T.E., and Saper, C.B. (2001). Melanopsin in cells of origin of the retinohypothalamic tract. Nat. Neurosci. *4*, 1165.

Gordon, S. (2016). Phagocytosis: An Immunobiologic Process. Immunity *44*, 463–475.

Grabert, K., Michoel, T., Karavolos, M.H., Clohisey, S., Baillie, J.K., Stevens, M.P., Freeman, T.C., Summers, K.M., and McColl, B.W. (2016a). Microglial brain region-dependent diversity and selective regional sensitivities to aging. Nat. Neurosci. *19*, 504–516.

Green, C.J., Knight, J., Precious, S., and Simpkin, S. (1981). Ketamine alone and combined with diazepam or xylazine in laboratory animals: a 10 year experience. Lab. Anim. *15*, 163–170.

Green, L.A., Nebiolo, J.C., and Smith, C.J. (2019). Microglia exit the CNS in spinal root avulsion. PLOS Biol. *17*, e3000159.

Grosmark, A.D., Mizuseki, K., Pastalkova, E., Diba, K., and Buzsáki, G. (2012). REM sleep reorganizes hippocampal excitability. Neuron *75*, 1001–1007.

Guido, W. (2008). Refinement of the retinogeniculate pathway. J. Physiol. *586*, 4357–4362.

Guneykaya, D., Ivanov, A., Hernandez, D.P., Haage, V., Wojtas, B., Meyer, N., Maricos, M., Jordan, P., Buonfiglioli, A., Gielniewski, B., et al. (2018). Transcriptional and Translational Differences of Microglia from Male and Female Brains. Cell Rep. *24*, 2773-2783.e6.

Gyoneva, S., and Traynelis, S.F. (2013). Norepinephrine modulates the motility of resting and activated microglia via different adrenergic receptors. J. Biol. Chem. *288*, 15291–15302.

Hager, A.M., and Dringenberg, H.C. (2010). Assessment of different induction protocols to elicit long-term depression (LTD) in the rat visual cortex in vivo. Brain Res. *1318*, 33–41.

Haider, B., Duque, A., Hasenstaub, A.R., and McCormick, D.A. (2006). Neocortical network activity in vivo is generated through a dynamic balance of excitation and inhibition. J. Neurosci. Off. J. Soc. Neurosci. *26*, 4535–4545.

Halassa, M.M., Florian, C., Fellin, T., Munoz, J.R., Lee, S.-Y., Abel, T., Haydon, P.G., and Frank, M.G. (2009). Astrocytic modulation of sleep homeostasis and cognitive consequences of sleep loss. Neuron *61*, 213–219.

Hamilton, N.B., and Attwell, D. (2010). Do astrocytes really exocytose neurotransmitters? Nat. Rev. Neurosci. *11*, 227–238.

Hammarberg, C., Schulte, G., and Fredholm, B.B. (2003). Evidence for functional adenosine A3 receptors in microglia cells. J. Neurochem. *86*, 1051–1054.

Hammond, T.R., Dufort, C., Dissing-Olesen, L., Giera, S., Young, A., Wysoker, A., Walker, A.J., Gergits, F., Segel, M., Nemesh, J., et al. (2019). Single-Cell RNA Sequencing of Microglia throughout the Mouse Lifespan and in the Injured Brain Reveals Complex Cell-State Changes. Immunity *50*, 253-271.e6.

Hanamsagar, R., Alter, M.D., Block, C.S., Sullivan, H., Bolton, J.L., and Bilbo, S.D. (2017). Generation of a microglial developmental index in mice and in humans reveals a sex difference in maturation and immune reactivity. Glia *65*, 1504–1520.

Hanisch, U.-K. (2013). Functional diversity of microglia - how heterogeneous are they to begin with? Front. Cell. Neurosci. *7*, 65.

Harris, K.D., Quiroga, R.Q., Freeman, J., and Smith, S.L. (2016). Improving data quality in neuronal population recordings. Nat. Neurosci. *19*, 1165–1174.

Hasselmo, null (1999). Neuromodulation: acetylcholine and memory consolidation. Trends Cogn. Sci. *3*, 351–359.

Hattar, S., Liao, H.W., Takao, M., Berson, D.M., and Yau, K.W. (2002). Melanopsin-containing retinal ganglion cells: architecture, projections, and intrinsic photosensitivity. Science *295*, 1065–1070.

Hayashi, Y. (2013). Diurnal Spatial Rearrangement of Microglial Processes through the Rhythmic Expression of P2Y12 Receptors. J. Neurol. Disord. *01*.

Hayashi, Y., Koyanagi, S., Kusunose, N., Okada, R., Wu, Z., Tozaki-Saitoh, H., Ukai, K., Kohsaka, S., Inoue, K., Ohdo, S., et al. (2013). The intrinsic microglial molecular clock controls synaptic strength via the circadian expression of cathepsin S. Sci. Rep. *3*.

Haynes, S.E., Hollopeter, G., Yang, G., Kurpius, D., Dailey, M.E., Gan, W.-B., and Julius, D. (2006). The P2Y12 receptor regulates microglial activation by extracellular nucleotides. Nat. Neurosci. *9*, 1512–1519.

Hellwig, S., Brioschi, S., Dieni, S., Frings, L., Masuch, A., Blank, T., and Biber, K. (2016). Altered microglia morphology and higher resilience to stress-induced depression-like behavior in CX3CR1-deficient mice. Brain. Behav. Immun. *55*, 126–137.

Heneka, M.T., Carson, M.J., El Khoury, J., Landreth, G.E., Brosseron, F., Feinstein, D.L., Jacobs, A.H., Wyss-Coray, T., Vitorica, J., Ransohoff, R.M., et al. (2015). Neuroinflammation in Alzheimer's disease. Lancet Neurol. *14*, 388–405.

Hengen, K.B., Torrado Pacheco, A., McGregor, J.N., Van Hooser, S.D., and Turrigiano, G.G. (2016). Neuronal Firing Rate Homeostasis Is Inhibited by Sleep and Promoted by Wake. Cell *165*, 180–191.

Hernandez, P.J., and Abel, T. (2008). The role of protein synthesis in memory consolidation: progress amid decades of debate. Neurobiol. Learn. Mem. *89*, 293–311.

Hide, I., Tanaka, M., Inoue, A., Nakajima, K., Kohsaka, S., Inoue, K., and Nakata, Y. (2000). Extracellular ATP triggers tumor necrosis factor-alpha release from rat microglia. J. Neurochem. *75*, 965–972.

Hines, D.J., Hines, R.M., Mulligan, S.J., and Macvicar, B.A. (2009). Microglia processes block the spread of damage in the brain and require functional chloride channels. Glia *57*, 1610–1618.

Hira, R., Ohkubo, F., Ozawa, K., Isomura, Y., Kitamura, K., Kano, M., Kasai, H., and Matsuzaki, M. (2013). Spatiotemporal dynamics of functional clusters of neurons in the mouse motor cortex during a voluntary movement. J. Neurosci. Off. J. Soc. Neurosci. *33*, 1377–1390.

Hirasawa, T., Ohsawa, K., Imai, Y., Ondo, Y., Akazawa, C., Uchino, S., and Kohsaka, S. (2005). Visualization of microglia in living tissues using Iba1-EGFP transgenic mice. J. Neurosci. Res. *81*, 357–362.

Hirsch, J.C., Fourment, A., and Marc, M.E. (1983). Sleep-related variations of membrane potential in the lateral geniculate body relay neurons of the cat. Brain Res. *259*, 308–312.

Ho, V.M., Lee, J.-A., and Martin, K.C. (2011). The cell biology of synaptic plasticity. Science *334*, 623–628.

Hoeffel, G., and Ginhoux, F. (2015). Ontogeny of Tissue-Resident Macrophages. Front. Immunol. *6*, 486.

Holloway, O.G., Canty, A.J., King, A.E., and Ziebell, J.M. (2019). Rod microglia and their role in neurological diseases. Semin. Cell Dev. Biol. *94*, 96–103.

Hoshiko, M., Arnoux, I., Avignone, E., Yamamoto, N., and Audinat, E. (2012). Deficiency of the microglial receptor CX3CR1 impairs postnatal functional development of thalamocortical synapses in the barrel cortex. J. Neurosci. Off. J. Soc. Neurosci. *32*, 15106–15111.

Hristovska, I., and Pascual, O. (2015). Deciphering Resting Microglial Morphology and Process Motility from a Synaptic Prospect. Front. Integr. Neurosci. *9*, 73.

Hsia, A.Y., Malenka, R.C., and Nicoll, R.A. (1998). Development of excitatory circuitry in the hippocampus. J. Neurophysiol. *79*, 2013–2024.

Huang, Z.-L., Urade, Y., and Hayaishi, O. (2011). The role of adenosine in the regulation of sleep. Curr. Top. Med. Chem. *11*, 1047–1057.

Huber, R., Deboer, T., and Tobler, I. (2000). Topography of EEG dynamics after sleep deprivation in mice. J. Neurophysiol. *84*, 1888–1893.

Huber, R., Ghilardi, M.F., Massimini, M., and Tononi, G. (2004). Local sleep and learning. Nature *430*, 78–81.

Huber, R., Ghilardi, M.F., Massimini, M., Ferrarelli, F., Riedner, B.A., Peterson, M.J., and Tononi, G. (2006). Arm immobilization causes cortical plastic changes and locally decreases sleep slow wave activity. Nat. Neurosci. *9*, 1169–1176.

Huh, G.S., Boulanger, L.M., Du, H., Riquelme, P.A., Brotz, T.M., and Shatz, C.J. (2000). Functional requirement for class I MHC in CNS development and plasticity. Science *290*, 2155–2159.

Hutt, A., Lefebvre, J., Hight, D., and Sleigh, J. (2018). Suppression of underlying neuronal fluctuations mediates EEG slowing during general anaesthesia. NeuroImage *179*, 414–428.

Iida, T., Tanaka, S., and Okabe, S. (2019). Spatial impact of microglial distribution on dynamics of dendritic spines.

Iliff, J.J., Wang, M., Liao, Y., Plogg, B.A., Peng, W., Gundersen, G.A., Benveniste, H., Vates, G.E., Deane, R., Goldman, S.A., et al. (2012). A Paravascular Pathway Facilitates CSF Flow Through the Brain Parenchyma and the Clearance of Interstitial Solutes, Including Amyloid. Sci. Transl. Med. *4*, 147ra111-147ra111.

Imeri, L., and Opp, M.R. (2009). How (and why) the immune system makes us sleep. Nat. Rev. Neurosci. *10*, 199–210.

Jewett, K.A., Taishi, P., Sengupta, P., Roy, S., Davis, C.J., and Krueger, J.M. (2015). Tumor necrosis factor enhances the sleep-like state and electrical stimulation induces a wake-like state in co-cultures of neurons and glia. Eur. J. Neurosci. *42*, 2078–2090.

Jha, M.K., and Morrison, B.M. (2018). Glia-neuron energy metabolism in health and diseases: New insights into the role of nervous system metabolic transporters. Exp. Neurol. *309*, 23–31.

Jiang, B., Akaneya, Y., Hata, Y., and Tsumoto, T. (2003). Long-term depression is not induced by low-frequency stimulation in rat visual cortex in vivo: a possible preventing role of endogenous brain-derived neurotrophic factor. J. Neurosci. Off. J. Soc. Neurosci. *23*, 3761–3770.

Joiner, W.J. (2018). The Neurobiological Basis of Sleep and Sleep Disorders. Physiol. Bethesda Md *33*, 317–327.

Jung, S., Aliberti, J., Graemmel, P., Sunshine, M.J., Kreutzberg, G.W., Sher, A., and Littman, D.R. (2000). Analysis of fractalkine receptor CX(3)CR1 function by targeted deletion and green fluorescent protein reporter gene insertion. Mol. Cell. Biol. *20*, 4106–4114.

Kabba, J.A., Xu, Y., Christian, H., Ruan, W., Chenai, K., Xiang, Y., Zhang, L., Saavedra, J.M., and Pang, T. (2018). Microglia: Housekeeper of the Central Nervous System. Cell. Mol. Neurobiol. *38*, 53–71.

Kaindl, A.M., Degos, V., Peineau, S., Gouadon, E., Chhor, V., Loron, G., Le Charpentier, T., Josserand, J., Ali, C., Vivien, D., et al. (2012). Activation of microglial N-methyl-D-aspartate receptors triggers inflammation and neuronal cell death in the developing and mature brain. Ann. Neurol. *72*, 536–549.

Kannan, G., Kambhampati, S.P., and Kudchadkar, S.R. (2017). Effect of anesthetics on microglial activation and nanoparticle uptake: Implications for drug delivery in traumatic brain injury. J. Control. Release Off. J. Control. Release Soc.

Karrer, M., Lopez, M.A., Meier, D., Mikhail, C., Ogunshola, O.O., Müller, A.F., Strauss, L., Tafti, M., and Fontana, A. (2015). Cytokine-induced sleep: Neurons respond to TNF with production of chemokines and increased expression of Homer1a in vitro. Brain. Behav. Immun. *47*, 186–192.

Kato, G., Inada, H., Wake, H., Akiyoshi, R., Miyamoto, A., Eto, K., Ishikawa, T., Moorhouse, A.J., Strassman, A.M., and Nabekura, J. (2016a). Microglial Contact Prevents Excess Depolarization and Rescues Neurons from Excitotoxicity. ENeuro *3*.

Kato, R., Yamanaka, M., Yokota, E., Koshikawa, N., and Kobayashi, M. (2016b). Spike Timing Rigidity Is Maintained in Bursting Neurons under Pentobarbital-Induced Anesthetic Conditions. Front. Neural Circuits *10*, 86.

Kékesi, K.A., Dobolyi, A., Salfay, O., Nyitrai, G., and Juhász, G. (1997). Slow wave sleep is accompanied by release of certain amino acids in the thalamus of cats. Neuroreport *8*, 1183–1186.

Keren-Shaul, H., Spinrad, A., Weiner, A., Matcovitch-Natan, O., Dvir-Szternfeld, R., Ulland, T.K., David, E., Baruch, K., Lara-Astaiso, D., Toth, B., et al. (2017). A Unique Microglia Type Associated with Restricting Development of Alzheimer's Disease. Cell *169*, 1276-1290.e17.

Kielian, T. (2006). Toll-like receptors in central nervous system glial inflammation and homeostasis. J. Neurosci. Res. *83*, 711–730.

Kierdorf, K., Erny, D., Goldmann, T., Sander, V., Schulz, C., Perdiguero, E.G., Wieghofer, P., Heinrich, A., Riemke, P., Hölscher, C., et al. (2013). Microglia emerge from erythromyeloid precursors via Pu.1- and Irf8-dependent pathways. Nat. Neurosci. *16*, 273–280.

Kigerl, K.A., de Rivero Vaccari, J.P., Dietrich, W.D., Popovich, P.G., and Keane, R.W. (2014). Pattern recognition receptors and central nervous system repair. Exp. Neurol. *258*, 5–16.

Klinzing, J.G., Niethard, N., and Born, J. (2019). Mechanisms of systems memory consolidation during sleep. Nat. Neurosci.

Knutson, K.L., Spiegel, K., Penev, P., and Van Cauter, E. (2007). The metabolic consequences of sleep deprivation. Sleep Med. Rev. *11*, 163–178.

Kolodziejczak, M., Béchade, C., Gervasi, N., Irinopoulou, T., Banas, S.M., Cordier, C., Rebsam, A., Roumier, A., and Maroteaux, L. (2015). Serotonin Modulates Developmental Microglia via 5-HT2B Receptors: Potential Implication during Synaptic Refinement of Retinogeniculate Projections. ACS Chem. Neurosci. *6*, 1219–1230.

Kompotis, K., Hubbard, J., Emmenegger, Y., Perrault, A., Mühlethaler, M., Schwartz, S., Bayer, L., and Franken, P. (2019). Rocking Promotes Sleep in Mice through Rhythmic Stimulation of the Vestibular System. Curr. Biol. CB *29*, 392-401.e4.

Krabbe, G., Matyash, V., Pannasch, U., Mamer, L., Boddeke, H.W.G.M., and Kettenmann, H. (2012). Activation of serotonin receptors promotes microglial injury-induced motility but attenuates phagocytic activity. Brain. Behav. Immun. *26*, 419–428.

von Krosigk, M., Bal, T., and McCormick, D. (1993). Cellular mechanisms of a synchronized oscillation in the thalamus. Science *261*, 361–364.

Krueger, J.M. (2008). The role of cytokines in sleep regulation. Curr. Pharm. Des. *14*, 3408–3416.

Krueger, J.M., and Obäl, F. (1993). A neuronal group theory of sleep function. J. Sleep Res. *2*, 63–69.

Krueger, J.M., Clinton, J.M., Winters, B.D., Zielinski, M.R., Taishi, P., Jewett, K.A., and Davis, C.J. (2011). Involvement of cytokines in slow wave sleep. In Progress in Brain Research, (Elsevier), pp. 39–47.

Kubota, T., Hirota, K., Yoshida, H., Takahashi, S., Anzawa, N., Ohkawa, H., Kushikata, T., and Matsuki, A. (1999). Effects of sedatives on noradrenaline release from the medial prefrontal cortex in rats. Psychopharmacology (Berl.) *146*, 335–338.

Kuhn, S.A., van Landeghem, F.K.H., Zacharias, R., Färber, K., Rappert, A., Pavlovic, S., Hoffmann, A., Nolte, C., and Kettenmann, H. (2004). Microglia express GABA(B) receptors to modulate interleukin release. Mol. Cell. Neurosci. *25*, 312–322.

Kurpius, D., Nolley, E.P., and Dailey, M.E. (2007). Purines induce directed migration and rapid homing of microglia to injured pyramidal neurons in developing hippocampus. Glia *55*, 873–884.

Kwon, H.-B., and Sabatini, B.L. (2011). Glutamate induces de novo growth of functional spines in developing cortex. Nature *474*, 100–104.

Kyrargyri, V., Madry, C., Rifat, A., Arancibia-Carcamo, I.L., Jones, S.P., Chan, V.T.T., Xu, Y., Robaye, B., and Attwell, D. (2019). P2Y $_{13}$ receptors regulate microglial morphology, surveillance, and resting levels of interleukin 1β release. Glia glia.23719.

Lang, C., Barco, A., Zablow, L., Kandel, E.R., Siegelbaum, S.A., and Zakharenko, S.S. (2004). Transient expansion of synaptically connected dendritic spines upon induction of hippocampal long-term potentiation. Proc. Natl. Acad. Sci. U. S. A. *101*, 16665–16670.

Lanser, A.J., Rezende, R.M., Rubino, S., Lorello, P.J., Donnelly, D.J., Xu, H., Lau, L.A., Dulla, C.G., Caldarone, B.J., Robson, S.C., et al. (2017). Disruption of the ATP/adenosine balance in CD39-/- mice is associated with handling-induced seizures. Immunology *152*, 589–601.

Lanté, F., Toledo-Salas, J.-C., Ondrejcak, T., Rowan, M.J., and Ulrich, D. (2011). Removal of synaptic Ca^2+-permeable AMPA receptors during sleep. J. Neurosci. Off. J. Soc. Neurosci. *31*, 3953–3961.

Latchoumane, C.-F.V., Ngo, H.-V.V., Born, J., and Shin, H.-S. (2017). Thalamic Spindles Promote Memory Formation during Sleep through Triple Phase-Locking of Cortical, Thalamic, and Hippocampal Rhythms. Neuron *95*, 424-435.e6.

Lawson, L.J., Perry, V.H., and Gordon, S. (1992). Turnover of resident microglia in the normal adult mouse brain. Neuroscience *48*, 405–415.

Leak, R.K., and Moore, R.Y. (2001). Topographic organization of suprachiasmatic nucleus projection neurons. J. Comp. Neurol. *433*, 312–334.

Lee, A.K., and Wilson, M.A. (2002). Memory of sequential experience in the hippocampus during slow wave sleep. Neuron *36*, 1183–1194.

Lee, H., Brott, B.K., Kirkby, L.A., Adelson, J.D., Cheng, S., Feller, M.B., Datwani, A., and Shatz, C.J. (2014). Synapse elimination and learning rules co-regulated by MHC class I H2-Db. Nature *509*, 195–200.

Lee, S., Varvel, N.H., Konerth, M.E., Xu, G., Cardona, A.E., Ransohoff, R.M., and Lamb, B.T. (2010). CX3CR1 deficiency alters microglial activation and reduces beta-amyloid deposition in two Alzheimer's disease mouse models. Am. J. Pathol. *177*, 2549–2562.

Lehrman, E.K., Wilton, D.K., Litvina, E.Y., Welsh, C.A., Chang, S.T., Frouin, A., Walker, A.J., Heller, M.D., Umemori, H., Chen, C., et al. (2018). CD47 Protects Synapses from Excess Microglia-Mediated Pruning during Development. Neuron *100*, 120-134.e6.

Lemieux, M., Chen, J.-Y., Lonjers, P., Bazhenov, M., and Timofeev, I. (2014). The impact of cortical deafferentation on the neocortical slow oscillation. J. Neurosci. Off. J. Soc. Neurosci. *34*, 5689–5703.

Lesburgueres, E., Gobbo, O.L., Alaux-Cantin, S., Hambucken, A., Trifilieff, P., and Bontempi, B. (2011). Early Tagging of Cortical Networks Is Required for the Formation of Enduring Associative Memory. Science *331*, 924–928.

Leung, L.S., Petropoulos, S., Shen, B., Luo, T., Herrick, I., Rajakumar, N., and Ma, J. (2011). Lesion of cholinergic neurons in nucleus basalis enhances response to general anesthetics. Exp. Neurol. *228*, 259–269.

Li, J.-W., Zong, Y., Cao, X.-P., Tan, L., and Tan, L. (2018). Microglial priming in Alzheimer's disease. Ann. Transl. Med. *6*, 176–176.

Li, Y., Du, X.-F., Liu, C.-S., Wen, Z.-L., and Du, J.-L. (2012). Reciprocal regulation between resting microglial dynamics and neuronal activity in vivo. Dev. Cell *23*, 1189–1202.

Lim, S.-H., Park, E., You, B., Jung, Y., Park, A.-R., Park, S.G., and Lee, J.-R. (2013). Neuronal synapse formation induced by microglia and interleukin 10. PloS One *8*, e81218.

Lima, S.L., and Rattenborg, N.C. (2007). A behavioural shutdown can make sleeping safer: a strategic perspective on the function of sleep. Anim. Behav. *74*, 189–197.

Lima, S.L., Rattenborg, N.C., Lesku, J.A., and Amlaner, C.J. (2005). Sleeping under the risk of predation. Anim. Behav. *70*, 723–736.

Liu, Z.-W., Faraguna, U., Cirelli, C., Tononi, G., and Gao, X.-B. (2010). Direct evidence for wake-related increases and sleep-related decreases in synaptic strength in rodent cortex. J. Neurosci. Off. J. Soc. Neurosci. *30*, 8671–8675.

Lőrincz, M.L., Gunner, D., Bao, Y., Connelly, W.M., Isaac, J.T.R., Hughes, S.W., and Crunelli, V. (2015). A distinct class of slow (~0.2-2 Hz) intrinsically bursting layer 5 pyramidal neurons determines UP/DOWN state dynamics in the neocortex. J. Neurosci. Off. J. Soc. Neurosci. *35*, 5442–5458.

Losi, G., Mariotti, L., Sessolo, M., and Carmignoto, G. (2017). New Tools to Study Astrocyte Ca2+ Signal Dynamics in Brain Networks In Vivo. Front. Cell. Neurosci. *11*, 134.

Lowery, R.L., Tremblay, M.-E., Hopkins, B.E., and Majewska, A.K. (2017). The microglial fractalkine receptor is not required for activity-dependent plasticity in the mouse visual system. Glia *65*, 1744–1761.

Lu, J., and Zuo, Y. (2015). Forgetfulness illuminated. Nature *525*, 324–325.

Lu, J., Nelson, L.E., Franks, N., Maze, M., Chamberlin, N.L., and Saper, C.B. (2008). Role of endogenous sleep-wake and analgesic systems in anesthesia. J. Comp. Neurol. *508*, 648–662.

Lucas, R.J., Douglas, R.H., and Foster, R.G. (2001). Characterization of an ocular photopigment capable of driving pupillary constriction in mice. Nat. Neurosci. *4*, 621–626.

Lukatch, H.S., Kiddoo, C.E., and MacIver, M.B. (2005). Anesthetic-induced Burst Suppression EEG Activity Requires Glutamate-mediated Excitatory Synaptic Transmission. Cereb. Cortex *15*, 1322–1331.

Luo, J., Phan, T.X., Yang, Y., Garelick, M.G., and Storm, D.R. (2013). Increases in cAMP, MAPK activity, and CREB phosphorylation during REM sleep: implications for REM sleep and memory consolidation. J. Neurosci. Off. J. Soc. Neurosci. *33*, 6460–6468.

Luppi, P.-H., Peyron, C., and Fort, P. (2017). Not a single but multiple populations of GABAergic neurons control sleep. Sleep Med. Rev. *32*, 85–94.

Lydic, R., and Baghdoyan, H.A. (2002). Ketamine and MK-801 decrease acetylcholine release in the pontine reticular formation, slow breathing, and disrupt sleep. Sleep *25*, 617–622.

Madry, C., and Attwell, D. (2015). Receptors, ion channels, and signaling mechanisms underlying microglial dynamics. J. Biol. Chem. *290*, 12443–12450.

Madry, C., Kyrargyri, V., Arancibia-Cárcamo, I.L., Jolivet, R., Kohsaka, S., Bryan, R.M., and Attwell, D. (2018a). Microglial Ramification, Surveillance, and Interleukin-1β Release Are Regulated by the Two-Pore Domain K+ Channel THIK-1. Neuron *97*, 299-312.e6.

Madry, C., Arancibia-Cárcamo, I.L., Kyrargyri, V., Chan, V.T.T., Hamilton, N.B., and Attwell, D. (2018b). Effects of the ecto-ATPase apyrase on microglial ramification and surveillance reflect cell depolarization, not ATP depletion. Proc. Natl. Acad. Sci. U. S. A. *115*, E1608–E1617.

Maggi, L. (2011). CX3CR1 deficiency alters hippocampal-dependent plasticity phenomena blunting the effects of enriched environment. Front. Cell. Neurosci. *5*.

Malatesta, P., Hartfuss, E., and Götz, M. (2000). Isolation of radial glial cells by fluorescent-activated cell sorting reveals a neuronal lineage. Dev. Camb. Engl. *127*, 5253–5263.

Malenka, R.C., Kauer, J.A., Perkel, D.J., and Nicoll, R.A. (1989). The impact of postsynaptic calcium on synaptic transmission--its role in long-term potentiation. Trends Neurosci. *12*, 444–450.

Maletic-Savatic, M., Malinow, R., and Svoboda, K. (1999). Rapid dendritic morphogenesis in CA1 hippocampal dendrites induced by synaptic activity. Science *283*, 1923–1927.

Malvache, A., Reichinnek, S., Villette, V., Haimerl, C., and Cossart, R. (2016). Awake hippocampal reactivations project onto orthogonal neuronal assemblies. Science *353*, 1280–1283.

Maret, S., Faraguna, U., Nelson, A.B., Cirelli, C., and Tononi, G. (2011). Sleep and waking modulate spine turnover in the adolescent mouse cortex. Nat. Neurosci. *14*, 1418–1420.

Marín-Teva, J.L., Dusart, I., Colin, C., Gervais, A., van Rooijen, N., and Mallat, M. (2004). Microglia promote the death of developing Purkinje cells. Neuron *41*, 535–547.

Markram, K., and Markram, H. (2010). The intense world theory - a unifying theory of the neurobiology of autism. Front. Hum. Neurosci. *4*, 224.

Marrosu, F., Portas, C., Mascia, M.S., Casu, M.A., Fà, M., Giagheddu, M., Imperato, A., and Gessa, G.L. (1995). Microdialysis measurement of cortical and hippocampal acetylcholine release during sleep-wake cycle in freely moving cats. Brain Res. *671*, 329–332.

Matcovitch-Natan, O., Winter, D.R., Giladi, A., Vargas Aguilar, S., Spinrad, A., Sarrazin, S., Ben-Yehuda, H., David, E., Zelada González, F., Perrin, P., et al. (2016). Microglia development follows a stepwise program to regulate brain homeostasis. Science *353*, aad8670.

Mathys, H., Adaikkan, C., Gao, F., Young, J.Z., Manet, E., Hemberg, M., De Jager, P.L., Ransohoff, R.M., Regev, A., and Tsai, L.-H. (2017). Temporal Tracking of Microglia Activation in Neurodegeneration at Single-Cell Resolution. Cell Rep. *21*, 366–380.

Matyash, M., Zabiegalov, O., Wendt, S., Matyash, V., and Kettenmann, H. (2017). The adenosine generating enzymes CD39/CD73 control microglial processes ramification in the mouse brain. PloS One *12*, e0175012.

Methippara, M.M., Kumar, S., Alam, M.N., Szymusiak, R., and McGinty, D. (2005). Effects on sleep of microdialysis of adenosine A1 and A2a receptor analogs into the lateral preoptic area of rats. Am. J. Physiol. Regul. Integr. Comp. Physiol. *289*, R1715-1723.

Michelson, N.J., and Kozai, T.D.Y. (2018). Isoflurane and ketamine differentially influence spontaneous and evoked laminar electrophysiology in mouse V1. J. Neurophysiol. *120*, 2232–2245.

Milior, G., Lecours, C., Samson, L., Bisht, K., Poggini, S., Pagani, F., Deflorio, C., Lauro, C., Alboni, S., Limatola, C., et al. (2016). Fractalkine receptor deficiency impairs microglial and neuronal responsiveness to chronic stress. Brain. Behav. Immun. *55*, 114–125.

Mistlberger, R.E. (2005). Circadian regulation of sleep in mammals: role of the suprachiasmatic nucleus. Brain Res. Brain Res. Rev. *49*, 429–454.

Mistlberger, R.E., Bergmann, B.M., Waldenar, W., and Rechtschaffen, A. (1983). Recovery sleep following sleep deprivation in intact and suprachiasmatic nuclei-lesioned rats. Sleep *6*, 217–233.

Miyamoto, A., Wake, H., Ishikawa, A.W., Eto, K., Shibata, K., Murakoshi, H., Koizumi, S., Moorhouse, A.J., Yoshimura, Y., and Nabekura, J. (2016). Microglia contact induces synapse formation in developing somatosensory cortex. Nat. Commun. *7*, 12540.

Miyawaki, H., and Diba, K. (2016). Regulation of Hippocampal Firing by Network Oscillations during Sleep. Curr. Biol. CB *26*, 893–902.

Miyawaki, H., Watson, B.O., and Diba, K. (2019). Neuronal firing rates diverge during REM and homogenize during non-REM. Sci. Rep. *9*.

Mizuseki, K., and Buzsáki, G. (2013). Preconfigured, skewed distribution of firing rates in the hippocampus and entorhinal cortex. Cell Rep. *4*, 1010–1021.

Mizuseki, K., and Miyawaki, H. (2017). Hippocampal information processing across sleep/wake cycles. Neurosci. Res. *118*, 30–47.

Moncada, D., Ballarini, F., and Viola, H. (2015). Behavioral Tagging: A Translation of the Synaptic Tagging and Capture Hypothesis. Neural Plast. *2015*, 650780.

Montgomery, S.M., Sirota, A., and Buzsáki, G. (2008). Theta and gamma coordination of hippocampal networks during waking and rapid eye movement sleep. J. Neurosci. Off. J. Soc. Neurosci. *28*, 6731–6741.

Moore, J.T., Chen, J., Han, B., Meng, Q.C., Veasey, S.C., Beck, S.G., and Kelz, M.B. (2012). Direct activation of sleep-promoting VLPO neurons by volatile anesthetics contributes to anesthetic hypnosis. Curr. Biol. CB *22*, 2008–2016.

Mosser, C.-A., Baptista, S., Arnoux, I., and Audinat, E. (2017). Microglia in CNS development: Shaping the brain for the future. Prog. Neurobiol. *149–150*, 1–20.

Naccarato, E.F., and Hunter, W.S. (1979). Anaesthetic effects of various ratios of ketamine and xylazine in rhesus monkeys (*Macaca mulatta*). Lab. Anim. *13*, 317–319.

Nagarajan, N., Jones, B.W., West, P.J., Marc, R.E., and Capecchi, M.R. (2018). Corticostriatal circuit defects in Hoxb8 mutant mice. Mol. Psychiatry *23*, 1868–1877.

Nagy, J.I., and Rash, J.E. (2000). Connexins and gap junctions of astrocytes and oligodendrocytes in the CNS. Brain Res. Rev. *32*, 29–44.

Nakajima, K., and Kohsaka, S. (2001). Microglia: activation and their significance in the central nervous system. J. Biochem. (Tokyo) *130*, 169–175.

Nakki, R., Nickolenko, J., Chang, J., Sagar, S.M., and Sharp, F.R. (1996). Haloperidol prevents ketamine- and phencyclidine-induced HSP70 protein expression but not microglial activation. Exp. Neurol. *137*, 234–241.

Nayak, D., Roth, T.L., and McGavern, D.B. (2014). Microglia development and function. Annu. Rev. Immunol. *32*, 367–402.

Nelson, L.E., Lu, J., Guo, T., Saper, C.B., Franks, N.P., and Maze, M. (2003). The alpha2-adrenoceptor agonist dexmedetomidine converges on an endogenous sleep-promoting pathway to exert its sedative effects. Anesthesiology *98*, 428–436.

Neske, G.T. (2015). The Slow Oscillation in Cortical and Thalamic Networks: Mechanisms and Functions. Front. Neural Circuits *9*, 88.

Niethard, N., Hasegawa, M., Itokazu, T., Oyanedel, C.N., Born, J., and Sato, T.R. (2016). Sleep-Stage-Specific Regulation of Cortical Excitation and Inhibition. Curr. Biol. CB *26*, 2739–2749.

Niethard, N., Ngo, H.-V.V., Ehrlich, I., and Born, J. (2018). Cortical circuit activity underlying sleep slow oscillations and spindles. Proc. Natl. Acad. Sci. *115*, E9220–E9229.

Nikodemova, M., Kimyon, R.S., De, I., Small, A.L., Collier, L.S., and Watters, J.J. (2015). Microglial numbers attain adult levels after undergoing a rapid decrease in cell number in the third postnatal week. J. Neuroimmunol. *278*, 280–288.

Nimmerjahn, A., Kirchhoff, F., and Helmchen, F. (2005). Resting microglial cells are highly dynamic surveillants of brain parenchyma in vivo. Science *308*, 1314–1318.

Nitz, D., and Siegel, J. (1997a). GABA release in the dorsal raphe nucleus: role in the control of REM sleep. Am. J. Physiol. *273*, R451-455.

Nitz, D., and Siegel, J.M. (1996). GABA release in posterior hypothalamus across sleep-wake cycle. Am. J. Physiol. *271*, R1707-1712.

Nitz, D., and Siegel, J.M. (1997b). GABA release in the locus coeruleus as a function of sleep/wake state. Neuroscience *78*, 795–801.

O'Donnell, J., Zeppenfeld, D., McConnell, E., Pena, S., and Nedergaard, M. (2012). Norepinephrine: a neuromodulator that boosts the function of multiple cell types to optimize CNS performance. Neurochem. Res. *37*, 2496–2512.

Ohsawa, K., Sanagi, T., Nakamura, Y., Suzuki, E., Inoue, K., and Kohsaka, S. (2012). Adenosine A3 receptor is involved in ADP-induced microglial process extension and migration. J. Neurochem. *121*, 217–227.

Olsen, M.L., Khakh, B.S., Skatchkov, S.N., Zhou, M., Lee, C.J., and Rouach, N. (2015). New Insights on Astrocyte Ion Channels: Critical for Homeostasis and Neuron-Glia Signaling. J. Neurosci. *35*, 13827–13835.

Orr, A.G., Orr, A.L., Li, X.-J., Gross, R.E., and Traynelis, S.F. (2009). Adenosine A(2A) receptor mediates microglial process retraction. Nat. Neurosci. *12*, 872–878.

Osterhout, D.J., Wolven, A., Wolf, R.M., Resh, M.D., and Chao, M.V. (1999). Morphological Differentiation of Oligodendrocytes Requires Activation of Fyn Tyrosine Kinase. J. Cell Biol. *145*, 1209–1218.

Oswald, I. (1980). Sleep as restorative process: human clues. Prog. Brain Res. *53*, 279–288.

Païdassi, H., Tacnet-Delorme, P., Garlatti, V., Darnault, C., Ghebrehiwet, B., Gaboriaud, C., Arlaud, G.J., and Frachet, P. (2008). C1q binds phosphatidylserine and likely acts as a multiligand-bridging molecule in apoptotic cell recognition. J. Immunol. Baltim. Md 1950 *180*, 2329–2338.

Pankratov, Y., Lalo, U., Verkhratsky, A., and North, R.A. (2006). Vesicular release of ATP at central synapses. Pflugers Arch. *452*, 589–597.

Paolicelli, R.C., Bolasco, G., Pagani, F., Maggi, L., Scianni, M., Panzanelli, P., Giustetto, M., Ferreira, T.A., Guiducci, E., Dumas, L., et al. (2011). Synaptic pruning by microglia is necessary for normal brain development. Science *333*, 1456–1458.

Paolicelli, R.C., Bisht, K., and Tremblay, M.-Ã. (2014). Fractalkine regulation of microglial physiology and consequences on the brain and behavior. Front. Cell. Neurosci. *8*.

Papadopoulos, M.C., and Verkman, A.S. (2013). Aquaporin water channels in the nervous system. Nat. Rev. Neurosci. *14*, 265–277.

Parkhurst, C.N., Yang, G., Ninan, I., Savas, J.N., Yates, J.R., Lafaille, J.J., Hempstead, B.L., Littman, D.R., and Gan, W.-B. (2013). Microglia promote learning-dependent synapse formation through brain-derived neurotrophic factor. Cell *155*, 1596–1609.

Pascual, O., Casper, K.B., Kubera, C., Zhang, J., Revilla-Sanchez, R., Sul, J.-Y., Takano, H., Moss, S.J., McCarthy, K., and Haydon, P.G. (2005). Astrocytic purinergic signaling coordinates synaptic networks. Science *310*, 113–116.

Pascual, O., Ben Achour, S., Rostaing, P., Triller, A., and Bessis, A. (2012). Microglia activation triggers astrocyte-mediated modulation of excitatory neurotransmission. Proc. Natl. Acad. Sci. *109*, E197–E205.

Pelluru, D., Konadhode, R.R., Bhat, N.R., and Shiromani, P.J. (2016). Optogenetic stimulation of astrocytes in the posterior hypothalamus increases sleep at night in C57BL/6J mice. Eur. J. Neurosci. *43*, 1298–1306.

Peng, J., Gu, N., Zhou, L., B Eyo, U., Murugan, M., Gan, W.-B., and Wu, L.-J. (2016). Microglia and monocytes synergistically promote the transition from acute to chronic pain after nerve injury. Nat. Commun. *7*, 12029.

Peng, J., Liu, Y., Umpierre, A.D., Xie, M., Tian, D.-S., Richardson, J.R., and Wu, L.-J. (2019). Microglial P2Y12 receptor regulates ventral hippocampal CA1 neuronal excitability and innate fear in mice. Mol. Brain *12*, 71.

Perry, J.S.A., and Ravichandran, K.S. (2017). Embryonic Trogocytosis: Neighborly Nibbling during Development. Curr. Biol. CB *27*, R68–R70.

Petrovic, J., Ciric, J., Lazic, K., Kalauzi, A., and Saponjic, J. (2013). Lesion of the pedunculopontine tegmental nucleus in rat augments cortical activation and disturbs sleep/wake state transitions structure. Exp. Neurol. *247*, 562–571.

Pfeiffer, T., Avignone, E., and Nägerl, U.V. (2016). Induction of hippocampal long-term potentiation increases the morphological dynamics of microglial processes and prolongs their contacts with dendritic spines. Sci. Rep. *6*.

Pigarev, I.N., Nothdurft, H.C., and Kastner, S. (1997). Evidence for asynchronous development of sleep in cortical areas. Neuroreport *8*, 2557–2560.

Polack, P.-O., Friedman, J., and Golshani, P. (2013). Cellular mechanisms of brain state-dependent gain modulation in visual cortex. Nat. Neurosci. *16*, 1331–1339.

Pont-Lezica, L., Beumer, W., Colasse, S., Drexhage, H., Versnel, M., and Bessis, A. (2014). Microglia shape corpus callosum axon tract fasciculation: functional impact of prenatal inflammation. Eur. J. Neurosci. *39*, 1551–1557.

Porkka-Heiskanen, T., Strecker, R.E., and McCarley, R.W. (2000). Brain site-specificity of extracellular adenosine concentration changes during sleep deprivation and spontaneous sleep: an in vivo microdialysis study. Neuroscience *99*, 507–517.

Portas, C.M., Bjorvatn, B., and Ursin, R. (2000). Serotonin and the sleep/wake cycle: special emphasis on microdialysis studies. Prog. Neurobiol. *60*, 13–35.

Poulet, J.F.A., and Petersen, C.C.H. (2008). Internal brain state regulates membrane potential synchrony in barrel cortex of behaving mice. Nature *454*, 881–885.

Prinz, M., and Priller, J. (2014). Microglia and brain macrophages in the molecular age: from origin to neuropsychiatric disease. Nat. Rev. Neurosci. *15*, 300–312.

Prinz, M., Erny, D., and Hagemeyer, N. (2017). Ontogeny and homeostasis of CNS myeloid cells. Nat. Immunol. *18*, 385–392.

Provencio, I., Rodriguez, I.R., Jiang, G., Hayes, W.P., Moreira, E.F., and Rollag, M.D. (2000). A novel human opsin in the inner retina. J. Neurosci. Off. J. Soc. Neurosci. *20*, 600–605.

Puchałowicz, K., Tarnowski, M., Baranowska-Bosiacka, I., Chlubek, D., and Dziedziejko, V. (2014). P2X and P2Y receptors—role in the pathophysiology of the nervous system. Int. J. Mol. Sci. *15*, 23672–23704.

Puentes-Mestril, C., and Aton, S.J. (2017). Linking Network Activity to Synaptic Plasticity during Sleep: Hypotheses and Recent Data. Front. Neural Circuits *11*.

Qian, X., Shen, Q., Goderie, S.K., He, W., Capela, A., Davis, A.A., and Temple, S. (2000). Timing of CNS Cell Generation. Neuron *28*, 69–80.

Raghuraman, R., Karthikeyan, A., Wei, W.L., Dheen, S.T., and Sajikumar, S. (2019). Activation of microglia in acute hippocampal slices affects activity-dependent long-term potentiation and synaptic tagging and capture in area CA1. Neurobiol. Learn. Mem. *163*, 107039.

Raj, D.D.A., Jaarsma, D., Holtman, I.R., Olah, M., Ferreira, F.M., Schaafsma, W., Brouwer, N., Meijer, M.M., de Waard, M.C., van der Pluijm, I., et al. (2014). Priming of microglia in a DNA-repair deficient model of accelerated aging. Neurobiol. Aging *35*, 2147–2160.

Ralph, M.R., Foster, R.G., Davis, F.C., and Menaker, M. (1990). Transplanted suprachiasmatic nucleus determines circadian period. Science *247*, 975–978.

Ransohoff, R.M. (2009). Chemokines and chemokine receptors: standing at the crossroads of immunobiology and neurobiology. Immunity *31*, 711–721.

Ransohoff, R.M. (2016). A polarizing question: do M1 and M2 microglia exist? Nat. Neurosci. *19*, 987–991.

Ransohoff, R.M., and Perry, V.H. (2009). Microglial physiology: unique stimuli, specialized responses. Annu. Rev. Immunol. *27*, 119–145.

Rasband, M.N. (2016). Glial Contributions to Neural Function and Disease. Mol. Cell. Proteomics *15*, 355–361.

Rasch, B., and Born, J. (2013). About sleep's role in memory. Physiol. Rev. *93*, 681–766.

Rector, D.M., Topchiy, I.A., Carter, K.M., and Rojas, M.J. (2005). Local functional state differences between rat cortical columns. Brain Res. *1047*, 45–55.

Rector, D.M., Schei, J.L., Van Dongen, H.P.A., Belenky, G., and Krueger, J.M. (2009). Physiological markers of local sleep. Eur. J. Neurosci. *29*, 1771–1778.

Redondo, R.L., and Morris, R.G.M. (2011). Making memories last: the synaptic tagging and capture hypothesis. Nat. Rev. Neurosci. *12*, 17–30.

Rex, C.S., Lin, C.-Y., Kramar, E.A., Chen, L.Y., Gall, C.M., and Lynch, G. (2007). Brain-Derived Neurotrophic Factor Promotes Long-Term Potentiation-Related Cytoskeletal Changes in Adult Hippocampus. J. Neurosci. *27*, 3017–3029.

Reyes-Vázquez, C., Prieto-Gómez, B., and Dafny, N. (2012). Interferon modulates central nervous system function. Brain Res. *1442*, 76–89.

Rogers, J.T., Morganti, J.M., Bachstetter, A.D., Hudson, C.E., Peters, M.M., Grimmig, B.A., Weeber, E.J., Bickford, P.C., and Gemma, C. (2011). CX3CR1 Deficiency Leads to Impairment of Hippocampal Cognitive Function and Synaptic Plasticity. J. Neurosci. *31*, 16241–16250.

Roumier, A., Béchade, C., Poncer, J.-C., Smalla, K.-H., Tomasello, E., Vivier, E., Gundelfinger, E.D., Triller, A., and Bessis, A. (2004). Impaired synaptic function in the microglial KARAP/DAP12-deficient mouse. J. Neurosci. Off. J. Soc. Neurosci. *24*, 11421–11428.

Roumier, A., Pascual, O., Béchade, C., Wakselman, S., Poncer, J.-C., Réal, E., Triller, A., and Bessis, A. (2008). Prenatal activation of microglia induces delayed impairment of glutamatergic synaptic function. PloS One *3*, e2595.

Rowland, D.C., Roudi, Y., Moser, M.-B., and Moser, E.I. (2016). Ten Years of Grid Cells. Annu. Rev. Neurosci. *39*, 19–40.

Roy, S., Krueger, J.M., Rector, D.M., and Wan, Y. (2008). A network model for activity-dependent sleep regulation. J. Theor. Biol. *253*, 462–468.

Rusak, B., and Zucker, I. (1979). Neural regulation of circadian rhythms. Physiol. Rev. *59*, 449–526.

Sadowski, J.H.L.P., Jones, M.W., and Mellor, J.R. (2016). Sharp-Wave Ripples Orchestrate the Induction of Synaptic Plasticity during Reactivation of Place Cell Firing Patterns in the Hippocampus. Cell Rep. *14*, 1916–1929.

Salvi, V., Sozio, F., Sozzani, S., and Del Prete, A. (2017). Role of Atypical Chemokine Receptors in Microglial Activation and Polarization. Front. Aging Neurosci. *9*, 148.

Sanchez-Vives, M.V., and McCormick, D.A. (2000). Cellular and network mechanisms of rhythmic recurrent activity in neocortex. Nat. Neurosci. *3*, 1027–1034.

Sanford, L.D., Tang, X., Xiao, J., Ross, R.J., and Morrison, A.R. (2003). GABAergic Regulation of REM Sleep in Reticularis Pontis Oralis and Caudalis in Rats. J. Neurophysiol. *90*, 938–945.

Saper, C.B., and Fuller, P.M. (2017). Wake–sleep circuitry: an overview. Curr. Opin. Neurobiol. *44*, 186–192.

Saper, C.B., Chou, T.C., and Scammell, T.E. (2001). The sleep switch: hypothalamic control of sleep and wakefulness. Trends Neurosci. *24*, 726–731.

Saper, C.B., Scammell, T.E., and Lu, J. (2005). Hypothalamic regulation of sleep and circadian rhythms. Nature *437*, 1257–1263.

Saper, C.B., Fuller, P.M., Pedersen, N.P., Lu, J., and Scammell, T.E. (2010). Sleep state switching. Neuron *68*, 1023–1042.

Sasaki, Y., Hoshi, M., Akazawa, C., Nakamura, Y., Tsuzuki, H., Inoue, K., and Kohsaka, S. (2003). Selective expression of Gi/o-coupled ATP receptor P2Y12 in microglia in rat brain. Glia *44*, 242–250.

Sato, K. (2015). Effects of Microglia on Neurogenesis. Glia *63*, 1394–1405.

Scammell, T.E., Arrigoni, E., and Lipton, J. (2017). Neural Circuitry of Wakefulness and Sleep. Neuron *93*, 747–765.

Schafer, D.P., Lehrman, E.K., Kautzman, A.G., Koyama, R., Mardinly, A.R., Yamasaki, R., Ransohoff, R.M., Greenberg, M.E., Barres, B.A., and Stevens, B. (2012). Microglia sculpt postnatal neural circuits in an activity and complement-dependent manner. Neuron *74*, 691–705.

Schuldiner, O., and Yaron, A. (2015). Mechanisms of developmental neurite pruning. Cell. Mol. Life Sci. CMLS *72*, 101–119.

Sedel, F., Béchade, C., Vyas, S., and Triller, A. (2004). Macrophage-derived tumor necrosis factor alpha, an early developmental signal for motoneuron death. J. Neurosci. Off. J. Soc. Neurosci. *24*, 2236–2246.

Seibt, J., Richard, C.J., Sigl-Glöckner, J., Takahashi, N., Kaplan, D.I., Doron, G., de Limoges, D., Bocklisch, C., and Larkum, M.E. (2017). Cortical dendritic activity correlates with spindle-rich oscillations during sleep in rodents. Nat. Commun. *8*, 684.

Seigneur, J., Kroeger, D., Nita, D.A., and Amzica, F. (2006). Cholinergic action on cortical glial cells in vivo. Cereb. Cortex N. Y. N 1991 *16*, 655–668.

Setiawan, E., Attwells, S., Wilson, A.A., Mizrahi, R., Rusjan, P.M., Miler, L., Xu, C., Sharma, S., Kish, S., Houle, S., et al. (2018). Association of translocator protein total distribution volume with duration of untreated major depressive disorder: a cross-sectional study. Lancet Psychiatry *5*, 339–347.

Shaham, S. (2005). Glia-neuron interactions in nervous system function and development. Curr. Top. Dev. Biol. *69*, 39–66.

Sheng, J., Ruedl, C., and Karjalainen, K. (2015a). Most Tissue-Resident Macrophages Except Microglia Are Derived from Fetal Hematopoietic Stem Cells. Immunity *43*, 382–393.

Sheng, L., Leshchyns'ka, I., and Sytnyk, V. (2015b). Neural cell adhesion molecule 2 promotes the formation of filopodia and neurite branching by inducing submembrane increases in Ca2+ levels. J. Neurosci. Off. J. Soc. Neurosci. *35*, 1739–1752.

Sherin, J.E., Shiromani, P.J., McCarley, R.W., and Saper, C.B. (1996). Activation of ventrolateral preoptic neurons during sleep. Science *271*, 216–219.

Shigemoto-Mogami, Y., Hoshikawa, K., Goldman, J.E., Sekino, Y., and Sato, K. (2014). Microglia Enhance Neurogenesis and Oligodendrogenesis in the Early Postnatal Subventricular Zone. J. Neurosci. *34*, 2231–2243.

Shih, A.Y., Mateo, C., Drew, P.J., Tsai, P.S., and Kleinfeld, D. (2012). A Polished and Reinforced Thinned-skull Window for Long-term Imaging of the Mouse Brain. J. Vis. Exp. 3742.

Siegel, J.M. (2008). Do all animals sleep? Trends Neurosci. *31*, 208–213.

Sigl-Glöckner, J., and Seibt, J. (2019). Peeking into the sleeping brain: Using in vivo imaging in rodents to understand the relationship between sleep and cognition. J. Neurosci. Methods *316*, 71–82.

Sipe, G.O., Lowery, R.L., Tremblay, M.-È., Kelly, E.A., Lamantia, C.E., and Majewska, A.K. (2016). Microglial P2Y12 is necessary for synaptic plasticity in mouse visual cortex. Nat. Commun. *7*.

Sogn, C.J.L., Puchades, M., and Gundersen, V. (2013). Rare contacts between synapses and microglial processes containing high levels of Iba1 and actin--a postembedding immunogold study in the healthy rat brain. Eur. J. Neurosci. *38*, 2030–2040.

Son, Y. (2010). Molecular mechanisms of general anesthesia. Korean J. Anesthesiol. *59*, 3–8.

Squarzoni, P., Oller, G., Hoeffel, G., Pont-Lezica, L., Rostaing, P., Low, D., Bessis, A., Ginhoux, F., and Garel, S. (2014). Microglia modulate wiring of the embryonic forebrain. Cell Rep. *8*, 1271–1279.

Stefani, J., Tschesnokowa, O., Parrilla, M., Robaye, B., Boeynaems, J.-M., Acker-Palmer, A., Zimmermann, H., and Gampe, K. (2018). Disruption of the Microglial ADP Receptor P2Y13 Enhances Adult Hippocampal Neurogenesis. Front. Cell. Neurosci. *12*, 134.

Stender, J., Mortensen, K.N., Thibaut, A., Darkner, S., Laureys, S., Gjedde, A., and Kupers, R. (2016). The Minimal Energetic Requirement of Sustained Awareness after Brain Injury. Curr. Biol. CB *26*, 1494–1499.

Steriade, M. (1994). Sleep oscillations and their blockage by activating systems. J. Psychiatry Neurosci. JPN *19*, 354–358.

Steriade, M., McCormick, D., and Sejnowski, T. (1993). Thalamocortical oscillations in the sleeping and aroused brain. Science *262*, 679–685.

Steriade, M., Timofeev, I., and Grenier, F. (2001). Natural waking and sleep states: a view from inside neocortical neurons. J. Neurophysiol. *85*, 1969–1985.

Stevens, B., Allen, N.J., Vazquez, L.E., Howell, G.R., Christopherson, K.S., Nouri, N., Micheva, K.D., Mehalow, A.K., Huberman, A.D., Stafford, B., et al. (2007). The classical complement cascade mediates CNS synapse elimination. Cell *131*, 1164–1178.

Stickgold, R., and Walker, M.P. (2013). Sleep-dependent memory triage: evolving generalization through selective processing. Nat. Neurosci. *16*, 139–145.

Stowell, R.D., Wong, E.L., Batchelor, H.N., Mendes, M.S., Lamantia, C.E., Whitelaw, B.S., and Majewska, A.K. (2018). Cerebellar microglia are dynamically unique and survey Purkinje neurons in vivo. Dev. Neurobiol. *78*, 627–644.

Sun, W., Suzuki, K., Toptunov, D., Stoyanov, S., Yuzaki, M., Khiroug, L., and Dityatev, A. (2019). In vivo Two-Photon Imaging of Anesthesia-Specific Alterations in Microglial Surveillance and Photodamage-Directed Motility in Mouse Cortex. Front. Neurosci. *13*, 421.

Suntsova, N., Guzman-Marin, R., Kumar, S., Alam, M.N., Szymusiak, R., and McGinty, D. (2007). The median preoptic nucleus reciprocally modulates activity of arousal-related and sleep-related neurons in the perifornical lateral hypothalamus. J. Neurosci. Off. J. Soc. Neurosci. *27*, 1616–1630.

Swinnen, N., Smolders, S., Avila, A., Notelaers, K., Paesen, R., Ameloot, M., Brône, B., Legendre, P., and Rigo, J.-M. (2013). Complex invasion pattern of the cerebral cortex bymicroglial cells during development of the mouse embryo. Glia *61*, 150–163.

Szepesi, Z., Manouchehrian, O., Bachiller, S., and Deierborg, T. (2018). Bidirectional Microglia-Neuron Communication in Health and Disease. Front. Cell. Neurosci. *12*, 323.

Tang, Y., and Le, W. (2016). Differential Roles of M1 and M2 Microglia in Neurodegenerative Diseases. Mol. Neurobiol. *53*, 1181–1194.

Tarozzo, G., Bortolazzi, S., Crochemore, C., Chen, S.-C., Lira, A.S., Abrams, J.S., and Beltramo, M. (2003). Fractalkine protein localization and gene expression in mouse brain. J. Neurosci. Res. *73*, 81–88.

Thion, M.S., and Garel, S. (2017). On place and time: microglia in embryonic and perinatal brain development. Curr. Opin. Neurobiol. *47*, 121–130.

Thion, M.S., Low, D., Silvin, A., Chen, J., Grisel, P., Schulte-Schrepping, J., Blecher, R., Ulas, T., Squarzoni, P., Hoeffel, G., et al. (2018). Microbiome Influences Prenatal and Adult Microglia in a Sex-Specific Manner. Cell *172*, 500-516.e16.

Thrane, A.S., Thrane, V.R., Zeppenfeld, D., Lou, N., Xu, Q., Nagelhus, E.A., and Nedergaard, M. (2012). General anesthesia selectively disrupts astrocyte calcium signaling in the awake mouse cortex. Proc. Natl. Acad. Sci. U. S. A. *109*, 18974–18979.

Tian, D.-S., Li, C.-Y., Qin, C., Murugan, M., Wu, L.-J., and Liu, J.-L. (2016). Deficiency in the voltage-gated proton channel Hv1 increases M2 polarization of microglia and attenuates brain damage from photothrombotic ischemic stroke. J. Neurochem. *139*, 96–105.

Tobler, I., Borbély, A.A., and Groos, G. (1983). The effect of sleep deprivation on sleep in rats with suprachiasmatic lesions. Neurosci. Lett. *42*, 49–54.

Tononi, G., and Cirelli, C. (2014). Sleep and the price of plasticity: from synaptic and cellular homeostasis to memory consolidation and integration. Neuron *81*, 12–34.

Town, T., Nikolic, V., and Tan, J. (2005). [No title found]. J. Neuroinflammation *2*, 24.

Trachsel, L., Edgar, D.M., Seidel, W.F., Heller, H.C., and Dement, W.C. (1992). Sleep homeostasis in suprachiasmatic nuclei-lesioned rats: effects of sleep deprivation and triazolam administration. Brain Res. *589*, 253–261.

Tremblay, M.-È., Lowery, R.L., and Majewska, A.K. (2010a). Microglial interactions with synapses are modulated by visual experience. PLoS Biol. *8*, e1000527.

Tremblay, M.-È., Lecours, C., Samson, L., Sánchez-Zafra, V., and Sierra, A. (2015). From the Cajal alumni Achúcarro and Río-Hortega to the rediscovery of never-resting microglia. Front. Neuroanat. *9*, 45.

Ueno, M., Fujita, Y., Tanaka, T., Nakamura, Y., Kikuta, J., Ishii, M., and Yamashita, T. (2013). Layer V cortical neurons require microglial support for survival during postnatal development. Nat. Neurosci. *16*, 543–551.

Ulmann, L., Levavasseur, F., Avignone, E., Peyroutou, R., Hirbec, H., Audinat, E., and Rassendren, F. (2013). Involvement of P2X4 receptors in hippocampal microglial activation after status epilepticus. Glia *61*, 1306–1319.

Urade, Y., and Hayaishi, O. (2011). Prostaglandin D2 and sleep/wake regulation. Sleep Med. Rev. *15*, 411–418.

Van Cauter, E., Spiegel, K., Tasali, E., and Leproult, R. (2008). Metabolic consequences of sleep and sleep loss. Sleep Med. *9 Suppl 1*, S23-28.

Van Dongen, H.P.A., Belenky, G., and Krueger, J.M. (2011). A local, bottom-up perspective on sleep deprivation and neurobehavioral performance. Curr. Top. Med. Chem. *11*, 2414–2422.

Vanini, G., Lydic, R., and Baghdoyan, H.A. (2012). GABA-to-ACh Ratio in Basal Forebrain and Cerebral Cortex Varies Significantly During Sleep. Sleep *35*, 1325–1334.

Vansteensel, M.J., Michel, S., and Meijer, J.H. (2008). Organization of cell and tissue circadian pacemakers: a comparison among species. Brain Res. Rev. *58*, 18–47.

Verdonk, F., Roux, P., Flamant, P., Fiette, L., Bozza, F.A., Simard, S., Lemaire, M., Plaud, B., Shorte, S.L., Sharshar, T., et al. (2016). Phenotypic clustering: a novel method for microglial morphology analysis. J. Neuroinflammation *13*, 153.

Verdonk, F., Petit, A.-C., Abdel-Ahad, P., Vinckier, F., Jouvion, G., de Maricourt, P., De Medeiros, G.F., Danckaert, A., Van Steenwinckel, J., Blatzer, M., et al. (2019). Microglial production of quinolinic acid as a target and a biomarker of the antidepressant effect of ketamine. Brain. Behav. Immun.

de Vivo, L., Bellesi, M., Marshall, W., Bushong, E.A., Ellisman, M.H., Tononi, G., and Cirelli, C. (2017). Ultrastructural evidence for synaptic scaling across the wake/sleep cycle. Science *355*, 507–510.

Vogel, D.Y.S., Vereyken, E.J.F., Glim, J.E., Heijnen, P.D.A.M., Moeton, M., van der Valk, P., Amor, S., Teunissen, C.E., van Horssen, J., and Dijkstra, C.D. (2013). Macrophages in inflammatory multiple sclerosis lesions have an intermediate activation status. J. Neuroinflammation *10*, 35.

Volterra, A., and Meldolesi, J. (2005). Astrocytes, from brain glue to communication elements: the revolution continues. Nat. Rev. Neurosci. *6*, 626–640.

Vutskits, L., and Xie, Z. (2016). Lasting impact of general anaesthesia on the brain: mechanisms and relevance. Nat. Rev. Neurosci. *17*, 705–717.

Vyazovskiy, V.V., Borbély, A.A., and Tobler, I. (2002). Interhemispheric sleep EEG asymmetry in the rat is enhanced by sleep deprivation. J. Neurophysiol. *88*, 2280–2286.

Vyazovskiy, V.V., Achermann, P., Borbély, A.A., and Tobler, I. (2004). The dynamics of spindles and EEG slow-wave activity in NREM sleep in mice. Arch. Ital. Biol. *142*, 511–523.

Vyazovskiy, V.V., Cirelli, C., Pfister-Genskow, M., Faraguna, U., and Tononi, G. (2008). Molecular and electrophysiological evidence for net synaptic potentiation in wake and depression in sleep. Nat. Neurosci. *11*, 200–208.

Vyazovskiy, V.V., Olcese, U., Lazimy, Y.M., Faraguna, U., Esser, S.K., Williams, J.C., Cirelli, C., and Tononi, G. (2009). Cortical firing and sleep homeostasis. Neuron *63*, 865–878.

Vyazovskiy, V.V., Olcese, U., Hanlon, E.C., Nir, Y., Cirelli, C., and Tononi, G. (2011). Local sleep in awake rats. Nature *472*, 443–447.

Wake, H., Moorhouse, A.J., Jinno, S., Kohsaka, S., and Nabekura, J. (2009). Resting microglia directly monitor the functional state of synapses in vivo and determine the fate of ischemic terminals. J. Neurosci. Off. J. Soc. Neurosci. *29*, 3974–3980.

Wakselman, S., Béchade, C., Roumier, A., Bernard, D., Triller, A., and Bessis, A. (2008). Developmental neuronal death in hippocampus requires the microglial CD11b integrin and DAP12 immunoreceptor. J. Neurosci. Off. J. Soc. Neurosci. *28*, 8138–8143.

Wang, T.F., and Guidotti, G. (1996). CD39 is an ecto-(Ca2+,Mg2+)-apyrase. J. Biol. Chem. *271*, 9898–9901.

Wang, Z., Ma, J., Miyoshi, C., Li, Y., Sato, M., Ogawa, Y., Lou, T., Ma, C., Gao, X., Lee, C., et al. (2018). Quantitative phosphoproteomic analysis of the molecular substrates of sleep need. Nature *558*, 435–439.

Watson, B.O., Levenstein, D., Greene, J.P., Gelinas, J.N., and Buzsáki, G. (2016). Network Homeostasis and State Dynamics of Neocortical Sleep. Neuron *90*, 839–852.

Watson, C.J., Soto-Calderon, H., Lydic, R., and Baghdoyan, H.A. (2008). Pontine reticular formation (PnO) administration of hypocretin-1 increases PnO GABA levels and wakefulness. Sleep *31*, 453–464.

Weinhard, L., di Bartolomei, G., Bolasco, G., Machado, P., Schieber, N.L., Neniskyte, U., Exiga, M., Vadisiute, A., Raggioli, A., Schertel, A., et al. (2018). Microglia remodel synapses by presynaptic trogocytosis and spine head filopodia induction. Nat. Commun. *9*, 1228.

Wigren, H.-K., and Porkka-Heiskanen, T. (2018). Novel concepts in sleep regulation. Acta Physiol. *222*, e13017.

Wilson, M.A., and McNaughton, B.L. (1994). Reactivation of hippocampal ensemble memories during sleep. Science *265*, 676–679.

Wisor, J.P., Schmidt, M.A., and Clegern, W.C. (2011). Evidence for neuroinflammatory and microglial changes in the cerebral response to sleep loss. Sleep *34*, 261–272.

Wolf, S.A., Boddeke, H.W.G.M., and Kettenmann, H. (2017). Microglia in Physiology and Disease. Annu. Rev. Physiol. *79*, 619–643.

Wu, L.-J., and Zhuo, M. (2008). Resting microglial motility is independent of synaptic plasticity in mammalian brain. J. Neurophysiol. *99*, 2026–2032.

Wu, L.-J., Vadakkan, K.I., and Zhuo, M. (2007). ATP-induced chemotaxis of microglial processes requires P2Y receptor-activated initiation of outward potassium currents. Glia *55*, 810–821.

Wu, L.-J., Wu, G., Akhavan Sharif, M.R., Baker, A., Jia, Y., Fahey, F.H., Luo, H.R., Feener, E.P., and Clapham, D.E. (2012). The voltage-gated proton channel Hv1 enhances brain damage from ischemic stroke. Nat. Neurosci. *15*, 565–573.

Wu, Y., Sun, X., Kaczmarek, E., Dwyer, K.M., Bianchi, E., Usheva, A., and Robson, S.C. (2006). RanBPM associates with CD39 and modulates ecto-nucleotidase activity. Biochem. J. *396*, 23–30.

Xavier, A.L., Menezes, J.R.L., Goldman, S.A., and Nedergaard, M. (2014). Fine-tuning the central nervous system: microglial modelling of cells and synapses. Philos. Trans. R. Soc. B Biol. Sci. *369*.

Xi, M.C., Morales, F.R., and Chase, M.H. (1999). Evidence that wakefulness and REM sleep are controlled by a GABAergic pontine mechanism. J. Neurophysiol. *82*, 2015–2019.

Xie, L., Kang, H., Xu, Q., Chen, M.J., Liao, Y., Thiyagarajan, M., O'Donnell, J., Christensen, D.J., Nicholson, C., Iliff, J.J., et al. (2013). Sleep Drives Metabolite Clearance from the Adult Brain. Science *342*, 373–377.

Xu, H.-T., Pan, F., Yang, G., and Gan, W.-B. (2007). Choice of cranial window type for in vivo imaging affects dendritic spine turnover in the cortex. Nat. Neurosci. *10*, 549–551.

Yamakura, T., Chavez-Noriega, L.E., and Harris, R.A. (2000). Subunit-dependent inhibition of human neuronal nicotinic acetylcholine receptors and other ligand-gated ion channels by dissociative anesthetics ketamine and dizocilpine. Anesthesiology *92*, 1144–1153.

Yang, G., and Gan, W.-B. (2012). Sleep contributes to dendritic spine formation and elimination in the developing mouse somatosensory cortex. Dev. Neurobiol. *72*, 1391–1398.

Yang, G., Lai, C.S.W., Cichon, J., Ma, L., Li, W., and Gan, W.-B. (2014). Sleep promotes branch-specific formation of dendritic spines after learning. Science *344*, 1173–1178.

Yasuda, K., Churchill, L., Yasuda, T., Blindheim, K., Falter, M., and Krueger, J.M. (2007). Unilateral cortical application of interleukin-1β (IL1β) induces asymmetry in fos, IL1β and nerve growth factor immunoreactivity: Implications for sleep regulation. Brain Res. *1131*, 44–59.

Yasuda, T., Yoshida, H., Garcia-Garcia, F., Kay, D., and Krueger, J.M. (2005). Interleukin-1β has a Role in Cerebral Cortical State-Dependent Electroencephalographic Slow-Wave Activity. Sleep *28*, 177–186.

Yüzgeç, Ö., Prsa, M., Zimmermann, R., and Huber, D. (2018). Pupil Size Coupling to Cortical States Protects the Stability of Deep Sleep via Parasympathetic Modulation. Curr. Biol. CB *28*, 392-400.e3.

Zhan, Y., Paolicelli, R.C., Sforazzini, F., Weinhard, L., Bolasco, G., Pagani, F., Vyssotski, A.L., Bifone, A., Gozzi, A., Ragozzino, D., et al. (2014). Deficient neuron-microglia signaling results in impaired functional brain connectivity and social behavior. Nat. Neurosci. *17*, 400–406.

Zhang, J., Malik, A., Choi, H.B., Ko, R.W.Y., Dissing-Olesen, L., and MacVicar, B.A. (2014a). Microglial CR3 activation triggers long-term synaptic depression in the hippocampus via NADPH oxidase. Neuron *82*, 195–207.

Zhang, Y., Chen, K., Sloan, S.A., Bennett, M.L., Scholze, A.R., O'Keeffe, S., Phatnani, H.P., Guarnieri, P., Caneda, C., Ruderisch, N., et al. (2014b). An RNA-sequencing transcriptome and splicing database of glia, neurons, and vascular cells of the cerebral cortex. J. Neurosci. Off. J. Soc. Neurosci. *34*, 11929–11947.

Zhao, Y., Huang, L., Xu, H., Wu, G., Zhu, M., Tian, J., Wang, H., Wang, X., Yu, W., Yang, L., et al. (2016). Neuroinflammation Induced by Surgery Does Not Impair the Reference Memory of Young Adult Mice. Mediators Inflamm. *2016*, 3271579.

Zusso, M., Methot, L., Lo, R., Greenhalgh, A.D., David, S., and Stifani, S. (2012). Regulation of postnatal forebrain amoeboid microglial cell proliferation and development by the transcription factor Runx1. J. Neurosci. Off. J. Soc. Neurosci. *32*, 11285–11298.

ANNEXES

1. *Article 3: In vivo imaging with multimodal NanoGd in a murine model of ischemic stroke*

2. *Article 4: The Shh receptor Boc is important for myelin formation and repair*

3. *Review: Deciphering resting microglial morphology and process motility from a synaptic prospect*

ARTICLE 3

In preparation

In-vivo Imaging of Phagocytes with Multimodal NanoGd in a Murine Model of Ischemic Stroke.

Violaine Hubert[1]*, **Inès Hristovska[2]***, Szilvia Karpati[3], Fréderic Lerouge[3], Maëlle Monteil[4], Emanuel Brun[5], Naura Chounlamountri[2], Chloé Dumot[1,6], Fabien Chauveau[7,8], Chantal Watrin[2], Patrice Marche[9], Marc Lecouvey[4], Stéphane Parola[3], Olivier Pascual*[2] and Marlène Wiart*[1,8].

1. Univ-Lyon, CarMeN laboratory, Inserm U1060, INRA U1397, INSA Lyon, Université Claude Bernard Lyon 1, F-69600, Oullins, France
2. Institut NeuroMyoGène, Université Claude Bernard Lyon 1, CNRS UMR 5310, INSERM U1217, Université Lyon, Villeurbanne 69100, France
3. Université de Lyon, Ecole Normale Supérieure de Lyon, CNRS UMR 5182, Université Lyon 1, Laboratoire de Chimie, 46 allée d'Italie, F69364 Lyon, France
4. Université Paris 13, Sorbonne Paris Cité, Laboratoire CSPBAT, CNRS UMR 7244, F-93017 Bobigny Cedex, France
5. European Synchrotron Radiation Facility, Grenoble, France
6. HCL, Lyon, France
7. BIORAN Team, Lyon Neurosciences Research Center, CNRS UMR5292, Inserm U1028, Université Claude Bernard Lyon 1, Lyon, France
8. CNRS, Lyon, France
9. Institute for Advanced Biosciences, Université Grenoble-Alpes, Saint-Martin-d'Hères, France.

*Both authors contributed equally

Abstract *(199 words)*

Neuroinflammation is known to be a major component of stroke, often associated with the worsening of outcome. Phagocyte cells, involving resident microglia and infiltrating macrophages, secrete toxic molecules and thus represent a potential therapeutic target in ischemic stroke. The aim of the present study was to investigate the feasibility of imaging phagocytic activity in-vivo after ischemic stroke using NanoGd, a new multimodal imaging probe. Following NanoGd intravenous injection in a mouse model of permanent middle cerebral artery occlusion, we identified with MRI an inflammatory response in the ischemic core and in the prolongation of the corpus callosum. Intravital microscopy performed back to back with MRI highlighted both an extravasation of NanoGd in the interstitial space of the ischemic lesion and an internalization of NanoGd by phagocytic cells. Ex-vivo analysis confirmed NanoGd accumulation within the ischemic lesion and their uptake by immune cells. This bimodal imaging approach was finally used to monitor the anti-inflammatory effects of a therapeutic molecule. In this study, we showed that NanoGd allowed to monitor phagocytic activity in-vivo at the subacute stage of ischemic stroke in a mouse model. Taking together, our data suggest that NanoGd-enhanced MRI might serve as an imaging biomarker of post-ischemic neuroinflammation.

Introduction

Ischemic stroke is a devastating neurological condition that represents the second cause of deaths in Western countries. Neuroinflammation is known to be a major component of stroke physiopathology, often associated with the worsening of outcome [1]. It is well established that phagocyte cells, including tissue-resident microglia/macrophages and blood-borne recruited macrophages, are main mediators of inflammation initiation and continuation following stroke. By secreting toxic molecules, they may contribute to tissue damages early in the acute phase of stroke, and thus represent potential therapeutic targets [2], [3].

The method of reference to image immune cells in-vivo in the pre-clinical setting is intravital two-photon microscopy coupled with the use of transgenic mouse lines and/or fluorescent dyes [4]. Two-photon microscopy have been used to investigate brain immune cell dynamic and interaction with neural environment in several neurological diseases [5], allowing exciting new discoveries in mouse models of focal blood brain barrier (BBB) disruption [6], traumatic brain injury [7], Alzheimer disease [8] or stroke [9], [10]. However, skull absorption of light prevents clinical translation of this method at this time. In addition, only part of the cortex may be imaged with this approach due to the low depth penetration of light. Therefore, a complementary 3D imaging technique is needed to provide information about macrophage activation into the whole brain. Positron emission tomography (PET) associated with radiotracers targeting the protein TSPO, biomarker of microglia, is the gold-standard to image inflammation in clinic. In patients with ischemic stroke, PET imaging reveals inflammatory phenomena at the lesion site as well as remote from the lesion [11]–[13], but only at the subacute (>72 hours) and chronic stages of the pathology [14]. Therefore, it cannot be used to study the early phagocytic activity following stroke. Over the last decades, contrast agents based on (ultrasmall) superparamagnetic particles of iron oxides (U)SPIOs) have been developed as magnetic resonance imaging (MRI) biomarkers of inflammation [15]. When injected intravenously, (U)SPIOs are internalized by

phagocytic cells, which become magnetic and may thus be detected with MRI. Thus, MRI coupled with the intravenous injection of USPIOs represents a non-invasive tool allowing to image immune cells trafficking across the inflamed central nervous system (CNS) [16], [17]. Notably, USPIO-enhanced MRI has been used for tracking phagocytic cells in rodent models at the acute and subacute phases of permanent ischemic stroke [18]–[21].

In this study, we investigate the potential of a novel contrast agent, NanoGd, for the multimodal in-vivo imaging (MRI back-to-back with two-photon intravital microscopy) of phagocytes after focal cerebral ischemia. Our aim was 2-fold: (1) to evaluate whether NanoGd-enhanced MRI allows to monitor in-vivo phagocytic cells following their internalization of NanoGd, and (2) to decipher the working mechanism of MRI signals using two-photon intravital imaging. Following NanoGd in-vitro characterization, we assessed the potential of NanoGd as an in-vivo multimodal phagocytic biomarker in transgenic CX3CR1-GFP mice submitted to permanent stroke. 3D high resolution gadolinium mapping and histological staining were performed post-mortem to corroborate our in-vivo results. Finally, we evaluated the ability of this technique to monitor the therapeutic effects of Simvastatin, molecule which have been shown to modulate phagocyte response following inflammatory challenges [22]–[24].

Material and Method

Contrast agent

The NanoGd nanoparticle is composed of a 16 nm magnetic core of gadolinium fluoride (GdF_3) [25], coated with bifunctional bisphosphonate polyethylene glycol (PEG) to ensure it biocompatibility and functionalized with a Lemke-type fluorophore (LEM-A) for fluorescence imaging. The hydrodynamic diameter of NanoGd is 29 nm with a polydispersity index (PDI) of 0.251+/-0.003 (PDI=[StDev/MeanSize]^2), and its zeta potential is – 40mV. NanoGd synthesis and in-vitro characterization are the subject of a specific paper currently in preparation

(Karpati S. et al), and we hope to complete this manuscript with a preliminary version of this article before the PhD defence. NanoGd cytotoxicity, biodistribution and pharmacokinetic were evaluated as described in the SI supplementary material.

For in-vivo experiments, a dose of 2 mmol gadolinium/kg body weight was injected intravenously (i.v.) into the tail vein 24 hours post-pMCAo, immediately after baseline MRI.

In-vitro microglial culture and immunocytology

Microglia were isolated from postnatal P0-P1 C57Bl/6 pups and prepared for primary cell culture. Briefly, brains were removed and rinsed in phosphate buffer saline with 0.6% glucose (PBS-glucose). After removal of the meninges, hemispheres were mechanically dissociated in PBS-glucose. Cells were collected and centrifuged, and then seeded in DMEM with 10% foetal calf serum (FCS). They were cultured at 37°C in humidified 5% CO_2/95% air and medium was exchanged at D1, D3 and D7. Microglial cells were collected at confluence (after 15-20 days): they were mechanically detached from the dish by agitation and freezing. Cells were then replated for 24 h in 12-wells plates containing glass coverslips coated with poly-l-ornithine, at a density of 80,000 cells per wells. The following day, microglia cultures were incubated with either 0 mM, 0.5 mM or 1.5 mM NanoGd for 24 h, in order to evaluate NanoGd internalization in a dose-dependent manner.

For microglial staining, cells were fixed with 4% paraformaldehyde (PFA). Cells were then rinsed in PBS and incubated 1 h with 0.30% Triton X, 1% bovine serum albumin (BSA) and 5% goat serum (GS) in PBS to block unspecific antibody labelling and permeabilize cell membrane. Microglia was stained using a rabbit anti-Iba-1 antibody (1:500; 019-19741, FUJIFILM Wako, Richmonds, USA) overnight at 4°C. Cells were then rinsed in PBS and incubated 90 min with an anti-rabbit secondary antibody labelled with Alexa fluor 488 (1:1000; A21433, Invitrogen, Carlsbad, USA). Finally, cells were rinsed three times in PBS, stained with Hoechst and investigated for the presence of NanoGd and Iba-1 positive cells. Images were

acquired using a Leica TCS-SP5X confocal microscope (Leica Biosystems, Wetzlar, Germany).

In-vivo study design

Figure 1 show the experimental design of the in-vivo studies. Table 1 summarizes the animal number for each group. At day 0 (D0), 22 mice underwent a permanent occlusion of the middle cerebral artery (pMCAO) in order to induce a reproducible cortical lesion. Baseline MRI was performed at day 1 (D1) post-pMCAO to document the presence of the lesion and of a potential brain blood barrier disruption. NanoGd was then immediately administered to 16 of the 22 operated mice (Group I). The 6 other operated mice did not receive NanoGd and served as controls (Group II). Three nonoperated mice (sham) received NanoGd the same day and at the same dose as in Group I (Group III). Among those animals, 11 mice (Group I: n=7; Group II: n=1; Group III: n=3) were prepared for longitudinal intravital two-photon microscopy. They were imaged on the day of injection (D1 post-pMCAO, approximatively 8h following NanoGd injection) and followed-up the next day (D2 post-pMCAO, approximatively 28h following NanoGd injection). Except for 3 mice (Group II: n=1; Group III: n=2) that were only imaged with intravital microscopy, all the mice (n=22) underwent post-contrast MRI at day 3 (D3) post-pMCAO (48 hours post-NanoGd administration).

To assess whether NanoGd multimodal imaging allow to detect the effect of an anti-inflammatory treatment, 6 additional mice were submitted to pMCAo (Group IV). All animals underwent a baseline MRI 1 hour after the occlusion (D0) and were then s.c. injected with simvastatin for 3 days, twice a day. A subgroup of mice (n=3) were imaged with two sessions of intravital two-photon microscopy (D1 and D2). All 6 mice were re-imaged with MRI at D3.

All animals were sacrificed at the end of the experiment and their brains were sampled for histology or X ray phase contrast tomography for 3D depiction of gadolinium brain distribution [26].

	Group I pMCAo + NanoGd (n = 16)		Group II pMCAo w/o NanoGd (n = 6)		Group III Sham + NanoGd (n =3)		Group IV pMCAo + NanoGd + Simva (n =6)	
	MRI only n = 9	MRI + 2γ n = 7	MRI only n = 5	2γ only n = 1	2γ only n = 2	MRI + 2γ n = 1	MRI only n = 3	MRI + 2γ n = 3
2γ 1		30h*			30h*	30h		30h*
2γ 2		54h		54h	54h	54h		54h
MRI	72h	72h	72h			72h	72h	72h

Table 1 | Subjects and studies design. Summary of imaging exams underwent by each mouse of the study, distributed in four experimental groups. 2γ1 and 2γ2 correspond to the first and the second intravital two-photon microscopy sessions, and MRI to the post-NanoGd MRI session. Times indicated in hour (30h, 54h or 72h) correspond to the exact time of imaging post-pMCAo. Baseline MRI was performed on D1, 24 hours after pMCAo induction, and immediately followed by NanoGd i.v. injection. *n=1, represents the mice that died before the end of the protocol. Simva: simvastatin; w/o: without.

Animal experiments

All experimental procedures involving animals and their care were carried out in accordance with the European regulation for animal use (EEC Council Directive 2010/63/UE, OJ L 276, Oct. 20, 2010) and this study was approved by our local ethic committee “Comité d’éthique pour l’Expérimentation Animale Neurosciences Lyon” (CELYNE - CNREEA number: C2EA – 42). The animals were housed in a temperature and humidity-controlled environment (21 ± 3°C), on 12:12h light-dark cycle, having free access to standard chow and tap water. Animal experiments were performed in 8-week-old (24.1 +/- 2.2 g) C57Bl/6 male mice (Janvier, France), and 8 to 12-week-old (22.7 +/- 1.9 g) CX3CR1-GFP transgenic male mice (originally donated by Serge Nataf in 2012 and bred at the INMG Institute, Claude Bernard University, Lyon).

Induction of focal Cerebral Ischemia

Focal ischemia was induced at day 0 in mice anesthetized with isoflurane (2%, ISO-VET, Piramal Healthcare, Morpeth, UK), by permanent occlusion of the distal middle cerebral artery (pMCAo) with iron chloride ($FeCl_3$), as previously described by Karatas et al. [27]. Briefly, the right MCA was exposed by subtemporal craniectomy and occluded by placement of a 10% $FeCl_3$-soaked filter paper strip on the dura mater, over the trunk of the distal MCA, for 10 minutes. To alleviate the pain, subcutaneous (s.c.) injection buprenorphine at the dose of 0.05 mg/kg was made prior to the surgery, and at the end of the surgery, the wound was covered with lidocaine. During surgery, body temperature was monitored with a rectal probe and maintained at 37 °C using a feedback-regulated heating pad.

Thinned skull cortical window preparation

Thinned skull cortical window preparation was performed one day after the permanent occlusion of the MCA. For surgery, mice were exposed to isoflurane anesthesia (3-4%) and mounted in a stereotaxic apparatus (D. Kopf Instruments). At the beginning of the surgery, buprenorphine was administered (0.05 mg/kg s.c.) for post-surgery pain relief. During surgery, mice were placed on a heating pad, and their body temperature was maintained at 37°C. After the skull was thoroughly cleaned and exposed, a 6 mm diameter custom-made polyamide cranial implant was glued. This material has an advantage over the commonly used metal-containing implants in being compatible with MR imaging. The implant was centered approximately -0.5 anterior and +2.5 lateral from Bregma, which corresponded to the periphery of the lesion; however, its position was adjusted according to the baseline T2-weighted MRI images and the size of the lesion. Thus, the 0.5 mm diameter area encircled both extralesional and ischemic tissue. The skull was carefully thinned over this area using a high-speed drill. To avoid heat-induced tissue injury, continuous cooling of the bone was performed by repeated application of cold, sterile saline solution. When the desired 20-30 μm bone thickness was

reached, a cover glass was placed on top of a thin layer of cyanoacrylate glue over the thinned skull.

Treatment

Simvastatin is a molecule from the statin family, competitive inhibitors of 3-hydroxy-3-methylglutaryl-CoA (HMG-CoA) reductase. which is also known to have immunomodulatory effects in vitro [23], [24]. Simvastatin (Sigma-Aldrich, Lyon, France) was activated and prepared for in-vivo injection as described on Çakmak et al study [28]: simvastatin was dissolved in the vehicle [95% ethanol (40%) and 0.1N NaOH (60%)], the solution was heated for 2 h at 50°C. Then, the solution was neutralized with HCl to pH 7.2. The final volume was completed by adding distilled water and the 4.0 mg/ml stock solution was stored at -20°C. At D0, one s.c. injection of activated simvastatin (40 mg/kg) was performed 1 hour post-pMCAo (40 mg/kg), and another one was performed 6 hours post-pMCAo. At D1 and D2, two s.c. injections (40 mg/kg) were performed per day 6 hours apart.

A first in-vivo study was performed to evaluate simvastatin impact on ischemic lesion volume. The experimental protocol is described in the SI supplementary material. The second study designed to assess whether NanoGd multimodal imaging allow to detect the anti-inflammatory effect of simvastatin is described in the "in-vivo study design" part of this M&M.

MRI

MRI was performed on a 7T horizontal-bore Bruker Avance II rodent imaging system (Bruker Biospin, Ettlingen, Germany).

To quantify the r1 and r2 relaxivities of NanoGd (in $mM^{-1}.s^{-1}$), phantoms were prepared with a range of twelve gadolinium concentrations going from 0 to 5 mM. To reach the appropriate concentrations, NanoGd phantoms were prepared using a 0.5 M stock solution dissolved in saline. Measurements were then performed at 25°C. T1 maps were obtained from a fast imaging with steady-state procession (FISP) sequence (TE/TR=2.1/4.2 ms; Inversion time (TI): 73,8ms;

32 echoes) by fitting an inversion/recuperation function to the data. T2 maps were obtained from a multiple spin-echo sequence (MSME; TE [interecho delay]/TR=50/5000 ms; 24 echoes) by fitting a monoexponential function to the data.

For in-vivo MRI, mouse anaesthesia was induced with a mixture of air and 3.5% isoflurane and then animals were placed in an MRI-compatible mouse cradle. During the acquisitions, anesthesia was maintained with 2% isoflurane. The respiratory rhythm was cautiously monitored by a pressure sensor linked to a monitoring system (ECG Trigger Unit HR V2.0, RAPID Biomedical, Rimpar, Germany), as well as the body temperature thanks to circulating heated water. A 50-mm inner diameter birdcage coil was used for transmission and a 15-mm diameter surface coil was used for reception.

For each sequence, 25 slices were acquired from the olfactory bulb to the cerebellum, using a field of view (FOV) of 20x20 mm^2, a slice thickness of 500 µm and a matrix size of 256x256. The in-vivo MRI protocol comprised the following axial sequences: a T1 weighted GRE FLASH sequence pre- and post-gadolinium i.v. injection, TE/TR= 3.5/350 ms, bandwidth= 101 kHz, number of average=3, acquisition time 4 min; a spin-echo T2 weighted image (T2-WI), TE/TR= 43.8/5000ms, bandwidth= 40 kHz, number of averages= 6, acquisition time 12 min; a T2-star gradient-echo (GRE) FLASH sequence (T2*-WI), TE/TR= 6/750 ms, bandwidth= 40 kHz, flip angle (FA)= 20°, number of averages= 8, acquisition time 19 min; these parameters yielded an in-plane resolution of 78 µm.

Two-photon intravital microscopy

For each imaging session, mice were anesthetized with intraperitoneal injection of a mixture of ketamine (100 mg/kg) and medetomidine (1 mg/kg). The mice were placed on a heating pad, and their body temperature was maintained at 37 °C. Imaging was performed using a two-photon microscope (Bruker Ultima) with an Insight 3X laser (Spectra Physics) tuned to 980 nm for simultaneous excitation of both fluorescent proteins, eGFP and LEM-A. For imaging, a 20x

water-immersion objective (0.95 N.A. Olympus) was used. To separate green and red fluorescence, 560 nm dichroic mirror coupled to 525/50 nm and 650/40 emission filters were used.

Images were acquired at a depth of 50-150 µm at three sites: 1) lesional area, corresponding to the ischemic core with mostly activated CX3CR1-GFP cells; 2) perilesional area, corresponding to the lesion border zone, containing both activated and ramified CX3CR1-GFP cells; and 3) extralesional area, corresponding to the zone furthest from the lesion and containing mostly ramified CX3CR1-GFP cells. These sites were determined by visual observation of the morphological characteristics of microglial cells and their localization with regards to the lesion. Thirty to forty-five consecutive Z-stacks with a resolution of 521x521 pixels were acquired every minute with a step size of 1µm. A typical recording lasted approximately 10-15 minutes (10-15 Z-stacks). To compare the evolution of: 1) CX3CR1-GFP cell morphology and number and 2) NanoGd internalization by CX3CR1-GFP cells, the same areas were imaged at day 1 and day 2.

Data analysis

MRI

The r1 and r2 relaxivities were calculated with T2 and T1 values obtained from T2- and T1-maps, using the following formulas: $1/\Delta T1 = r1 \times C$; $1/\Delta T2 = r2 \times C$ (T1 and T2 in sec; C= molar concentration in mmol/L). For r1 calculation, a linear regression was made between the gadolinium concentration (mM) of NanoGd phantoms and the value 1/T1 associated. The slope of the line represents r1 ($mM^{-1}.s^{-1}$). The same process was applied for r2 measurement.

Hypointense MR signal volumes in the ischemic lesion were measured, 1) to quantify NanoGd accumulation in the ischemic lesion following pMCAo, and 2) to compare this accumulation between the vehicle-treated and the simvastatin-treated groups (respectively Group I and Group IV in Table I). Hypointense MR signals in the ischemic lesion were thus manually outlining on

T2*-WI for both groups. Volumes were then calculated by summation of the hypointense signals of all brain slices showing brain damage and integrated by slice thickness. For each mouse, hypointense signal volume in the lesion was normalized by the ischemic lesion volume at 24 hours post-pMCAO determined on baseline T2-WI. Analyses was performed using ImageJ software (National Institute of Mental Health, Bethesda, USA, imagej.nih.gox/ij/).

Two-photon microscopy

Image processing and analysis were performed using ImageJ, Icy (open source software created by BioImage Analysis Lab, Institut Pasteur, France; http://icy.bioimageanalysis.org/) and custom-written Matlab software. We first corrected the images for drift in x, y, and z-axis during acquisition using a custom-written Matlab program. The correction was accomplished by shift estimation from the cross-correlation peak by FFT (fast Fourier transform) between the first stack of each acquisition (reference Z-stack) and the following Z-stacks. After realignment, CX3CR1-GFP images were uniformly adjusted for contrast and brightness to reduce background noise.

For CX3CR1-GFP cell density count, the first Z-stack from each acquisition was used to generate an average intensity projection. The threshold was adjusted for object detection for each projection and quantified the number of cells using Spot Detector (Icy). The total number of CX3CR1-GFP cell was then divided by the imaging volume/field to generate a measure of cell density.

For the nanoparticle internalization analysis, the first Z-stacks from both channels were used. A threshold was set to convert the nanoparticle images to binary and used a median filter to remove background noise. Then, the AND function from Image Calculator (ImageJ) was used, to obtain the resulting Z-stack containing the colocalized signal from both channels. An average Z-projection was generated, and the number of cells that have internalized the nanoparticle was

counted using Spot Detector. This number was subtracted from the total number of cells in the field, providing the percentage of cells that have internalized the nanoparticle.

Confocal microscopy

For the in-vitro study, 5 representative areas of 246x246 μm^2 were acquired (6-9 Z-stacks) for each condition (control, NanoGd 0.5 mM and NanoGd 1.5 mM). The quantification of NanoGd internalization by Iba-1 positive microglial cells on these areas will be performed using ImageJ, using the same methods described in the subsection "M&M - Data analyses – Two photon microscopy".

Histology

For histological analysis, mice were euthanized by intracardiac perfusion with PBS followed by perfusion with 4% PFA. Brains were then removed, post-fixed with 4% PFA for 24 hours and frozen in methylbutane with dry ice. Finally, tissues were cut into 12 µm sections on a cryostat. For the fluorescence analyses, slides were rinsed three times in 0.5% PBS-Triton (PBST) and then mounted with Roti-Mount® Fluocare with DAPI. Then, the slices were investigated for the presence of NanoGd and CX3CR1-GFP cells. Images were acquired from the 12 µm section using an Axio Scope A.1 fluorescence microscope (4 filters, Carl Zeiss, Oberkochen, Germany) equipped with a x0.63 AxioCam MRc (Carl Zeiss, Oberkochen, Germany).

X ray phase contrast tomography

For ex-vivo phase contrast tomography, mice were euthanized by intracardiac perfusion with PBS followed by 4% PFA. Brains were then extracted and dehydrated in successive ethanol baths: 25% ethanol (24h), 50% ethanol (24h), 75% ethanol (24h) and 96% ethanol (24h). Finally, mouse brains were placed inside 2 ml syringes to maintain them in a static position. In-line phase contrast tomography was performed on beamline ID17 of the European Synchrotron

Radiation Facility (ESRF) in Grenoble at 26 keV. An indirect detection-based detector with a LuAg scintillator, standard microscope optics and a 2048x2048 pixel CCD camera was positioned 3-m from the sample to obtain phase contrast. The whole-brain data set was acquired at an isotropic pixel size of 7.5-µm. Acquisition time of the 3000 projections was <5 minutes per brain. Reconstruction was performed with Paganin algorithm by setting δ/β to 1000 as in [26].

Results

NanoGd has optimal properties for in-vivo multimodal imaging of phagocytic cells

First, NanoGd cytotoxicity was evaluated on several human cell lines, including THP-1 monocytes, HepG2 hepatocytes, A549 epithelial-like cells and HEK 293T kidneys cells. Mortality and viability cell tests (LDH and MTT assays) revealed an absence of cytotoxic impact for NanoGd on these cell lines (Suppl Figure S1). As a second step, we investigated 1) NanoGd fluorescence detection in-vitro and 2) the ability of microglial cells to phagocyte NanoGd particles (Figure 2A). NanoGd red fluorescent signal was detected on microglial cultures incubated with NanoGd (Figure 2A2 and 2A3), but not in control microglial culture (Figure 2A1). Moreover, confocal images showed an internalization of NanoGd by Iba-1 stained cells following NanoGd incubation (Figure 2A2 and 2A3, white arrowheads). Higher magnification highlighted a cytoplasmic location for the NanoGd particles in the microglial cells (Figure 2A2 and 2A3, insets). Quantitative analyses are ongoing to see if the proportion of NanoGd-labelled Iba-1 cells increases in a dose-dependent manner, and this experiment will be repeated in order to obtain n=3 replicates/condition.

MR signal drops increased on T2 map with increasing NanoGd concentration (Figure 2B1) and MR signal enhancement increase on T1 map with increasing NanoGd concentration (Figure 2B2). Relaxivity parameters were then calculated (Figure 2C). NanoGd r1 relaxivity was 0.98

$mM^{-1}.s^{-1}$ and r2 relaxivity was 20 $mM^{-1}.s^{-1}$. Then, NanoGd biodistribution and pharmacokinetic were evaluated in-vivo in healthy mice (n=4). Dynamic images showed an accumulation of NanoGd in the liver, the spleen but not in the kidneys immediately after NanoGd injection (Suppl Figure S2A), which was constant during the first hour following injection (Suppl Figure S2B). From this data, we concluded that NanoGd has a long vascular remanence. This was also seen with two-photon microscopy, where NanoGd was still detected in the vessels 24 hours after i.v. injection. Therefore, we scheduled the post-NanoGd MRI scan 48h post-injection to allow time for the nanoparticle to be eliminated from the vascular compartment at the time of scanning.

NanoGd accumulation in the ischemic core of the lesion is detected with in-vivo MRI

On baseline T2-WI, a cortical edema indicative of the ischemic lesion was detected for all the mice submitted to pMCAo surgery (Dotted white line, Figure 3A). A strong contrast enhancement was detected in the ischemic area of pMCAo mice on baseline post-gadolinium images (white arrowheads, Figure 3B), indicative of a BBB disruption. Of note, three pMCAo mice were not imaged with pre- and post-gadolinium T1 sequences for technical reasons. In sham-operated animals, neither cortical lesion nor BBB leakage were detected (Figures 3A et 3B).

Due to experimental reasons related to mouse anaesthesia during intravital microscopy sessions, two mice died before the post-NanoGd MRI session (Table 1. Group I, n=1; Group III, n=1). T2- and T2*-WI acquired 48 hours after NanoGd injection (D3 post-pMCAO) showed an accumulation of strong hypointense MR signals within the ischemic lesion of the fifteen pMCAo mice from group I (red arrowheads, Figures 3C and 3D). These hypointense signals were not found in sham-operated mice (n=1; Figures 3C and 3D) or in pMCAo mice not injected with NanoGd (n=5; Figures 3C and 3D).

For all group I animals, hypointense MR signals were mainly detected on the central part of the ischemic lesion, also called ischemic core. Less hypointense signals were observed in the border zone of the lesion which surrounds the ischemic core, and we did not detect any signal drops in the cortical extralesional area. Examples of this spatial distribution are shown in Figures 4C and 4D (see the T2 and T2* hypointense signals delineated by dotted red lines), for four representative pMCAo mice. Visually, contrast enhancement in the ischemic core on T2- and T2*-WI were quite heterogeneous from one mouse to another (Figures 4C and 4D). Quantifications of these MR hypointense signals in the ischemic lesion of group I mice are ongoing. Visual analysis of MR images showed a strong co-localization of T1 contrast enhancement and T2 hypointense signals for n=6/15 mice, a partial co-localization for n=5/15 mice and no co-localization for n=1/15 mouse (see examples on Figures 4B and 4C). For the three mice that were not imaged with gadolinium sequences, this analysis was not performed. Of note, extralesional hypointense MR signals were also detected in several pMCAo mice (n=8/15), in the corpus callosum (red arrowheads, Figures 4B and 4C).

NanoGd accumulation in activated CX3CR1-GFP+ cells is revealed by two-photon intravital microscopy.

To understand the biological substrates of MR hypointense signals, we examined NanoGd fate in mouse brains using two-photon intravital microscopy. In a subgroup of pMCAo mice injected with NanoGd (n=6), two sessions of microscopy were performed to image the same three cortical areas at D1 and D2 following pMCAo: 1) the extralesional area, 2) the border zone and 3) the ischemic core (Figure 5A). The extralesional area was characterized by the presence of resting-state branched CX3CR1-GFP positive cells (Figure 5B and Suppl online movies), the ischemic core by the presence of highly activated round CX3CR1+ cells (Figure 5D and Suppl online movies) and the border zone by the presence of the two types of cell phenotype (Figure 5C and Suppl online movies). To ensure that CX3CR1+ cell activation was not associated with

NanoGd injection, we imaged a pMCAo mouse not injected with NanoGd. With intravital microscopy, highly activated round CX3CR1+ cells were also detected in the ischemic lesion (dotted white lines on Suppl Figure S3C).

Following NanoGd injection, two-photon images showed NanoGd diffusion from the blood sector to the brain parenchyma in the ischemic core. This phenomenon was moderate in the border zone and almost non-existent in the extralesional area (Figures 5B-D and Suppl online movies). Our analyses also stressed out the high amount of CX3CR1+ cells that have internalized NanoGd particles in the ischemic core and to a lesser extent, in the border zone (yellow signal on the right images, Figures 5C and 5D). When looking at CX3CR1+ cells that have internalized NanoGd, we distinguished two type of cell phenotype: large "jellyfish" like cells, which probably correspond to activated microglia (white arrowheads on Suppl Figure S4; Figures 5C-D and Suppl online movies) and small round shape cells, very mobile, which probably correspond to infiltrated macrophages (white arrows on Suppl Figure S4; Figures 5C-D and online movies). We also detected red signal that seems to correspond to NanoGd accumulation in CX3CR1-GFP negative cells, on the ischemic core and the border zone (blue arrows on Suppl Figure S4; Figures 5C-D and online movies). By contrast, we did not observe colocalization of CX3CR1+ cells and NanoGd in the extralesional area (yellow signal on the right images, Figure 5B). Cortical two-photon imaging of sham-operated mice revealed neither CX3CR1+ cell activation, NanoGd diffusion in the brain parenchyma, nor NanoGd internalization by CX3CR1+ cells (Suppl Figure S3A).

These observations were supported by our first quantitative analyses. Quantification of CX3CR1-GFP cell numbers per area showed an increase of CX3CR1+ cells in the ischemic core and in the border zone from D1 to D2, but not in the extralesional area (data not shown). The percentage of CX3CR1+/NanoGd+ cells was quantitatively higher in the ischemic core (80 to 90%) than in the border zone (60 to 65%) and it was negligible in the extralesional areas. In

addition, this percentage of CX3CR1+/NanoGd+ cells increased from D1 to D2 (Figure 5E). Quantitative analyses presented in this part were made for four of the seven pMCAo mice imaged with intravital microscopy. The global analysis is ongoing.

Post-mortem analyses confirm NanoGd presence in the ischemic lesion and its internalization by phagocytic cells.

To make sure that MR signal drops did not come from NanoGd within brain capillaries mice were euthanized by intracardiac perfusion in order to remove any NanoGd particle that could remain within the blood sector. On high resolution X ray phase contrast images, hyperintense signals were still visualized inside the ischemic core (dotted red line, Figure 6B), and they co-localized with in-vivo hypointense MR signals (dotted red line, Figure 6A). Beside the ischemic hyperintense signals, extralesional hyperintense signals were also detected in the prolongation of the corpus callosum on phase contrast images (red arrowheads Figure 6B), as observed in-vivo on T2-WI (red arrowheads Figure 4B and 6A).

Histological analyses highlighted the same spatial distribution for CX3CR1+ cells as described with intravital microscopy: 1) ramified CX3CR1+ cells characteristic of resting-state microglia were found on the extralesional areas of the brain and closed to the border zone, 2) large round shape CX3CR1+ cells surrounded the ischemic core, corresponding to the border zone and 3) the ischemic core was rich with both large round shape CX3CR1+ cells and small CX3CR1+ cells (Figure 6C). We then focused on each of these areas. In the ischemic core of the pMCAo mice injected with NanoGd, highly activated CX3CR1+ cells were often associated with red fluorescent signal corresponding to the NanoGd (white arrowheads, Figure $6D_3$). Higher magnification suggested an intracellular location for NanoGd (magnified inset, Figure $6D_3$). In the border zone, CX3CR1+ cells also presented an activated phenotype and some of them colocalized with NanoGd (white arrowheads and magnified inset, Figure $6D_2$) whereas in the extralesional area, CX3CR1+ cells were not associated with red fluorescence (Figure $6D_1$). In

the sham-operated mice, histological staining showed resting-state microglia in the cortical area but no NanoGd presence was observed (Suppl Figure S3B).

Assessment of simvastatin anti-inflammatory effects using NanoGd multimodal imaging. Finally, to investigate the potential of NanoGd multimodal imaging to measure the impact of an anti-inflammatory treatment, we worked with simvastatin, which have been shown to have neuroprotective effects in stroke rodent models [29]–[31]. First, we wanted to assess the impact of simvastatin treatment on ischemic lesion volume in our pMCAo mouse model. Suppl Figure S5A represents the experimental protocol designed to evaluate this impact. There was no significative difference of lesion volume between simvastatin-treated mice (n=9) and vehicle-treated mice (n=9) (Suppl Figure S5C).

In parallel, we imaged a group of simvastatin-treated pMCAo mice injected with NanoGd (Table I, Group IV) using our bimodal (MRI/two-photon microscopy) imaging method, to evaluate whether this method could give some insights on potential anti-inflammatory impact of simvastatin following ischemic stroke (see experimental design on Figure 1B). Du to experimental reasons related to intravital microscopy anaesthesia protocol, one mouse died before the post-NanoGd MRI session. On T2- and T2*-WI, we compared the presence of hypointense MR signals in the ischemic lesion between simvastatin-treated pMCAo mice (n=5) and non-treated pMCAo mice injected with NanoGd (respectively Group IV and Group I in Table I). Example of T2-WI for representative mice from both groups are showed on the Figure 7A, where dotted red lines delineated the hypointense MR signals in the ischemic core. Quantitative analyses are ongoing to measure and compare the volume of these hypointense MR signals for simvastatin-treated group and non-treated group. Of note, hypointense MR signal were also detected for simvastatin-treated mice in the corpus callosum (red arrowheads, Figure 7A1). To go further, a subgroup of simvastatin-treated pMCAo mice (n=2) were also imaged with two-photon microscopy, on D1 and D2 following pMCAO surgery. As for non-

treated mice (Figures 5B and 7B and Suppl online movies), we observed the same phenomena of NanoGd diffusion in the brain parenchyma and internalization by CX3CR1+ cells in the border zone (Figure 7B) and the ischemic core, but not in the extralesional area (Suppl online movies). Quantification of CX3CR1+ cells number and of CX3CR1+/NanoGd+ cell percentage in these areas are ongoing and will offer more precise information regarding simvastatin impact on NanoGd internalization and CX3CR1+ activation.

Figures

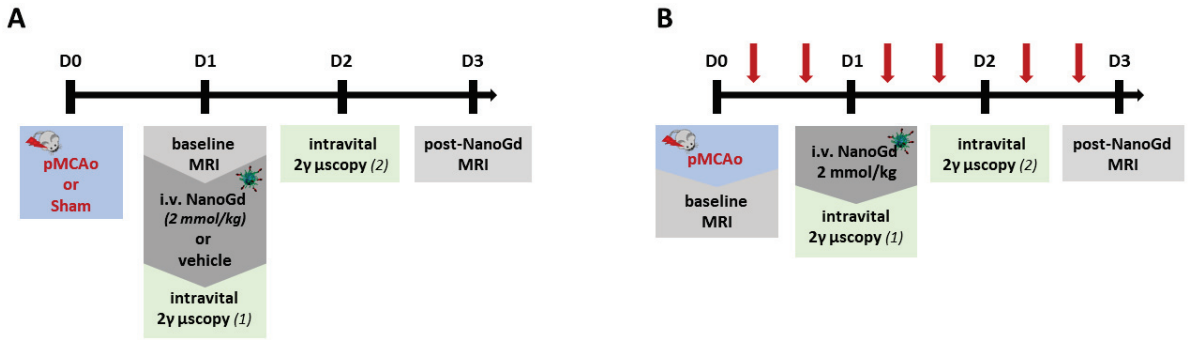

Figure 1 | Experimental design. A. Experimental timeline for Group I (pMCAo + NanoGd), Group II (pMCAo without NanoGd) and Group III (Sham + NanoGd). **B.** Experimental timeline for Group IV (pMCAo + NanoGd + Simvastatin). Red arrows represent simvastatin s.c. injection, spaced from 6 hours each day. Intravital 2γ µscopy (1): intravital two-photon microscopy, session 1; Intravital 2γ µscopy (2): intravital two-photon microscopy, session 2.

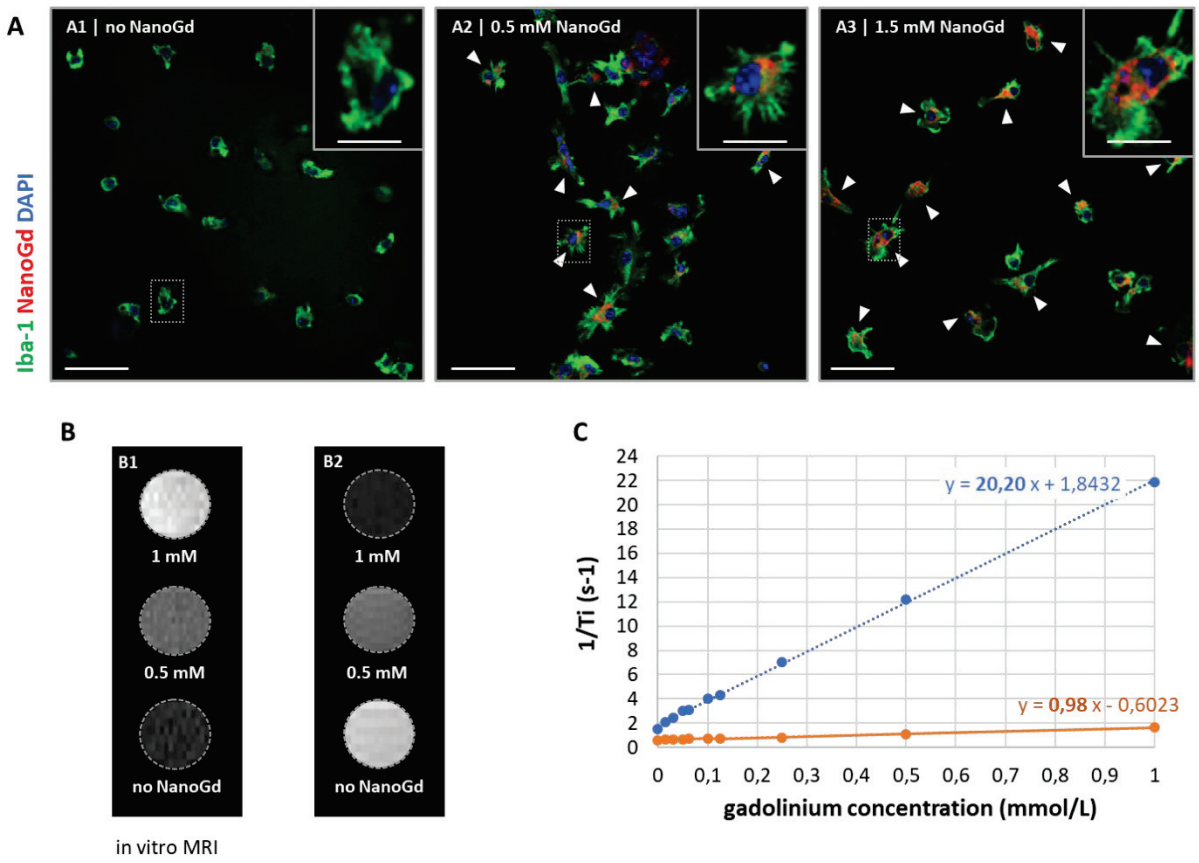

Figure 2 | NanoGd in-vitro characterization. A. Microglia primary cultures internalized NanoGd. Confocal images of Iba-1 stained microglial cells incubated with (A2, 0.5 mmol/L; A3, 1.5 mmol/L) or without NanoGd (A1). (Scale bars: 50 µm for overview images; 10 µm for magnified insets). **B**. NanoGd increased T1 and T2 MR contrast. On T1 cartography, MR signal increases with gadolinium concentration increase (B1) whereas on T2 cartography, MR signal drops with the increase of gadolinium concentration (B2). **C**. Measurement of r1 (orange) and r2 (blue) relaxivities by linear regression connecting NanoGd phantoms gadolinium concentration to the value "1/Ti", where Ti means either T1 or T2.

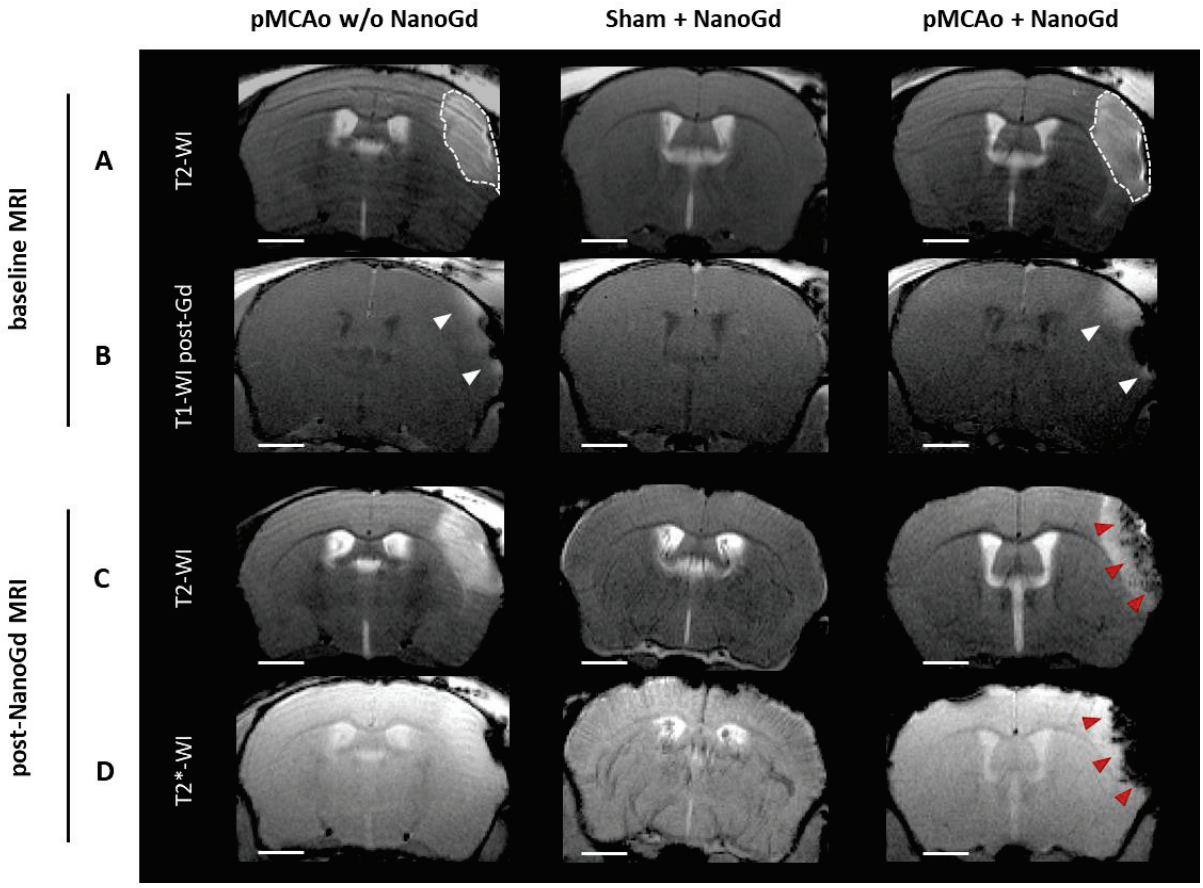

Figure 3 | In-vivo multiparametric MRI. Pre- (A-B) and post-NanoGd (C-D) MRI for three representative mice, a pMCAo mouse and a sham-operated mouse both injected with NanoGd, and a pMCAo mouse not injected with NanoGd. For each sequence, only one transversal slice is showed. T2 weighted images (A) show the presence of an ischemic lesion in pMCAo mice (dotted white lines), but not in the sham mouse. Blood brain barrier (BBB) breakdown was assessed using a T1 weighted sequence, pre and post (B) gadolinium injection. T1 enhancement in pMACo mouse brain is indicative of BBB disruption (white arrowheads). 48 hours following NanoGd injection, its presence at the ischemic lesion was observed using T2 (C) and T2* (D) weighted sequences. Red arrowheads indicate the presence of hypointense signals in the ischemic lesion of the pMCAo mouse. NanoGd is also detected in the vessels of the sham-operated mouse, illustrating a slight heterogeneity in NanoGd pharmacokinetic from one mouse to another. Gd: gadolinium. w/o: without. (Scale bars: 1mm).

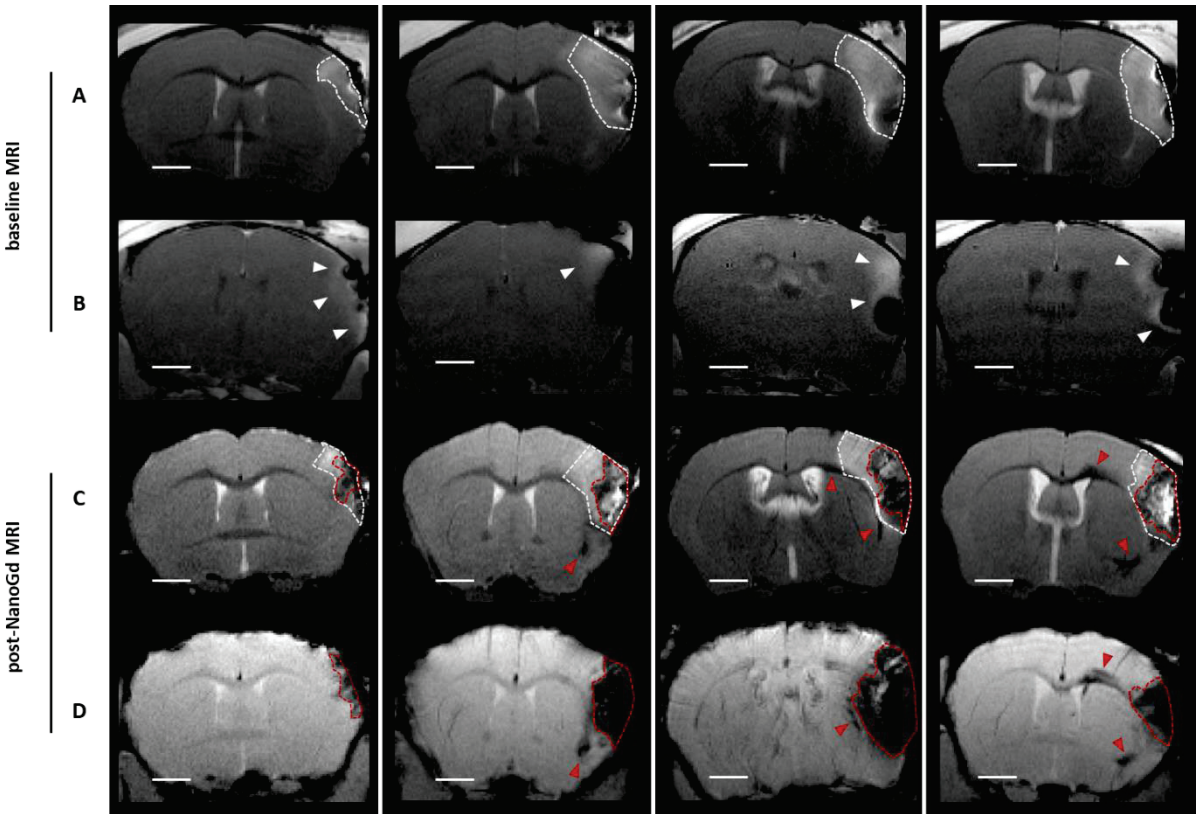

Figure 4 | Spatiotemporal pattern of NanoGd distribution following pMCAo. Baseline MRI (A-B) and post-NanoGd MRI (B-D) for 4 representative pMCAo mice injected with NanoGd. For each sequence, only one transversal slice is showed. Dotted white lines delineate the ischemic lesion on baseline T2-WI (A). White arrowheads indicate T1 enhancement following gadolinium injection on T1 weighted images (B), indicative of BBB disruption. On post-NanoGd T2-WI (C), dotted white lines delineate the ischemic lesion and dotted red lines the hypointense signals within the lesion, indicative of NanoGd presence. Red arrowheads point out hypointense signals remote from the lesion, along the corpus callosum. The same legend is used for post-NanoGd T2*-WI (D). On these T2*-WI, NanoGd is still detected on the vessels of some mice, highlighting the heterogeneity in NanoGd pharmacokinetic from one mouse to another. (Scale bars: 1mm)

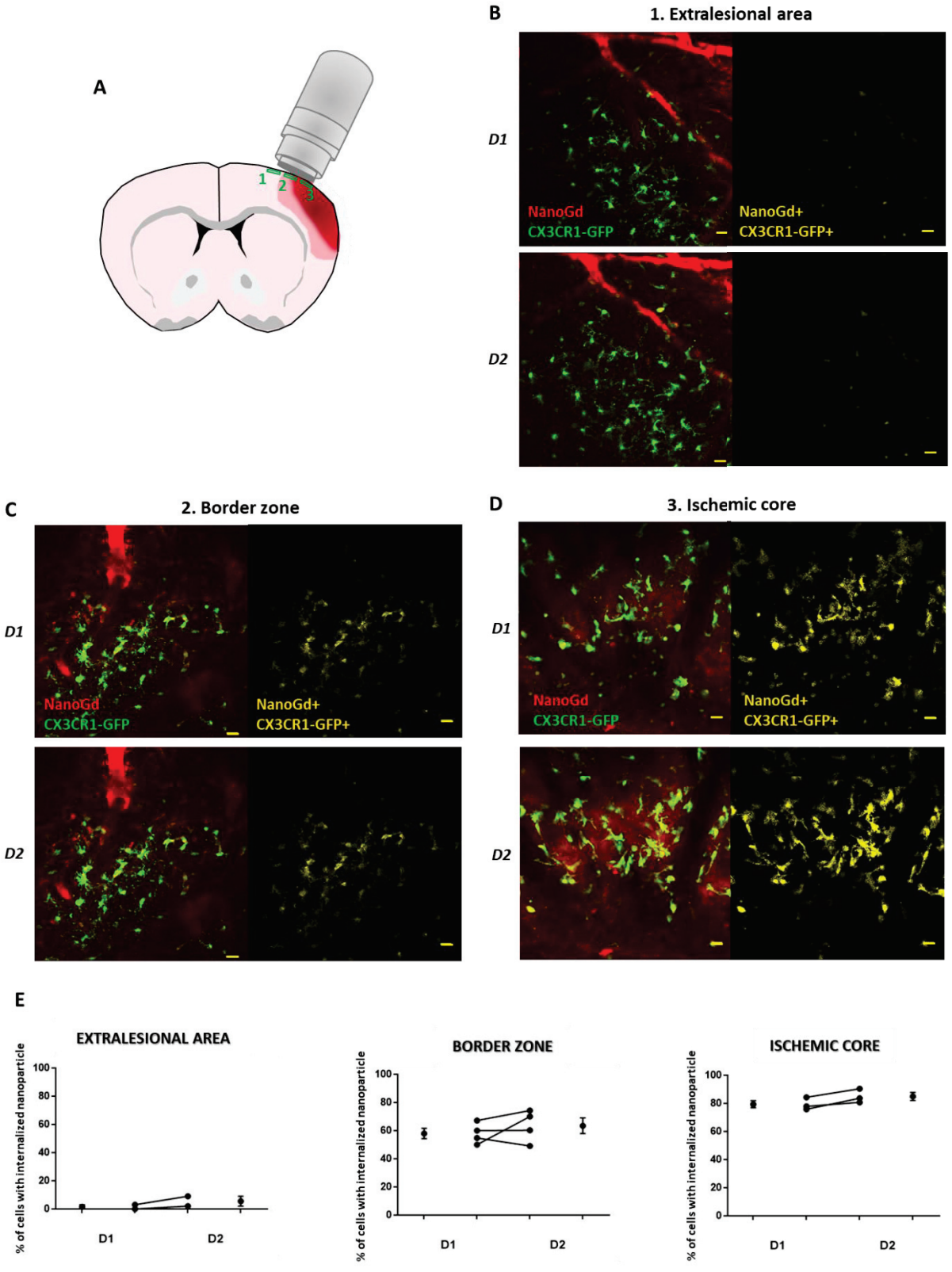

Figure 5 | Characterization of NanoGd interaction with phagocytic cells with two-photon intravital microscopy. A. Schematic representation of the ischemic brain for a pMACo mouse. The three areas imaged with two-photon microscope are represented (green boxes): 1= the extralesional area; 2= the perilesional area or border

zone; 3= the ischemic core. **B-D.** For a pMCAo mouse injected with NanoGd, representative images from two-photon microscopy sessions are showed, for the first imaging session (D1) and the second one (D2). For each brain localization, left images represent fluorescent signals from CX3CR1-GFP positive cells (in green) and NanoGd (in red), and the right images showed the area where CX3CR1-GFP positive cells and NanoGd colocalize (in yellow). (Scale bar: 20μm). **E.** Percentage of CX3CR1-GFP cells that have internalized the nanoparticle in the extralesional area (n=2), the border zone (n=4) and the ischemic core (n=3).

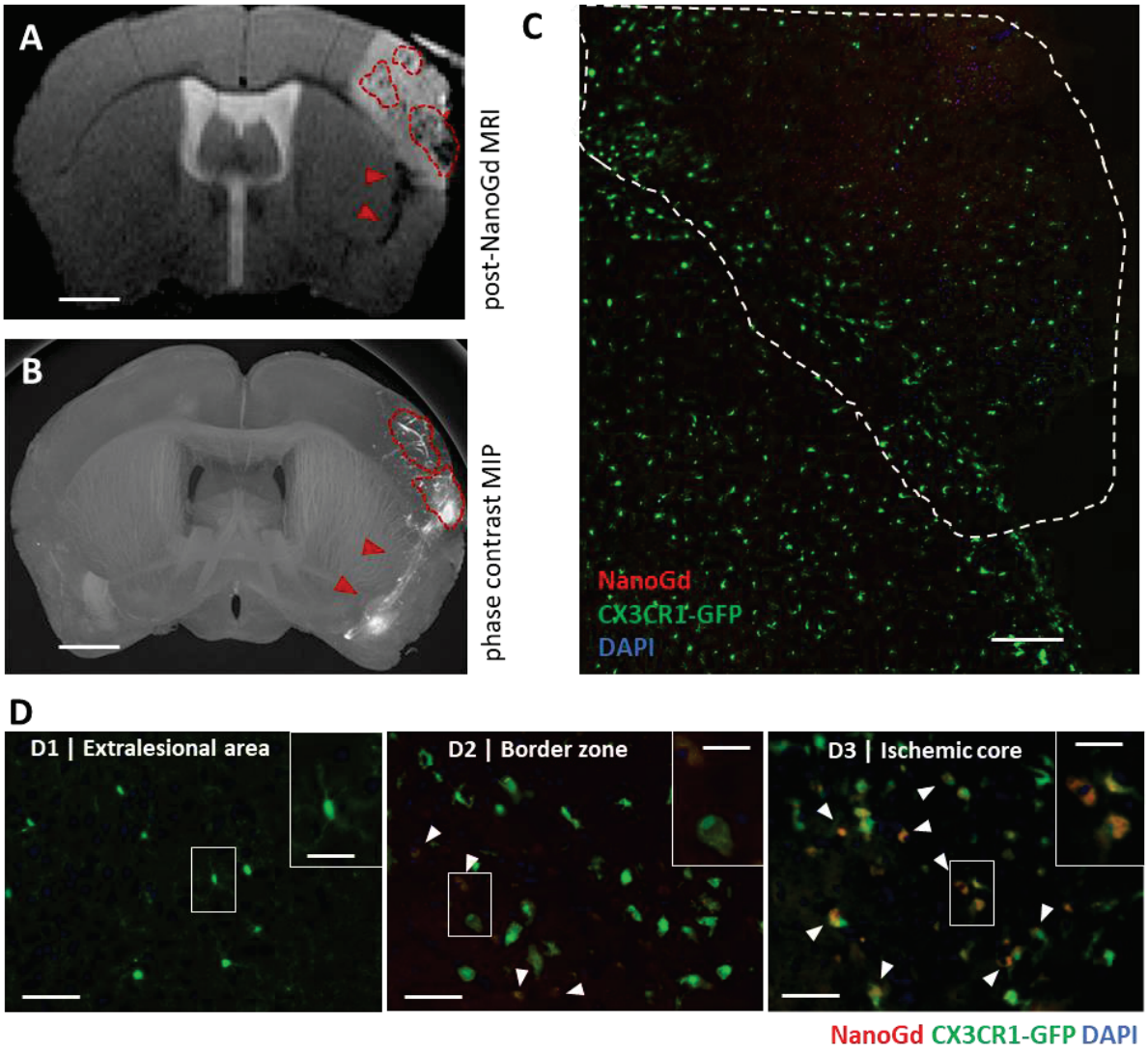

Figure 6 | Ex-vivo detection of NanoGd following pMCAo. Hypointense signals on in-vivo T2-WI (**A**) colocalized with hyperdense signals observed on maximum intensity projection (MIP) obtained from ex vivo X ray phase contrast image (**B**). Dotted red lines represent signal observed in the ischemic lesion and red arrowheads signals exterior from the lesion. Both images were obtained from the same pMCAo mouse injected with NanoGd. (Scale bar: 1 mm). Brain stained sections of a representative pMCAo mouse (C-D). **C.** The ischemic lesion is delineated with dotted white line on a macroscopic view of the ischemic hemisphere. (Scale bar: 250 µm). **D.** Higher magnifications show CX3CR1-GFP cells and NanoGd in the extralesional area (D1), the border zone (D2) and the ischemic core (D3). White arrowheads point at the area of colocalization between CX3CR1-GFP cells and NanoGd. (Scale bars: 50 µm for overview images; 20 µm for magnified insets).

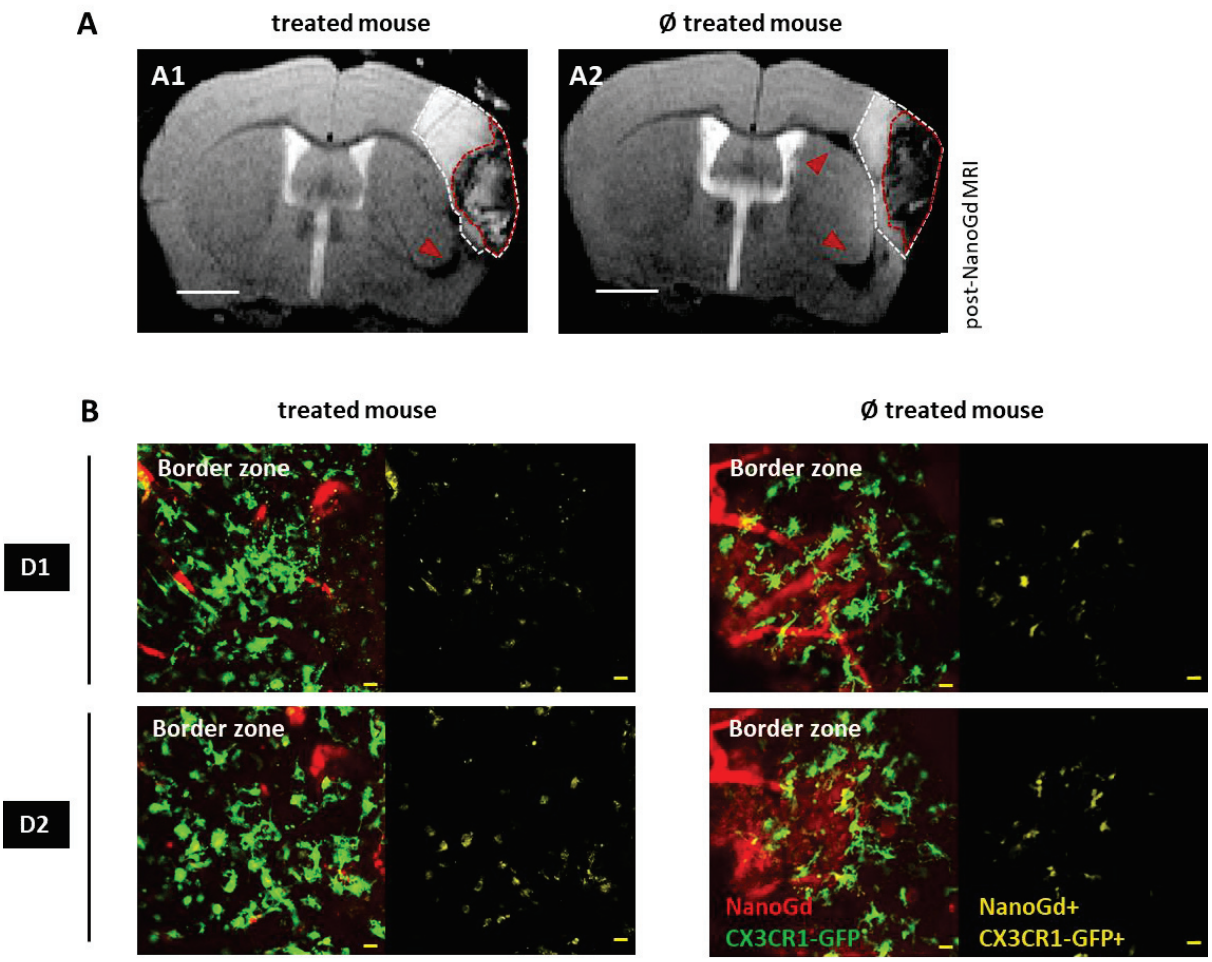

Figure 7 | Multimodal NanoGd imaging to investigate Simvastatin anti-inflammatory effect. A. Qualitative evaluation of simvastatin effect on MR signal related to NanoGd in a pMCAo treated mouse (A1) compare to a pMCAo non treated mouse (A2). On the T2-WI, the dotted white line delineated the ischemic lesion, the dotted red line the hypointense signals within the lesion and the red arrowheads point out hypointense signals exterior from the lesion. (Scale bars: 1mm). **B.** Two-photon intravital microscopy images show CX3CR1-GFP positive cells and NanoGd interaction in the border zone of a pMCAo treated mouse and a pMCAo non treated mouse, at D1 (session 1) and D2 (session 2). Ø treated mice: non-treated mouse. (Scale bar: 20µm).

Discussion

Tissue-resident microglia and recruited macrophages are important mediators of tissue damage following ischemic stroke. However, in vivo monitoring of phagocytic activity is currently limited at the acute stage of this condition. New tools enabling in vivo assessment of early phagocytic activity would thus be highly desirable. In this study we have developed a multimodal protocol to image in-vivo phagocytic cells in a mouse model of permanent ischemia. Our MRI results highlighted a systematic accumulation of T2/T2* signals in the ischemic core of the pMCAo mice, associated with remote MR signal voids in the corpus callosum. With two-photon microscopy, we confirmed the correlation between MR signals and NanoGd internalization by CX3CR1-GFP phagocytic cells, validating the potential of NanoGd-enhanced MRI for phagocyte tracking at the acute and subacute stages of ischemic stroke.

The originality of our method is based the use of a new multimodal nanoprobe, the NanoGd. In the present study, we demonstrated its optimal properties for MR imaging, with a r2 relaxivity equivalent to (U)SPIO relaxivities [32], [33], reference as T2/T2* contrast agent. NanoGd fluorescence spectra have already been measured with fluorescence spectroscopy on NanoGd phantoms (Karpati et al., in preparation), and here we confirmed its efficient detection both in-vitro and in vivo with fluorescence, confocal and two-photon microscopies. Moreover, NanoGd detection with new generation spectral photon-counting computed tomography (SPCCT) was demonstrated in a recent study performed on healthy rodents [25], which highlighted its potential as contrast agent for X-ray imaging. Regarding NanoGd physicochemical properties, our nanoparticle has a small hydrodynamic diameter, a long vascular remanence and a negative zeta potential characteristic of anionic compounds. These properties are known to be associated with great uptake by circulating macrophages [15], [34]. Except for the zeta potential, they are quite similar to the ones of (U)SPIOs [15], [35], widely used nanoparticles for phagocyte labelling and immune cell tracking imaging [36]. In a primary model of microglia cell culture,

we confirmed this hypothesis, demonstrating its efficient internalization by phagocytic cells. All these data, taking together with our results showing the absence of NanoGd cytotoxic effects, confirmed the great properties of our nanoprobe as a trimodal contrast agent and promising biomarker of phagocytosis.

Following NanoGd injection in mice submitted to permanent ischemia, reproducible hypointense MR signals were almost systematically detected in the ischemic core of the lesion. Post-mortem high-resolution phase contrast images confirmed this spatial distribution of NanoGd in the mouse ischemic brains. Two distinct and probably complementary mechanisms may explain NanoGd accumulation within the ischemic brains of pMCAo mice. The first mechanism is the so-called “Trojan horse mechanism” by which activated peripheral immune cells may internalize NanoGd in the blood stream before being subsequently recruited at the ischemic lesion by inflammatory signals. The second mechanism is represented by the crossing of disrupted BBB by free NanoGd, followed by secondary internalization by phagocytic cells present at the lesion site [37], [38]. In the ischemic core and to a lesser extent, in the border zone, we observed with two-photon microscopy sessions both NanoGd diffusion from the vessels to the brain parenchyma and activated CX3CR1-GFP cells phagocytosing NanoGd. Moreover, observation and preliminary quantifications of two-photon images obtained during these two imaging sessions pointed out: 1) an increase in CX3CR1-GFP+ cells presence in the ischemic core and the border zone, associated with 2) an increase of NanoGd internalization by CX3CR1-GFP cells. In the current study, we used the fractalkine receptor CX3CR1, expressed on the surface of both resident microglia and recruited macrophages [39], [40], to image and characterize phagocytic cells. While this marker is common to both cell types, visual observations of CX3CR1-GFP cell morphologies highlighted the presence of two distinct cell population: first, small round shape CX3CR1-GFP cells, essentially in the ischemic core, which are most probably recruited macrophages [41], and second, highly activated “jellyfish” like

CX3CR1-GFP microglial cells [42] in the ischemic core and border zone. Moreover, highly mobile NanoGd-laden CX3CR1-GFP negative cells were detected in the ischemic core. We hypothesized that these cells may correspond to neutrophils, which are CX3CR1 negative immune cells [43] presents at the lesion at the acute and subacute phases of permanent stroke [44], and which have the potential to internalize magnetic nanoparticles [45]. These results are in line with literature studies performed on pMCAo mice, showing that the presence and activation of immune phagocytic cells is major at the lesion site from 1 day to 5 days following ischemic stroke [46]. If microglia and neutrophils presence and activation in the lesion in this model have been well documented using specific histological markers [44] or fluorescent reporter mice [47], it is more challenging to obtain temporal information that is specific from recruited macrophages, and data regarding the kinetic of macrophage infiltration following pMCAo are scarce [48], [49]. Several studies have described the temporal dynamic of blood-borne macrophage infiltration in mouse models of transient cerebral ischemia and photothrombosis permanent stroke [50]–[52], but inflammatory mechanisms differ from one model to another [44], [53]. Thus, the precise characterisation of cellular population associated with NanoGd internalisation following pMCAo warrants further investigation. Nonetheless, regardless of the cell origin, these first analyses suggest that MR hypointense signals observed in the ischemic lesion 48 hours following NanoGd injection reflect at least in part phagocytic activity in the ischemic lesion.

Interestingly, the spatial distribution of NanoGd-associated hypointense MR signals differs from the results obtained in USPIO-enhanced MRI studies in the same stroke model, despite quite similar experimental chronologies [19], [54], [55]. In these studies, strong hypointense MR signals were observed surrounding the ischemic lesion, and ex-vivo analyses revealed a colocalization between the iron oxide particles and immune phagocytic cells in the same area [54]. NanoGd and USPIOs biocompatibility is ensured by distinct types of coating [19], [55],

chemical component which is known to strongly influence nanoparticle uptake by phagocytes [15]. Thus, an internalization of these nanoparticles by different cell populations based on their affinity for nanoparticles coating could be one hypothesis to explain MR signal spatial difference following permanent ischemia. Indeed, following pMCAo in mice, microglia cells/recruited macrophages and their anti/pro-inflammatory subsets had been associated with specific localizations in the ischemic core and in the border zone [46], [47], [56]. In this study, sample preparation for post-mortem analyses did not offer the possibility to assess the phenotype of immune cells that have internalized NanoGd. Thus, future studies should aim at confirming this hypothesis.

To give some therapeutic perspectives to our study, we wanted to determine whether the NanoGd imaging approach could provide a marker of disease regression upon anti-inflammatory treatment, and we tested its efficiency to monitor the potential therapeutic effects of a treatment with simvastatin in pMCAo mice. Indeed, in-vitro studies highlighted promising immunomodulatory properties for simvastatin, showing an effect on immune cell migration and phagocytic properties [23], [24], [57]. To the best of our knowledge, this study is the first investigating the impact of a treatment with simvastatin in a pMCAo mouse model. At first sight, our results suggest that simvastatin does not impact the lesion size on this model. Quantifications of NanoGd accumulation in the ischemic lesion on MRI and two-intravital microscopy data are ongoing and will allow to obtain in-vivo information on simvastatin impact on phagocytic activity following ischemic stroke.

In the present study, we extended the work done with nanoparticle-enhanced MRI for in-vivo phagocyte tracking, using for the first time MRI and intravital microscopy back-to-back in a murine model of ischemic stroke. Two-photon intravital microscopy is a powerful method, complementary to noninvasive 3D imaging techniques by providing the spatial and temporal resolution required to monitor the dynamics of immune cells in CNS diseases, including stroke.

Notably, it has been used in a mouse model of photothrombosis stroke, to monitor and characterize in-vivo neutrophils interaction with microglia at the acute phase of ischemic stroke [10], [58], highlighting a potential protective role for microglia against tissue damages induced by neutrophils [47]. As mentioned above, microglia/macrophage dynamic differs from one stroke model to another [53], and still have to be characterized following pMCAo. Due to the reproducible cortical localization of the pMCAO infarct, intravital microscopy is ideal to investigate immune cell involvement in this model. This technique has already been used in pMCAo mice to investigate T cell behavior following stroke, but to our knowledge, our study provides the first two-photon intravital microscopy data on CX3CR1-GFP cell activation in the ischemic lesion following pMCAo.

The absence of efficient treatment to protect the brain following stroke has resulted in a clear need to develop surrogate markers for monitoring the clinical response to therapy. In this study, we proposed a multimodal imaging method to assess in-vivo phagocytic activity following stroke, based on the injection of a novel nanoprobe, the NanoGd. We have shown that minimally-invasive NanoGd-enhanced MRI provides an in-vivo surrogate marker of inflammation. Most importantly, we demonstrated that this method is a promising tool for studying phagocyte spatiotemporal dynamic associated with the ischemic lesion in transgenic animals.

Acknowledgments

The authors thank Radu Bolbos and Jean-Baptiste Langlois of the Animage platform (CERMEP, Lyon) for their technical assistance.

This research was funded by the French national research agency (ANR) project NanoBrain (grant # ANR-15-CE18-0026-01) and was performed within the framework of the RHU

MARVELOUS (ANR16-RHUS-0009) of University Claude Bernard Lyon 1 (UCBL), within the program “Investissements d’Avenir”. We also thank ESRF for allocation of beamtime.

Author Contributions

V.H, I.H, O.P and M.W. designed all experiments. V.H, I.H, N.C, C.W, E.B, P.M, F.C, O.P and M.W performed experiments. S.K, F.L, M.M, M.L and S.P provided the nanoprobe. V.H, I.H, O.P and M.W analyzed data. V.H. I.H, O.P and M.W. wrote the manuscript with inputs from all the co-authors. All authors approved final version of manuscript.

Additional information

Supplementary information accompanies this paper.

Competing interest statement: this project is part of a public-private partnership with a society that may commercialize the investigated nanoparticle. Otherwise, the authors declare that the research was conducted in the absence of any commercial or financial relationships that could be construed as a potential conflict of interest.

References

[1] C. Iadecola and J. Anrather, “The immunology of stroke: from mechanism to translation,” *Nat. Med.*, vol. 17, no. 7, pp. 796–808, 2011.

[2] X. Y. Xiong, L. Liu, and Q. W. Yang, “Functions and mechanisms of microglia/macrophages in neuroinflammation and neurogenesis after stroke,” *Prog. Neurobiol.*, vol. 142, pp. 23–44, 2016.

[3] M. Kanazawa, I. Ninomiya, M. Hatakeyama, T. Takahashi, and T. Shimohata, “Microglia and monocytes/macrophages polarization reveal novel therapeutic mechanism against stroke,” *Int. J. Mol. Sci.*, vol. 18, no. 10, 2017.

[4] J. Secklehner, C. Lo Celso, and L. M. Carlin, “Intravital microscopy in historic and contemporary immunology,” *Immunol Cell Biol*, vol. 95, pp. 506–513, 2017.

[5] D. Nayak, B. H. Zinselmeyer, K. N. Corps, and D. B. McGavern, “In vivo dynamics of innate immune sentinels in the CNS,” *Intravital*, vol. 100, no. 2, pp. 130–134, 2012.

[6] A. Nimmerjahn, F. Kirchhoff, and F. Helmchen, “Resting microglial cells are highly dynamic surveillants of brain parenchyma in vivo.,” *Science (80-.).*, vol. 308, no. 5726, pp. 1314–8, May 2005.

[7] T. L. Roth, D. Nayak, T. Atanasijevic, A. P. Koretsky, L. L. Latour, and D. B. McGavern, “Transcranial amelioration of inflammation and cell death after brain injury.,” *Nature*, vol. 505, no. 7482, pp. 223–8, 2014.

[8] E. Pietronigro, Z. Elena, V. Della Bianca, S. Dusi, and E. Terrabuio, “Blockade of α 4 integrins reduces leukocyte – endothelial interactions in cerebral vessels and improves memory in a mouse model of Alzheimer ’ s disease,” *Sci. Rep.*, no. May, pp. 1–15, 2019.

[9] S. Fumagalli, F. Ortolano, and M. G. De Simoni, “A close look at brain dynamics: Cells and vessels seen by in vivo two-photon microscopy,” *Prog. Neurobiol.*, vol. 121, pp. 36–54, 2014.

[10] J. Neumann *et al.*, “Beware the intruder: Real time observation of infiltrated neutrophils and neutrophil-Microglia interaction during stroke in vivo,” *PLoS One*, vol. 13, no. 3, pp. 1–9, 2018.

[11] C. J. S. Price *et al.*, “Intrinsic Activated Microglia Map to the Peri-infarct Zone in the Subacute Phase of Ischemic Stroke,” *Stroke*, vol. 37, no. 7, pp. 1749–1753, Jul. 2006.

[12] B. A. Radlinska *et al.*, “Multimodal microglia imaging of fiber tracts in acute subcortical stroke.,” *Ann. Neurol.*, vol. 66, no. 6, pp. 825–32, Dec. 2009.

[13] A. Gerhard, J. Schwarz, R. Myers, R. Wise, and R. B. Banati, “Evolution of microglial activation in patients after ischemic stroke: a [11C](R)-PK11195 PET study,” *Neuroimage*, vol. 24, no. 2, pp. 591–595, Jan. 2005.

[14] B. Zinnhardt *et al.*, “In vivo imaging biomarkers of neuroinflammation in the development and assessment of stroke therapies-towards clinical translation,” *Theranostics*, vol. 8, no. 10, pp. 2603–2620, 2018.

[15] C. Corot, P. Robert, J.-M. Idée, and M. Port, “Recent advances in iron oxide nanocrystal technology for medical imaging ☆,” *Adv. Drug Deliv. Rev.*, vol. 58, pp. 1471–1504, 2006.

[16] M. Gkagkanasiou, A. Ploussi, M. Gazouli, and E. P. Efstathopoulos, “USPIO-Enhanced MRI Neuroimaging: A Review,” *J. Neuroimaging*, vol. 26, no. 2, pp. 161–168, Mar. 2016.

[17] F. Chauveau, T. H. Cho, Y. Berthezène, N. Nighoghossian, and M. Wiart, “Imaging inflammation in stroke using magnetic resonance imaging.,” *Int. J. Clin. Pharmacol. Ther.*, vol. 48, no. 11, pp. 718–28, Nov. 2010.

[18] M. Rausch, A. Sauter, J. Frohlich, U. Neubacher, E. W. Radu, and M. Rudin, “Dynamic patterns of USPIO enhancement can be observed in macrophages after ischemic brain damage,” *Magn. Reson. Med.*, vol. 46, no. 5, pp. 1018–1022, 2001.

[19] M. Wiart *et al.*, “MRI monitoring of neuroinflammation in mouse focal ischemia,” *Stroke*, vol. 38, no. 1, pp. 131–137, 2007.

[20] A. Saleh, D. Wiedermann, M. Schroeter, C. Jonkmanns, S. Jander, and M. Hoehn, “Central nervous system inflammatory response after cerebral infarction as detected by magnetic resonance imaging,” *NMR Biomed.*, vol. 17, no. 4, pp. 163–169, 2004.

[21] C. Kleinschnitz, M. Bendszus, M. Frank, L. Solymosi, K. V Toyka, and G. Stoll, “In vivo monitoring of macrophage infiltration in experimental ischemic brain lesions by magnetic resonance imaging.,” *J. Cereb. Blood Flow Metab.*, vol. 23, no. 11, pp. 1356–1361, 2003.

[22] C. Lindberg, M. Crisby, B. Winblad, and M. Schultzberg, “Effects of statins on microglia,” *J. Neurosci. Res.*, vol. 82, no. 1, pp. 10–19, 2005.

[23] H. Salman, M. Bergman, M. Djaldetti, and H. Bessler, “Hydrophobic but not hydrophilic statins enhance phagocytosis and decrease apoptosis of human peripheral blood cells in vitro.,” *Biomed. Pharmacother.*, vol. 62, no. 1, pp. 41–45, 2008.

[24] M. M. Sadeghi, M. Collinge, R. Pardi, and J. R. Bender, “Simvastatin modulates cytokine-mediated endothelial cell adhesion molecule induction: involvement of an inhibitory G protein.,” *J. Immunol.*, vol. 165, pp. 2712–2718, 2000.

[25] N. Halttunen *et al.*, “Hybrid Nano-GdF 3 contrast media allows pre-clinical in vivo element- specific K-edge imaging and quantification,” *Sci. Rep.*, no. August, pp. 1–8, 2019.

[26] M. Marinescu *et al.*, “Synchrotron radiation X-ray phase micro-computed tomography as a new method to detect iron oxide nanoparticles in the brain,” *Mol. Imaging Biol.*, vol. 15, no. 5, pp. 552–559, 2013.

[27] H. Karatas *et al.*, “Thrombotic distal middle cerebral artery occlusion produced by topical FeCl 3 application: A novel model suitable for intravital microscopy and thrombolysis studies,” *J. Cereb. Blood Flow Metab.*, vol. 31, no. 6, pp. 1452–1460, 2011.

[28] A. Çakmak, M. Yemişçi, C. Köksoy, U. Yazgan, D. Dinçer, and T. Dalkara, “Statin Pre-Treatment Protects Brain Against Focal Cerebral Ischemia in Diabetic Mice,” *J. Surg. Res.*, vol. 138, no. 2, pp. 254–258, 2007.

[29] L. García-Bonilla, M. Campos-Martorell, and J. Montaner, “Evidence for the efficacy of statins in animal stroke models: a meta-analysis,” *J Neurochem.*, pp. 233–243, 2012.

[30] J. Zhang, Q. Bai, and Y. Zhang, “Pretreatment with simvastatin upregulates expression of BK-2R and CD11b in the ischemic penumbra of rats,” *JBR*, vol. 32(5), pp. 354–360, 2018.

[31] K.-S. Hong and J. S. Lee, “Statins in Acute Ischemic Stroke: A Systematic Review.,” *J. Stroke*, vol. 17, no. 3, pp. 282–301, Sep. 2015.

[32] CheMatech, “P904 – USPIO – www.chematech-mdt.com.” [Online]. Available: https://www.chematech-mdt.com/produit/p904-uspio/. [Accessed: 21-Sep-2019].

[33] S. Liu, J. C. Brisset, J. Hu, E. M. Haacke, and Y. Ge, “Susceptibility weighted imaging and quantitative susceptibility mapping of the cerebral vasculature using ferumoxytol,” *J. Magn. Reson. Imaging*, vol. 47, no. 3, pp. 621–633, 2018.

[34] E. Fröhlich, “The role of surface charge in cellular uptake and cytotoxicity of medical nanoparticles,” *Int. J. Nanomedicine*, vol. 7, pp. 5577–5591, 2012.

[35] H. E. Daldrup-Link, “Ten Things You Might Not Know about Iron Oxide Nanoparticles,” *Radiology*, vol. 284, no. 3, pp. 616–629, 2017.

[36] D. A. Hammoud, “Molecular Imaging of Inflammation: Current Status,” *J Nucl Med*, vol. 57, no. 8, pp. 1161–1165, 2016.

[37] J. Brisset *et al.*, “INFLAM – INFLAMmation in Brain and Vessels with Iron Nanoparticles and Cell Trafficking: A Multiscale Approach of Tissue Microenvironment, Iron Nanostructure and Iron Biotransformation,” *IRBM*, vol. 39, no. 2, pp. 93–102, Apr. 2018.

[38] S. Floris *et al.*, “Blood-brain barrier permeability and monocyte infiltration in experimental allergic encephalomyelitis: a quantitative MRI study.,” *Brain*, vol. 127, no. Pt 3, pp. 616–27, Mar. 2004.

[39] M. Prinz and J. Priller, “Tickets to the brain: Role of CCR2 and CX3CR1 in myeloid cell entry in the CNS,” *J. Neuroimmunol.*, vol. 224, no. 1–2, pp. 80–84, Jul. 2010.

[40] S. Fumagalli, C. Perego, F. Ortolano, and M. G. De Simoni, “CX3CR1 deficiency induces an early protective inflammatory environment in ischemic mice,” *Glia*, vol. 61, no. 6, pp. 827–842, 2013.

[41] R. Shechter *et al.*, “Recruitment of Beneficial M2 Macrophages to Injured Spinal Cord Is Orchestrated by Remote Brain Choroid Plexus,” *Immunity*, vol. 38, no. 3, pp. 555–569, 2013.

[42] T. L. Roth, D. Nayak, T. Atanasijevic, A. P. Koretsky, L. L. Latour, and D. B. McGavern, “Transcranial amelioration of inflammation and cell death after brain injury,” *Nature*, vol. 505, no. 7482, pp. 223–228, 2014.

[43] M. Lee, Y. Lee, J. Song, J. Lee, and S.-Y. Chang, “Tissue-specific Role of CX3CR1 Expressing Immune Cells and Their Relationships with Human Disease.,” *Immune Netw.*, vol. 18, no. 1, p. e5, Feb. 2018.

[44] W. Zhou *et al.*, “Postischemic Brain Infiltration of Leukocyte Subpopulations Differs among Murine Permanent and Transient Focal Cerebral Ischemia Models,” *Brain Pathol.*, vol. 23, no. 1, pp. 34–44, Jan. 2013.

[45] K. Kirschbaum *et al.*, “In vivo nanoparticle imaging of innate immune cells can serve as a marker of

disease severity in a model of multiple sclerosis," *Proc. Natl. Acad. Sci.*, vol. 113, no. 46, p. 201609397, 2016.

[46] C. Perego, S. Fumagalli, and M.-G. De Simoni, "Temporal pattern of expression and colocalization of microglia/macrophage phenotype markers following brain ischemic injury in mice," *J. Neuroinflammation*, vol. 8, no. 1, p. 174, 2011.

[47] A. Otxoa-de-Amezaga *et al.*, "Microglial cell loss after ischemic stroke favors brain neutrophil accumulation," *Acta Neuropathol.*, vol. 137, no. 2, pp. 321–341, 2019.

[48] H. X. Chu *et al.*, "Immune cell infiltration in malignant middle cerebral artery infarction: Comparison with transient cerebral ischemia," *J. Cereb. Blood Flow Metab.*, vol. 34, no. 3, pp. 450–459, 2014.

[49] J. G. Zarruk, A. D. Greenhalgh, and S. David, "Microglia and macrophages differ in their inflammatory profile after permanent brain ischemia," *Exp. Neurol.*, vol. 301, no. August 2017, pp. 120–132, 2018.

[50] M. Gelderblom *et al.*, "Temporal and Spatial Dynamics of Cerebral Immune Cell Accumulation in Stroke," *Stroke*, vol. 40, pp. 1849–1857, 2009.

[51] R. Jin, G. Yang, and G. Li, "Inflammatory mechanisms in ischemic stroke: role of inflammatory cells," *J. Leukoc. Biol.*, vol. 87, no. 5, pp. 779–789, 2010.

[52] T. Li, S. Pang, Y. Yu, X. Wu, J. Guo, and S. Zhang, "Proliferation of parenchymal microglia is the main source of microgliosis after ischaemic stroke.," *Brain*, vol. 136, no. Pt 12, pp. 3578–3588, 2013.

[53] M. L. Cotrina, N. Lou, J. Tome-Garcia, J. Goldman, and M. Nedergaard, "Direct comparison of microglial dynamics and inflammatory profile in photothrombotic and arterial occlusion evoked stroke," *Neuroscience*, vol. 343, pp. 483–494, 2017.

[54] V. Desestret *et al.*, "Early-stage investigations of ultrasmall superparamagnetic iron oxide-induced signal change after permanent middle cerebral artery occlusion in mice," *Stroke*, vol. 40, no. 5, pp. 1834–1841, 2009.

[55] M. Marinescu *et al.*, "Monitoring therapeutic effects in experimental stroke by serial USPIO-enhanced MRI," *Eur. Radiol.*, vol. 23, no. 1, pp. 37–47, 2013.

[56] S. Fumagalli, C. Perego, F. Pischiutta, E. R. Zanier, and M.-G. De Simoni, "The ischemic environment drives microglia and macrophage function.," *Front. Neurol.*, vol. 6, no. April, p. 81, 2015.

[57] M. R. Jensen *et al.*, "Structural basis for simvastatin competitive antagonism of complement receptor 3," *J. Biol. Chem.*, vol. 291, no. 33, pp. 16963–16976, 2016.

[58] J. Neumann *et al.*, "Very-late-antigen-4 (VLA-4)-mediated brain invasion by neutrophils leads to interactions with microglia, increased ischemic injury and impaired behavior in experimental stroke," *Acta*

Neuropathol., vol. 129, no. 2, pp. 259–277, 2015.

Supporting Information

SI Material and Method

NanoGd cytotoxicity study

Cell lines

NanoGd potential cytotoxicity was assessed on 4 human cell lines, all supplied by the American Type Culture Collection (ATCC). A549, epithelial-like cells from human lung, were cultivated in DMEM 4.5 g/L glucose + Glutamax medium supplemented with 10% fetal calf serum (FCS) and 1% penicillin-streptomycin. THP-1, monocytes from human peripheral blood, were cultivated in RPMI 1640 + Glutamax medium supplemented with 10% FCS, 1% penicillin-streptomycin, 1% pyruvate and 4.5 g/L glucose. HepG2, human hepatocytes, were cultivated in MEM _ + Glutamax medium supplemented with 10% FCS, 1% penicillin-streptomycin and 1% pyruvate. Finally, HEK 293T, embryonic kidney cells from human, were cultivated in the same medium than HepG2 cells.

Cell survival assays

NanoGd impact on cell lines was evaluated using two complementary assays: the LDH assay, assessing cell membrane damages and the MTT assay, assessing mitochondrial activity. Briefly, the different cell lines were seeded in 96-well plates at 10^5 cells/mL for A549, HEK and HepG2, and 5.10^5 cells/mL for THP-1, and incubated for 24 h at 37°C and 5% CO_2. After 24h, cells were exposed to different NanoGd concentrations (0.5 nM to 5000 nM). Cell survival assays were performed at 48 hours and 72 hours after NanoGd incubation.

For LDH assay, cells were incubated with 100 µL of CytoToxOne reagent for 10 minutes at 22°C. 50 µL of Stop solution were then added in each well and cell death was measured by fluorescence with ELISA plate reader (Victor, Perkin Elmer) at λ_{ex}= 544 nm and λ_{em}=572 nm.

For MTT assay, 10 µL of MTT Sigma-Aldrich solution (5 mg/mL in PBS) were added to each well, and the 96-well plates were incubated for 2 hours at 37°C. 100 µL of lysis buffer (SDS 10%) were then added to each well, and after 3 hours of agitation, cell viability was determined by absorption measurement (λ = 570 nm) with ELISA plate reader (Victor, Perkin Elmer).

Simvastatin treatment study design

An experimental protocol was designed to evaluate simvastatin impact on ischemic lesion volume, based on the protocols of two studies: the study of Marinescu and colleagues on minocycline treatment [1] and the study of Potey et al investigating atorvastatin impact following mouse ischemic stroke [2]. Suppl Figure S4A describes this experimental design. On day 0 (D0), 18 mice underwent permanent occlusion of the MCA, immediately followed by a baseline MRI. Simvastatin (n=9) or its vehicle (n=9) was randomly administered as a two-dose per day subcutaneous injection once every 6 h starting 1 hour after pMCAO induction, at D0 and D1. MRI was repeated 24h (D1) and 48h (D2) after pMCAo. The lesion volume was extracted from the MRI data to compare Simvastatin-treated versus vehicle-treated animals: it was delineated on apparent diffusion coefficient (ADC) map at D0, and on T2-weighted images at D1 and D2. The imaging protocol was followed by animal sacrifice and brain preparation for histology.

MRI

Evaluation of biodistribution, pharmacokinetic and Simvastatin treatment with MRI were performed on the same 7T magnet, using the same anesthesia protocol and mouse monitoring.

Biodistribution and pharmacokinetic

To evaluate biodistribution and pharmacokinetic, healthy mice (n=4) were imaged using a 35 mm inner diameter whole-body transmit-receive coil for signal acquisition. To avoid movement artifacts due to the respiration, the acquired sequence was triggered on mouse respiratory

rhythms. Abdominal axial T1 images were obtained with a dynamic RARE 2D sequence (TE/TR= 7.51/960.77 ms; FA= 90; number of averages= 2; acquisition time 1.32 min; number of repetitions= 25). NanoGd (2.0 mmol/kg) was injected i.v in the magnet between the second and the third repetitions. For this scan, 37 slices were acquired from the top of the heart to the bottom of the liver, using a FOV of 35x35 mm^2, a slice thickness of 1 mm and a matrix of 128x128.

Simvastatin treatment study

To measure the lesion volume at D0 (baseline MRI), EPI-diffusion images (acquisition time 4 min) were acquired with TE/TR= 23.3/5000 ms using 3 b-values (0, 1532 and 3045 s/mm^2 in slice direction). Apparent diffusion coefficients (in mm^2/s) were then calculated by fitting monoexponential model function on a pixel-by-pixels basis. At D1 and D2, T2 weighted images were acquired using a spin-echo sequence (TE/TR= 75/5000 ms; number of averages= 4, acquisition time 8 min). For all scans, the field of view was 20x20 mm^2, slice thickness 0.8 mm and the number of slices 17. Matrix size was 256x256 for the T2 sequence and 128x128 for the diffusion sequence.

Data analysis

Image analysis was performed using ImageJ software (National Institute of Mental Health, Bethesda, USA imagej.nih.gox/ij/).

Biodistribution and pharmacokinetic

Biodistribution in the liver, the spleen, the kidneys and the vascular sector was assessed by looking at contrast enhancement on the T1 weighted images obtained before contrast agent injection (1^{st} repetition), and at the end (25^{th} repetition) of the dynamic RARE sequence post-injection. To study NanoGd pharmacokinetic, MR signal changes during the time was observed by delineated one region of interest (ROI) for the liver, one for the spleen, one for each kidney

and three on the abdominal aorta on T1-WI for each mouse. MR signal intensity values in these ROI were averaged for the four mice, for each sequence repetition time. Results are expressed in a graph representing the variation of the mean MR signal value in relation to the time.

Simvastatin treatment study

On ADC maps (D0) and T2 maps (D1 and D2), three ROI were outlined: the ischemic lesion, the ipsilateral hemisphere and the contralateral hemisphere. Volumes were calculated by summation of the lesion areas of all brain slices showing brain damage and integrated by slice thickness. Brain swelling (increased ipsilateral hemisphere volume compared with contralateral) was assessed by dividing the ipsilateral (IH) by the contralateral hemisphere (CH) value: IH/CH. To avoid overestimation attributable to brain swelling, lesion volume (V) was normalized by the ratio: Vx(CH/IH).

Statistical analysis

To determine differences in ischemic lesion volume between simvastatin-treated mice and not-treated mice, a Student t-test (BiostaTGV website, Institut Pierre Louis UMR 1136 and UPMC, France) was used. In all comparisons, a p-value <0.05 was considered statistically significant.

SI Supplementary Figures

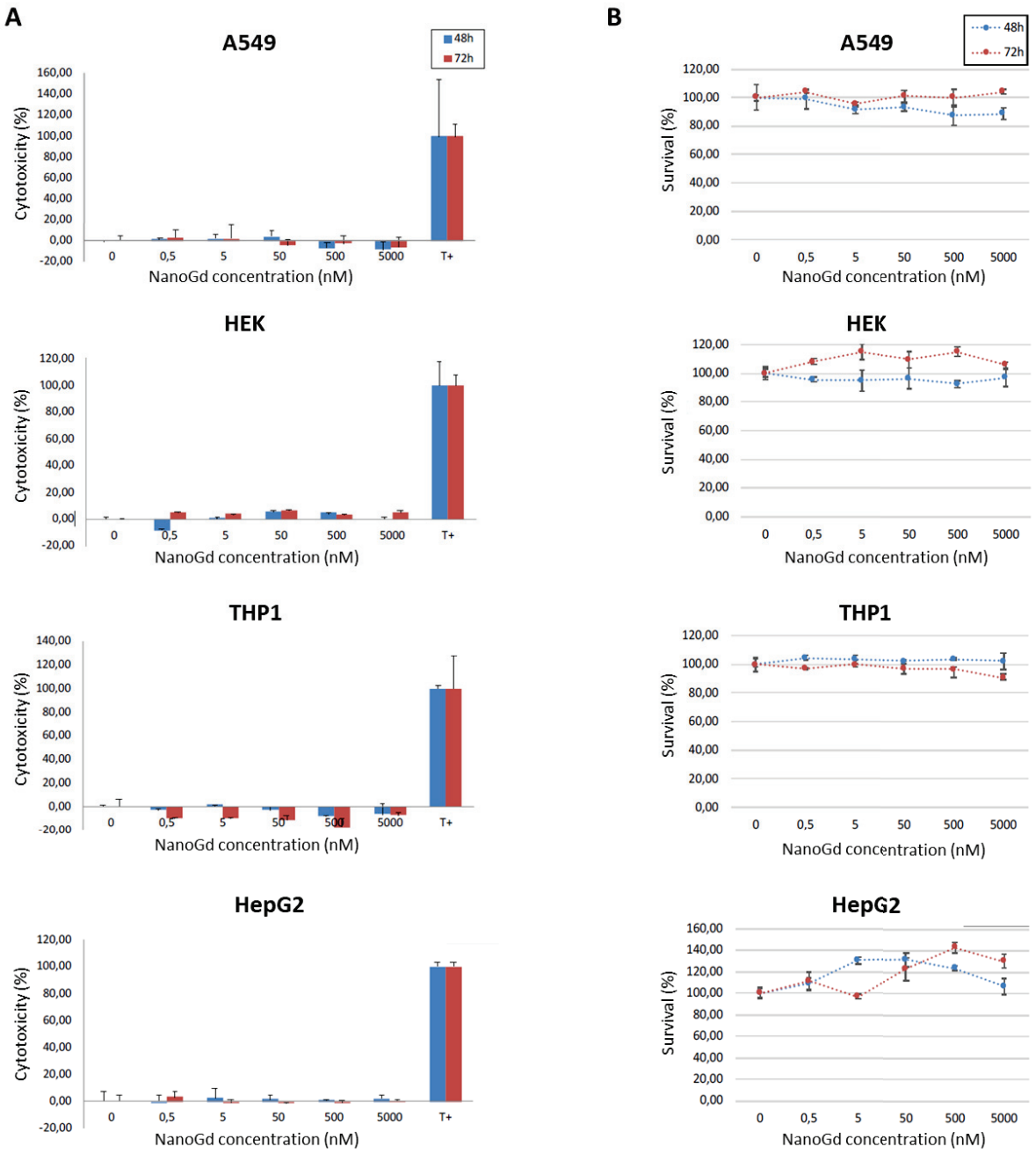

Supplementary Figure 1 | Evaluation of NanoGd cytotoxicity. Cytotoxicity was measured in different human cultured cells: HepG2, HEK, A549 and THP1. Cells were in contact with 0-5000 nM of NanoGd for 48h and 72h. **A.** NanoGd impact on cell survival assessed by LDH assay. "T+" correspond to the positive control with 100% cell death. Mean ±SD of duplicate. **B.** NanoGd effect on cell viability assessed by MTT assay. Mean ±SD of duplicate.

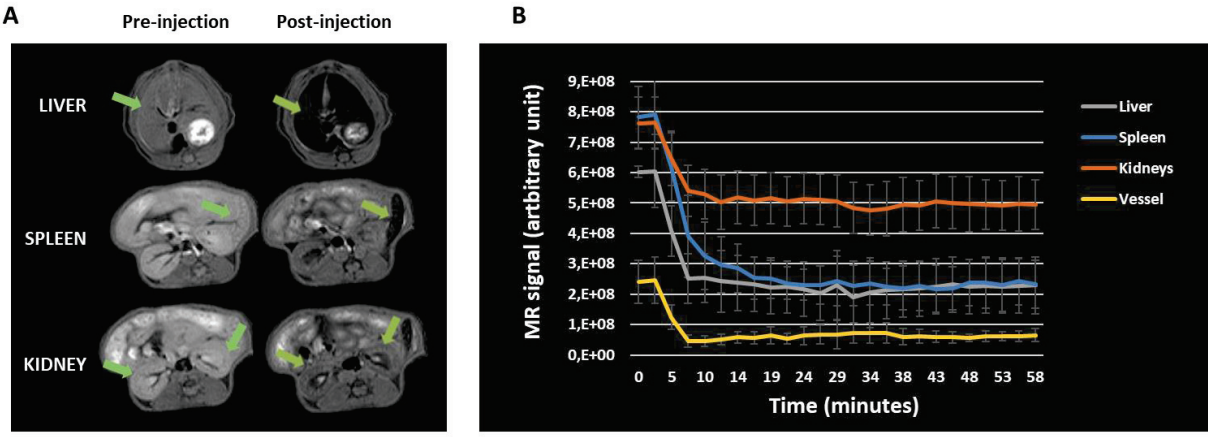

Supplementary Figure 2 | Biodistribution and Pharmacokinetic. A. NanoGd biodistribution was assessed with a dynamic T1 sequence for the liver, the spleen and the kidneys. Left T1-WI were acquired before gadolinium injection and right T1-WI after gadolinium injection, at the end of the dynamic sequence. Green arrows point the organs of interest ant the MR contrast enhancement. **B.** Graph represents the evolution of MR signal intensities in the liver, the spleen, the kidneys and the blood compartment across the time. Mean ±SD (n= 4 mice).

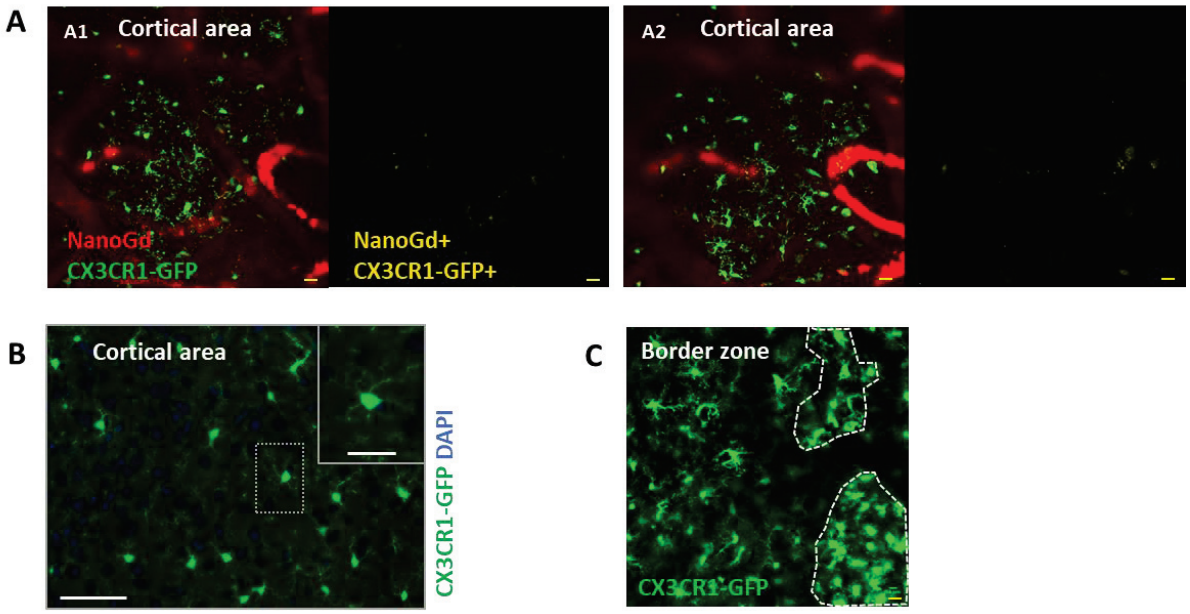

Supplementary Figure 3 | Fluorescence imaging in the control groups. Fluorescence imaging of NanoGd in a sham-operated mouse injected with NanoGd (**A-B**). **A.** Two-photon intravital microscope images of a cortical area at D1 (A1) and D2 (A2) following sham-operation. Right images represent fluorescent signals from CX3CR1-GFP positive cells and NanoGd, and the left images showed areas where CX3CR1-GFP positive cells and NanoGd

colocalize (in yellow). (Scale bar: 20µm). **B.** Brain stained sections show CX3CR1-GFP cells in a cortical area of a sham-operated mouse. NanoGd was not detected with histological analyses in sham-operated mouse brains. (Scale bars: 50 µm for overview images; 10 µm for magnified insets). **C**. Two-photon intravital microscope image for a pMCAo-operated mouse non injected with NanoGd, showing the border zone of the ischemic lesion at D2 following pMCAo. Dotted white lines delineated areas with activated CX3CR1-GFP cells. (Scale bar: 20µm).

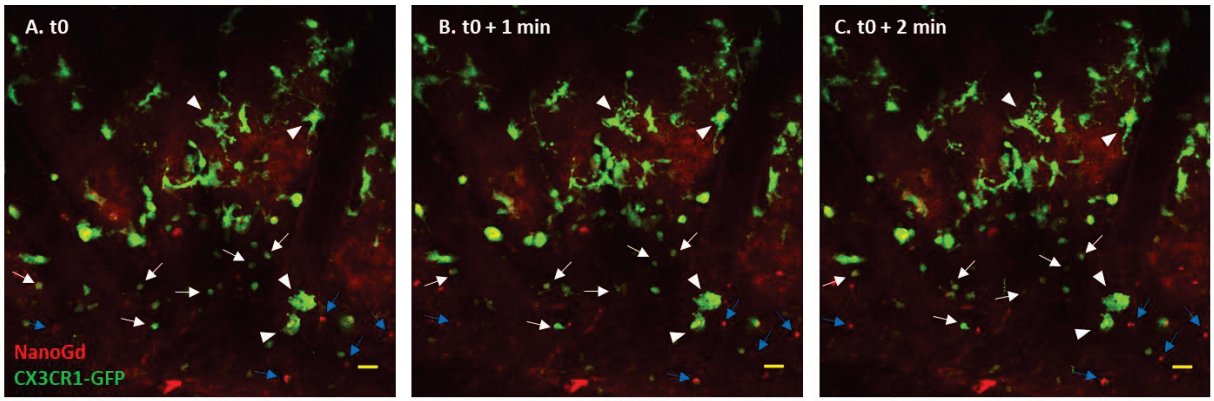

Supplementary Figure 4 | Cellular populations within the ischemic core. Two-photon intravital microscope images A to C are screenshots from a movie of the ischemic core, for a representative pMCAo mouse. White arrowheads point at some of the "jellyfish" like CX3CR1-GFP positive cells that we assume to be microglia cells. White arrows show some of the small round shape, highly mobile CX3CR1-GFP positive cells, which are likely to be recruited macrophages. Blue arrows point at red signal that seems to correspond to NanoGd accumulation in CX3CR1-GFP negative cells and which may be neutrophils. All of these cells are highly dynamic across the time. (Scale bar: 20µm).

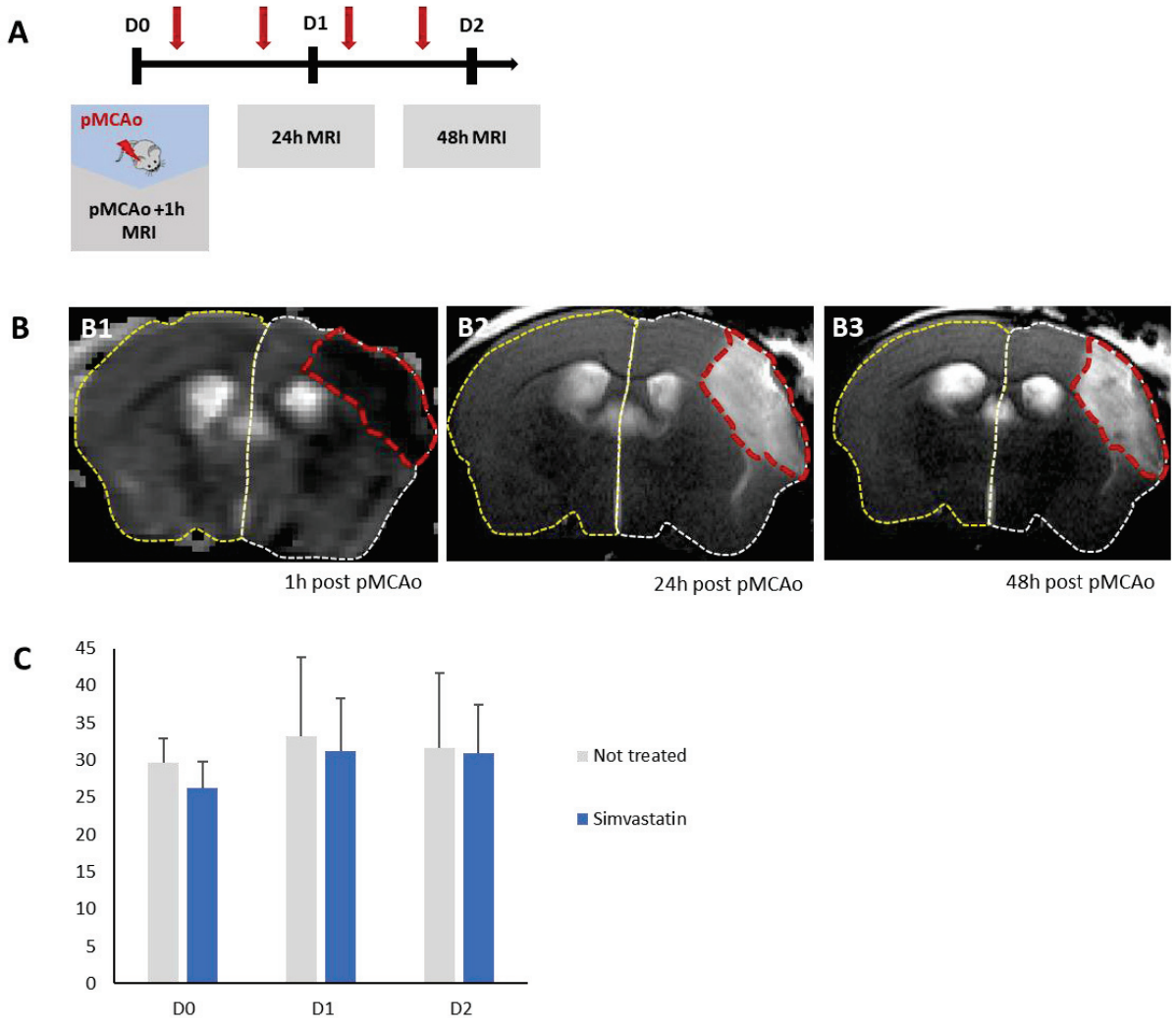

Supplementary Figure 5 | Measurement of simvastatin impact on ischemic lesion with MRI. A. Experimental timeline of simvastatin treatment study. **B.** Example of ROI delineation in ADC map at D0 (B1) and T2-WI at D1 (B2) and D2 (B3). Dotted red line represent the ROI "ischemic lesion", dotted white line the ROI "ipsilateral hemisphere" and dotted yellow line the ROI "contralateral hemisphere". **C.** Quantification of ischemic lesion volume at D0, D1 and D2 for the not treated group and the simvastatin group. Volume were normalized to ipsilateral and contralateral hemisphere volumes. Results are expressed in mean ±SD.

ARTICLE 4

Published in Development (2019)

The Shh receptor Boc is important for myelin formation and repair

Zakaria M[1], Ferent J[2], **Hristovska I**[3], Laouarem Y[1], Zahaf A[1], Kassoussi A[1], Mayeur ME[3], Pascual O[3], Charron F[2], Traiffort E[4].

[1] INSERM-University Paris-Sud/Paris-Saclay; Diseases and Hormones of the Nervous System, U1195, 80 rue du Général Leclerc, F-94276, Le Kremlin-Bicêtre, France.

[2] IRCM, Molecular Biology of Neural Development, 110 Pine Avenue West, Montreal, Quebec H2W 1R7, Canada; Department of Medicine, University of Montreal, Montreal, Quebec, Canada; McGill University, Montreal, Quebec, Canada.

[3] Institut NeuroMyoGène CNRS UMR 5310-INSERM U1217-Université Claude Bernard Lyon 1, Faculté de Médecine et de Pharmacie 69008 Lyon, France.

[4] INSERM-University Paris-Sud/Paris-Saclay; Diseases and Hormones of the Nervous System, U1195, 80 rue du Général Leclerc, F-94276, Le Kremlin-Bicêtre, France elisabeth.traiffort@inserm.fr.

© 2019. Published by The Company of Biologists Ltd | Development (2019) 146, dev172502. doi:10.1242/dev.172502

STEM CELLS AND REGENERATION

RESEARCH ARTICLE

The Shh receptor Boc is important for myelin formation and repair

Mary Zakaria[1], Julien Ferent[2], Ines Hristovska[3], Yousra Laouarem[1], Amina Zahaf[1], Abdelmoumen Kassoussi[1], Marie-Eve Mayeur[3], Olivier Pascual[3], Frederic Charron[2] and Elisabeth Traiffort[1,*]

ABSTRACT

Myelination leads to the formation of myelin sheaths surrounding neuronal axons and is crucial for function, plasticity and repair of the central nervous system (CNS). It relies on the interaction of the axons and the oligodendrocytes: the glial cells producing CNS myelin. Here, we have investigated the role of a crucial component of the Sonic hedgehog (Shh) signalling pathway, the co-receptor Boc, in developmental and repairing myelination. During development, *Boc* mutant mice display a transient decrease in oligodendroglial cell density together with delayed myelination. Despite recovery of oligodendroglial cells at later stages, adult mutants still exhibit a lower production of myelin basic protein correlated with a significant decrease in the calibre of callosal axons and a reduced amount of the neurofilament NF-M. During myelin repair, the altered OPC differentiation observed in the mutant is reminiscent of the phenotype observed after blockade of Shh signalling. In addition, *Boc* mutant microglia/macrophages unexpectedly exhibit the apparent inability to transition from a highly to a faintly ramified morphology *in vivo*. Altogether, these results identify Boc as an important component of myelin formation and repair.

KEY WORDS: Myelin, Oligodendrocyte, Axon, Hedgehog signalling

INTRODUCTION

Myelination in vertebrates is fundamental for the rapid conduction of action potentials along axons, and stands as a crucial regulator of function, plasticity and repair in the central nervous system (CNS) (Fields, 2008; Tomassy et al., 2016). This complex process relies on reciprocal interactions between neurons and oligodendrocytes: the CNS myelin-forming cells. Oligodendrocytes are the progeny of oligodendrocyte precursor cells (OPCs) and arise in multiple waves (Kessaris et al., 2006). In the dorsal forebrain, a major wave of OPC production arises from the germinative zone located just beneath the developing corpus callosum at the perinatal period. This wave coincides with the bulk of myelination occurring early after birth (Kessaris et al., 2006; Tong et al., 2015; Azim et al., 2016; Naruse et al., 2016). OPCs are maintained in the adult CNS, continue to divide, and generate new myelinating oligodendrocytes that participate in the myelin-remodelling (Young et al., 2013) and the learning processes (Gibson et al., 2014; McKenzie et al., 2014). Importantly, these progenitors also constitute a major reserve of cells scattered throughout the whole CNS that are able to be recruited towards a demyelinated area, which leads to myelin regeneration (Lopez Juarez et al., 2016; Franklin and Ffrench-Constant, 2017).

The type l transmembrane receptor Boc (brother of Cdo) is related to cell-adhesion molecules of the immunoglobulin superfamily and was initially implicated in the positive regulation of myogenic differentiation (Kang et al., 2002). Besides this role, Boc is a target and signalling component of the sonic hedgehog (Shh) pathway (Tenzen et al., 2006; Allen et al., 2011; Sanchez-Arrones et al., 2012; Yam and Charron, 2013). By binding Shh with high affinity, Boc transduces Shh signal in the guidance of commissural axons in the embryonic spinal cord (Okada et al., 2006; Tenzen et al., 2006) and in the segregation of ipsilateral retinal ganglion cell axons at the optic chiasm (Fabre et al., 2010). Later during postnatal development, Boc forms a Shh receptor complex with the main receptor patched 1 and is required for Shh-mediated cell proliferation of cerebellar granule neuron progenitors (Izzi et al., 2011). Finally, the strong expression of Boc in neurons of the cerebral cortex revealed its requirement for circuit-specific synapse formation (Harwell et al., 2012).

Recently, the Shh signalling pathway has been implicated in oligodendrocyte and myelin production during development and repair. A Shh-dependent domain in the germinal zone of the dorsal forebrain was found to produce large numbers of oligodendroglial lineage cells in the postnatal brain (Tong et al., 2015). Moreover, we and others have shown that modulation of Shh signalling can promote myelin repair (Ferent et al., 2013; Samanta et al., 2015; Sanchez et al., 2018). However, the role of Boc in oligodendrogenesis and myelination remains unexplored.

Here, we have examined the endogenous expression and function of Boc during OPC and myelin production, and in the context of CNS demyelination. During development, we show that, besides its previously described expression in callosal projection neurons, Boc can be detected in progenitors arising from the dorsal forebrain that are fated to the glial cell lineage. The *Boc*-null mutant revealed a transient oligodendroglial phenotype that delayed myelination and was associated with a decrease in the calibre of callosal axons. In the context of CNS demyelination, we demonstrate a high upregulation of *Boc* in the lesion. Together with the impaired myelin regeneration reminiscent of the phenotype observed when Shh signalling is inhibited, *Boc* mutant mice reveal morphological differences of microglia and/or macrophages *in vivo*, suggesting an inability to switch from a highly to a faintly ramified morphology. Altogether, this work identifies the Boc receptor as a new regulator of developmental myelination and remyelination.

RESULTS

Boc is expressed in neurons and neural progenitors that are fated to the glial cell lineage

The first two postnatal weeks correspond to an intense period of production and differentiation of OPCs derived from the germinative zone of the dorsal forebrain and leading to active myelination in the

[1]INSERM-University Paris-Sud/Paris-Saclay; Diseases and Hormones of the Nervous System, U1195, 80 rue du Général Leclerc, F-94276, Le Kremlin-Bicêtre, France. [2]IRCM, Molecular Biology of Neural Development, 110 Pine Avenue West, Montreal, Quebec H2W 1R7, Canada; Department of Medicine, University of Montreal, Montreal, Quebec, Canada; McGill University, Montreal, Quebec, Canada. [3]Institut NeuroMyoGène CNRS UMR 5310-INSERM U1217-Université Claude Bernard Lyon 1, Faculté de Médecine et de Pharmacie 69008 Lyon, France.

*Author for correspondence (elisabeth.traiffort@inserm.fr)

J.F., 0000-0002-4659-230X; E.T., 0000-0002-9645-6269

Received 6 October 2018; Accepted 28 March 2019

Development (2019) 146, dev172502. doi:10.1242/dev.172502

rodent brain (Kessaris et al., 2006). On day 8 after birth (P8), the highest Boc expression was detected in the cerebral cortex, and in the external granular and Purkinje cell layers of the cerebellum, as previously described (Izzi et al., 2011; Harwell et al., 2012). In addition, Boc could be observed in the germinative zone located just beneath the developing subcortical white matter (Fig. 1A). This area comprises undifferentiated progenitors, which give rise to oligodendroglial lineage cells that notably migrate to and populate the developing corpus callosum and the cerebral cortex during the first postnatal weeks (Menn et al., 2006; Seri et al., 2006; Kim et al., 2011; Azim et al., 2016; Naruse et al., 2016). At P8, in the germinative zone, 79±3% of Boc$^+$ cells co-expressed the proliferation marker Ki67 (Fig. 1B,D), while 32±2% were labelled for the Olig2 marker (Fig. 1C,D), which at this developmental stage is expressed in both oligodendrocyte and astrocyte progenitors (Naruse et al., 2017). Remarkably, most Olig2$^+$ cells detected at a distance from the germinative area were devoid of Boc expression (white arrowheads in Fig. 1C). At P15, Boc-expressing cells were mainly observed in layers II to V of the cerebral cortex (Fig. 1E). The majority of these cells (97±1%) co-expressed the marker of mature neurons NeuN and corresponded to 58.5±4.9% of the neuronal population (Fig. 1F and data not shown). The remaining 3±1% co-expressed Olig2 and constituted only 2±1% of all the Olig2$^+$ oligodendroglial cells in the cortex (Fig. 1G,H). In the corpus callosum, a faint Boc immunofluorescence was detected in the cytoplasm of a few scattered cells co-expressing Olig2 and the adenomatous polyposis coli (APC/CC1) marker. Boc$^+$ cells represented only 15±2% of the oligodendroglial population in the corpus callosum at P15 (Fig. 1H). Given the decrease of Boc immunostaining from P8 to P15, we investigated Boc expression at earlier time points (Fig. 1I). *In situ* hybridization led to the detection of a high level of *Boc* transcription at P0 and P5 in the dorsal germinative zone. A much weaker signal

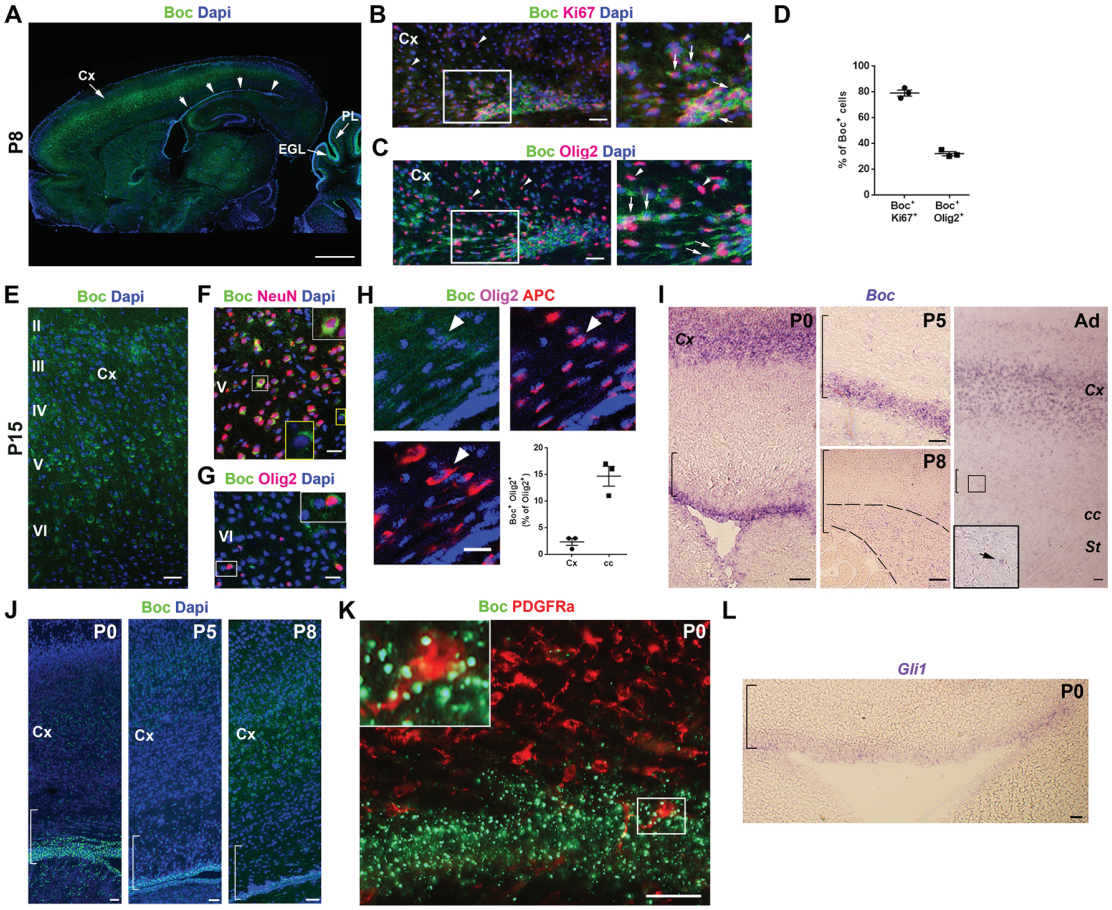

Fig. 1. Boc is expressed in neurons and neural progenitors of the dorsal forebrain germinative zone. (A) Tiled image visualizing Boc immunoreactivity in the P8 mouse brain. The four white arrows indicate the germinative zone of the dorsal forebrain. (B,C) Double immunohistofluorescence at the level of the germinative zone showing Boc$^+$ cells co-expressing (white arrows) or not (white arrowheads) the proliferation and oligodendroglial markers Ki67 and Olig2, respectively. The right panels are magnifications of the boxed areas. (D) Quantification of Boc$^+$ Ki67$^+$ and Boc$^+$ Olig2$^+$cells. (E-G) Visualization of Boc expression in the cerebral cortex from a P15 mouse (E, cortical layers are indicated on the left) and its co-expression with markers of mature neurons (NeuN, F) and of oligodendroglial cells (Olig2, G). Insets show boxed areas at higher magnification. (H) Triple immunostaining using Boc, Olig2 and APC antibodies visualizes a Boc$^+$ cell co-expressing Olig2 and APC in the corpus callosum at P15 (white arrowhead). The graph shows the quantification of the percentage of Olig2$^+$ cells co-expressing Boc in the cerebral cortex or corpus callosum. (I) *Boc in situ* hybridization of brain slices from P0, P5, P8 and adult mice at the level of the dorsal germinative zone. The dotted lines delineate the germinal zone at P8. The boxed area in the adult shows a scattered Boc$^+$ cell in the corpus callosum. (J) Boc immunostaining of brain slices from P0, P5 and P8 *Boc* knockout mice. (K) Boc$^+$ and PDGFRa$^+$ immunostaining in the dorsal germinative zone and developing corpus callosum in the P0 *Boc* mutant. The boxed area indicates an OPC still present in the germinative zone and likely expressing Boc (yellow puncta). (L) *Gli1 in situ* hybridization in the dorsal germinative zone at P0. The brackets in I,J,L indicate the position of the germinative zone and developing corpus callosum. Scale bars: 500 µm in A; 50 µm in B,C,E,H-L; 25 µm in F,G. Data are mean±s.e.m. cc, corpus callosum; Cx, cerebral cortex; EGL, external granular cell layer; PL, Purkinje layer; St, striatum.

Development (2019) 146, dev172502. doi:10.1242/dev.172502

was observed at P8 and became restricted to a few scattered cells in the corpus callosum of the adult animal (boxed area in Fig. 1I). In contrast, Boc$^+$ cells were clearly detected at all time points in the cerebral cortex (Fig. 1I and data not shown). To improve the visualization of low Boc protein levels, we took advantage of the insertion of a gene-trap β-galactosidase cassette inside the Boc gene of the *Boc* mutant mouse strain (Okada et al., 2006). A fragment of the N-terminal extracellular domain of Boc is still expressed in these mutants. We have shown previously that the Boc antibody reacts with this inactive fragment, which is retained intracellularly but inactive, and that the signal from this antibody disappears in *Boc*-null mutant mice (Allen et al., 2011). Therefore, we immunostained brain slices derived from P0, P5 and P8 mutant mice. In agreement with *in situ* hybridization experiments, we detected a high Boc signal in the dorsal germinative zone from P0 pups progressively decreasing until P8 (Fig. 1J). Moreover, double immunostaining of mutant P0 brain slices by using antibodies against Boc and PDGFRa, a marker of OPCs, showed that most OPCs were devoid of Boc expression, although we could not completely exclude the possibility that a subset may maintain Boc expression (boxed area in Fig. 1K). Remarkably, transcripts of Gli1, the transcriptional effector of Shh signalling, were also detected at a low level in the P0 dorsal germinative zone (Fig. 1L). These data thus indicate that, besides its neuronal expression during the early postnatal period, Boc is present in proliferating progenitors of the dorsal germinative zone.

Boc regulates the perinatal production of undifferentiated neural progenitors and OPCs

The expression of Boc in progenitors of the dorsal germinal zone during the period of oligodendrocyte production raised the possibility that Boc could be involved in the dorsal wave of oligodendrogenesis. To test this hypothesis, we analysed *Boc* mutant mice and immunolabelled P0 forebrain sections derived from wild-type and *Boc* mutant pups for Olig2 and the neural stem cell marker Sox2 (Ellis et al., 2004; Dai et al., 2015). In the germinative zone of the dorsal forebrain, the neural progenitors co-express both markers, but progressively reduce Sox2 expression while they migrate towards the developing subcortical white matter and commit into astro- or oligodendroglial progenitors. As expected, immediately after birth, we observed a high number of Sox2$^+$ and Olig2$^+$ cells in the developing subcortical white matter from the wild-type animals (Fig. 2A). Olig2$^+$ cells co-expressed either a high or a low level of Sox2, reflecting the ongoing reduction in Sox2 expression (Fig. 2A, top, inset). In the P0 *Boc* mutant animals, we observed a significant decrease in the density of Sox2$^+$ (132±13 versus 210±12 cells/0.1 mm^2, P=0.002) and Olig2$^+$ (92±8 versus 164±7 cells/0.1 mm^2, P=0.0005) cells compared with the wild-type animals (Fig. 2A,B). However, the proportion of Sox2$^+$ neural progenitors upregulating Olig2 was not changed, suggesting that the absence of Boc reduced the production of Sox2$^+$ neural progenitors but not their commitment into Olig2$^+$ progenitors.

Although Boc was mostly expressed in neural progenitors and not in OPCs, we next tested whether the absence of Boc in the former may nevertheless alter the proliferation of OPCs. Therefore, we immunostained P0-P1 slices with the OPC and proliferation markers PDGFRa and Ki67, respectively. The density of PDGFRa$^+$ OPCs was significantly decreased in *Boc* mutant compared with the wild-type pups (140±15 versus 196±18 cells/0.1 mm^2, P=0.04). The proportion of proliferating PDGFRa$^+$ Ki67$^+$ cells was also decreased (31±5 versus 42±2%, P=0.03) not only at P0 (Fig. 2C,D) but also at P5 (Fig. 2E,F). In contrast, this percentage collapsed at P8 in the wild-type animals (20±2 versus 49±3%, P=0.0001), whereas it remained stable in the mutant (33±1 versus 29±4%) (Fig. 2E,F), suggesting a prolonged OPC proliferation in the mutant beyond that observed in wild-type animals. To determine whether Boc may be involved in the previously reported Shh-mediated proliferation of OPCs, we used a mixed glial cell culture containing astrocytes, oligodendroglial cells and microglia derived from the dorsal forebrain of P0-P1 wild-type and *Boc* mutant pups. In agreement with the reduced number of oligodendroglial cells generated in the dorsal germinal zone of the mutants, the percentage of Olig2$^+$ cells was significantly reduced (18.5±1.1 versus 28.8±3.2%, P=0.023; Fig. 2G,H). Two hours after a short pulse of the proliferation marker BrdU, we observed a lower percentage of Olig2$^+$ cells able to incorporate BrdU in the mutant than in the wild type (11.5±0.8 versus 19.3±0.7%; P=0.0002). Moreover, supplementation of the culture medium with recombinant Shh protein (4 nM), which is able to bind its receptor complex (Izzi et al., 2011), significantly increased the percentage of wild-type Olig2$^+$ BrdU$^+$ cells (29.1±2.4 versus 19.3±0.7%, P=0.002). In contrast, Shh stimulation only slightly and non-significantly increased the proliferation of OPCs derived from *Boc* mutants (13.0±0.5 versus 11.5±0.8%) (Fig. 2G,H). *Gli1* transcription was increased by about fourfold when Shh was added to the wild-type cells (4.4±0.8 versus 1.2±0.5, P=0.02), although it was not significantly upregulated when Shh was added to the mutant cell culture (2.1±0.5 versus 1.3±0.4; Fig. 2I), suggesting that Boc is required in neural progenitors from the dorsal germinative zone for their progeny to respond to Shh. In a consistent manner, Gli1 transcription level determined by quantitative RT-PCR in the forebrain from wild-type and Boc mutant mice indicated significant *Gli1* downregulation in P8 and P15 animals (Fig. 2J). Then, to evaluate whether mutant OPCs could be refractory to any stimulation, the mixed glial cell cultures were treated with SAG (3×10^{-7}M), an agonist of the key transducer of Shh signalling smoothened (Smo). SAG induced an increase in the percentage of Olig2$^+$ cells incorporating BrdU in both the wild-type (28±2 versus 18±1, P=0.003) and the mutant (18±2 versus 11±1, P=0.02; Fig. 2K, L) cultures, in disagreement with the idea of a full refractory state of Boc mutant progenitors. In addition, purified OPCs derived from wild-type and mutant pups responded to Shh in a similar manner to the mixed glial cell cultures (Fig. 2M,N), further supporting the hypothesis that Boc inactivation affects OPC proliferation independently of the other glial cells present in the culture.

The absence of Boc decreases MBP production in the dorsal forebrain

The decrease in OPC production at the perinatal period suggested that the absence of Boc may influence developmental myelination of axons that takes place during the first three postnatal weeks in rodents. Therefore, we performed western blot analysis using the dorsal forebrain from P8, P15 and adult wild-type or mutant mice (Fig. 3A,B). MBP protein was significantly decreased in *Boc* mutant compared with wild-type mice at P8 (0.631±0.009 versus 1.018±0.022, P<0.0001), P15 (0.807±0.018 versus 1.036±0.017, P=0.0001) and in adulthood (0.845±0.007 versus 1.093±0.04, P=0.0001). In order to determine whether MBP decrease was related to a reduced density of oligodendroglial cells throughout the whole process of developmental myelination, we first analysed the transcription of *Olig2* using quantitative RT-PCR. In *Boc* mutants, as expected, *Olig2* transcription was significantly decreased at P0-P1 (0.73±0.01 versus 1.00±0.02, P=0.005) and remained lower compared with the wild type at P8 (Fig. 3C). To further support this observation, we analysed the generation of OPCs

Development (2019) 146, dev172502. doi:10.1242/dev.172502

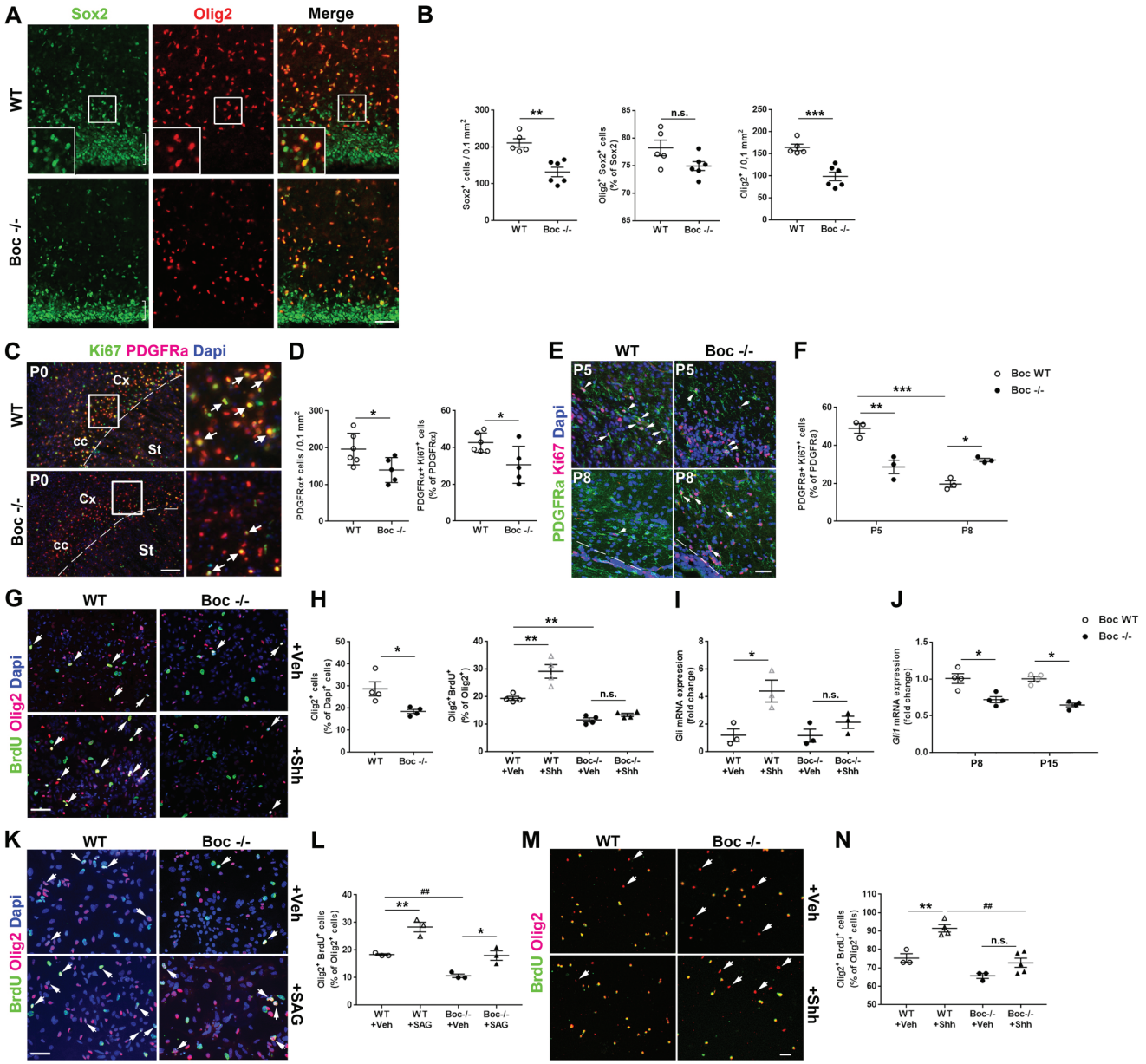

Fig. 2. Boc regulates the perinatal production of neural progenitors and OPCs. (A) Immunostaining of slices derived from P0-P1 wild-type or *Boc*$^{-/-}$ pups at the level of the germinative zone (white bracket) of the dorsal forebrain identified by Sox2 expression. Cells arising from this area and co-expressing the Olig2 marker are pre-OPCs and/or OPCs. (B) Quantification of Sox2^{+} and Olig2^{+} cells, and of the percentage of Sox2^{+} Olig2^{+} cells in the Sox2^{+} population. (C-F) Immunostaining and quantification of slices from P0-P1 (C,D), P5 and P8 (E,F) pups using Ki67 and PDGFRa as cell proliferation and OPC markers, respectively. (G,H) Primary mixed glial cell cultures derived from the forebrain of P0-P1 wild-type and *Boc*$^{-/-}$ mice assessed for cell proliferation after incorporation of the proliferation marker BrdU in the presence (+Shh) or absence (+Veh) of recombinant Shh protein. (I,J) Determination of *Gli1* transcription in the indicated culture conditions (I) and in the forebrain of P8 and P15 wild-type and *Boc*$^{-/-}$ mice (J) using quantitative RT-PCR. (K,L) Primary mixed glial cell cultures assessed for cell proliferation in the presence (+SAG) or absence (+Veh) of the Smo agonist SAG. (M,N) Purified OPCs prepared from P0-P1 wild-type and *Boc*$^{-/-}$ mice, and assessed for cell proliferation in the presence (+Shh) or absence (+Veh) of recombinant Shh protein. The white arrows show Olig2^{+} BrdU^{+} cells in G,K, PDGFRa^{+} Ki67^{+} in C,E and Olig2^{+} BrdU^{-} cells in M. Scale bars: 50 µm in E,K,M; 100 µm in A,G; 200 µm in C. Each point in the graphs corresponds to one animal or one culture. Statistical analysis used unpaired two-tailed *t*-test (B,D,H, left), two-way ANOVA and Tukey's multiple comparisons (F,H, right; I,J,L,N). **P*<0.05; ** and $^{\#\#}$*P*<0.01, ****P*<0.001; n.s. not significant. Data are mean±s.e.m.

and oligodendrocytes by immunostaining P8, P15 and adult brain slices with markers of OPCs (PDGFRa) and mature oligodendrocytes (APC). At P8, the density of PDGFRa^{+} OPCs was slightly but significantly lower in the mutant compared with the wild-type corpus callosum (Fig. 3D,E). Similarly, we observed a lower density of Olig2^{+} and APC^{+} cells. However, the percentage of APC^{+} cells in the Olig2 population (19±2 versus 22±2%) was unchanged, indicating that the absence of Boc did not alter the capacity of OPCs to differentiate into mature oligodendrocytes (Fig. 3F,G). At P15, in agreement with the absence of regulation of *Olig2* transcription observed at this age, the populations of Olig2^{+} and APC^{+} cells remained comparable in both genotypes (Fig. 3H,I). Similarly, no significant modification in the ability of OPCs to differentiate into APC^{+} oligodendrocytes was observed in

Development (2019) 146, dev172502. doi:10.1242/dev.172502

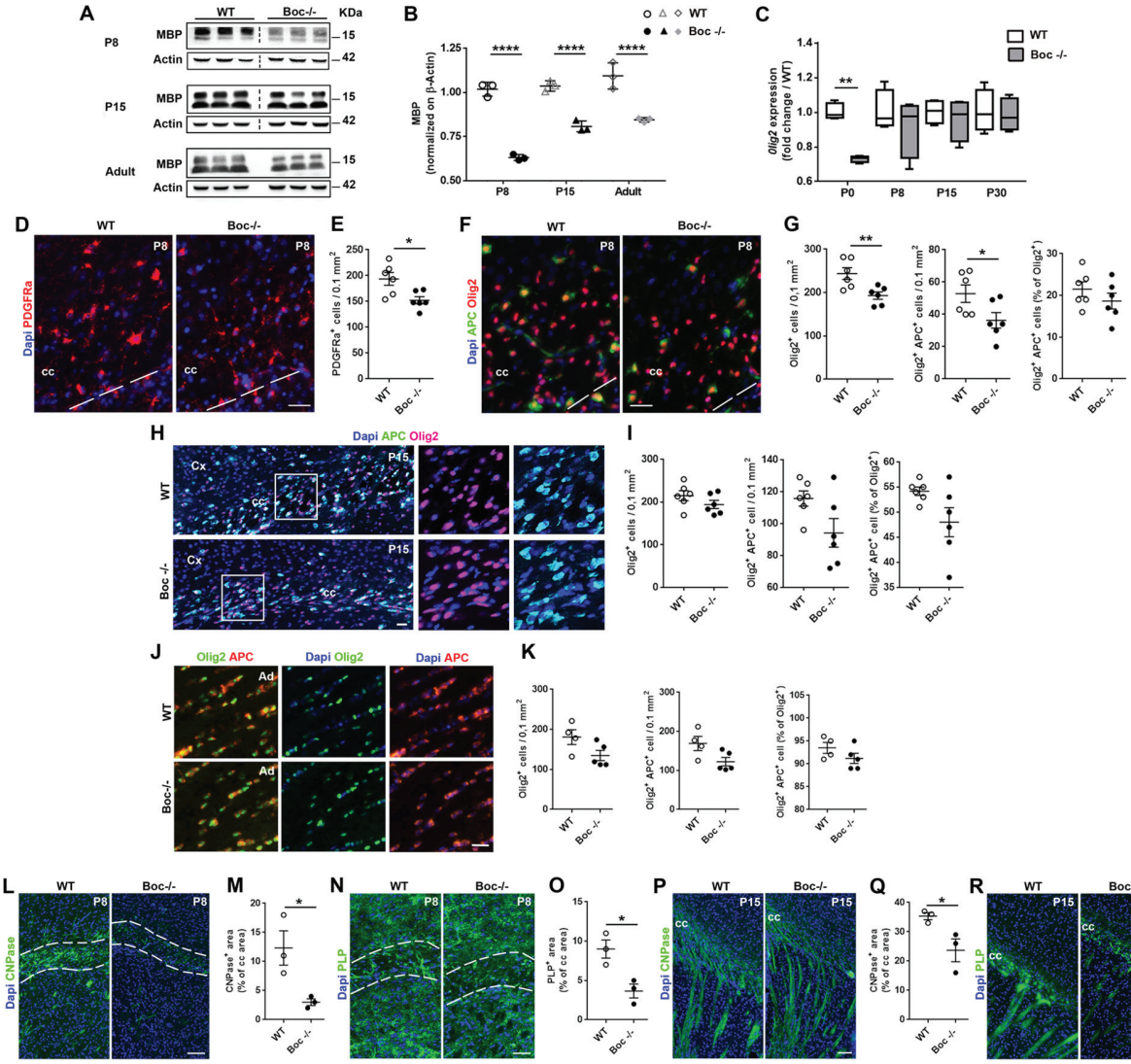

Fig. 3. Boc KO mice display a decreased production of myelin in the developing dorsal forebrain. (A) Western blot analysis of dorsal forebrain homogenates derived from P8, P15 and adult wild-type and *Boc*$^{-/-}$ mice. (B) Densitometric analysis of MBP immunoreactive signals normalized to β-actin expression. (C) *Olig2* transcript level determined by quantitative RT-PCR in the developing dorsal forebrain from P0, P8, P15 and P30 wild-type and *Boc*$^{-/-}$ mutant mice (*n*=3). Boxes and whiskers indicate minimal to maximal values and corresponding s.e.m., respectively. (D-G) PDGFRa and Olig2/APC immunostaining and corresponding quantifications carried out in slices from P8 wild-type or *Boc*$^{-/-}$ mice. The dashed line indicates the position of the germinative zone. (H-K) Visualization and quantification of Olig2$^+$ cells and APC$^+$ differentiated oligodendrocytes in the corpus callosum of P15 (H,I) and adult (J,K) wild-type and *Boc*$^{-/-}$ mice. (L-S) Visualization and quantification of CNPase$^+$ and PLP$^+$ immunostaining in the developing corpus callosum at P8 (L-O) and P15 (P-S) in wild-type and *Boc*$^{-/-}$ animals. The dashed lines in (L,N) delineate the developing corpus callosum. cc, corpus callosum; Cx, cerebral cortex. Scale bars: 50 µm in D,F,H,J,N; 100 µm in L,P,R. Statistical analysis used unpaired two-tailed *t*-test (E,G,I,K,M,O,Q,S), two-way ANOVA and Sidak's multiple comparisons (B,C). **P*<0.05; ***P*<0.01, *****P*<0.0001. Data are mean±s.e.m.

the mutant (48±3 versus 54±1%) (Fig. 3I). A similar result was obtained in adulthood, where 92±1 and 94±1% of Olig2$^+$ cells co-expressed the APC marker in the mutant and wild-type corpus callosum, respectively (Fig. 3J,K). However, consistent with the decrease in MBP previously observed, visualization of other myelin proteins, including the 2′,3′-cyclic-nucleotide 3′-phosphodiesterase (CNPase) and the proteolipid protein (PLP) indicated a significantly lower level of these proteins in P8 and P15 *Boc* mutants (Fig. 3L-S) compared with wild type. Collectively, these results indicate that the decreased production of OPCs observed in *Boc* mutants at birth can still be detected at P8 but recovers from P15 onwards, in contrast to the level of myelin proteins, which remains persistently reduced.

Impaired upregulation of gelsolin and delayed myelination in *Boc* mutant mice

To further characterize the decrease in MBP protein observed at P8 and because the heterozygous *Mbp*$^{+/-}$ mice have been shown to display only a subtle hypomyelination phenotype (Poggi et al., 2016), we determined whether the decrease in MBP observed in *Boc* mutant mice was associated with abnormal myelination of axons. At this age, myelination had already started in the lateral corpus callosum of control mice, but was significantly reduced in *Boc* mutant mice (Fig. 4A), as indicated by the determination of the area occupied by MBP$^+$ myelin sheaths in this region (25±1 versus 42±2%; *P*=0.0002; Fig. 4B). Consistently, the proportion of APC$^+$ oligodendrocytes co-expressing MBP was significantly lower in

Development (2019) 146, dev172502. doi:10.1242/dev.172502

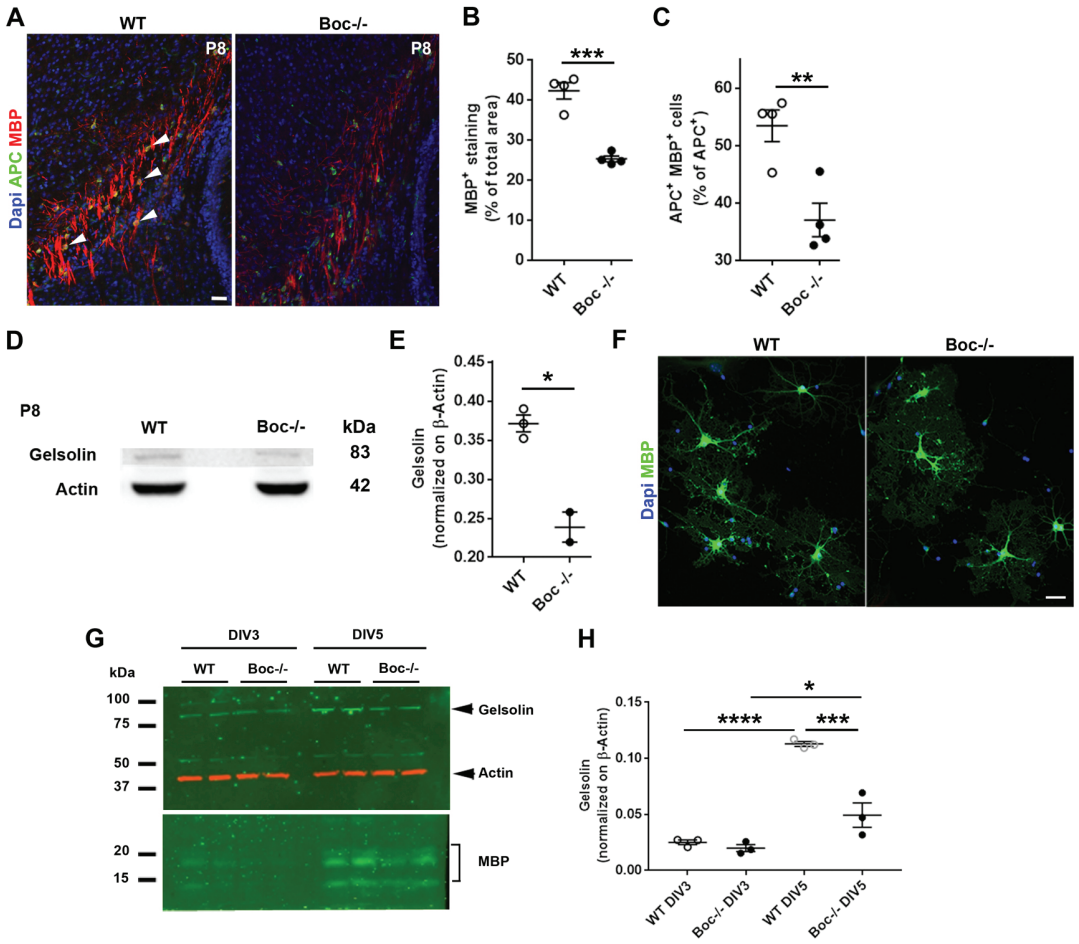

Fig. 4. The *Boc* mutant fails to induce actin disassembly proteins and leads to a delay of myelination. (A) Initiation of myelination detected by MBP upregulation in APC$^+$ oligodendrocytes and first MBP$^+$ myelin sheaths occurring in P8 wild-type and mutant mice. White arrowheads indicate APC$^+$ MBP$^+$ cells in the wild-type developing corpus callosum. (B,C) Quantification of the area occupied by MBP and the percentage of APC$^+$ MBP$^+$ cells in each genotype. (D) Detection of gelsolin immunoreactivity by western blot analysis of dorsal forebrain homogenates derived from P8 wild-type and *Boc*$^{-/-}$ mice. (E) Densitometric analysis of gelsolin signals normalized to β-actin expression. (F) Oligodendrocyte-enriched cultures prepared from the dorsal forebrain of wild-type or *Boc* mutant pups immunostained with MBP after 3 DIV show no major morphological differences. (G) Western blot analysis evaluating gelsolin and MBP expression in these cultures at 3 and 5 DIV. (H) Densitometric analysis of the immunoreactive gelsolin signal normalized to β-actin expression. Scale bars: 50 µm. Statistical analysis used unpaired two-tailed *t*-test (B,C,E), two-way ANOVA and Tukey's multiple comparisons (H). **P*<0.05, ***P*<0.01, ****P*<0.001. Data are mean±s.e.m.

Boc mutants compared with controls (37±3 versus 53±3%; *P*=0.006; Fig. 4C). Moreover, the release of gelsolin, one of the proteins required for oligodendrocyte actin disassembly, which is a step that is necessary to promote myelin wrapping around axons (Zuchero et al., 2015), was also reduced in the mutant. Indeed, forebrain homogenates from P8 wild-type or mutant animals analysed by western blot revealed a slight but significant decrease of gelsolin in the mutant (0.238±0.019 versus 0.371±0.011; *P*=0.04; Fig. 4D,E). In addition, we evaluated the ability of enriched oligodendrocyte cultures to differentiate for 5 DIV. No major morphological differences (Fig. 4F) were observed according to the genotype, suggesting that the absence of Boc in the neural progenitors did not impair the ability of OPCs to differentiate into oligodendrocytes. However, western blot analysis of such cultures at DIV 3 and DIV 5 revealed an increase in gelsolin signal in both genotypes from DIV 3 to DIV 5, with a much lower upregulation of gelsolin in the mutant (0.04±0.01 versus 0.11±0.01; *P*=0.0001; Fig. 4G,H). Thus, in *Boc* mutants, the delayed production of OPCs at birth is correlated with a decrease in MBP production and a defective gelsolin upregulation, both of which are consistent with the delay in developmental myelination observed at P8.

The absence of *Boc* causes/is associated with a decrease in myelinated axon calibre

Despite the recovery of regular oligodendroglial density in adult *Boc* mutants, the persistent decrease in MBP production remained intriguing. Therefore, we analysed the adult corpus callosum at the ultrastructural level. A striking observation was that axons appeared smaller in *Boc* mutants compared with wild-type corpus callosum (Fig. 5A,B). The analysis of more than 1000 axons from the three animals studied for each genotype indicated that the total number of axons was not significantly different in *Boc* mutants compared with wild-type animals (135±9 versus 128±11 axons per 100 µm^2; Fig. 5C). In a similar manner, no significant difference was found in the proportion of myelinated axons (68±3 versus 62±3%; Fig. 5D). In contrast, the mean diameter evaluated for 200 wild-type and 150 *Boc* mutant myelinated axons was significantly lower in the mutants (0.574±0.033 versus 0.773±0.061; *P*=0.047; Fig. 5E). Characterized as a structure containing mainly small-calibre axons

Development (2019) 146, dev172502. doi:10.1242/dev.172502

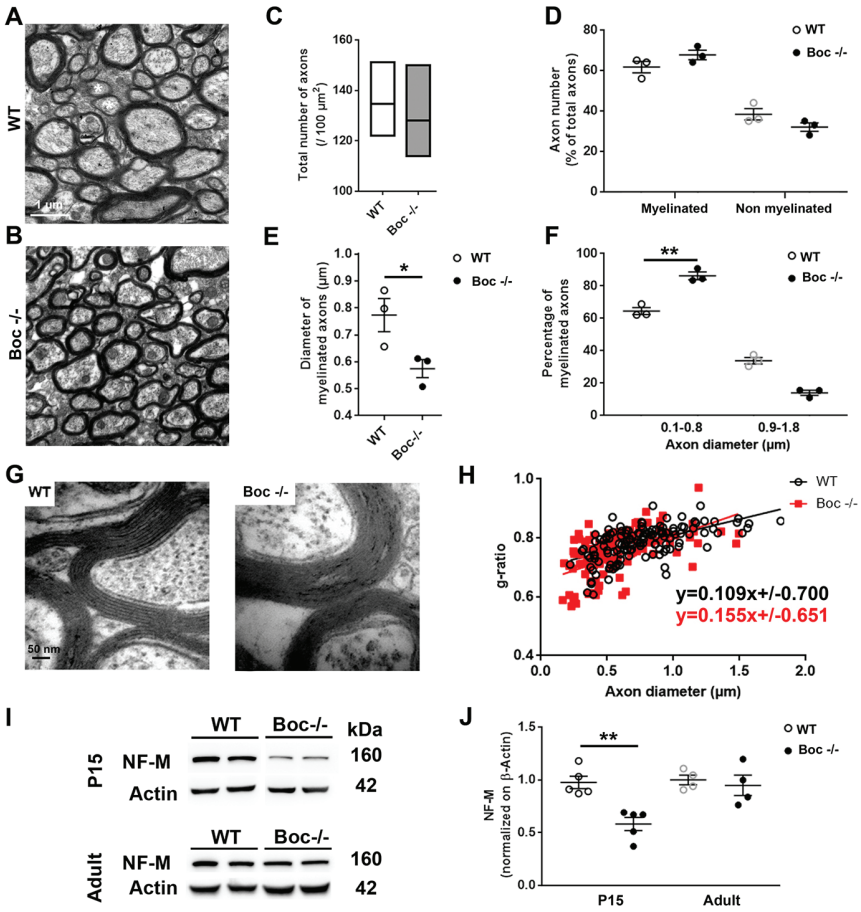

Fig. 5. The absence of Boc induces a decrease in the diameter of axons. (A,B) Visualization of coronal sections of the corpus callosum derived from wild-type (A) or *Boc*$^{-/-}$ (B) adult mice using electron microscopy. (C,D) The total number of axons (C, *n*=3 mice) and the percentage of myelinated axons (D) do not significantly differ according to the genotype. Boxes indicate minimal to maximal values in C. (E) The diameter of myelinated axons is decreased in the mutant animals. (F) The mutant displays a significantly higher proportion of myelinated axons with a diameter in the range 0.1-0.8 µm at the expense of larger calibre axons. (G,H) Visualization of myelin sheaths at high magnification and linear regression of the g-ratio (axon diameter/axon+myelin diameter). (I) Western blot analysis of the neurofilament NF-M in the dorsal forebrain from P15 and adult wild-type or *Boc* mutant animals. (J) Densitometric analysis of NF-M immunoreactive signals normalized to β-actin expression. Statistical analysis used unpaired two-tailed *t*-test (C-F,J). *P<0.05; **P<0.01. Data are mean±s.e.m.

(Hildebrand et al., 1993), the corpus callosum from the wild-type mice contained a high percentage of axons narrower than 0.8 µm. Remarkably, this percentage was even higher in the mutant (86±2 versus 65±2%; P=0.002) at the expense of axons with a diameter in the range 0.9-1.8 µm (14±2 versus 34±2; Fig. 5A,B,F). The g-ratio (the ratio of the axon diameter to axon+myelin diameter) was determined and the values were plotted against the axon diameter from n=134 and n=119 axons derived from three animals of each genotype (Fig. 5G,H). The equations were y=0.155x+0.651 and y=0.109x+0.700 for *Boc* mutants and wild type, respectively. The differences observed in the slopes and the intercepts did not reached significance (P=0.06). Because of the role of the neurofilament medium NF-M recognized in the control of axon calibre mostly in the peripheral nervous system, we looked for a change in the expression level of NF-M using western blot analysis. Consistent with the globally reduced axon calibre, *Boc* mutants showed a significantly reduced amount of NF-M at P15 (0.573±0.064 versus 0.927±0.077; P=0.008). In adulthood, no significant difference was observed (0.948±0.096 versus 1.000±0.046). Taken together, these results indicate that, in adulthood, the reduced production of MBP is not associated with hypomyelination, but could be the indirect result of the decreased axon diameter in *Boc* mutants. Moreover, the absence of Boc is associated with a reduced amount of the neurofilament NF-M.

The absence of Boc prevents spontaneous remyelination in LPC-treated animals

Given the oligodendroglial phenotype of the *Boc* mutant during development, we evaluated the possible consequences of inactivating *Boc* in the spontaneous regeneration of myelin that occurs upon demyelination. We used a model based on the injection of lysolecithin (LPC) into the corpus callosum. In this model, repair of the tissue comprises several successive and stereotyped steps, including the recruitment and proliferation of OPCs (at 5 days post-lesion, dpl), their differentiation into immature oligodendrocytes (at 10 dpl) and their maturation into myelinating cells (at 15 dpl). This process finally leads to the regression of the lesion size. We compared the main steps of the remyelination process in the corpus callosum from wild-type and *Boc* mutant animals. At 5 dpl, while Olig2$^+$ cells have already populated the demyelinated area in the wild-type mice, only rare Olig2$^+$ cells could be detected in the lesion from *Boc* mutants, indicating altered/delayed recruitment of new oligodendroglial cells. In a consistent manner, at 10 dpl, the density of differentiated APC$^+$ oligodendrocytes was largely reduced in the lesion from *Boc* mutants compared with wild type (Fig. 6A). The quantification of Olig2$^+$ and APC$^+$ cells at the different steps of the regeneration process confirmed a significantly lower density of oligodendroglial lineage cells in the mutant lesion until 15 dpl. However, at a later time point (21 dpl), the difference was largely attenuated, suggesting that Boc delays rather than impedes OPC recruitment (Fig. 6B). In contrast, the absence of Boc appeared to prevent OPC differentiation, as APC$^+$ immature oligodendrocytes were detected at a much lower level in the mutant than in the wild type at all time points. APC$^+$ cells reached a plateau between 15 and 21 dpl, representing 60-70% of the level observed in the wild type (Fig. 6C). In agreement with the delay for recruiting new Olig2$^+$ cells, the number of PDGFRa$^+$ OPCs (43±2 versus 72±5; P=0.001) and the percentage of proliferating OPCs (13±1 versus 18±2%;

Development (2019) 146, dev172502. doi:10.1242/dev.172502

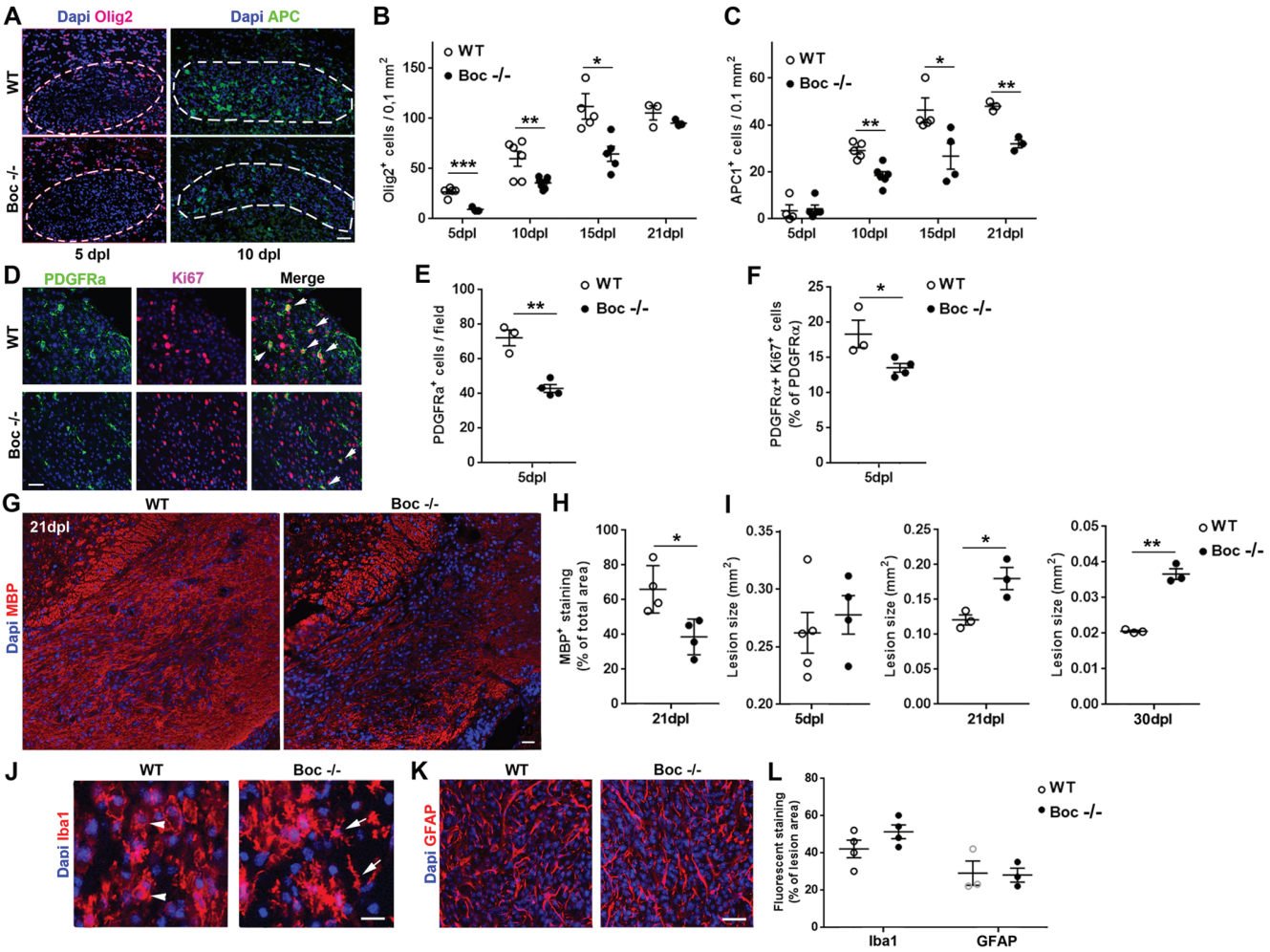

Fig. 6. The absence of functional Boc impedes complete remyelination. (A) Visualization of Olig2$^+$ and APC$^+$ cells in the lesion after the stereotaxic injection of LPC into the corpus callosum of wild-type and *Boc* mutant mice. The white dotted lines delineate the lesion. (B,C) The histograms show the densities of Olig2$^+$ (B) and APC$^+$ (C) cells quantified in the lesion of the wild-type and mutant mice at the indicated time points. (D-F) Double immunostaining using PDGFRa and Ki67 in the lesion at 5 dpl (D) and quantifications of the density of OPCs and the percentage of proliferating OPCs (E,F). Arrows in D indicate double-labelled cells. (G) Immunodetection of MBP in the lesion from the wild-type and mutant mice at 21 dpl. (H) The determination of MBP immunofluorescent area is shown in the histogram. (I) Evaluation of the lesion size at 5, 21 and 30 dpl. (J-L) Visualization of Iba1$^+$ microglia and GFAP$^+$ astrocytes at 10 dpl in the lesion from the wild-type and mutant mice. (J) Microglia and/or macrophage morphology appears more ameboid in the wild type (arrowheads) and more multipolar (arrows) in the mutant. (K) In contrast, no morphological differences are observed for astrocytes. (L) Quantification of Iba1 and GFAP fluorescent areas indicates no significant difference according to the genotype. Scale bars: 100 µm in A; 50 µm in D,G,K; 25 µm in J. Statistical analysis used multiple *t*-test (B,C) and unpaired two-tailed *t*-test (E,F,H,I,L). **P*<0.05; ***P*<0.01. Data are mean±s.e.m.

P=0.04; Fig. 6D,E,F) were decreased in the mutant at 5 dpl. Moreover, in a manner consistent with the impairment of OPC differentiation, *Boc* mutants displayed a lower ability to repair myelin, as indicated by the significantly lower MBP immunolabelling in the demyelinated area at 21 dpl (38±5 versus 66±6%, *P*=0.02; Fig. 6G,H). The lesion size was also determined by measuring the area in which a high cell nuclei density persists or the area devoid of small chains of cells compared with the unlesioned corpus callosum. Although the extent of the lesion significantly decreased in both the wild-type and mutant animals between 5 and 30 dpl, the lesion remained significantly larger in the mutant at 21 (0.180±0.016 versus 0.121±0.007 mm^2, *P*=0.03) and 30 dpl (0.035±0.003 versus 0.021±0.001 mm^2; *P*=0.001) (Fig. 6I).

Finally, we immunolabelled astrocytes and microglia and/or macrophages using Iba1 and GFAP markers in each animal group. Both cell types were detected in *Boc* mutants, as shown at 10 dpl (Fig. 6J-L), suggesting that the absence of Boc did not prevent the astro- and microgliosis in the lesion. However, microglia and/or macrophages appeared to display some discrete morphological differences, with cells apparently more ameboid in the wild type and more multipolar in *Boc* mutants (Fig. 6J). In contrast, no morphological differences could be observed for astrocytes (Fig. 6K). Moreover, the extent of the response determined by the measure of the area occupied by Iba1 and GFAP fluorescent signals did not differ according to the genotype. *In situ* hybridization using the *Boc* riboprobe showed that, as early as 2 dpl, *Boc* was upregulated not only at the site of LPC injection, but also in the ipsilateral SVZ compared with the contralateral hemisphere (Fig. 7A,B). Co-immunolabelling of the slices with the Olig2 marker indicated that some *Boc*$^+$ cells co-expressed Olig2 both in the lesion and in the SVZ (Fig. 7C), suggesting that, besides the reduced proliferation of OPCs shown above, OPC migration from

Development (2019) 146, dev172502. doi:10.1242/dev.172502

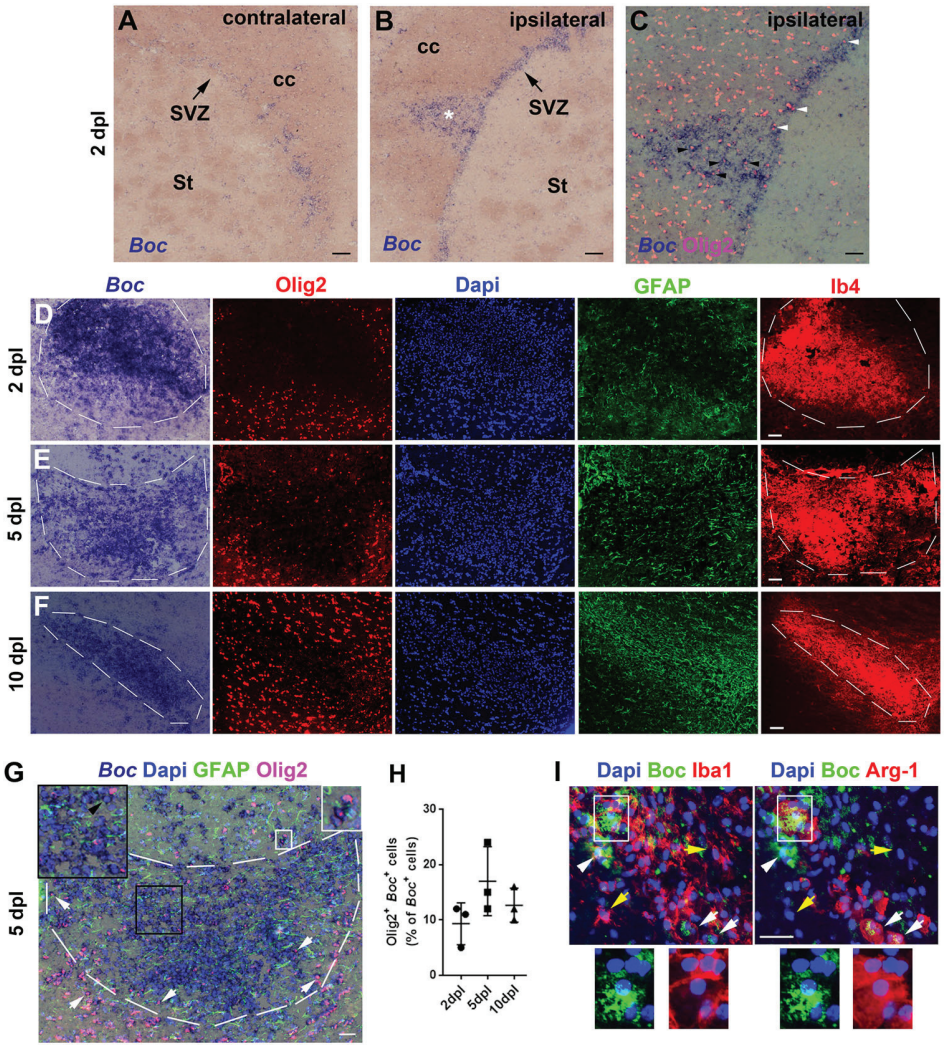

Fig. 7. Boc is highly upregulated upon focal demyelination of the corpus callosum. (A-C) *In situ* hybridization of slices derived from wild-type animals 2 days after LPC injection. *Boc* transcription is detected at a low level in the contralateral SVZ (A) and clearly upregulated in the ipsilateral side in the SVZ and the corpus callosum at a level corresponding to the LPC injection site (white star, B). (C) Immunostaining using the Olig2 antibody shows that most Olig2$^+$ cells arising from the SVZ (white arrowheads) or already recruited into the lesion (black arrowheads) co-express *Boc*. (D-F) *In situ* hybridization and double immunolabelling using the Olig2 and GFAP markers performed on the same slice derived from animals at 2 (D), 5 (E) and 10 (F) dpl. Ib4 staining was performed on the consecutive slice at each time point. The highest level of *Boc* is observed in the centre of the lesion in which Ib4$^+$ microglia and/or macrophages are the most abundant. The dashed lines outline the lesion area. (G,H) At 5 dpl, the merged images indicate the presence of *Boc*$^+$ cells co-expressing the Olig2 marker (white arrows and white box in G) and the vast majority of cells co-expressing neither Olig2 nor GFAP (black arrowhead in the black inset in G). Only a tiny number of GFAP$^+$ cell bodies colocalize with *Boc*$^+$ staining (not shown). The quantification of *Boc*$^+$ Olig2$^+$ cells is shown in H. Data are mean±s.e.m. (I) Triple immunolabelling of a brain slice derived from an animal demyelinated via LPC injection into the corpus callosum at 5 dpl. Boc signal is observed in Iba1$^+$ cells (white arrowheads) as well as in Iba1$^+$ Arg-1$^+$ (white arrows and boxed area) cells. Bottom panels are magnifications of the boxed area. The yellow arrows indicate Iba1$^+$ Boc$^-$ microglia and/or macrophages. Scale bars: 100 µm in A,B,D-F; 50 µm in C,G,I.

the SVZ towards the lesion might also be impaired in the mutant. However, the hypothesis remains to be investigated. Our previous work has shown that, in the lesion of wild-type animals, the *Gli1* effector was upregulated at a much lower level than other components of Shh signalling, such as Smo (Ferent et al., 2013). Given the decrease of *Gli1* transcription in the healthy Boc mutant mice (present work), *Gli1* upregulation was barely detectable in the lesion of the Boc mutant (data not shown). In contrast, the visualization of *Boc* transcription at 2, 5 and 10 dpl clearly indicated that a high upregulation of *Boc* was maintained throughout the repair process. The immunodetection of the oligodendroglial (Olig2$^+$) and astroglial (GFAP$^+$) cells on the same section, and microglia and/or macrophage (Ib4$^+$) on an adjacent section showed a notable similarity between the *Boc* signal and the Ib4$^+$ microglia and/or macrophage staining (Fig. 7D-F). The analysis of the merged images for *Boc*$^+$ and Olig2$^+$ cells at each time point allowed the detection of *Boc*$^+$ cells co-expressing the Olig2 marker and corresponding to a small and non-significantly different proportion (9±3, 17±4 and 13±2% for 2, 5 and 10 dpl, respectively) of all Boc$^+$ cells (Fig. 7G,H). The co-expression of Boc and GFAP was even more restricted (Fig. 7G) and thus most *Boc*$^+$ cells appeared to be neither oligodendroglial nor astroglial cells. Therefore, many *Boc*$^+$ cells could be microglia or macrophages. In order to check such hypothesis, we performed triple immunolabelling of brain slices derived from LPC-demyelinated animals at 5 dpl by using Iba1 as a global marker of microglia and/or macrophages and Arg-1 as a

Development (2019) 146, dev172502. doi:10.1242/dev.172502

marker of microglia and/or macrophages displaying pro-regenerative activity (Miron et al., 2013). The images evidenced Boc$^+$ cells expressing Iba1 alone or together with Arg-1 (Fig. 7I). Together, these results indicate that the absence of Boc prevents myelin repair by impairing OPC recruitment/differentiation, and also results in discrete morphological differences in microglia and/or macrophages that are consistent with Boc expression in this cell type.

Boc expression is required for microglia and/or macrophage transition from a highly to a faintly ramified morphology

Under healthy conditions, the so-called 'resting' microglia and/or macrophages display highly dynamic processes continuously elongating and retracting to explore the tissue environment (Nimmerjahn et al., 2005). Upon recognition of inflammatory stimuli, microglia and/or macrophages can rapidly retract their processes in order to become more ameboid and therefore efficient mobile effector cells able to fulfil local immune-related functions (Kierdorf and Prinz, 2013). The morphological differences detected for microglia and/or macrophages in the *Boc* mutant upon LPC-mediated demyelination led us to investigate whether the presence or the absence of Boc could influence the morphological transition between highly and faintly ramified cells. We took advantage of live-imaging approaches (Hristovska and Pascual, 2015) to visualize microglia and/or macrophages in the context of myelin repair in living animals. We crossed the *Boc* mutant mice with a strain expressing the YFP reporter under the promoter of the chemokine receptor CX3CR1, prominently expressed in microglia and/or macrophages (Wolf et al., 2013; Yona et al., 2013). Animals received the copper chelator cuprizone in their food for 12 weeks to induce an extensive demyelination of the cerebral cortex (Skripuletz et al., 2008; Gudi et al., 2009), as shown in Fig. 8A-C. Transcranial live-imaging of YFP$^+$ microglia and/or macrophages was carried out in the somatosensory cortex from both genotypes using two-photon microscopy. Animals were live-imaged on day 3 (D3) and day 8 (D8) after cuprizone removal from the diet while remyelination was already ongoing (Skripuletz et al., 2008; Gudi et al., 2009). On D3, microglia and/or macrophages appeared to be more ramified in *Boc* mutant mice compared with wild-type mice (Fig. 8D). Indeed, the cell processes were highly ramified in the mutant, similar to a resting phenotype, whereas they were retracted in the wild-type animals. In agreement with this observation, the quantification of processes complexity indicated a significantly higher value in *Boc* mutants compared with wild type (1.63±0.003 versus 1.57±0.013; P=0.05; Fig. 8E). Remarkably, the density of microglia and/or macrophages did not significantly differ with regards to the genotype or cuprizone treatment (Fig. 8F). Moreover, as already shown in the context of injury (Eyo et al., 2016), we visualized spontaneous focal events (SFE) corresponding to the attraction of microglia and/or macrophage processes within minutes at a focal point, followed by the subsequent invasion of the area by

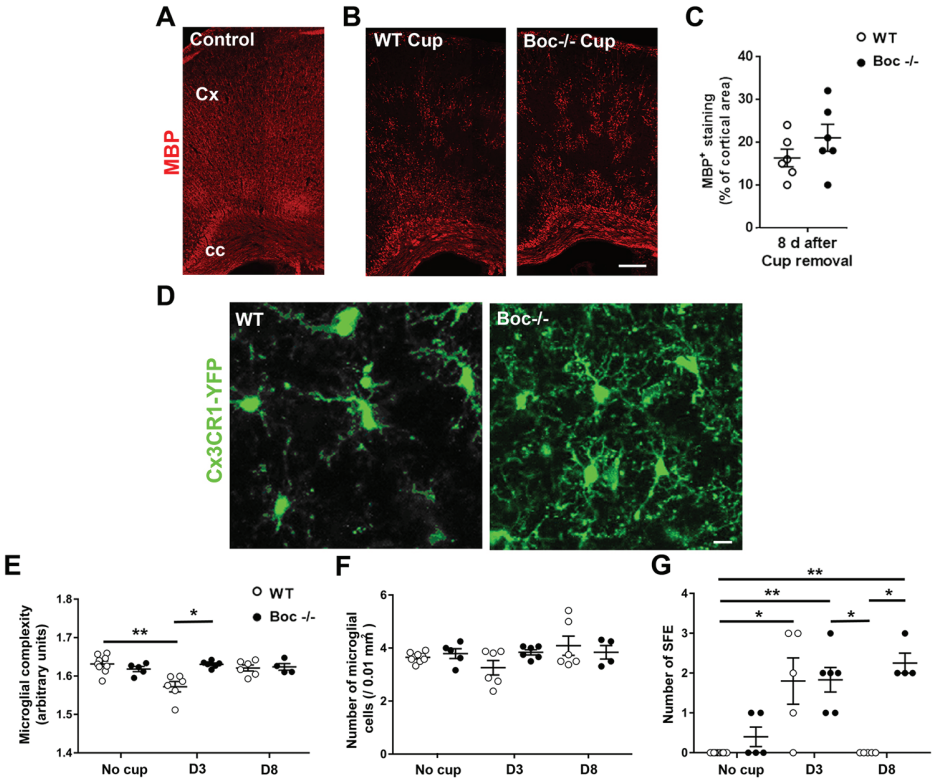

Fig. 8. Microglia and/or macrophages fail to switch from a resting-like to an activated-like state in the demyelinated cerebral cortex of the Boc mutant mice. (A) MBP immunostaining in the dorsal forebrain of a wild-type mouse (control). (B) MBP staining in wild-type and Boc mutant animals fed with cuprizone-supplemented (Cup) chow for 12 weeks and analysed 8 days after cuprizone removal. (C) Comparable levels of MBP immunofluorescence are observed, reflecting a similar extent of demyelination at this early time point after cuprizone removal. (D) Live images of CX3CR1-YFP microglia and/or macrophages in the cerebral cortex of wild-type and Boc mutant mice 3 days after cuprizone removal. (E,F) Quantification of the complexity of microglia and/or macrophages shows their inability to display the activated morphology observed for the wild-type cells 3 days after cuprizone removal (E). In contrast, the densities of cells are not significantly different under any conditions (F). (G) Quantification of the number of spontaneous focal events shows that, in the mutant, microglia and/or macrophage processes remain attracted towards focal events. Scale bars: 200 µm in B; 10 µm in D. Statistical analysis used Kruskal-Wallis and Dunn's multiple comparison test (E-G). *P<0.05; **P<0.01. Data are mean±s.e.m.

Development (2019) 146, dev172502. doi:10.1242/dev.172502

those processes (Movie 1). As expected, SFE could be detected in the cuprizone-treated wild-type and *Boc* mutant mice at D3. However, although SFE completely disappeared in the wild-type animals at D8, indicating a significant recovery, they were still detected in *Boc* mutants at this time point (P=0.05; Fig. 8G). Remarkably, in *Boc* mutant mice receiving a regular diet, some SFE could be detected, whereas they were completely absent from their wild-type counterparts. Together, these results indicate that, during myelin repair, *Boc* inactivation is associated with morphological differences in microglia and/or macrophages that mimic the transition between a 'resting-like' and an 'activated-like' state. In addition, *Boc* mutant mice display impaired responses in demyelinating conditions.

DISCUSSION

The investigation of *Boc* mutants performed in the present work provides evidence for the involvement of Boc in both developmental and repairing myelination. The first phenotypic feature observed in *Boc* mutants was the transient decrease in OPC production related to a reduced number of $Sox2^+$ neural progenitors and the decreased capacity of OPCs to proliferate. Together with the inability of *Boc* mutant glial cells to upregulate *Gli1 in vitro*, these data support the hypothesis that Boc may be positively involved in Shh-mediated dorsal oligodendrogenesis. Although questioned for a long time (Kessaris et al., 2006), Shh involvement in this process was recently demonstrated. Indeed, the neural progenitors located in the dorsal germinative zone of the forebrain are Shh-responding cells (Ahn and Joyner, 2005), which proliferate in a Shh-dependent manner (Balordi and Fishell, 2007) and give rise to oligodendroglial lineage cells at the neonatal period (Tong et al., 2015; Sanchez and Armstrong, 2018). However, whereas the conditional inactivation of the key transducer of Shh signalling, Smo, leads to a persistent oligodendrocyte decrease (Tong et al., 2015), *Boc* mutant mice display a rapid recovery of oligodendrocyte density. To account for this discrepancy, a first hypothesis relies on the existence of partially redundant functions of Boc with other Shh co-receptors, including Cdo and Gas1 as previously proposed in Shh-mediated proliferation of cerebellar progenitors (Izzi et al., 2011). This hypothesis is nevertheless unlikely because, if Cdo and/or Gas1 had redundant functions with Boc, the Boc-deficient glial cells should have upregulated *Gli1* in response to exogenous Shh. However, our data indicate no *Gli1* upregulation *in vitro*. Moreover, *Gli1* transcription is clearly downregulated in the early postnatal dorsal forebrain of the x*Boc* mutant. On the other hand, the recent report that Cdo promotes oligodendrocyte differentiation and myelination *in vitro* (Wang and Almazan, 2016) is not in support of a putative role for Cdo in oligodendroglial proliferation. A more plausible hypothesis could be the existence of compensatory mechanisms mediated by one of the other potent positive regulators of dorsal OPC production, such as Wnt or FGF (Azim et al., 2012, 2014, 2016; Ortega et al., 2013). If so, the absence of compensation observed upon conditional inactivation of *Smo* could be related to the experimental approach, based on the administration of an adenoviral vector at birth, which probably induced a massive and abrupt drop in oligodendrogenesis that may conceivably be more difficult to be compensated for.

Contrasting with its limited expression in cells of the oligodendroglial lineage, the wide expression of Boc in neurons is in support of a major neuronal function susceptible to indirectly influence myelination. In agreement with this hypothesis, Boc has initially been characterized as a member of the family of membrane-bound cell-adhesion molecules that provide axon-derived instructive cues for myelination (Emery, 2010; Hughes and Appel, 2016; Klingseisen and Lyons, 2018). Therefore, we tested the Src-family tyrosine kinase (SFK) Fyn (data not shown) as the most well-known integrator of neuronal signals during active myelination and notably for its role in the site-specific translation of MBP (White et al., 2008; White and Kramer-Albers, 2014). Although we were unable to detect any modification in SFK phosphorylation that might support the involvement of neuronal Boc-mediated signals in the spatiotemporal regulation of MBP production, we cannot exclude the possibility that Boc may mediate such a signal via a signalling cascade different from Fyn. However, our work importantly shows that the absence of functional Boc results in a clear reduction in the calibre of callosal axons and in a significant decrease in the neurofilament NF-M. The former observation is able to account for the persistence of a lower production of MBP given that small calibre axons require less MBP for their ensheathment by myelin. The latter deserves to be considered in the molecular mechanism possibly contributing to the defective radial growth of callosal axons. Remarkably, the decrease in NF-M is consistent with the role of Boc in neurite outgrowth previously reported in cultures of cortical neural progenitor cells. Indeed, the induction of Boc expression in those cells was found to specifically induce a high NF-M expression (Vuong et al., 2017). The role of NF-M in the radial growth of both large (>2 µm) and small (<2 µm) classes of myelinated fibres has been thoroughly investigated mainly in the peripheral nervous system where this process is necessary for the rapid impulse transmission in axons with a diameter over 1 µm (Eyer and Peterson, 1994; Garcia et al., 2003; Barry et al., 2012; Yuan and Nixon, 2016). Therefore, although further work is required to demonstrate a potential link between the altered radial growth of the callosal axons and the decreased expression of the neurofilament NF-M, both phenotypic features are likely to impair the fine tuning of postnatal active myelination in the absence of functional Boc.

In the context of demyelination, the Boc phenotype on cells of the oligodendroglial lineage is reminiscent of the phenotype previously reported when Shh signalling is inhibited (Ferent et al., 2013), as shown by the delay of OPC recruitment into the lesion, the decrease in the proliferation of these cells and the defect in their differentiation into immature oligodendrocytes. In contrast, *Boc* mutants do not phenocopy Shh signalling blockade at the level of astrocytes, microglia and/or macrophages (Ferent et al., 2013) because those cells were not increased in the *Boc* mutants. Moreover, the fact that the mutant fails to reach the level of myelin regeneration observed in the control animals was surprising given the apparent inability of Boc to regulate OPC differentiation during development. However, the unexpected consequences of non-functional Boc on microglia and/or macrophages provide an answer to these discordant observations. The high upregulation of Boc in an area encompassing the region populated by activated microglia and/or macrophages, most importantly the colocalization of Boc with one of the markers of pro-regenerative microglia and/or macrophages, as well as the inability of the mutant microglia and/or macrophages to retract their processes both support the hypothesis that OPC differentiation failure in the mutant may likely be related to defective microglia and/or macrophage activation. Consistently, during the past few years, a plethora of evidence have highlighted the pro-remyelination roles of microglia and/or macrophages, notably in the clearance of myelin debris, the secretion of growth factors or the remodelling of the extracellular matrix in myelin repair (Lloyd et al., 2017). Therefore, it is conceivable that the behavioural anomalies of microglia and/or macrophages observed in *Boc*

Development (2019) 146, dev172502. doi:10.1242/dev.172502

mutants disturb the ability of these cells to play their pro-remyelinating role, by altering microglia and/or macrophage reactive state (Kotter et al., 2006; Miron et al., 2013; Orihuela et al., 2016; Ransohoff, 2016; Church et al., 2017). Moreover, the recent observation that the dynamic state of the actin cytoskeleton profoundly affects microglia and/or macrophage behaviour (Uhlemann et al., 2016) might open the way to further investigations regarding a potential relationship between Boc and cell cytoskeletal dynamics in microglia and/or macrophages.

The recent identification of *Boc* variants in individuals with holoprosencephaly and the characterization of *Boc* as a modifier locus in this pathology, which is the most common malformation of the forebrain in humans, pinpoint Boc as a new therapeutic target (Roessler and Muenke, 2010; Hong et al., 2017). Given the accurate tuning of CNS myelination according to a precise spatiotemporal pattern, which coincides with the appearance of cognitive and behavioural functions (Nagy et al., 2004; Fields, 2008; Dean et al., 2016; Poggi et al., 2016), the delayed myelination, together with the reduction in axon calibre, may likely be associated with potential cortical dysfunctions in the absence of functional Boc. Moreover, Boc variants in individuals presenting with a demyelinating disease should be considered in the therapeutic strategy used, in particular when the Shh pathway is known to contribute to the remyelinating effects of the selected treatment, as recently shown for the drug Fingolimod (Zhang et al., 2015).

MATERIALS AND METHODS

Animals

The *Boc* knockout mouse strain (Okada et al., 2006) was obtained and maintained on a C57BL/6 background. The mouse strain *CX3CR1tm2.1(Cre/ERT2)* (thereafter called *CX3CR1^{CreER}-YFP*) expressing the YFP reporter under the promoter of the chemokine receptor CX3CR1 (Wolf et al., 2013; Yona et al., 2013) was provided by the Jackson Laboratory. Surgeries and perfusions were performed under ketamine (100 mg/kg)/xylazine (10 mg/kg)-induced anaesthesia. Two-month-old male animals were used unless otherwise indicated. The number of animals is indicated in each graph as the data obtained for each animal are shown. All animal studies were carried out according to the guidelines established by the European Communities Council Directive (86/806/EEC) for the care and use of laboratory animals. All experimental and surgical protocols were approved by the Regional Ethics Committee CEEA26, Ministère de L'Education Nationale, de l'Enseignement Supérieur et de la Recherche. Animals were housed under standard conditions with access to water and food *ad libitum* on a normal 12 h light/dark cycle.

LPC-induced focal demyelination

The lysolecithin (LPC)-induced demyelination was carried out as previously described (Ferent et al., 2013). The injection was performed at the following coordinates (to the bregma): anteroposterior (AP) +1 mm, lateral +1 mm, dorsoventral (DV) −2.2 mm. Mice were sacrificed at different survival time points: 2, 5, 10, 15, 21 and 30 days postlesion (dpl). The brain was removed, frozen in liquid nitrogen and cryostat sections (14 µm) were cut.

Cuprizone-induced demyelination

Boc$^{-/-}$;CX3CR1^{CreER}-YFP male animals were placed on a diet containing 0.2% cuprizone (Sigma-Aldrich) mixed into powdered food. The food was available *ad libitum* for 12 weeks and replaced every 2 days.

Primary glial cell cultures

Primary glial cell cultures were prepared from postnatal day (P) 1-2 mouse dorsal forebrain derived from each genotype as previously described (Feutz et al., 2001). Cultures containing astrocytes, oligodendrocytes and microglia cells were then incubated in 5% CO_2 and 95% air in a humidified atmosphere (90%) at 37°C. After 5 DIV, the medium was replaced by fresh medium supplemented or not with the recombinant Shh protein [4 nM; Shh (C24II) N-Terminus, BioTechne; 4 nM] or SAG (DC Chemicals; 3×10^{-7} M) which was renewed at 7 DIV. At 9 DIV, the cells were either collected in Trizol reagent for RNA extraction and quantitative RT-PCR analysis or incubated for 2 h with BrdU (3 µg/ml) before PFA 4% fixation for immunocytofluorescence. For enriched oligodendrocyte cultures, shaking of the flasks containing the primary mixed glial cells was carried out at 9 DIV in order to detach the oligodendroglial cells that were further cultured for 3 or 5 additional DIV in an oligodendrocyte medium as described previously (O'Meara et al., 2011). The number of independent cultures is indicated in each graph in which the data obtained from each culture is individually represented.

Histological procedures

The animals were deeply anesthetized before perfusion with 4% paraformaldehyde (PFA). Brains were post-fixed in 4% PFA for 4 h and incubated overnight in a 30% sucrose solution. Hemispheres were then frozen into a Shandon Cryomatrix and stored at −80°C before performing cryostat sections (14 µm). For immunohistochemistry the primary antibodies were as follows: anti-Boc (goat polyclonal, R&D, AF2385, 1:100; Izzi et al., 2011), anti-NeuN (mouse monoclonal, Millipore, MAB377, 1:500; Ferent et al., 2014), anti-Sox2 (goat polyclonal, Santa Cruz, sc-17320, 1:500), anti-Olig2 (rabbit polyclonal, Millipore, AB9610, 1:500; mouse monoclonal, Millipore, MABN50, 1:200; Ferent et al., 2013), anti-PDGFRa (rat; BD Pharmingen, 558774, 1:500; Ferent et al., 2013), anti-myelin basic protein (MBP) (rabbit polyclonal, Millipore, AB980, 1:500; Ferent et al., 2013), anti-adenomatus polyposis coli (APC/CC1) (mouse monoclonal, Calbiochem, OP80, 1:250; Ferent et al., 2013), anti-Ki67 (mouse monoclonal; BD Pharmingen, 550609, 1:100; Ferent et al., 2013), anti-BrdU antibody (rat monoclonal, Abcam, Ab6326, 1:250; Ferent et al., 2013), anti-glial fibrillary acidic protein (GFAP) (rabbit polyclonal, Dako, ZO334, 1:1000; mouse monoclonal, Sigma-Aldrich, G3893, 1:1000; Ferent et al., 2013), Iba1 (rabbit, Wako, W1W019-19741, 1:250), isolectin GS-IB4 conjugated to Alexa Fluor 568 (Thermo Fisher Scientific, I21412, 1:250; Ferent et al., 2013), arginase 1 (goat, Santa-Cruz, sc-18355, 1:100), CNPase (mouse, Sigma-Aldrich, 11-5B, 1:500), PLP (mouse, Millipore, Mab388, 1:250). The secondary antibodies were: donkey anti-goat Alexa 488, anti-mouse 647 and anti-rabbit 546 (Thermo Fisher Scientific, A11055, 1:250; A31571, 1:750; A10040, 1:250); goat anti-rabbit cyanine 3 conjugated (Jackson Immunoresearch, 111-165-003, 1:250); goat anti-mouse Alexa 488 and anti-rabbit Alexa 633 (Thermo Fisher Scientific, A11026, 1:250 and A21070, 1:750).

In situ hybridization experiments were performed as previously described (Ferent et al., 2013). The *Boc* riboprobe was kindly provided by Dr R.S. Krauss (Mount Sinai, New York, USA).

Image acquisition and analysis

Images were taken using the microscope analysing system Axiovision 4.2 (Carl Zeiss), the confocal Zeiss LSM 510-Meta Confocor 2, Leica TCS SP8 with LAS AF software and slide scanner Model Panoramic 250 Flash II 3DHISTECH with CaseViewer software. Analyses were performed using ImageJ software. Immunofluorescent-positive cells were counted in one sitting for every other five sections throughout the whole demyelinated lesion per mouse and averaged for each animal. Cell counts are the results from at least three animals (the exact number is indicated in each graph) or three independent cultures and are expressed per surface unit. Alternatively, the area occupied by marker immunofluorescence is expressed as percentage of the studied area. The lesion surface was determined by measuring the area of the nuclear densification or the absence of small cell chains (correlated with myelin loss visualized by MBP staining) on every other five slices throughout the whole demyelinated lesion per mouse.

Electron microscopy

Three 12-week-old male mice per genotype were perfused with 2% PFA and 2% glutaraldehyde. Ultrathin slices of resin-embedded osmium post-fixed corpus callosum (related to the genu part) were examined using a transmission electron microscope (1011 JEOL) equipped with a Gatan digital camera. The g ratio (the ratio between the axon diameter and fibre diameter corresponding to myelin sheath+axon diameter) was estimated by measuring the minimum and maximum axon diameter and fibre diameter for each axon using ImageJ software. At least 50 randomly chosen myelinated axons were evaluated for each animal.

RT-qPCR analysis

Three animals per group were sacrificed by decapitation. Brains were dissected and frozen in liquid nitrogen for further processing. Total RNA was isolated by using the Trizol Technique (Thermo Fisher Scientific) and RNeasy Mini Kit (Qiagen). For the primary glial cell cultures, the cells were directly collected in Trizol reagent. Reverse transcription was performed using the High Capacity cDNA Reverse Transcription kit (Applied Biosystems). Quantitative real-time PCR was carried out by using the Power SYBR-Green Master mix (Applied Biosystems) and gene expression was analysed with the 7300 Systems SDS Software (Applied Biosystems) normalized to reference genes GAPDH. The primers used were as follows: GAPDH fwd, 5′-GTCGGTGTGAACGGATTTGG-3′; GAPDH rev, 5′-GACTCCACGACATACTCAGC-3′; Olig2 fwd, 5′-GCAGCGAGCACCTCAAATCT-3′; Olig2 rev, 5′-GGGATGATCTAAGCTCTCGAATG-3′; Gli1 fwd, 5′-ACAAGTGCACGTTTGAAGGCTGTC-3′; Gli rev, 5′-GCTGCAACCTTCTTGCTCACACAT-3′.

Western blotting

Tissues were homogenized in cold RIPA lysis buffer (Biorad) in the presence of protease inhibitors (Sigma-Aldrich). The protein extract concentration was measured using the BCA method (Thermo Fisher Scientific). Proteins (30 µg) were separated using a 12% polyacrylamide gel followed by blotting onto a PVDF membrane using the trans-blot Turbo Transfer Pack (Biorad). Blots were incubated with the following antibodies: anti-MBP (rabbit, Millipore, Mab386), anti-gelsolin (rabbit, Abcam; Zuchero et al., 2015), anti-NF-M (mouse, Abcam, Ab7794) and anti-β-actin (mouse, Sigma-Aldrich; Ferent et al., 2014). Goat anti-mouse- and anti-rabbit Dylight-conjugated secondary antibodies were used (Thermo Fisher Scientific) and membranes were scanned with the Odyssey InfraRed Scanner (Li-Cor). Bands of interest were quantified by measuring their integrated intensities using the Odyssey software V3.0. Alternatively, goat anti-rabbit or anti-mouse horseradish peroxydase (Biorad) were used and immunoreactivity was revealed with enhanced chemiluminescence. The membranes were exposed to the chemiluminescent substrate Radiance Plus (Biorad) according to the manufacturer's instructions and then quantified using the Bio-Rad ChemiDoc MP Imaging System (Biorad). The densitometric values were systematically normalized to β-actin expression.

Two-photon *in vivo* imaging

For transcranial imaging, we performed thin-skull window preparation over the somatosensory cortex. Briefly, mice were deeply anesthetized with isoflurane (3-4%, Isovet, Piramal Healthcare) and mounted in a stereotaxic apparatus (D. Kopf Instruments). Carprofen (5 mg/kg s.c.) was injected at the beginning of the surgery to diminish post-surgical pain and inflammation. After the skull was exposed, a thin custom-made metal implant was glued, allowing delimitation of the area over the somatosensory cortex. The skull was then carefully thinned using a high-speed dental drill. To avoid heat-induced damage, we repeatedly interrupted drilling and applied cold sterile saline. When a 20 to 30 µm skull thickness was reached, we applied a thin layer of cyanoacrylate glue and placed a cover glass on top of the thinned skull. Mice were imaged on the 2nd and 7th post-operatory days, which are respectively the 3rd and 8th day of the end of cuprizone treatment. These two time points represent early remyelination and a more advanced remyelination. For each imaging session, mice were anesthetized with a mixture of ketamine (100 mg/kg) and xylazine (10 mg/kg), and their body temperature was maintained at 37°C. Imaging was performed using a two-photon microscope (Olympus) with a Ti:Sapphire laser (Mai-Tai, Spectra-Physics) tuned to 940 nm. We used a 20× water-immersion objective (0.95 N.A. Olympus) to acquire images and maintained the laser power below 30 mW. Fluorescence was detected using a 560 nm dichroic mirror coupled to a 525/50 nm emission filter and a photomultiplier tube in whole-field detection mode. We imaged microglia and/or macrophages at a depth of 50-150 µm. Every 30 s we acquired 30-35 consecutive stack images with a step size of 1 µm/optical section over an area of 200×200 µm and a resolution of 521×521 pixels. Recordings generally lasted 10-15 min (20-30 stacks).

Live imaging analysis

Image processing and analysis were performed using custom-written program under MatLab and ImageJ software. Regions of interest containing the totality of one microglia and/or one macrophage were delimited manually. Brightness/contrast and drift correction in x, y and z planes of images were adjusted by an automated post-processing. Drift correction was performed by registering each volume to a reference volume (the first volume) using shift estimation from the cross-correlation peak by FFT (fast Fourier transform). After realignment, 2D time-lapse movies were generated from standard deviation intensity projections of z-stacks. To quantitatively measure cell complexity, the images were first converted into binary. The cell complexity index was obtained by assessing the fractal dimension of the cell by calculating the Hausdorff dimension using a custom-written MatLab program. For each cell, the cell complexity index corresponded to the complexity value obtained at the beginning of the recording (t0). We identified spontaneous microglia and/or macrophage process convergence as events during which processes from one or (more frequently) several cells converged toward a focal point. All observed spontaneous microglia and/or macrophage process convergence events, regardless of size, were manually counted in a 200×200×30 µm visual field from all our recordings. Microglia and/or macrophage density was manually counted by marking each cell body in the visual field. The total number of microglia and/or macrophages was then divided to generate a measure of cell density for 10^4 µm^2.

Statistical analysis

Size sample was defined on the basis of our previous experiments. For cell counts, the mean number of immunopositive cells was evaluated per image area to determine the density of cells/surface area. Mice were allocated into experimental groups based on their genotype. Data analysis was carried out blind to the genotype of the mice. Data are expressed as mean±s.e.m. Statistical analysis was performed with GraphPad Prism 7.0 software. The significance of differences between means was evaluated using Student's unpaired t-test for two independent group comparisons and ANOVA followed by ad hoc post-tests for comparisons of more than two groups and/or several variables. In case of absence of distribution normality, non-parametric tests (Mann–Whitney, Kruskal-Wallis) were used. Appropriate corrections were carried out according to the determination of the variance of each sample. Dixon's Q test was used to identify potential outliers. Significance of $P<0.05$ was used for all analyses.

Acknowledgements

We thank Prof. Dr Leda Dimou for preliminary discussions regarding this work, Olivier Trassard and Alain Schmitt for technical assistance in imaging and transmission electron microscopy, respectively.

Competing interests

The authors declare no competing or financial interests.

Author contributions

Conceptualization: J.F., E.T.; Methodology: M.Z., J.F., I.H., Y.L., A.Z., A.K., O.P., E.T.; Validation: O.P., E.T.; Formal analysis: M.Z., I.H., Y.L., O.P., E.T.; Investigation: M.Z., J.F., I.H., Y.L., A.Z., A.K., M.-E.M.; Data curation: O.P., E.T.; Writing - original draft: E.T.; Writing - review & editing: J.F., O.P., F.C., E.T.; Visualization: M.Z., I.H., Y.L., A.Z., A.K.; Supervision: E.T.; Project administration: E.T.; Funding acquisition: E.T.

Funding

This work was supported by the Fondation pour l'Aide à la Recherche sur la Sclérose en Plaques (RAK14147LLA and RAK17128LLA to E.T.) and the Agence Nationale de la Recherche (RPV15198LLA to E.T.). M.Z. was the recipient of a PhD student fellowship from the Ministère de l'Enseignement Supérieur et de la Recherche.

Supplementary information

Supplementary information available online at
http://dev.biologists.org/lookup/doi/10.1242/dev.172502.supplemental

References

Ahn, S. and Joyner, A. L. (2005). In vivo analysis of quiescent adult neural stem cells responding to Sonic hedgehog. *Nature* **437**, 894-897. doi:10.1038/nature03994

Allen, B. L., Song, J. Y., Izzi, L., Althaus, I. W., Kang, J.-S., Charron, F., Krauss, R. S. and McMahon, A. P. (2011). Overlapping roles and collective requirement for the coreceptors GAS1, CDO, and BOC in SHH pathway function. *Dev. Cell* **20**, 775-787. doi:10.1016/j.devcel.2011.04.018

Azim, K., Raineteau, O. and Butt, A. M. (2012). Intraventricular injection of FGF-2 promotes generation of oligodendrocyte-lineage cells in the postnatal and adult forebrain. *Glia* **60**, 1977-1990. doi:10.1002/glia.22413

Azim, K., Rivera, A., Raineteau, O. and Butt, A. M. (2014). GSK3beta regulates oligodendrogenesis in the dorsal microdomain of the subventricular zone via Wnt-beta-catenin signaling. *Glia* **62**, 778-779. doi:10.1002/glia.22641

Azim, K., Berninger, B. and Raineteau, O. (2016). Mosaic subventricular origins of forebrain oligodendrogenesis. *Front. Neurosci.* **10**, 107. doi:10.3389/fnins.2016.00107

Balordi, F. and Fishell, G. (2007). Hedgehog signaling in the subventricular zone is required for both the maintenance of stem cells and the migration of newborn neurons. *J. Neurosci.* **27**, 5936-5947. doi:10.1523/JNEUROSCI.1040-07.2007

Barry, D. M., Stevenson, W., Bober, B. G., Wiese, P. J., Dale, J. M., Barry, G. S., Byers, N. S., Strope, J. D., Chang, R., Schulz, D. J. et al. (2012). Expansion of neurofilament medium C terminus increases axonal diameter independent of increases in conduction velocity or myelin thickness. *J. Neurosci.* **32**, 6209-6219. doi:10.1523/JNEUROSCI.0647-12.2012

Church, J. S., Milich, L. M., Lerch, J. K., Popovich, P. G. and McTigue, D. M. (2017). E6020, a synthetic TLR4 agonist, accelerates myelin debris clearance, Schwann cell infiltration, and remyelination in the rat spinal cord. *Glia* **65**, 883-899. doi:10.1002/glia.23132

Dai, J., Bercury, K. K., Ahrendsen, J. T. and Macklin, W. B. (2015). Olig1 function is required for oligodendrocyte differentiation in the mouse brain. *J. Neurosci.* **35**, 4386-4402. doi:10.1523/JNEUROSCI.4962-14.2015

Dean, D. C., III, O'Muircheartaigh, J., Dirks, H., Travers, B. G., Adluru, N., Alexander, A. L. and Deoni, S. C. (2016). Mapping an index of the myelin g-ratio in infants using magnetic resonance imaging. *Neuroimage* **132**: 225-237. doi:10.1016/j.neuroimage.2016.02.040

Ellis, P., Fagan, B. M., Magness, S. T., Hutton, S., Taranova, O., Hayashi, S., McMahon, A., Rao, M. and Pevny, L. (2004). SOX2, a persistent marker for multipotential neural stem cells derived from embryonic stem cells, the embryo or the adult. *Dev. Neurosci.* **26**, 148-165. doi:10.1159/000082134

Emery, B. (2010). Regulation of oligodendrocyte differentiation and myelination. *Science* **330**, 779-782. doi:10.1126/science.1190927

Eyer, J. and Peterson, A. (1994). Neurofilament-deficient axons and perikaryal aggregates in viable transgenic mice expressing a neurofilament-beta-galactosidase fusion protein. *Neuron* **12**, 389-405. doi:10.1016/0896-6273(94)90280-1

Eyo, U. B., Peng, J., Murugan, M., Mo, M., Lalani, A., Xie, P., Xu, P., Margolis, D. J. and Wu, L. J. (2016). Regulation of physical microglia-neuron interactions by fractalkine signaling after status epilepticus. *eNeuro* **3**, 1-14. ENEURO.0209-16.2016. doi:10.1523/ENEURO.0209-16.2016

Fabre, P. J., Shimogori, T. and Charron, F. (2010). Segregation of ipsilateral retinal ganglion cell axons at the optic chiasm requires the Shh receptor Boc. *J. Neurosci.* **30**, 266-275. doi:10.1523/JNEUROSCI.3778-09.2010

Ferent, J., Zimmer, C., Durbec, P., Ruat, M. and Traiffort, E. (2013). Sonic Hedgehog signaling is a positive oligodendrocyte regulator during demyelination. *J. Neurosci.* **33**, 1759-1772. doi:10.1523/JNEUROSCI.3334-12.2013

Ferent, J., Cochard, L., Faure, H., Taddei, M., Hahn, H., Ruat, M. and Traiffort, E. (2014). Genetic activation of Hedgehog signaling unbalances the rate of neural stem cell renewal by increasing symmetric divisions. *Stem Cell Rep.* **3**, 312-323. doi:10.1016/j.stemcr.2014.05.016

Feutz, A. C., Pham-Dinh, D., Allinquant, B., Miehe, M. and Ghandour, M. S. (2001). An immortalized jimpy oligodendrocyte cell line: defects in cell cycle and cAMP pathway. *Glia* **34**, 241-252. doi:10.1002/glia.1058

Fields, R. D. (2008). White matter in learning, cognition and psychiatric disorders. *Trends Neurosci.* **31**, 361-370. doi:10.1016/j.tins.2008.04.001

Franklin, R. J. M. and Ffrench-Constant, C. (2017). Regenerating CNS myelin - from mechanisms to experimental medicines. *Nat. Rev. Neurosci.* **18**, 753-769. doi:10.1038/nrn.2017.136

Garcia, M. L., Lobsiger, C. S., Shah, S. B., Deerinck, T. J., Crum, J., Young, D., Ward, C. M., Crawford, T. O., Gotow, T., Uchiyama, Y. et al. (2003). NF-M is an essential target for the myelin-directed "outside-in" signaling cascade that mediates radial axonal growth. *J. Cell Biol.* **163**, 1011-1020. doi:10.1083/jcb.200308159

Gibson, E. M., Purger, D., Mount, C. W., Goldstein, A. K., Lin, G. L., Wood, L. S., Inema, I., Miller, S. E., Bieri, G., Zuchero, J. B. et al. (2014). Neuronal activity promotes oligodendrogenesis and adaptive myelination in the mammalian brain. *Science* **344**, 1252304. doi:10.1126/science.1252304

Gudi, V., Moharregh-Khiabani, D., Skripuletz, T., Koutsoudaki, P. N., Kotsiari, A., Skuljec, J., Trebst, C. and Stangel, M. (2009). Regional differences between grey and white matter in cuprizone induced demyelination. *Brain Res.* **1283**, 127-138. doi:10.1016/j.brainres.2009.06.005

Harwell, C. C., Parker, P. R. L., Gee, S. M., Okada, A., McConnell, S. K., Kreitzer, A. C. and Kriegstein, A. R. (2012). Sonic hedgehog expression in corticofugal projection neurons directs cortical microcircuit formation. *Neuron* **73**, 1116-1126. doi:10.1016/j.neuron.2012.02.009

Hildebrand, C., Remahl, S., Persson, H. and Bjartmar, C. (1993). Myelinated nerve fibres in the CNS. *Prog. Neurobiol.* **40**, 319-384. doi:10.1016/0301-0082(93)90015-K

Hong, M., Srivastava, K., Kim, S., Allen, B. L., Leahy, D. J., Hu, P., Roessler, E., Krauss, R. S. and Muenke, M. (2017). BOC is a modifier gene in holoprosencephaly. *Hum. Mutat.* **38**, 1464-1470. doi:10.1002/humu.23286

Hristovska, I. and Pascual, O. (2015). Deciphering resting microglial morphology and process motility from a synaptic prospect. *Front. Integr. Neurosci.* **9**, 73. doi:10.3389/fnint.2015.00073

Hughes, E. G. and Appel, B. (2016). The cell biology of CNS myelination. *Curr. Opin. Neurobiol.* **39**, 93-100. doi:10.1016/j.conb.2016.04.013

Izzi, L., Lévesque, M., Morin, S., Laniel, D., Wilkes, B. C., Mille, F., Krauss, R. S., McMahon, A. P., Allen, B. L. and Charron, F. (2011). Boc and Gas1 each form distinct Shh receptor complexes with Ptch1 and are required for Shh-mediated cell proliferation. *Dev. Cell* **20**, 788-801. doi:10.1016/j.devcel.2011.04.017

Kang, J.-S., Mulieri, P. J., Hu, Y., Taliana, L. and Krauss, R. S. (2002). BOC, an Ig superfamily member, associates with CDO to positively regulate myogenic differentiation. *EMBO J.* **21**, 114-124. doi:10.1093/emboj/21.1.114

Kessaris, N., Fogarty, M., Iannarelli, P., Grist, M., Wegner, M. and Richardson, W. D. (2006). Competing waves of oligodendrocytes in the forebrain and postnatal elimination of an embryonic lineage. *Nat. Neurosci.* **9**, 173-179. doi:10.1038/nn1620

Kierdorf, K. and Prinz, M. (2013). Factors regulating microglia activation. *Front. Cell Neurosci.* **7**, 44. doi:10.3389/fncel.2013.00044

Kim, W. R., Chun, S. K., Kim, T. W., Kim, H., Ono, K., Takebayashi, H., Ikenaka, K., Oppenheim, R. W. and Sun, W. (2011). Evidence for the spontaneous production but massive programmed cell death of new neurons in the subcallosal zone of the postnatal mouse brain. *Eur. J. Neurosci.* **33**, 599-611. doi:10.1111/j.1460-9568.2010.07557.x

Klingseisen, A. and Lyons, D. A. (2018). Axonal regulation of central nervous system myelination: structure and function. *Neuroscientist* **24**, 7-21. doi:10.1177/1073858417703030

Kotter, M. R., Li, W. W., Zhao, C. and Franklin, R. J. (2006). Myelin impairs CNS remyelination by inhibiting oligodendrocyte precursor cell differentiation. *J. Neurosci.* **26**, 328-332. doi:10.1523/JNEUROSCI.2615-05.2006

Lloyd, A. F., Davies, C. L. and Miron, V. E. (2017). Microglia: origins, homeostasis, and roles in myelin repair. *Curr. Opin. Neurobiol.* **47**, 113-120. doi:10.1016/j.conb.2017.10.001

Lopez Juarez, A., He, D. and Richard Lu, Q. (2016). Oligodendrocyte progenitor programming and reprogramming: toward myelin regeneration. *Brain Res.* **1638**, 209-220. doi:10.1016/j.brainres.2015.10.051

McKenzie, I. A., Ohayon, D., Li, H., de Faria, J. P., Emery, B., Tohyama, K. and Richardson, W. D. (2014). Motor skill learning requires active central myelination. *Science* **346**, 318-322. doi:10.1126/science.1254960

Menn, B., Garcia-Verdugo, J. M., Yaschine, C., Gonzalez-Perez, O., Rowitch, D. and Alvarez-Buylla, A. (2006). Origin of oligodendrocytes in the subventricular zone of the adult brain. *J. Neurosci.* **26**, 7907-7918. doi:10.1523/JNEUROSCI.1299-06.2006

Miron, V. E., Boyd, A., Zhao, J. W., Yuen, T. J., Ruckh, J. M., Shadrach, J. L., van Wijngaarden, P., Wagers, A. J., Williams, A., Franklin, R. J. et al. (2013). M2 microglia and macrophages drive oligodendrocyte differentiation during CNS remyelination. *Nat. Neurosci.* **16**, 1211-1218. doi:10.1038/nn.3469

Nagy, Z., Westerberg, H. and Klingberg, T. (2004). Maturation of white matter is associated with the development of cognitive functions during childhood. *J. Cogn. Neurosci.* **16**, 1227-1233. doi:10.1162/0898929041920441

Naruse, M., Ishino, Y., Kumar, A., Ono, K., Takebayashi, H., Yamaguchi, M., Ishizaki, Y., Ikenaka, K. and Hitoshi, S. (2016). The dorsoventral boundary of the germinal zone is a specialized niche for the generation of cortical oligodendrocytes during a restricted temporal window. *Cereb. Cortex* **26**, 2800-2810. doi:10.1093/cercor/bhv141

Naruse, M., Ishizaki, Y., Ikenaka, K., Tanaka, A. and Hitoshi, S. (2017). Origin of oligodendrocytes in mammalian forebrains: a revised perspective. *J. Physiol. Sci.* **67**, 63-70. doi:10.1007/s12576-016-0479-7

Nimmerjahn, A., Kirchhoff, F. and Helmchen, F. (2005). Resting microglial cells are highly dynamic surveillants of brain parenchyma in vivo. *Science* **308**, 1314-1318. doi:10.1126/science.1110647

Okada, A., Charron, F., Morin, S., Shin, D. S., Wong, K., Fabre, P. J., Tessier-Lavigne, M. and McConnell, S. K. (2006). Boc is a receptor for sonic hedgehog in the guidance of commissural axons. *Nature* **444**, 369-373. doi:10.1038/nature05246

O'Meara, R. W., Ryan, S. D., Colognato, H. and Kothary, R. (2011). Derivation of enriched oligodendrocyte cultures and oligodendrocyte/neuron myelinating co-cultures from post-natal murine tissues. *J. Vis. Exp.* **54**, e3324. doi:10.3791/3324

Orihuela, R., McPherson, C. A. and Harry, G. J. (2016). Microglial M1/M2 polarization and metabolic states. *Br. J. Pharmacol.* **173**, 649-665. doi:10.1111/bph.13139

Ortega, F., Gascón, S., Masserdotti, G., Deshpande, A., Simon, C., Fischer, J., Dimou, L., Chichung Lie, D., Schroeder, T. and Berninger, B. (2013).

Oligodendrogliogenic and neurogenic adult subependymal zone neural stem cells constitute distinct lineages and exhibit differential responsiveness to Wnt signalling. *Nat. Cell Biol.* **15**, 602-613. doi:10.1038/ncb2736

Poggi, G., Boretius, S., Möbius, W., Moschny, N., Baudewig, J., Ruhwedel, T., Hassouna, I., Wieser, G. L., Werner, H. B., Goebbels, S. et al. (2016). Cortical network dysfunction caused by a subtle defect of myelination. *Glia* **64**, 2025-2040. doi:10.1002/glia.23039

Ransohoff, R. M. (2016). A polarizing question: do M1 and M2 microglia exist? *Nat. Neurosci.* **19**, 987-991. doi:10.1038/nn.4338

Roessler, E. and Muenke, M. (2010). The molecular genetics of holoprosencephaly. *Am. J. Med. Genet. C Semin. Med. Genet.* **154C**, 52-61. doi:10.1002/ajmg.c.30236

Samanta, J., Grund, E. M., Silva, H. M., Lafaille, J. J., Fishell, G. and Salzer, J. L. (2015). Inhibition of Gli1 mobilizes endogenous neural stem cells for remyelination. *Nature* **526**, 448-452. doi:10.1038/nature14957

Sanchez, M. A. and Armstrong, R. C. (2018). Postnatal Sonic hedgehog (Shh) responsive cells give rise to oligodendrocyte lineage cells during myelination and in adulthood contribute to remyelination. *Exp. Neurol.* **299**, 122-136. doi:10.1016/j.expneurol.2017.10.010

Sanchez-Arrones, L., Cardozo, M., Nieto-Lopez, F. and Bovolenta, P. (2012). Cdon and Boc: Two transmembrane proteins implicated in cell-cell communication. *Int. J. Biochem. Cell Biol.* **44**, 698-702. doi:10.1016/j.biocel.2012.01.019

Sanchez, M. A., Sullivan, G. M. and Armstrong, R. C. (2018). Genetic detection of Sonic hedgehog (Shh) expression and cellular response in the progression of acute through chronic demyelination and remyelination. *Neurobiol. Dis.* **115**, 145-156. doi:10.1016/j.nbd.2018.04.003

Seri, B., Herrera, D. G., Gritti, A., Ferron, S., Collado, L., Vescovi, A., Garcia-Verdugo, J. M. and Alvarez-Buylla, A. (2006). Composition and organization of the SCZ: a large germinal layer containing neural stem cells in the adult mammalian brain. *Cereb. Cortex* **16** Suppl. 1, i103-i111. doi:10.1093/cercor/bhk027

Skripuletz, T., Lindner, M., Kotsiari, A., Garde, N., Fokuhl, J., Linsmeier, F., Trebst, C. and Stangel, M. (2008). Cortical demyelination is prominent in the murine cuprizone model and is strain-dependent. *Am. J. Pathol.* **172**, 1053-1061. doi:10.2353/ajpath.2008.070850

Tenzen, T., Allen, B. L., Cole, F., Kang, J.-S., Krauss, R. S. and McMahon, A. P. (2006). The cell surface membrane proteins Cdo and Boc are components and targets of the Hedgehog signaling pathway and feedback network in mice. *Dev. Cell* **10**, 647-656. doi:10.1016/j.devcel.2006.04.004

Tomassy, G. S., Dershowitz, L. B. and Arlotta, P. (2016). Diversity matters: a revised guide to myelination. *Trends Cell Biol.* **26**, 135-147. doi:10.1016/j.tcb.2015.09.002

Tong, C. K., Fuentealba, L. C., Shah, J. K., Lindquist, R. A., Ihrie, R. A., Guinto, C. D., Rodas-Rodriguez, J. L. and Alvarez-Buylla, A. (2015). A dorsal SHH-dependent domain in the V-SVZ produces large numbers of oligodendroglial lineage cells in the postnatal brain. *Stem Cell Rep.* **5**, 461-470. doi:10.1016/j.stemcr.2015.08.013

Uhlemann, R., Gertz, K., Boehmerle, W., Schwarz, T., Nolte, C., Freyer, D., Kettenmann, H., Endres, M. and Kronenberg, G. (2016). Actin dynamics shape microglia effector functions. *Brain Struct. Funct.* **221**, 2717-2734. doi:10.1007/s00429-015-1067-y

Vuong, T. A., Leem, Y.-E., Kim, B.-G., Cho, H., Lee, S.-J., Bae, G.-U. and Kang, J.-S. (2017). A Sonic hedgehog coreceptor, BOC regulates neuronal differentiation and neurite outgrowth via interaction with ABL and JNK activation. *Cell. Signal.* **30**, 30-40. doi:10.1016/j.cellsig.2016.11.013

Wang, L. C. and Almazan, G. (2016). Cdon, a cell surface protein, mediates oligodendrocyte differentiation and myelination. *Glia* **64**, 1021-1033. doi:10.1002/glia.22980

White, R. and Krämer-Albers, E. M. (2014). Axon-glia interaction and membrane traffic in myelin formation. *Front. Cell. Neurosci.* **7**, 1-8. doi:10.3389/fncel.2013.00284

White, R., Gonsior, C., Krämer-Albers, E. M., Stöhr, N., Hüttelmaier, S. and Trotter, J. (2008). Activation of oligodendroglial Fyn kinase enhances translation of mRNAs transported in hnRNP A2-dependent RNA granules. *J. Cell Biol.* **181**, 579-586. doi:10.1083/jcb.200706164

Wolf, Y., Yona, S., Kim, K.-W. and Jung, S. (2013). Microglia, seen from the CX3CR1 angle. *Front. Cell Neurosci.* **7**, 26. doi:10.3389/fncel.2013.00026

Yam, P. T. and Charron, F. (2013). Signaling mechanisms of non-conventional axon guidance cues: the Shh, BMP and Wnt morphogens. *Curr. Opin. Neurobiol.* **23**, 965-973. doi:10.1016/j.conb.2013.09.002

Yona, S., Kim, K.-W., Wolf, Y., Mildner, A., Varol, D., Breker, M., Strauss-Ayali, D., Viukov, S., Guilliams, M., Misharin, A. et al. (2013). Fate mapping reveals origins and dynamics of monocytes and tissue macrophages under homeostasis. *Immunity* **38**, 79-91. doi:10.1016/j.immuni.2012.12.001

Young, K. M., Psachoulia, K., Tripathi, R. B., Dunn, S.-J., Cossell, L., Attwell, D., Tohyama, K. and Richardson, W. D. (2013). Oligodendrocyte dynamics in the healthy adult CNS: evidence for myelin remodeling. *Neuron* **77**, 873-885. doi:10.1016/j.neuron.2013.01.006

Yuan, A. and Nixon, R. A. (2016). Specialized roles of neurofilament proteins in synapses: Relevance to neuropsychiatric disorders. *Brain Res. Bull.* **126**, 334-346. doi:10.1016/j.brainresbull.2016.09.002

Zhang, J., Zhang, Z. G., Li, Y., Ding, X., Shang, X., Lu, M., Elias, S. B. and Chopp, M. (2015). Fingolimod treatment promotes proliferation and differentiation of oligodendrocyte progenitor cells in mice with experimental autoimmune encephalomyelitis. *Neurobiol. Dis.* **76**, 57-66. doi:10.1016/j.nbd.2015.01.006

Zuchero, J. B., Fu, M.-M., Sloan, S. A., Ibrahim, A., Olson, A., Zaremba, A., Dugas, J. C., Wienbar, S., Caprariello, A. V., Kantor, C. et al. (2015). CNS myelin wrapping is driven by actin disassembly. *Dev. Cell* **34**, 152-167. doi:10.1016/j.devcel.2015.06.011

REVIEW 1

Published in Frontiers in Integrative Neuroscience (2016)

Deciphering resting microglial morphology and process motility from a synaptic prospect

Ines Hristovska*[1], Olivier Pascual*[1]

1. Institut NeuroMyoGène, Université Claude Bernard Lyon 1, CNRS UMR 5310, INSERM U1217, Université Lyon, Villeurbanne 69100, France

frontiers in Integrative Neuroscience

MINI REVIEW
published: 19 January 2016
doi: 10.3389/fnint.2015.00073

Deciphering Resting Microglial Morphology and Process Motility from a Synaptic Prospect

Ines Hristovska[1,2] *and Olivier Pascual*[1,2]*

[1] INSERM U1028, CNRS UMR5292, Lyon Neuroscience Research Center, Lyon, France, [2] Université Claude Bernard Lyon 1, Lyon, France

Microglia, the resident immune cells of the central nervous system (CNS), were traditionally believed to be set into action only in case of injury or disease. Accordingly, microglia were assumed to be inactive or resting in the healthy brain. However, recent studies revealed that microglia carry out active tissue sampling in the intact brain by extending and retracting their ramified processes while periodically contacting synapses. Microglial morphology and motility as well as the frequency and duration of physical contacts with synaptic elements were found to be modulated by neuronal activity, sensory experience and neurotransmission; however findings have not been straightforward. Microglial cells are the most morphologically plastic element of the CNS. This unique feature confers them the possibility to locally sense activity, and to respond adequately by establishing synaptic contacts to regulate synaptic inputs by the secretion of signaling molecules. Indeed, microglial cells can hold new roles as critical players in maintaining brain homeostasis and regulating synaptic number, maturation and plasticity. For this reason, a better characterization of microglial cells and cues mediating neuron-to-microglia communication under physiological conditions may help advance our understanding of the microglial behavior and its regulation in the healthy brain. This review highlights recent findings on the instructive role of neuronal activity on microglial motility and microglia-synapse interactions, focusing on the main transmitters involved in this communication and including newly described communication at the tripartite synapse.

Keywords: microglia, motility, neuronal activity, ATP, glutamate

OPEN ACCESS

Edited by:
Ye Chen,
Naval Medical Research Center, USA

Reviewed by:
Alexej Verkhratsky,
The University of Manchester, UK
Marie-Eve Tremblay,
Université Laval, Canada
Jiu-lin Du,
Chinese Academy of Sciences, China

***Correspondence:**
Olivier Pascual
olivier.pascual@inserm.fr

Received: *28 October 2015*
Accepted: *21 December 2015*
Published: *19 January 2016*

Citation:
Hristovska I and Pascual O (2016) Deciphering Resting Microglial Morphology and Process Motility from a Synaptic Prospect. Front. Integr. Neurosci. 9:73. doi: 10.3389/fnint.2015.00073

INTRODUCTION

Microglia are the resident immunocompetent cells of the central nervous system (CNS) and they comprise around 5–12% of the glial cell population (Gomez-Nicola and Perry, 2015). Microglia emerge from two sources: erythromyeloid precursors of the embryonic yolk sac, and myeloid progenitors that invade the CNS and proliferate during embryonic and postnatal development (Ginhoux et al., 2013).

Considered as the resident immune cells of the brain, microglia have been mostly studied in immune and inflammatory contexts (Prinz and Priller, 2014). However, recent *in vivo* data indicate that under physiological conditions, microglial cells exhibit a highly ramified morphology characterized by motile processes that constantly monitor their immediate surrounding by extending and retracting their processes (Davalos et al., 2005; Nimmerjahn et al., 2005).

This constant movement of microglial processes while the soma remains stationary is called microglial motility (**Figure 1**). The unexpected finding of microglial process motility led scientists to enquire and identify new roles in the non-pathological brain (Kettenmann et al., 2013). Since then, microglia were shown to be involved in the phagocytosis of synaptic elements during the entire lifespan, and the formation of learning-dependent synapses in the mature brain, as well as maturation and plasticity of excitatory synapses (Tremblay et al., 2010; Paolicelli et al., 2011; Hoshiko et al., 2012; Schafer et al., 2012; Parkhurst et al., 2013). These functions require localized fine-tuning involving specialized cellular function to deliver targeted messages at individual synapses. This targeted delivery could be compatible with the rapid process motility described earlier. A growing body of evidence also suggests that process motility and the frequency and duration of physical contacts with synaptic elements are regulated by neuronal activity, sensory experience and neurotransmission. It is thus crucial to better understand the mechanisms guiding neuron-to-microglia communication to further comprehend microglial functions in a healthy brain. In this review, we synthetize the recent discoveries on the properties of microglia in physiological conditions. Then, we report findings on the instructive role of neuronal activity on microglial motility and microglia-synapse interactions. Finally, we describe the current understanding of the molecular mechanisms underlying these interactions.

MICROGLIA, HIGHLY MOTILE CELLS THAT CONTACT SYNAPSES

Until fairly recently, due to lack of proper tools to study the microglial cells in a healthy brain, these cells were believed to be immunologically quiescent and were qualified as resting/dormant under physiological conditions. Two pioneer studies using two-photon microscopy observation of microglial motility in the intact cortical micro-environment reversed the common belief that "resting" microglia in the healthy brain were morphologically static (Davalos et al., 2005; Nimmerjahn et al., 2005). They shifted the concept of microglia from "resting" to "surveying" (Hanisch and Kettenmann, 2007). Visualization of microglia was made possible by the development of $CX3CR1^{GFP}$ and $Iba1^{GFP}$ transgenic mice (Jung et al., 2000; Hirasawa et al., 2005). Small-shaped soma of microglial cells remained still overtime, with only 5% moving by 1–2 μm/h (Nimmerjahn et al., 2005). In contrast, microglial processes were morphologically plastic with considerable motility. They presented a similar rate of extension and retraction of around 1.47 μm/min (Nimmerjahn et al., 2005). These findings position microglial cells as the most dynamic CNS cells as no other cells display such morphological plasticity *in vivo*. The dynamism of microglial processes was also confirmed in the mouse spinal cord and retinal explants (Davalos et al., 2005; Lee et al., 2008) and in the zebrafish embryo (Peri and Nüsslein-Volhard, 2008).

These groundbreaking discoveries confirmed the morphological plasticity of microglial ramifications under physiological conditions in distinct CNS structures and species led scientists to envisage a possible contribution in neuronal physiology. Specific, direct and activity-dependent microglia-to-synaptic element contacts in the adult mouse visual and somatosensory cortex *in vivo* were thus demonstrated for the first time (Wake et al., 2009). Using $CX3CR1^{GFP}/Thy1^{YFP}$ mice, Tremblay et al. (2010) were able to distinguish microglial cells from neurons in the superficial layers of the developing mouse visual cortex at 4 weeks of age. Intriguingly, microglial processes made physical contacts especially with axon terminals and dendritic spines, but also with perisynaptic astrocytic processes and synaptic clefts. They preferentially localized

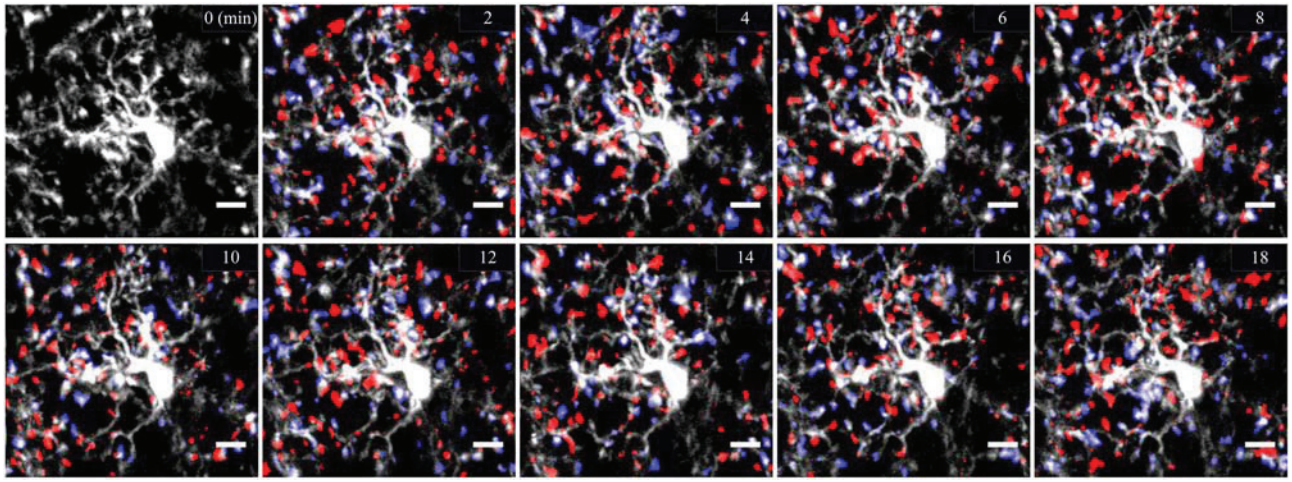

FIGURE 1 | Cortical two-photon imaging on awake mouse. Resting microglia are highly ramified and motile in the mouse cerebral cortex. Microglia are labeled by enhanced green fluorescent protein (eGFP) expressed under the control of microglial promoter CX3CR1. Microglial motility is shown by means of representative color-coded time-lapse images of a single microglial cell showing rapid process extensions (in blue) and retractions (in red) with a 2 min interval over the time course of 18 min. Scale bar = 10 μm.

at the proximity of small, more motile and more frequently eliminated dendritic spines rather than larger dendritic spines. Microglial distal processes enveloped dendritic spines by forming finger-like protrusions (Tremblay et al., 2010). Microglia-neuron contacts were brief and transient, at a frequency of one per hour (Wake et al., 2009), whereas in the developing visual cortex contacts varied in duration between 5 and 30 min (Tremblay et al., 2010). These data suggest that under physiological conditions *in vivo*, microglial processes are highly motile and make direct contacts with synaptic elements at regular frequencies during all stages of life.

MICROGLIAL MOTILITY IS MODULATED BY NEURONAL ACTIVITY

The discovery of the incessant dynamism of microglial processes and the transient contacts with synapses under physiological conditions led to new questions: are microglial processes specifically guided by neuronal activity and do they respond to the functional status of synapses? To investigate whether neuronal activity instructs microglial motility and contact with synaptic elements, global excitatory and inhibitory activity were modulated by pharmacological, physiological and genetic means. Initial results were rather negative. Silencing neuronal activity by applying tetrodotoxin (TTX) onto cortical surface *in vivo* had no impact on microglial motility (Nimmerjahn et al., 2005), as well as high frequency stimulation inducing long term potentiation (LTP) in acute hippocampal slices (Wu and Zhuo, 2008). Likewise, reduction of basal activity in the visual cortex *in vivo* by several independent approaches, including binocular eye enucleation, retinal TTX injection and reduction of body temperature, had no effect on basal velocity of microglial processes (Wake et al., 2009). However, with a simultaneous visualization of neurons and microglia, Wake et al. (2009), showed a reduced frequency of microglia-synapse contacts. Since this effect resulted from the aforementioned manipulations of neuronal activity, apart from TTX application, neuronal activity could at least modulate microglia-synapse interaction.

Using physiological approach by modulating sensory experience, Tremblay et al. (2010), studied neuronal activity-dependent microglial behavior in the developing mouse visual cortex. Mice were housed in dark conditions and thus deprived of visual experience during a critical period of development. During deprivation, average sampling and motility of microglial processes were significantly reduced, but the frequency and duration of microglia-synapse contacts remained unchanged. The synaptic target changed: microglia no longer localized next to small spines, but interacted preferentially with larger dendritic spines that subsequently shrank. Re-exposure to daylight restored microglial motility and contact with small dendritic spines.

Microglial motility and activity-dependent interactions with synaptic elements were also studied in the zebrafish optic tectum. By simultaneously monitoring GFP-labeled microglia and levels of spontaneous activity by Ca^{2+} imaging, Li et al. (2012) found that neurons with high level of spontaneous activity steer microglial processes, causing an increased contact frequency between these two elements. Conversely, reducing global activity by overexpressing human inward rectifier K+ channel (Kir2.1) in tectal neurons lowered the likelihood of physical contact (Hua et al., 2005). Visual stimuli increased the total number of bulbous endings, inferring microglia-neuron interaction, which were considerably reduced by TTX application (Li et al., 2012).

Overall, these findings suggest that under physiological conditions the motility of microglial processes and their interaction with synaptic elements can be modulated by neuronal activity.

NEUROTRANSMITTERS AND MECHANISMS AFFECTING MICROGLIAL MOTILITY

The molecular cues which maintain the movement of microglial processes and by which neuronal activity may signal to microglia are under investigation. A variety of classical neurotransmitter and neuromodulator receptors are expressed at the surface of microglia from culture assays, which in turn can cause changes in cytokine release, in membrane potential, cellular morphology and motility (Kettenmann et al., 2011). However, these *in vitro* preparations should be interpreted with caution because microglial phenotype resembles activated state (Ransohoff and Perry, 2009). Recent *in situ* studies indicate that microglia express functional purinergic receptors, whereas local application of other neurotransmitters did not elicit electrical responses, most probably reflecting lack of neurotransmitter receptors (Fontainhas et al., 2011).

ROLE OF PURINES

Adenosine triphosphate (ATP), a neurotransmitter of the CNS, has been identified as the key regulator of microglial morphology and baseline dynamics. Disruption of ATP-dependent signaling in the presence of ATP/ADP hydrolyzing enzyme apyrase decreased the basal motility of microglial processes (Davalos et al., 2005) while application of ATP increased basal motility and cell complexity (Fontainhas et al., 2011). ATP is also involved in directed microglial process outgrowth because focal applications of ATP caused a striking extension of microglial processes towards the source of ATP (Davalos et al., 2005; Dissing-Olesen et al., 2014) and process outgrowth persisted as long as ATP was applied (Dissing-Olesen et al., 2014). In addition, ATP critically mediated microglial process outgrowth towards sites of increased neuronal activity (Li et al., 2012; Eyo et al., 2014). Finally, the extension of microglial processes was found to be propelled by a cell autonomous release of ATP contained in lysosomes, serving ultimately as a motor for motility (Dou et al., 2012).

ATP acts at specific ionotropic (P2X) and metabotropic (P2Y) purinergic receptors that are largely distributed in neurons and glial cells. Initial studies *in vitro* showed that ATP signaling through P2YR induced microglial membrane ruffling (Honda et al., 2001), and that P2YR inhibition, but

not P2XR, affected the number and motility of microglial processes towards ablation site (Davalos et al., 2005). The requirement of P2R signaling for neuronal activity oriented motility and formation of bulbous contacts was also observed in the zebrafish optic tectum (Li et al., 2012). A major receptor candidate is P2Y12R, selectively expressed by microglia in the physiological brain. Following ATP release, the extension of microglial processes, but not basal motility, was critically dependent on the activation of P2Y12R, as shown by experiments performed on acute hippocampal slices from P2Y12 KO mice (Haynes et al., 2006; Eyo et al., 2014). P2Y12R accumulated at the tip of microglial processes during ATP-induced process outgrowth, along with Rho GTPase Rac, a key molecule in the cytoskeleton reorganization, whose downregulation abolished oriented microglial process movement in response to neuronal activity (Li et al., 2012; Dissing-Olesen et al., 2014).

Additional factors such as gradient formation and generation of ATP metabolites may be important in mediating motility. ATP is quickly catabolized to other purine molecules by ecto-nucleotidases in the extracellular space (Dunwiddie et al., 1997). Constant release of non-hydrolysable ATP in presence of apyrase was unable to attract microglial processes (Davalos et al., 2005). Furthermore, the contribution of ATP hydrolysis products seem to be critical because blocking ATP hydrolysis using selective ectonucleotidases inhibitor altered microglial outgrowth (Dissing-Olesen et al., 2014). When ATP and metabolites diffuse in the extracellular space and form a chemotactic gradient critical for microglial process outgrowth, their elimination reduced the extent and speed of microglial processes (Davalos et al., 2005). Adenosine seems to be a potential candidate for regulating microglial motility because high levels of adenosine receptors A1 and A3 are expressed on microglia in physiological conditions (Hammarberg et al., 2003) and an interplay of simultaneous purinergic stimulation of both A3 and P2Y12 receptors was found necessary for process outgrowth (Ohsawa et al., 2012). Adenosine was also involved in the retraction of microglial processes in the pathological brain due to signaling involving A2A receptors (Orr et al., 2009).

ATP appears to be released in an activity-dependent manner by neurons and astrocytes through hemichannels (pannexin and connexin), transporters and secretory vesicles (Burnstock, 2008). Studies reviewed below focus on ATP release from hemichannels, since this particular mode of communication has been predominantly investigated in relation to microglial motility. The precise distribution of the three pannexin subtypes (Panx1 to Panx3) between cell types and subcellular location has not been fully understood, but could partly account for discrepancies in the literature (Penuela et al., 2013). Initial studies found that probenecid, a non-selective pannexin channel antagonist, caused a general decrease in morphological parameters and basal velocity (Fontainhas et al., 2011). In the zebrafish optic tectum, glutamate uncaging-induced movement of microglial processes and the formation of bulbous endings were abolished using probenecid and more importantly, by specifically downregulating *pannexin-1* expression while keeping unchanged basal cell area and velocity (Li et al., 2012). Consequently, pannexin-1 emerged as the main hemichannel mediating ATP release and subsequently microglial outgrowth. However, a recent study found that during pannexin-1 blockage and in pannexin-1 deficient mice, microglial outgrowth following NMDAR activation in acute hippocampal slices was unaffected (Dissing-Olesen et al., 2014). This mechanism remained probenecid-dependent, raising possibilities for involvement of other pannexin channels mediating ATP efflux, such as pannexin-2 or prepackaged vesicles (Dissing-Olesen et al., 2014; Eyo et al., 2014).

Another important component affecting microglial dynamics could involve connexin hemichannels that mediate ATP released from astrocytes. They seem to be of particular importance for basal velocity of microglial processes *in vivo* because pharmacological blockade of connexins decreased it significantly (Davalos et al., 2005). However, fluoroacetate, an astrocytic function blocker, did not affect glutamate-induced microglial process extension (Eyo et al., 2014). In acute hippocampal slices, blocking connexin channels did not prevent NMDA-mediated microglial extension (Dissing-Olesen et al., 2014; Eyo et al., 2014). The discrepancy in these findings could be due to tissue specificity, microglia heterogeneity, *in vivo* and *ex vivo* preparation and the type and concentration of the pharmacological substances utilized.

These studies clearly demonstrate that purinergic signaling, in particular ATP and its derivates, are crucial for mediating microglial basal motility and neuronal activity-oriented motility. Further studies need to be performed to address the specific effects and contribution of purinergic molecules, as well as the exact downstream signaling pathways elicited in microglia.

ROLE OF GLUTAMATE AND GABA

Direct action of glutamate and γ-aminobutyric acid (GABA) neurotransmission on microglial morphology and motility was also investigated. Initial studies failed to demonstrate any effect of local application of glutamate and GABA on microglial motility. No change was provoked by enhancing neuronal activity with the application of GABA antagonist on the cortical surface (Nimmerjahn et al., 2005) or the application of glutamate and GABA on acute hippocampal slices and spinal cord dorsal horn (Wu and Zhuo, 2008; Chen et al., 2010). A more recent study found that glutamatergic and GABAergic neurotransmission modulated microglial morphology and motility in retinal explants, an *ex vivo* model with minimal CNS damage: GABA application decreased microglial motility, whereas bicuculline increased both the size and basal velocity of microglial processes (Fontainhas et al., 2011). Both agonist and antagonist of ionotropic glutamatergic receptors affected the size and motility of microglial processes mainly through fast AMPA/kainate receptors in retinal explants. This effect was mediated to a much lesser extent through NMDA receptors. Strangely, application of glutamate alone did not result in

any change of the above-mentioned parameters (Fontainhas et al., 2011). We must note that variations exist between brain areas. In the hippocampus, two recent studies used acute slices to show an important glutamate-induced microglial process outgrowth requiring NMDAR activation that was independent of AMPA/kainate receptor activation (Dissing-Olesen et al., 2014; Eyo et al., 2014). These differences between structures may attest for striking tissue-specific regulation of microglial motility through fast AMPA/kainate receptors in the retina and slow NMDA receptors in the hippocampus (**Figure 2**). Glutamate signaling also affected microglial motility in the zebrafish optic tectum. Glutamate uncaging, a noninvasive approach for upregulating neuronal activity, caused outgrowth of microglial processes towards the glutamate source as well as formation of bulbous endings (Li et al., 2012).

Studies have suggested that glutamate and GABA neurotransmission do not signal directly to microglial cells, but affect microglial motility and outgrowth by modulating extracellular levels of nucleotides, such as ATP and metabolites. Local application of glutamatergic or GABAergic agonists did not induce detectable electrophysiological responses in microglia. This is in agreement with the discovery that ionotropic glutamatergic receptors were not present on microglial processes and soma (Fontainhas et al., 2011; Eyo et al., 2014). On the contrary, ATP induced large inward currents in microglia and seems to be indeed implicated downstream glutamatergic transmission because reduction of process length and motility, obtained with glutamate receptor blockade, was inversed by ATP (Fontainhas et al., 2011).

Future studies should investigate whether the activation of all three main ionotropic glutamatergic receptors can activate a common pathway.

OTHER NEUROTRANSMITTERS

Other than glutamate and GABA, very few studies have investigated the impact of neurotransmitter application on microglial motility. Acetylcholine, norepinephrine or serotonin did not cause changes in the dynamism of microglial processes in the spinal dorsal horn (Chen et al., 2010). However, Gyoneva and Traynelis (2013) has shown that norepinephrine was responsible for the retraction of microglial processes in acute brain slices in physiological conditions through β2 adrenergic receptors present in resting microglia. Process extension caused by ATP was inhibited by co-application of norepinephrine. Propranolol, an antagonist of β2 receptor, reversed this effect. These findings raise an interesting question: can signaling mediated by norepinephrine modify the microglial reactivity to ATP release *in vivo*? We believe further studies of the influence of various neurotransmitters in more physiological conditions are needed to obtain a more complete understanding of the mechanisms underlying neuron-to-microglia communication.

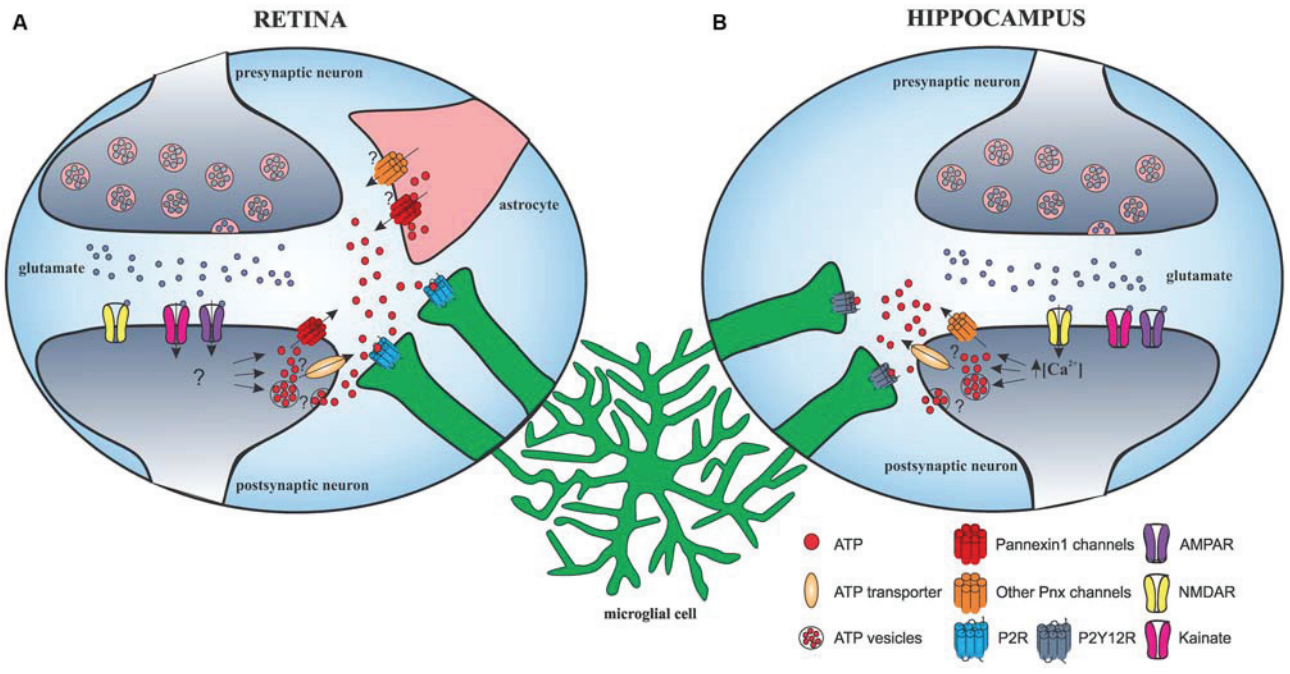

FIGURE 2 | Schematic representation of glutamatergic neurotransmission-induced microglial process outgrowth in the retina and hippocampus. **(A)** In the retina, AMPAR/kainate activation leads to release of ATP through pannexin-1 and possibly other mechanisms from neurons and astrocytes, ultimately leading to microglial response through P2 receptors. **(B)** In the hippocampus, glutamate-induced microglial process outgrowth is dependent on NMDA receptor. NMDAR activation leads to a significant Ca^{2+} influx that is required for ATP release through currently unknown mechanisms but independent of pannexin-1 and astrocyte hemichannels. ATP diffuses into the extracellular space and activates microglial purinergic receptor P2Y12, eliciting microglial process extension.

MICROGLIA-ASTROCYTE INTERACTIONS

In addition to interacting structurally with pre- and postsynaptic elements, microglia closely affix perisynaptic astrocytic processes (Tremblay et al., 2010). Accumulating evidence demonstrate that astrocytes not only play an important role in maintaining homeostasis, but also in regulating synaptic transmission (Perea et al., 2014; Oliveira et al., 2015). Thus, it appears that these glial cells may cooperate in the modulation of synaptic function taking into consideration their occasional structural proximity and emerging roles. Despite the possible influence of astrocytic ATP on microglial motility and morphology previously described, astrocyte-derived ATP was also found to induce microvesicle shedding from microglial cells, ultimately generating an increase of excitatory transmission (Bianco et al., 2005; Antonucci et al., 2012). Two recent studies provided compelling data on microglia-to-astrocyte interactions. Pascual et al. (2012) found that LPS stimulation of microglia in acute hippocampal slices resulted in a rapid ATP release. ATP bound to astrocytic P2Y receptor, which led to glutamate release by astrocytes, ultimately increasing excitatory transmission (Pascual et al., 2012). Another study found that fractalkine signaling, mediated exclusively by microglia, caused adenosine release, which in turn increased the release of D-serine most probably from both astrocytes and microglia, finally resulting in potentiation of NMDAR function (Scianni et al., 2013). Future studies must elucidate the context and molecular mechanisms governing interactions between microglia and astrocytes, as well as the functional consequences at the regulation of synaptic transmission and neural circuits.

CONCLUSION

Considerable progress has been made to decipher signaling mechanisms that regulate microglia-synapse interactions, which is only a token of its complexity. It is now crucial to better understand these mechanisms because the degree to which and how microglia interact with other cell types is most probably dependent on their morphology and motility. Several studies reveal functional importance of microglia in physiological conditions as they contribute to the fine-tuning of neuronal circuits and engage in synaptic and structural plasticity. These microglial functions are at least partly mediated by their motile processes, which can engulf synaptic terminals, thus homeostatically regulating neuronal activity and secrete a plethora of signaling molecules, including cytokines, neurotrophines, microvesicles etc. Their dynamism and functional capabilities position them perfectly to regulate individual synapses and to be undoubtedly involved in optimizing information processing, learning and memory, and cognition.

AUTHOR CONTRIBUTIONS

IH and OP wrote the review.

ACKNOWLEDGMENTS

We gratefully acknowledge the research support provided by Institut pour le recherche sur la Moelle Epinière (IRME) and J-F Labbé for its help on the manuscript.

REFERENCES

Antonucci, F., Turola, E., Riganti, L., Caleo, M., Gabrielli, M., Perrotta, C., et al. (2012). Microvesicles released from microglia stimulate synaptic activity via enhanced sphingolipid metabolism. *EMBO J.* 31, 1231–1340. doi: 10.1038/emboj.2011.489

Bianco, F., Pravettoni, E., Colombo, A., Schenk, U., Möller, T., Matteoli, M., et al. (2005). Astrocyte-derived ATP induces vesicle shedding and IL-1 beta release from microglia. *J. Immunol.* 174, 7268–7277. doi: 10.4049/jimmunol.174.11.7268

Burnstock, G. (2008). Purinergic signalling and disorders of the central nervous system. *Nat. Rev. Drug Discov.* 7, 575–590. doi: 10.1038/nrd2605

Chen, T., Koga, K., Li, X.-Y., and Zhuo, M. (2010). Spinal microglial motility is independent of neuronal activity and plasticity in adult mice. *Mol. Pain* 6:19. doi: 10.1186/1744-8069-6-19

Davalos, D., Grutzendler, J., Yang, G., Kim, J. V., Zuo, Y., Jung, S., et al. (2005). ATP mediates rapid microglial response to local brain injury *in vivo*. *Nat. Neurosci.* 8, 752–758. doi: 10.1038/nn1472

Dissing-Olesen, L., LeDue, J. M., Rungta, R. L., Hefendehl, J. K., Choi, H. B., and MacVicar, B. A. (2014). Activation of neuronal NMDA receptors triggers transient ATP-mediated microglial process outgrowth. *J. Neurosci.* 34, 10511–10527. doi: 10.1523/JNEUROSCI.0405-14.2014

Dou, Y., Wu, H.-J., Li, H.-Q., Qin, S., Wang, Y.-E., Li, J., et al. (2012). Microglial migration mediated by ATP-induced ATP release from lysosomes. *Cell Res.* 22, 1022–1033. doi: 10.1038/cr.2012.10

Dunwiddie, T. V., Diao, L., and Proctor, W. R. (1997). Adenine nucleotides undergo rapid, quantitative conversion to adenosine in the extracellular space in rat hippocampus. *J. Neurosci.* 17, 7673–7682.

Eyo, U. B., Peng, J., Swiatkowski, P., Mukherjee, A., Bispo, A., and Wu, L.-J. (2014). Neuronal hyperactivity recruits microglial processes via neuronal NMDA receptors and microglial P2Y12 receptors after status epilepticus. *J. Neurosci.* 34, 10528–10540. doi: 10.1523/JNEUROSCI.0416-14.2014

Fontainhas, A. M., Wang, M., Liang, K. J., Chen, S., Mettu, P., Damani, M., et al. (2011). Microglial morphology and dynamic behavior is regulated by ionotropic glutamatergic and GABAergic neurotransmission. *PLoS One* 6:e15973. doi: 10.1371/journal.pone.0015973

Ginhoux, F., Lim, S., Hoeffel, G., Low, D., and Huber, T. (2013). Origin and differentiation of microglia. *Front. Cell. Neurosci.* 7:45. doi: 10.3389/fncel.2013.00045

Gomez-Nicola, D., and Perry, V. H. (2015). Microglial dynamics and role in the healthy and diseased brain: a paradigm of functional plasticity. *Neuroscientist* 21, 169–184. doi: 10.1177/1073858414530512

Gyoneva, S., and Traynelis, S. F. (2013). Norepinephrine modulates the motility of resting and activated microglia via different adrenergic receptors. *J. Biol. Chem.* 288, 15291–15302. doi: 10.1074/jbc.M113.458901

Hammarberg, C., Schulte, G., and Fredholm, B. B. (2003). Evidence for functional adenosine A3 receptors in microglia cells. *J. Neurochem.* 86, 1051–1054. doi: 10.1046/j.1471-4159.2003.01919.x

Hanisch, U.-K., and Kettenmann, H. (2007). Microglia: active sensor and versatile effector cells in the normal and pathologic brain. *Nat. Neurosci.* 10, 1387–1394. doi: 10.1038/nn1997

Haynes, S. E., Hollopeter, G., Yang, G., Kurpius, D., Dailey, M. E., Gan, W.-B., et al. (2006). The P2Y12 receptor regulates microglial activation by extracellular nucleotides. *Nat. Neurosci.* 9, 1512–1519. doi: 10.1038/nn1805

Hirasawa, T., Ohsawa, K., Imai, Y., Ondo, Y., Akazawa, C., Uchino, S., et al. (2005). Visualization of microglia in living tissues using Iba1-EGFP transgenic mice. *J. Neurosci. Res.* 81, 357–362. doi: 10.1002/jnr.20480

Honda, S., Sasaki, Y., Ohsawa, K., Imai, Y., Nakamura, Y., Inoue, K., et al. (2001). Extracellular ATP or ADP induce chemotaxis of cultured microglia through Gi/o-coupled P2Y receptors. *J. Neurosci.* 21, 1975–1982.

Hoshiko, M., Arnoux, I., Avignone, E., Yamamoto, N., and Audinat, E. (2012). Deficiency of the microglial receptor CX3CR1 impairs postnatal functional development of thalamocortical synapses in the barrel cortex. *J. Neurosci.* 32, 15106–15111. doi: 10.1523/JNEUROSCI.1167-12.2012

Hua, Y. J., Smear, M. C., Baier, H., and Smith, S. J. (2005). Regulation of axon growth *in vivo* by activity-based competition. *Nature* 434, 1022–1026. doi: 10.1038/nature03409

Jung, S., Aliberti, J., Graemmel, P., Sunshine, M. J., Kreutzberg, G. W., Sher, A., et al. (2000). Analysis of fractalkine receptor CX(3)CR1 function by targeted deletion and green fluorescent protein reporter gene insertion. *Mol. Cell. Biol.* 20, 4106–4114. doi: 10.1128/mcb.20.11.4106-4114.2000

Kettenmann, H., Hanisch, U.-K., Noda, M., and Verkhratsky, A. (2011). Physiology of microglia. *Physiol. Rev.* 91, 461–553. doi: 10.1152/physrev.00011.2010

Kettenmann, H., Kirchhoff, F., and Verkhratsky, A. (2013). Microglia: new roles for the synaptic stripper. *Neuron* 77, 10–18. doi: 10.1016/j.neuron.2012.12.023

Lee, J. E., Liang, K. J., Fariss, R. N., and Wong, W. T. (2008). *Ex vivo* dynamic imaging of retinal microglia using time-lapse confocal microscopy. *Invest. Ophthalmol. Vis. Sci.* 49, 4169–4176. doi: 10.1167/iovs.08-2076

Li, Y., Du, X.-F., Liu, C.-S., Wen, Z.-L., and Du, J.-L. (2012). Reciprocal regulation between resting microglial dynamics and neuronal activity *in vivo*. *Dev. Cell* 23, 1189–1202. doi: 10.1016/j.devcel.2012.10.027

Nimmerjahn, A., Kirchhoff, F., and Helmchen, F. (2005). Resting microglial cells are highly dynamic surveillants of brain parenchyma *in vivo*. *Science* 308, 1314–1318. doi: 10.1126/science.1110647

Ohsawa, K., Sanagi, T., Nakamura, Y., Suzuki, E., Inoue, K., and Kohsaka, S. (2012). Adenosine A3 receptor is involved in ADP-induced microglial process extension and migration. *J. Neurochem.* 121, 217–227. doi: 10.1111/j.1471-4159.2012.07693.x

Oliveira, J. F., Sardinha, V. M., Guerra-Gomes, S., Araque, A., and Sousa, N. (2015). Do stars govern our actions? Astrocyte involvement in rodent behavior. *Trends Neurosci.* 38, 535–549. doi: 10.1016/j.tins.2015.07.006

Orr, A. G., Orr, A. L., Li, X.-J., Gross, R. E., and Traynelis, S. F. (2009). Adenosine A(2A) receptor mediates microglial process retraction. *Nat. Neurosci.* 12, 872–878. doi: 10.1038/nn.2341

Paolicelli, R. C., Bolasco, G., Pagani, F., Maggi, L., Scianni, M., Panzanelli, P., et al. (2011). Synaptic pruning by microglia is necessary for normal brain development. *Science* 333, 1456–1458. doi: 10.1126/science.1202529

Parkhurst, C. N., Yang, G., Ninan, I., Savas, J. N., Yates, J. R., Lafaille, J. J., et al. (2013). Microglia promote learning-dependent synapse formation through brain-derived neurotrophic factor. *Cell* 155, 1596–1609. doi: 10.1016/j.cell.2013.11.030

Pascual, O., Ben Achour, S., Rostaing, P., Triller, A., and Bessis, A. (2012). Microglia activation triggers astrocyte-mediated modulation of excitatory neurotransmission. *Proc. Natl. Acad. Sci. U S A* 109, E197–E205. doi: 10.1073/pnas.1111098109

Penuela, S., Gehi, R., and Laird, D. W. (2013). The biochemistry and function of pannexin channels. *Biochim. Biophys. Acta* 1828, 15–22. doi: 10.1016/j.bbamem.2012.01.017

Perea, G., Sur, M., and Araque, A. (2014). Neuron-glia networks: integral gear of brain function. *Front. Cell. Neurosci.* 8:378. doi: 10.3389/fncel.2014.00378

Peri, F., and Nüsslein-Volhard, C. (2008). Live imaging of neuronal degradation by microglia reveals a role for v0-ATPase a1 in phagosomal fusion *in vivo*. *Cell* 133, 916–927. doi: 10.1016/j.cell.2008.04.037

Prinz, M., and Priller, J. (2014). Microglia and brain macrophages in the molecular age: from origin to neuropsychiatric disease. *Nat. Rev. Neurosci.* 15, 300–312. doi: 10.1038/nrn3722

Ransohoff, R. M., and Perry, V. H. (2009). Microglial physiology: unique stimuli, specialized responses. *Annu. Rev. Immunol.* 27, 119–145. doi: 10.1146/annurev.immunol.021908.132528

Schafer, D. P., Lehrman, E. K., Kautzman, A. G., Koyama, R., Mardinly, A. R., Yamasaki, R., et al. (2012). Microglia sculpt postnatal neural circuits in an activity and complement-dependent manner. *Neuron* 74, 691–705. doi: 10.1016/j.neuron.2012.03.026

Scianni, M., Antonilli, L., Chece, G., Cristalli, G., Di Castro, M. A., Limatola, C., et al. (2013). Fractalkine (CX3CL1) enhances hippocampal N-methyl-D-aspartate receptor (NMDAR) function via D-serine and adenosine receptor type A2 (A2AR) activity. *J. Neuroinflammation* 10:108. doi: 10.1186/1742-2094-10-108

Tremblay, M. E., Lowery, R. L., and Majewska, A. K. (2010). Microglial interactions with synapses are modulated by visual experience. *PLoS Biol.* 8:e1000527. doi: 10.1371/journal.pbio.1000527

Wake, H., Moorhouse, A. J., Jinno, S., Kohsaka, S., and Nabekura, J. (2009). Resting microglia directly monitor the functional state of synapses *in vivo* and determine the fate of ischemic terminals. *J. Neurosci.* 29, 3974–3980. doi: 10.1523/JNEUROSCI.4363-08.2009

Wu, L.-J., and Zhuo, M. (2008). Resting microglial motility is independent of synaptic plasticity in mammalian brain. *J. Neurophysiol.* 99, 2026–2032. doi: 10.1152/jn.01210.2007

Conflict of Interest Statement: The authors declare that the research was conducted in the absence of any commercial or financial relationships that could be construed as a potential conflict of interest.

Copyright © 2016 Hristovska and Pascual. This is an open-access article distributed under the terms of the Creative Commons Attribution License (CC BY). The use, distribution and reproduction in other forums is permitted, provided the original author(s) or licensor are credited and that the original publication in this journal is cited, in accordance with accepted academic practice. No use, distribution or reproduction is permitted which does not comply with these terms.